UNIVERSITY OF BELGRADE

FACULTY OF TECHNOLOGY AND METALLURGY

Mohamed H. Assaleh

# IMINO DERIVATIVES OF CARBONOTHIOIC DIHYDRAZIDES AND CINNAMIC ACIDS AMIDES: STRUCTURE-ACTIVITY RELATIONSHIP STUDIES

Doctoral Dissertation

Belgrade, 2022

УНИВЕРЗИТЕТ У БЕОГРАДУ

ТЕХНОЛОШКО-МЕТАЛУРШКИ ФАКУЛТЕТ

Мохамед Х. Асалех

# ИМИНО ДЕРИВАТИ ДИХИДРАЗИДА ТИОУГЉЕНЕ И АМИДА ЦИМЕТНИХ КИСЕЛИНА: КОРЕЛАЦИЈЕ СТРУКТУРЕ И АКТИВНОСТИ

докторска дисертација

Београд, 2022

**Supervisor**:

Dr Aleksandar Marinković, associate professor
University of Belgrade, Faculty of Technology and Metallurgy

Dr. Sc. Med. Snežana Bjelogrlić, associate research professor
Institute for Oncology and Radiology of Serbia

Members of committee:

Dr Nevena Prlainović, assistant professor
University of Belgrade, Faculty of Technology and Metallurgy

Dr Dušan Mijin, full professor
University of Belgrade, Faculty of Technology and Metallurgy

Dr Irena Arandjelovic, assistant professor
University of Belgrade, Faculty of Medicine

Date of defense:_____

# IMINO DERIVATIVES OF CARBONOTHIOIC DIHYDRAZIDES AND CINNAMIC ACIDS AMIDES: STRUCTURE-ACTIVITY RELATIONSHIP STUDIES

## ABSTRACT


Two series of compounds were synthesized in this PhD thesis: Salicylaldehyde (**sal**) and 2-Acetylpyridine (**2ap**) mono- and *bis*-(thiocarbohydrazones), **m-TCH** and **b-TCH**, respectively (first series), and cinnamic acids amides (second series), in overall twenty eigth compounds.

All synthesized compounds are characterized using both experimental and theoretical methods. Experimental techniques include FT-IR, NMR and UV-Vis spectroscopy, as well as elemental analysis used for structural and purity characterization. The use of UV-Vis and NMR spectroscopy, and theoretical ("quantum chemical") calculations was applied to get a deeper insight into experimental data related to the ratio of Z/E isomer and thion/thio tautomerism *versus* related antioxidant activity induced by water addition to dimethyl sulfoxide (DMSO) TCHs solution. Water-induced breakage of intra-molecular hydrogen bond in mono- and *bis*(salicylaldehyde)**TCH**, i.e. [(2-hydroxyphenyl)methylene]carbonothioichydrazide, **m-TCH$_{sal}$**, and 2,2'-*bis*[(2-hydroxyphenyl)methylene]carbonothioic dihydrazide, **b-TCH$_{sal}$**, lead to *E* to *Z* isomerization. Good accordance of experimental data, from $^{1}$H and $^{13}$C NMR and 2D NOESY spectra, and theoretical ones, obtained using GIAO/B3LYP-6-311G++(d,p), with respect to geometrical *E*:*Z* isomer ratio, e.g. 81:19 for **m-TCH$_{sal}$** was obtained. Destabilization of the ground state lowers bond dissociation enthalpy (BDE) for 11 kcal/mol, and as consequence leads to more extensive electron spin delocalization in Z-isomers.

Additionally, 2-acetylpyridine based **TCH**, *i.e.* *E*-[1-(2-pyridinyl)ethylidene]-carbonothioic dihydrazide, **m-TCH$_{2ap}$**, and 2,2'-*bis*[1-(2-pyridinyl)ethylidene]carbonothioic dihydrazide, **b-TCH$_{2ap}$**, are susceptible to thione/thiol tautomerism as a phenomenon which contributes to lower BDE and effectiveness of the hydrogen transfer to DPPH$^{\bullet}$ is facilitated in that manner. Analogously, experimental and theoretical results confirmed the shift of **m-TCH$_{2ap}$** and **b-TCH$_{2ap}$** to thiol form by water addition. These data were observed from the calculation of ZPE-corrected energy, enthalpy, BDEs, and the extent of radical spin delocalization of the isomers of studied compounds. Results indicate that increased participation of the thiol group in thiol/thion equilibria highly contributes to increased radical scavenging activity of compounds **m-TCH$_{2ap}$** and **b-TCH$_{2ap}$**. The spin density delocalization in thiol form of **m-TCH$_{2ap}$** and **b-TCH$_{2ap}$** occupy almost entire structure. Opposite is true for thione radicals. This fact is observed by a significant increase of antioxidant activity of all compounds, e.g. 0.67 for **b-TCH$_{2ap}$** in DMSO and 0.13 in DMSO:$H_2O$ = 4:1 ($IC_{50}$ in mM).

A second part includes the synthesis of twenty four cinnamic acid amides (cinnamamides) with TCHs pharmacophore, synthesized by coupling of acid chlorides: cinnamic, 3-chlorocinnamic, 4-chlorocinnamic and 4-methoxycinnamic acid with **m-TCH** containing: pyridine-2-yl, salicyl, 8-hydroxyquinoline-2-yl and 2-acetyl moiety. Synthesized compounds have been investigated for their biological properties in terms of anticancer and antimycobacterial activity. Analogous synthesis was applied with 3-hydroxycinnamic acid using the same set of **m-TCH** and HATU coupling agent. Finally, amides based on Caffeic and Ferulic acids with **m-TCH** containing pyridine-2-yl and salicyl moieties were synthesized in the same manner, and used for study of their antioxidative potential. Within assessment of compounds' ability to induce death of malignant cells, five human cell lines were treated over 24 h: colorectal adenocarcinoma (LoVo), ovarian adenocarcinoma (SkOV-3), lung adenocarcinoma (A549), breast adenocarcinoma (MCF-7) and pancreatic adenocarcinoma (AsPC-1). Obtained results showed that A549 cells were the most sensitive to tested treatments, whereas compounds **3-ClCimTCH$_{sal}$** and **4-ClCimTCH$_{8OH2qu}$** revealed superior activity and were set as the focus of a further anticancer investigation. Although **4-ClCimTCH$_{8OH2qu}$** acted as a more powerful inducer of apoptotic death than **3-ClCimTCH$_{sal}$**, both compounds in A549 cells stimulated cell cycle arrest at the G0/G1 phase, as well as activation of the intrinsic caspase cascade. A notable difference

in mechanisms of their pro-apoptotic activity refers to the ability of **4-ClCimTCH$_{8OH2qu}$** to strongly arouse generation of superoxide anion in mitochondria, which was not seen in A549 cells subjected to **3-ClCimTCH$_{sal}$**. Evaluation of their antimigratory properties demonstrated that compound **3-ClCimTCH$_{sal}$** significantly inhibited mobility of A549 cells, which was not recorded in samples treated with **4-ClCimTCH$_{8OH2qu}$**. Finally, powerful cytotoxicity of **4-ClCimTCH$_{8OH2qu}$** on HaCat (human keratinocytes) and HepG-2 (hepatocellular adenocarcinoma) cells that were employed as models for skin and liver toxicity, uncovered that this compound has disadvantageous toxicity profile. On the contrary, **3-ClCimTCH$_{sal}$** had only a moderate impact on the vitality of HaCaT cells, and therefore proved as suitable for future investigations of its anticancer properties. The capacity of compounds to interfere with proliferation and survival of *Mycobacterium tuberculosis* (Mtb), which is a pathogen responsible for the development of tuberculosis (TB), was assessed on three strains from clinical isolates, each comprising a specific resistance genotype: Mtb-InhRif-S with no specific mutations associated with resistance to isoniazid (INH) and/or rifampicin (RIF), Mtb-Inh-R harboring specific mutation for resistance to RIF, and Mtb-Rif-R holding specific mutation associated with resistance to INH. After 6 days of incubation with investigated drugs, with INH and RIF as positive controls, **CimTCH$_{8OH2qu}$** was the only one that successfully reduced Mtb viability for more than 90 % in all three treated strains. Moreover, compound **CimTCH$_{8OH2qu}$** did not induce the death of HepG-2 cells, which indicates its favorable hepatotoxicity profile compared to current therapeutic options for the treatment of TB.

A third part of the present study included an antimicrobial study of three series of cinnamic acid amides: cinnamic, 4-chlorocinnamic and 4-methoxy cinnamic acid and **m-TCH** containing: pyridine-2-yl, salicyl, 8-hydroxyquinoline-2-yl, and 2-acetyl moiety. The antimicrobial study against *Enterococcus cloacae* ATCC13047, *Staphylococcus aureus* NCTC 6571, *Klebsiella pneumoniae* ATCC 13883, *Acinetobacter baumannii* ATCC 19606, *Pseudomonas aeruginosa* NCTC 10662, and *Escherichia coli* ATCC 1175 was performed. Some of the cinnamic amides showed good *in vitro* activity against all strains tested, *i.e*. amides based on cinnamic, 4-chlorocinnamic and 4-methoxy cinnamic acid and **m-TCH$_{2ap}$**, *i.e*. **CimTCH$_{2ap}$**, **4-MeOCimTCH$_{2ap}$** и **4-ClCimTCH$_{2ap}$**. Moreover, all compounds showed acceptable to high activities with respect to *A. baumannii*, a widely spread opportunistic pathogen in hospitals. The most active derivative was **4-MeOCimTCH$_{2fp}$**, with $MIC_{50}$ value of 10.4 (μmol). Additionally, in order to establish relation of structure and antibacterial activity against *A. baumanii* an alignment-independent 3D QSAR model was developed for the identification of pharmacophoric hotspots. In order to rationalize antimicrobial mechanism, the iron chelation capability of synthesized compounds was determined using UV-Vis spectrophotometric method. Due to the presence of strong donor sites the synthesized compounds showed strong iron chelating ability by creating complexes with the stability constant in the range from $10^7$ to $10^9$. Determined stability constants indicate that interaction of iron and synthesized compounds is an important step in the reaction pathway of antimicrobial activity against A. baumannii.

**Keywords**: Thiocarbohydrazide; Cinnamic acid amides; *E*/*Z* isomerism; Tautomerism; Antioxidant Activity; Antibacterial activity; *Mycobacterium tuberculosis*; Anticancer; Hepatotoxicity; Acinetobacter baumannii; 3D QSAR.

Scientific field: Chemical sciences
Scientific subfield: Organic chemistry

# ИМИНО ДЕРИВАТИ ДИХИДРАЗИДА ТИОУГЉЕНЕ И АМИДА ЦИМЕТНИХ КИСЕЛИНА: КОРЕЛАЦИЈЕ СТРУКТУРЕ И АКТИВНОСТИ

## ИЗВОД


У овој докторској дисертацији синтетисане су две серије једињења: салицилалдехид и 2-ацетилпиридин моно- и дитиокарбохидразони, **TCH** (прва серија), и амиди циметних киселина (друга серија), укупно двадесетосам једињења.

У првом делу дисертације, применом експерименталних и теоријских метода су окарактерисана сва синтетисана једињења. Експерименталне технике су укључиле: FT-IR, NMR и UV-Vis спектроскопију, као и елементалну анализу. Употреба UV-Vis и NMR спектроскопије и теоријских прорачуна примењена је да би се добио бољи увид у експерименталне податке који се односе на однос *Z/E* изомера и повећану антиоксидативну активност након додатка воде у раствор диметил-сулфоксида (ДМСО) **TCH**s. Вода раскида интрамолекуларне водоничне везе у [(2-хидроксифенил)-метилен]карботиохидразид, **m-TCH$_{sal}$** и 2,2'-*bis*[(2-хидроксифенил)метилен]карботио-дихидразид, **b-TCH$_{sal}$**, који доводе до *E* и *Z* изомеризације. Резултати из $^{1}$H и $^{13}$C NMR и 2D NOESY спектара и теоријских израчунавања, добијених коришћењем GIAO/B3LYP-6-311G++(d,p) базиз сета, указују на 81:19 однос *E*:*Z* изомера за **m-TCH$_{sal}$**. Такође, израчунато је да услед дестабилизације основног стања, енталпија дисоцијације везе (енгл. Bond Dissociation Energy, BDE) је мања за 11 kcal/mol, а делокализација спина електрона у *Z* -изомерима је значајнија.

Поред тога, *E*-[1-(2-пиридинил)етилиден]карботиохидразид, **m-TCH$_{2ap}$**, и 2,2'-*bis*[1-(2-пиридинил)етилиден]карботио-дихидразид, **b-TCH$_{2ap}$**, су подложни тион/тиол таутомеризацији што доприноси смањењу BDE и тиме олакшава пренос атома водоника у DPPH$^{\cdot}$ тесту. Експериментални и теоријски резултати потврдили су да тион/тиол равнотежа, код **m-TCH$_{2ap}$** и **b-TCH$_{2ap}$**, додавањем воде помера равнотежу ка тиолном облику. Ови подаци су добијени из израчунавања ZPE-кориговане енергије, енталпије, BDE и степена делокализације спина радикала одговарајућих таутомера. Резултати показују да повећан удео тиолне групе у великој мери доприноси повећању активности једињења **m-TCH$_{2ap}$** и **b-TCH$_{2ap}$**. Густина спина радикала у тиолном облику једињења **m-TCH$_{2ap}$** и **b-TCH$_{2ap}$** делокализована је скоро преко целе структуре, што није случај код тион облика. Ова чињеница објашњава значајно повећање антиоксидативне активности, нпр. IC$_{50}$ за **b-TCH$_{2ap}$** је 0,67 у ДМСО и 0,13 у ДМСО:H$_2$O = 4:1 (у mM).

Други део дисертације је укључивао синтезу дванаест амида циметне киселине укључујући **TCH** фармакофоре, синтетисаних куповањем хлорида киселина: циметне, 3-хлорциметне и 4-хлорциметне киселине, као и **m-TCH** који садрже: пиридин-2-ил, салицил, 8-хидроксихинолин-2-ил и 2-ацетил групе. Синтетисаним једињењима је испитиван спектар биолошких активности укључујући антиканцерску и антимикобактеријску активност. Аналогна синтеза је примењена са 3-хидроксициметном киселином коришћењем истог сета **m-TCH** и HATU средства за куповање. На исти начин су синтетисани амиди кафеинске и ферулинске киселине са **m-TCH** који садрже пиридин-2-ил и салицил делове који су коришћени за одређивање антиоксидативног потенцијала. У оквиру процене способности једињења да индукују смрт малигних ћелија, пет хуманих ћелијских линија је третирано током 24 сата: колоректални аденокарцином (LoVo), аденокарцином јајника (SkOV-3), аденокарцином плућа (A549), аденокарцином дојке (MCF-7) и аденокарцином панкреаса (AsPC-1). Добијени резултати су показали да су ћелије A549 биле најосетљивије на тестирана једињења док су једињења **3-ClCimTCH$_{sal}$** и **4-ClCimTCH$_{8OH2qu}$** показала супериорну

активност и изабрана су за даља истраживања антиканцерске активности. Иако је **4-ClCimTCH$_{8OH2qu}$** деловао као снажнији индуктор апоптозне смрти од **3-ClCimTCH$_{sal}$**, оба једињења у A549 ћелијама су стимулисала заустављање ћелијског циклуса у G0/G1 фази, као и активацију интринзичне каспазне каскаде. Значајна разлика у механизмима њихове про-апоптозне активности односи се на способност **4-ClCimTCH$_{8OH2qu}$** да снажно побуди стварање супероксидног анјона у митохондријама, што није детектовано у ћелијама A549 подвргнутим **3-ClCimTCH$_{sal}$**. Процена њихових антимиграционих својстава показала је да једињење **3-ClCimTCH$_{sal}$** значајно инхибира покретљивост A549 ћелија, што није забележено у узорцима третираним са **4-ClCimTCH$_{8OH2qu}$.** Висок проценат ћелијске смрти које је изазвало једињење **4-ClCimTCH$_{8OH2qu}$** у ћелијама HaCaT (хумани кератиноцити) и HepG-2 (хумани хепатоцити), коришћених као модели за процену могућих нежељених дејстава, указало је да ово једињење има неповољан токсиколошки профил. Напротив, **3-ClCimTCH$_{sal}$** је имао само умерен утицај на виталност HaCaT ћелија и стога се показао погодним за будућа истраживања његових антиканцерских својстава.

Капацитет једињења да омета пролиферацију *Mycobacterium tuberculosis* (*Mtb*), патогена одговорног за развој туберкулозе (ТБ), процењен је на три соја из клиничких изолата, од којих сваки садржи специфичан генотип отпорности на лекове који се користе у првој линији анти-ТБ терапије: *Mtb-InhRif-S* без специфичних мутација повезаних са резистенцијом на изониазид (INH) и/или рифампицин (RIF), *Mtb-Inh-R* који има специфичну мутацију за отпорност на INH, и *Mtb-Rif-R* који има специфичну мутацију повезану са отпорношћу на RIF. После шест дана инкубације са испитиваним лековима и INH и RIF као позитивним контролама, **CimTCH$_{8OH2qu}$** је био једини који је успешно смањио раст и размножавање *Mtb* за више од 90% у сва три третирана соја. Штавише, једињење **CimTCH$_{8OH2qu}$** није изазвало смрт HepG-2 ћелија, што указује на његов повољан профил хепатотоксичности за разлику од тренутно доступних терапијских опција за лечење ТБ.

Трећи део ове студије обухватао је испитивање антибактеријске активности четири серије амида: циметне, 4-хлороциметне и 4-метокси циметне киселине које у амидном делу садрже: пиридин-2-ил, салицил, 8-хидрокси хинолин-2-ил и 2-ацетил групу. Антибактеријска студија изведена је на *Enterococcus cloacae* ATCC13047, *Staphylococcus aureus* NCTC 6571, *Klebsiella pneumoniae* ATCC 13883, *Acinetobacter baumannii* ATCC 19606, *Pseudomonas aeruginosa* NCTC 10662, and *Escherichia coli* ATCC 1175, применом методе разблаживања. Поједини амиди циметне киселине су показали добру *in vitro* активност према свим испитиваним сојевима, односно амиди циметне, 4-хлорциметне и 4-метоксициметне киселине са 2-ацетилпиридинил групом, тј. **CimTCH$_{2ap}$**, **4-MeOCimTCH$_{2ap}$** и **4-ClCimTCH$_{2ap}$**. Штавише, сва једињења су показала значајну активност у односу на *A. baumannii*, широко распрострањени опортунистички интрахоспитални патоген. Најактивнији дериват био је **4-MeOCimTCH$_{2fp}$**, чија је минимална инхибиторна концентрација способна да инхибира раст и размножавање за 50 % (МИК$_{50}$) износила 10,4 μmol. Поред тога, да би се успоставила веза између структуре и антибактеријске активности против *A. baumannii*, развијен је 3D QSAR модел (an alignment-independent 3D QSAR model) за идентификацију битних фармакофора. У циљу рационализације антимикробног механизма, способност хелације (координације) гвожђа синтетисаних једињења је одређена UV-Vis спектрофотометријском методом. Због присуства јаких донорских места, синтетисана једињења су показала високу способност хелације гвожђа стварањем комплекса са константом стабилности у опсегу од $10^7$ до $10^9$. Вредности константи стабилности указује да је интеракција гвожђа са овим једињењима важан корак у метаболитичком

путу што је потврђено тиме што је антибактеријска активност према *A. Baumannii* у корелацији са променом вредности константе стабилности.

**Кључне речи**: Тиокарбохидразиди; Амиди циметне киселине; *E/Z* изомеризација; Таутомеризација; Антиоксидатвна активност; Антибактеријска активност; *Mycobacterium tuberculosis*; Антиканцер; Хепатоксичност; *Acinetobacter baumannii*; 3D QSAR

Научна област: Хемијске науке
Ужа научна област: Органска хемија

## LIST OF ABBREVIATIONS AND SYMBOLS

●$O_2^-$ - mitochondrial superoxide radical
$^{13}$C NMR – Carbon Nuclear Magnetic Resonance Spectroscopy
$^{1}$H NMR – Proton Nuclear Magnetic Resonance Spectroscopy
2D NMR – Two-dimensional Nuclear Magnetic Resonance Spectroscopy
3-AP – 3-aminopyridine-2-carboxaldehyde TSC
5-HP - 2-formylpyridine TSC
A549 – human lung non-small cell carcinoma cell line
$ABTS^{\bullet+}$ – 2,2'-Azino-bis(3-ethylbenzothiazoline-6-sulfonic acid)
ACD – Accidental Cell Death
ADME – absorption, distribution, metabolism and excretion properties
AsPC-1 – human pancreatic adenocarcinoma cell line
ATP – adenosine-3-phosphate
ATR – attenuated total reflectance
AU – arbitrary units
BBB – blood-brain barrier
BCS – biopharmaceutics classification system
BDE – Bond Dissociation Enthalpy
br. m. ovlp. – broar multiplet overlapping
b-TCH – dithiocarbohydrazones
CA – cinnamic acid
CADs – cinnamic acid derivatives
CAM – Calcein acetoxymethil
CAT – catalase
$CdC_{50}$ – concentration that induces death in 50 % of treated cells
CNS – central nervous system
COSY – Correlation Spectroscopy
CUPRAC – Cupric reducing antioxidant power
d – doublet
dd – doublet of doublets
DFT – Density functional Theory
DHS – Thiocarbohydrazide
DIPEA - Diisopropylethylamine
DMEM – Dulbecco's Modified Eagle's Medium
DMF – Dimethylformamide
DMSO - dimethyl sulfoxide
DMSO-*d*6 – Deuterated Dimethyl sulfoxide
$DPPH^{\bullet}$ – 2,2-diphenyl-1-picrylhydrazyl radical
DPPH4 – Dipeptidyl peptidase 4
ECM – extracellular Matrix
EDTA – Ethylenediaminetetraacetic acid
EOF – Enthalpy of Formation
ESI – electronic supplementary information
ESM – Electronic Supplementary Material
ESOL – estimated solubility
FBS – fetal bovine serum
FT-IR – Fourier Transform Infrared Spectroscopy
GGA – Generalized-Gradient Approximation

GIAO – Gauge Independent Atomic Orbital
GPx – glutathione peroxidase
HaCaT – human keratinocytes cell line
HAT – Hydrogen Atom Transfer
HepG-2 – human hepatocellular carcinoma cell line
HFS – Hartree-Fock Slater
HMBC – Heteronuclear Multiple Bond Correlation
HSQC – Heteronuclear Single Quantum Coherence
IHB – Intramolecular H-bond
IMP - inosine 5'-monophosphate.
IMPDH2 - inosine 5'-monophosphate dehydrogenase 2
INH – Isoniazid
IR – infrared spectroscopy
*J* - coupling constant
LCAO – linear combination of atomic orbitals
LDA – Local Density Approximation
LJ - Löwenstein-Jensen medium
m – Multiplet
MBC – Minimal Bactericidal Concentration
MCF-7 – human mammary adenocarcinoma cell line
MeOH – Methanol
MFI – mean fluorescent intensity
MIC – minimal inhibitory concentration
Mp – melting point
MPT – Mitochondrial Permeability Transition
*Mtb – Mycobacterium tuberculosis*
*Mtb-Inh-R – Mtb* strain with detected INH resistance-associated *KatG* mutations
*Mtb-InhRif-S – Mtb* strain with no detected mutations associated with resistance to either INH or RIF
*Mtb-Rif-R – Mtb* strain with detected RIF resistance-associated *rpoB* mutations
m-TCH - monothiocarbohydrazones
MTT – 3-(4,5-dimethylthiazol-2-yl)-2,5-diphenyltetrazolium bromide
N-HATU - 1-[*Bis*(dimethylamino)methylene]-1*H*-1,2,3-triazolo[4,5-*b*]pyridinium 3-oxid hexafluorophosphate
NMR – Nuclear Magnetic Resonance Spectroscopy
NOESY – Nuclear Overhauser Effect Spectroscopy
$P_{app}$ – apparent permeability coefficient
PDB – Protein data bank
PI – propidium iodide
ppm – Parts Per Million
PTP1B - tyrosine-protein phosphatase non-receptor type 1
RCD – Regulated Cell Death
RIF – Rifampicin
RNase A – ribonuclease A
RO5 – Lipinski rule of 5
ROS – reactive oxygen species
s – singlet
SDS – sodium dodecyl sulfate
SET – Single-electron Transfer
SkOV-3 - human ovary adenocarcinoma cell line

SOD – superoxide dismutase
SOD2 - mitochondrial (manganese) superoxide dismutase
SPLET – Sequential Proton Loss Electron Transfer
t – triplet
TAC – Total antioxidant capacity
TB – tuberculosis
TCH – Thiocarbohydrazones
TMS – tetramethylsilane
TPSA – total polar surface area
UV-Vis – Ultraviolet visible spectroscopy
VWA – Vosko, Wilks, and Nusair

**TABLE OF CONTENTS**

## 1. Introduction

Cinnamic acid (CA) is an aromatic carboxylic acid with nine-carbon atoms (C6-C3) structure, moreover, cinnamic acid derivatives (CADs) naturally appear in the plant kingdom found in the vegetables, fruits, cereals and flowers that are consumed as phenolic compounds in the diet.[1–4] Cinnamic acid derivatives exhibited a broad range of biological activity and low toxicity, are of particular interest in the development of novel highly active drugs.[5] It has played an intermediate role in the synthesis of pharmaceutical ingredients which potential to have antioxidant activity, and their ability to decrease oxidative stress-induced tissue damage caused by chronic diseases, and reported as lipid-lowering action, several biological interests were mentioned in the literature review including anticancer, antioxidant, antimicrobial, antifungal, anti-inflammatory, and antituberculosis.[6–10] Besides, CADs have been widely used all over the world as cosmetics because of their floral odour including perfumes, face creams, body lotions, antiperspirants, bath products, shampoos, and soaps.[11,12]

Thiocarbohydrazide (DHS) and its derivative are an important class of compounds that have many useful applications as well as their valuable reactions; the chemistry of DHS has considerable interest in the synthesis of organic chemistry and biological filed besides their therapeutic importance.[13,14]

The condensation of DHS with an aldehyde or ketone leads to poly-function thiocarbohydrazones (**TCH**), which gained wide interest due to their various use. Furthermore, (**TCH**) that contain an azomethine (–C=N–) linkage that may stitch together two or more heterocyclic/ aromatic scaffolds to create different molecular hybrids that may have biological properties.[15–17]

Moreover, DHS especially their Schiff bases obtained from condensation with various carbonyl compounds – (**TCH**), have recently become important compounds in the medicinal and pharmaceutical field. The chemistry of carbon-nitrogen double bond present in those molecules is rapidly becoming the backbone of the condensation reaction, and hydrazones containing azometine N=CH moiety are utilized as starting materials in the synthesis of industrial[16] and biological compounds.[17–26]

Furthermore, during our interest in (**TCH**) in the past several years, we have successfully synthesized a considerable number of different derivatives of mono-thiocarbohydazones (**m-TCH**) and bis-thiocarbohydrazones (**b-TCH**). Results of anti-cancer activity of quinoline-containing compounds are already reported[27], while data supporting the anti-cancer activity of compounds containing pyridine and hydroxyphenyl nucleus are in the preparation phase. **m-TCH$_{2ap}$** have been reported as "inactivators of Herpes Simplex Virus (HSV-1) ribonucleotide reductase, [28,29] and a large number of hydrazones that contain the quinoline core in their structure have shown promising results in testing on various cancer cells[30–35].

The urge for new, even more potent, compounds initiates the idea of making hybrid molecules by combining two pharmacophores to produce a third molecule with a more potent effect. As it has been documented that introduction of cinnamoyl functionality ameliorate anticancer activity of compounds[36], we have decided to upgrade, already detected (proven, confirmed) anti-cancer activity of **m-TCH**.[27] Due to this we synthesized sixteen amide derivatives by combining 2-pyridinyl-, salicyl-, 8-hydroxy-2-quinolinyl- or 2-acetylpyridynil- monothiocarbohydrazones with cinnamic-, 3-chlorocinnamic-, 4-chlorocinnamic acids or 4-Methoxycinnamic acid. To the best of our knowledge, all synthesized compounds are new and unknown in the literature, so they are fully characterized using melting temperature, elemental analysis, $^{1}$H NMR and $^{13}$C NMR, FT-IR, spectroscopy. Also, 2D spectroscopic characterization (COSY, NOESY, $^{1}$H-$^{13}$C HSQC, $^{1}$H-$^{13}$C HMBC) of specific representatives of each group of synthesized compounds has been given.

## 1.1. Literature review

### 1.1.1. Cinnamic acid and its derivatives

Cinnamic acids and their derivatives are aromatic fatty acids of low toxicity, which are important components of our daily diet, and readily available naturally from the plant. They are created in the biochemical manner that produces lignin, which is an aromatic polymeric that provides mechanical strength to plant walls, facilitates water transport and solutes through the vascular system. These compounds have received considerable attention in recent years because of their health benefits and multiple uses.[1,3,37]

Hydroxycinnamic acid derivatives represent a group of amino acids: L-tyrosine, L-phenylalanine, and L-tryptophan which include a number of organic acid isomers, most of them from plant origin, manufactured industrially or synthesized in the laboratory.[38]

In addition, the aromatic amino acids (AAA) are major molecules in plant metabolism, which are ubiquitously involved in the synthesis of proteins. Likewise, they are important nutritive compounds in the humans and monogastric livestock diet which are not able to create them.[39–41]

Hydroxycinnamic acids amides are a varied category of secondary metabolites found abundantly in high plants, which are nitrogenous compounds that have low molecular weight. Furthermore, they are one of the most common types of phenylpropanoids distributed in plant tissues which are important participant in a growth and development processes including cytomorphogenesis, cell division, sexual differentiation, plant defence, flowering, root growth, cell wall cross-linking, and leaf senescence.[42–46]

Cinnamic acid and its derivatives are the essential groups of phenolic acids that have existed naturally in fruits, vegetables, flowers, and grains and spread throughout the plant in stems, roots, seeds and leaves.[47]

Antitumor activity of cinnamic acids dates back to 1905 when Dr. Drage used salt of *ortho*-coumaric acid to treat patients[48]. However, despite promising results, until the beginning of the 20st century those compounds have been unfairly neglected and underutilized and only in the in last fifteen years the extreme potency of molecules with cinnamic acid moiety has attracted great attention of medicinal chemists[49]. Although a great number of scientific papers has been published recently, no direct conclusions of their mechanism of action have been proposed, but it is most likely that multi-activities can be correlated with the presence of α,β-unsaturated carbonyl moiety.[36]

In the molecule of cinnamic acid, there are three different reactivity centers, which results in the possibility of forming various types of derivatives such as esters, amides, hydrazides, glycosides and others. Among all of them, esters and amides are the most common, and while both exhibit a broad spectrum of biological activities,[36,50–53] reduced chemical stability of esters, compared to amides, limits their use. The high stability of amides under physiological conditions, provided by specific three-dimensional structures of the amide bond, is responsible for the highest share of these derivatives in both natural and synthetic drugs.[54]

### 1.1.2. History of Cinnamic acid and its derivative

The term "cinnamic" used since antiquity derives from the spice cinnamon (*Cinnamomum zeilanicum*) which has been used in several fields such as a flavouring agent and for carminative, antiseptic, insecticide, and stimulant. The brown bark of Cinnamomum has a large amount of E-Cinnamaldehyde, which is a volatile compound responsible for the hot, sweet, and pungent flavour of cinnamon.[3]

The first reported use of commercial sunscreen was in the USA in 1928 but with limited use, had benzyl cinnamate and benzyl salicylate in their composition, the structure of these filters has the ability to convert harmful UV rays into low energy radiation, which is supposed to be relatively safe. Currently, it considers, as one of the most UV chemical filters used is octyl methoxycinnamate. [55–58] Furthermore, the first biological activity of CA was reported in 1935 by Haagen-Smit and Went win

they discovered that it has like auxin activity and thus cis-CA has long been believed to be an analogue of auxin.[59–61] In the 1970s, Japanese scientists were reported that Ferulic acid has a strong antioxidant activity that exhibits chain breaking and prevents ischemia-reperfusion-connected intestinal injury. A few years later, they adopted using Ferulic acid as an antioxidant food additive.[62,63]

### 1.1.3. Structure and classification of cinnamic acid and its derivatives

Cinnamic acid is an organic aromatic compound with a white crystalline form that is slightly water-soluble and easily soluble in several chemical solvents. CA has formula $C_6H_5CH=CHCOOH$, classified as unsaturated carboxylic acid, presents in both *cis*- and *trans*-isomerism as shown in Figure 1, although the second is more popular and both of them are endogenous to plants.[61]

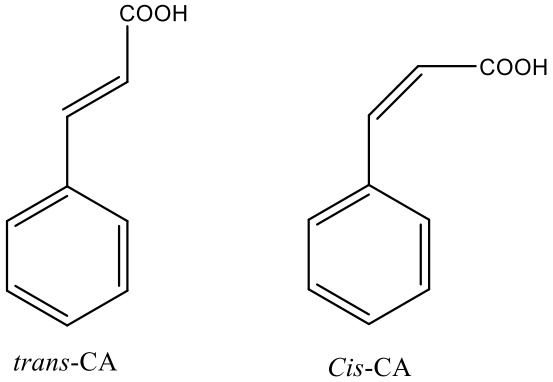


Figure 1. Structure of *trans*-cinnamic acid (*trans*-CA) and *cis*-cinnamic (*cis*-CA) acid.

The starting compounds used in this study are shown in Figure 2 (a-f), including cinnamic acid in (Figure 1), 3-Chloro Cinnamic acid (Figure 2 a), 4-Chloro Cinnamic Acid (Figure 2 b), 4-Methoxy Cinnamic acid (Figure 2 c), 3-Hydroxy Cinnamic acid (Figure 2 d), Ferulic Acid (Figure 2 e) and Caffeic acid (Figure 2 f).

The most plentiful hydroxycinnamic acid in the plant world is Ferulic acid which is found abundant in plant cell walls such as vegetables, grains, and fruits. It shows a great antioxidant source well as anticancer, antimicrobial, anti-angiogenic and antidiabetic activity.[64,65]

Caffeic acid is mostly found in coffee beans, regular drinking coffee provides 250 to 500 mg of Caffeic acid, likewise, coffee is an important source of methoxy derivatives of cinnamic acid including *p*-methoxycinnamic acid and 3,4-dimethoxycinnamic acid (690 mg/kg dry weight of coffee beans), in addition, Caffeic acid is present in olives, potatoes, fruits, and carrots [62,66].

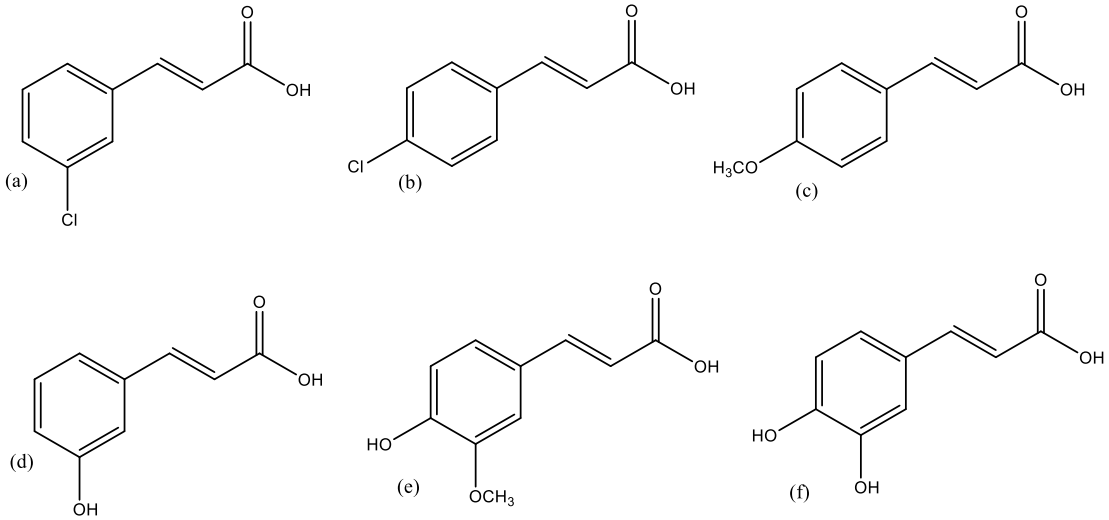


Figure 2. Structure of Cinnamic Acid and Its Derivatives.

## 1.2. Thiocarbohydrazones

Thiocarbohydrazides (DHS) are important compounds that have a wide range of uses. The chemistry of DHS has sparked interest in biological fields and synthetic organic chemistry; it also has important applications besides its therapeutic value as exampled by estimation of three-dimensional ultrastructure investigation method of interphase nuclei and tissues. Moreover, it is also known as fogging factor, and it is defined as a safe, storable, and cool-burning pyrotechnic compound for dispersing smoke and chemical warfare weapons. On the other hand, DHS is employed as a complex factor for solvent extraction separation methods as well as an extremely selective for adsorbing heavy metal ion.[16]

DHS is a commercially accessible polynucleophile with five nucleophilic sites, giving it a wide range of synthetic applications. It was utilized to produce functionalized heterocyclic compounds with improved biological activity.[67]

In recent years, the coordination chemistry of TCHs, molecules with the formula shown in Figure 3 a-c and which can be estimated as higher homologues of thiosemicarbazones (TSCs) (Figure 3 d). The condensation of ketones and aldehydes with DHS was reported in the first synthesis of these systems in 1925. The close of hetero-ring of aldehyde-derived of TCHs was the first application of these compounds.[68]

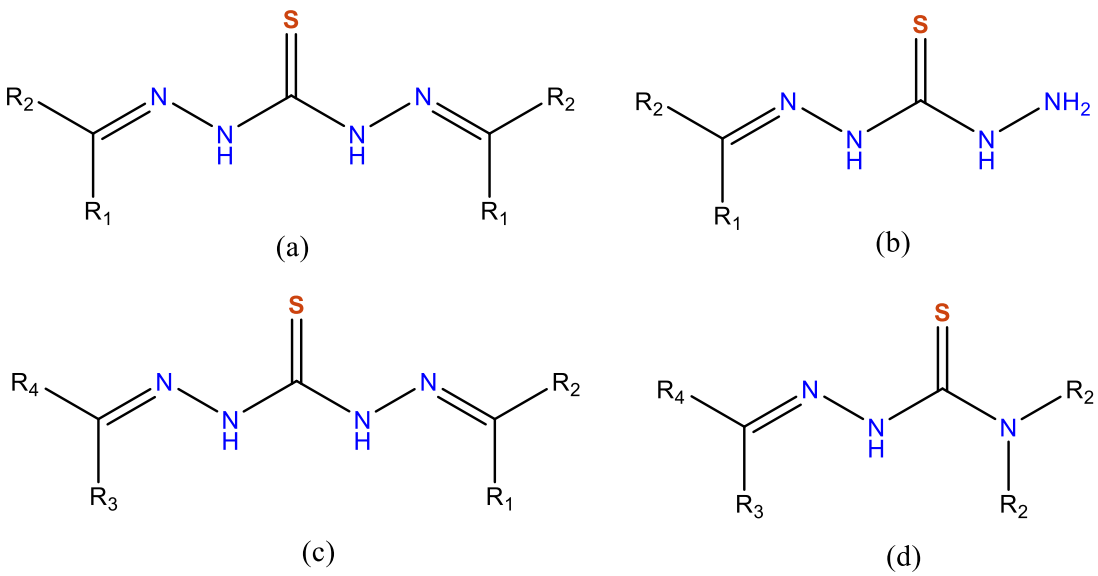


Figure 3. The formula of TCHs (a-c) and TSCHs (d).

### 1.2.1. Structure of TCHs

We can identify symmetric and asymmetric systems from the point of structural standpoint. In the first case, When the condensation reaction is the equivalent of an aldehyde or a ketone, yield 1,5-b-TCHs. (Figure 3 a); in the second case, the yield is a terminal non-functionalized hydrazine moiety by condensation with one equivalent of the carbonyl derivative. (Figure 3 b) for the following insertion of various carbonyl compounds (Figure 3 c).

The thioketo-thioenol tautomerism is also conceivable for the TCHs, as it is for the parent thiocarbohydrazides (Figure 4). Because of the double bond nature of the core N-C linkage, the thioenol tautomers might exist such an *syn* (Figure 4 b) or *anti* (Figure 4 c) geometric isomers.[68]

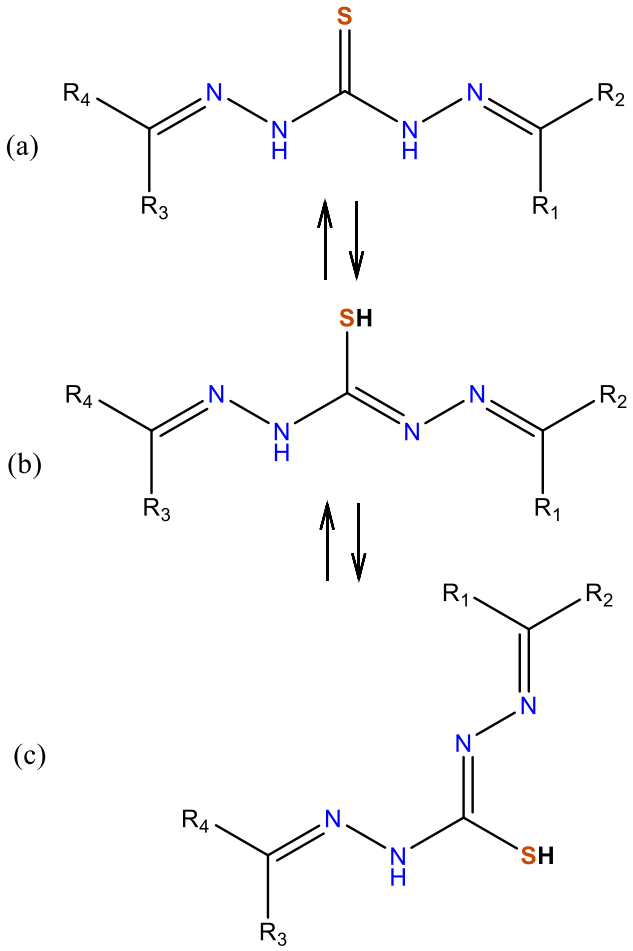


Figure 4. TCHs tautomers; (a) thioketo form, (b) thioenol *syn*, and (c) thioenol *anti* isomers.

Because of the availability of numerous possible donor sites, (**TCH**) are fascinating ligand systems. They usually function as a neutral ligand or negatively charged that links the metal through one imine nitrogen atom and the sulfur atom, this phenomenon is caused by a tautomeric equilibrium between the thioketo and thioenol forms. The kind of metal ion and its counterion, circumstances of reaction, solvent composition, and medium pH influence all this equilibrium. The inclusion of additional coordination sites on the side substituents might impact the selectivity and stoichiometry of metal ion binding.

These qualities can be used in a variety of biological applications, and the ability to accurately control chelate stability/properties by changing the substituents' coordinating residues might have significant implications. Only a few publications on TCHs biological activity are known, and they have only been studied for medical purposes occasionally in terms of their putative antiviral action against herpes via stimulation of HSV-1 ribonucleotide reductase inactivation.

The complexes of **TCH** have received significantly less attention than TSCHs complexes for metal complex synthesis with uses of anticancer, antibacterial, or antifungal. This is remarkable given the striking parallels between these two types of ligands, both of which may couple metal centers in a multidentate manner. Few **TCH**-based metal compounds with Fe(III), Cr(III), Mn(II), Ni(II), Co(II), Cu(II), or Zn(II) centers, for example, have been evaluated for their activity from strains of bacterial, fungal infections or cancer.[68]

## 1.3. Synthesis of Cinnamic Acid and its derivatives

### 1.3.1. Perkin reaction

A Perkin reaction is an organic chemical reaction method used to synthesize cinnamic acid and its derivatives, the reaction was named after William Henry Perkin and developed in the 19th century. In this procedure, an aromatic aldehyde, and acid anhydride are condensed in the presence of an alkali salt of the acid [Sodium acetate], which serves as a base catalyst and produces, *α, β*-unsaturated aromatic acid which is an example of an aldol condensation. Otherwise, the Perkin reaction cannot be used with a simple aliphatic aldehyde or aromatic ketones.[11,69]

The most common method to synthesize cinnamic acid and its analogues is using benzaldehyde in acetic anhydride and anhydrous sodium acetate as shown in Scheme 1. The reaction disadvantage is unwanted side products formation as a result of aldehydes in the presence of a base.[70]

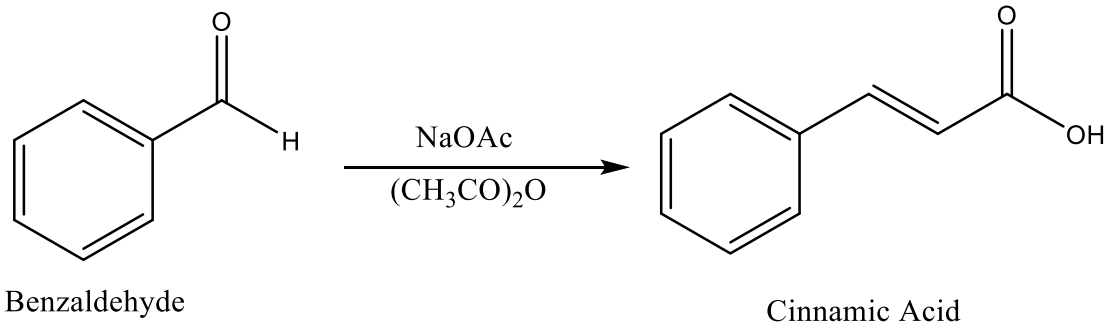


Scheme 1. Synthesis of cinnamic acid by Perkin reaction using benzaldehyde in acetic anhydride and anhydrous sodium acetate.

As shown in Scheme 2, Cinnamic acid was also synthesized via Perkin reaction using deep eutectic solvent (DES), which convert Benzaldehyde into cinnamic acid in the presence of acetic anhydride and biodegradable DES based on choline chloride and urea at 30±2°C in 4 hours with yield 92%.[69,71]

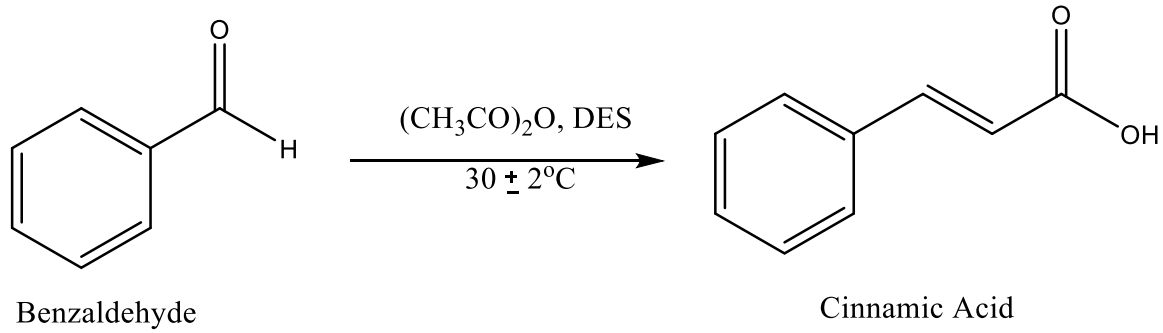


Scheme 2. Synthesis of cinnamic acid by Perkin reaction using DES.

### 1.3.2. Microwave irradiation methods (Knoevenagel condensation)

In a solvent-free environment, analogues of Cinnamic acid are produced by microwave irradiation of aryl aldehydes and malonic acid using polyphosphate ester (PPE) as a catalyst as shown in (Scheme 3) which is considered as a suitable method of synthesizing of cinnamic acid, as it avoids the drawbacks of the Perkin reaction. On the other hand, the main disadvantage of this method is the long reaction time.[7,70]

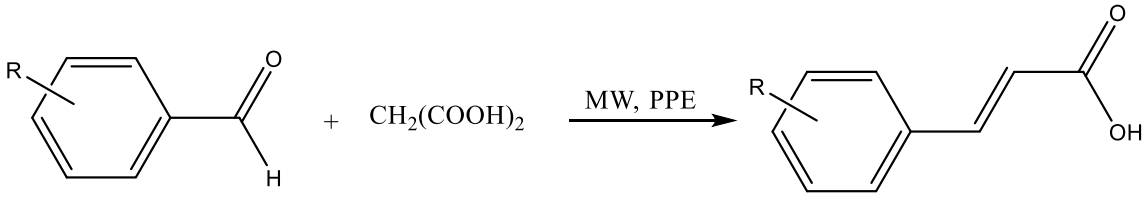


R = 4-Br, 3, 4$(OMe)_2$, 4-OH, 4-$NO_2$, 2, 5$(OMe)_2$, OMe, 4-Me, 3-Cl, H.

Scheme 3. Synthesis of cinnamic acid derivatives by microwave irradiation methods (Knoevenagel condensation).

Cinnamic acids are produced when ketones or aromatic aldehydes and malonic acid are microwaves irradiated in the presence of tetra butylammonium bromide (TBAB) and $K_2CO_3$ as shown in Scheme 4.[7,69,70]

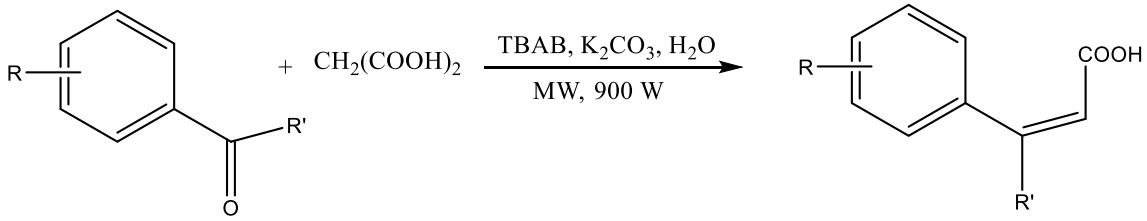


R/R'=H/H, 4-O $CH_3$/H, 4-$NO_2$/H, 3- Br/H, 2,4-Cl/H, 4-OH/H, H/ $CH_3$, 4-Br/ $CH_3$, 4-$NO_2$/ $CH_3$

Scheme 4. Synthesis of cinnamic acids by ketones or Aromatic aldehydes and malonic acid.

### 1.3.3. Enzymatic method

The enzymatic method was carried out as described by *Lee et al*. 2006 in presence of Novozym 435 as a catalyst, successfully synthesized ethyl ferulate from 4-hydroxy 3-methoxy cinnamic acid (Ferulic acid) and ethanol, as well as, octyl methoxycinnamate from p-methoxycinnamic acid and 2-ethyl hexanol which is shown in Figure 5. This reaction method is more useful than other methods reported because it achieves the highest rate of yield and allows the enzyme to be used again without considerable loss of activity.[7,70,72]

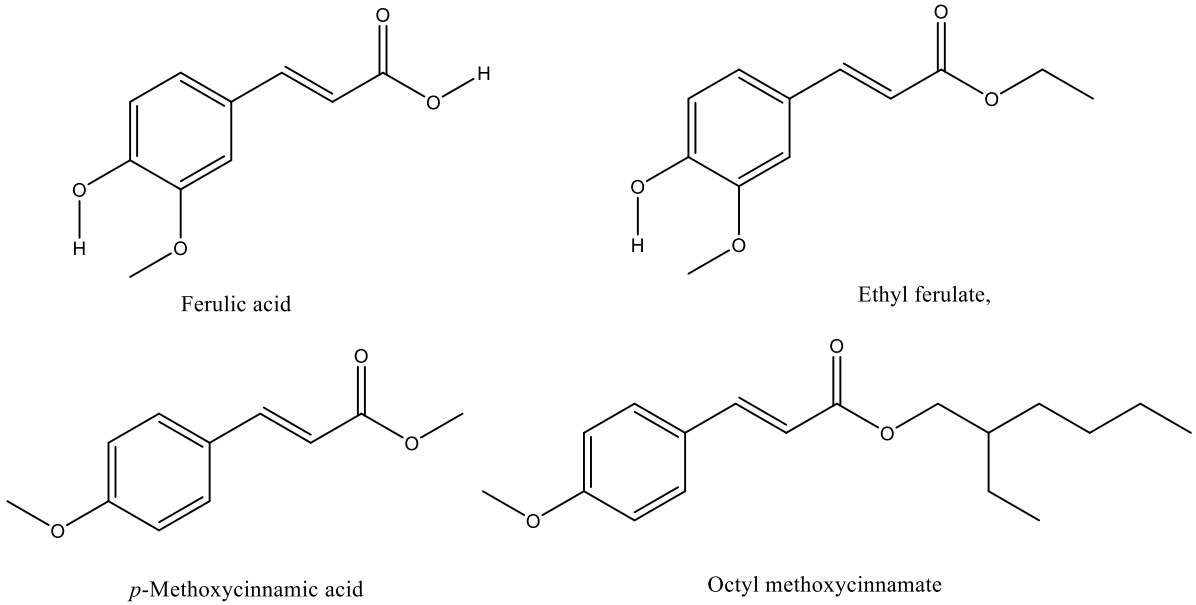


Figure 5. Molecular structure of reactants and products compounds.

### 1.3.4. By using Heck coupling reaction

The Heck coupling reaction occurs when aryl halide is coupled with an alkene in the use of a base and palladium as a catalyst. Under different circumstances, this procedure is also utilized to produce cinnamic acid utilizing iodobenzene and methyl acrylate as reactants in the presence of palladium as a catalyst.[69]

#### 1.3.4.1. Using palladium on charcoal as a catalyst

Methyl esters of cinnamic acid were synthesized under ultrasonic conditions from iodobenzene and methyl acrylatecatalyst Pd/C and N-methyl pyrolidine (NMP) as a solvent.[7,69] the reaction synthesis is shown in Scheme 5.

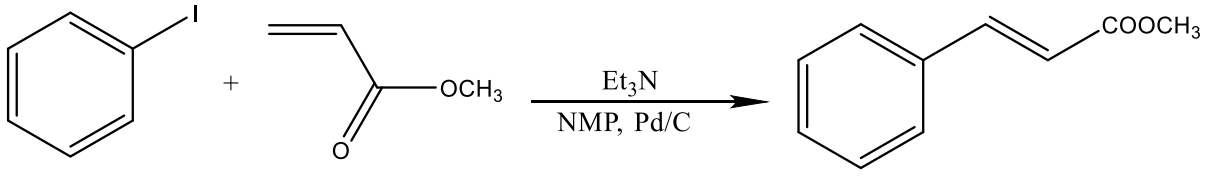


Iodobenzene Methyl acrylate Methyl ester of cinnamic acid

Scheme 5. Synthesis of methyl ester of cinnamic acid using palladium on charcoal as a catalyst.

#### 1.3.4.2. Using palladium chloride as a catalyst

Cinnamic acid esters were synthesized from various aryl halides in presence of $PdCl_2$ as a catalyst under ultrasonic conditions (where X = COOMe) as showed in Scheme 6. TBAB (tetra butyl ammonium bromide) serves as a phase transport catalyst, whereas $Na_2CO_3$ serves as a base. Commercially, this reaction is particularly beneficial because it was carried out at room temperature, water was used as a solvent under ultrasonic conditions.[7,69,73]

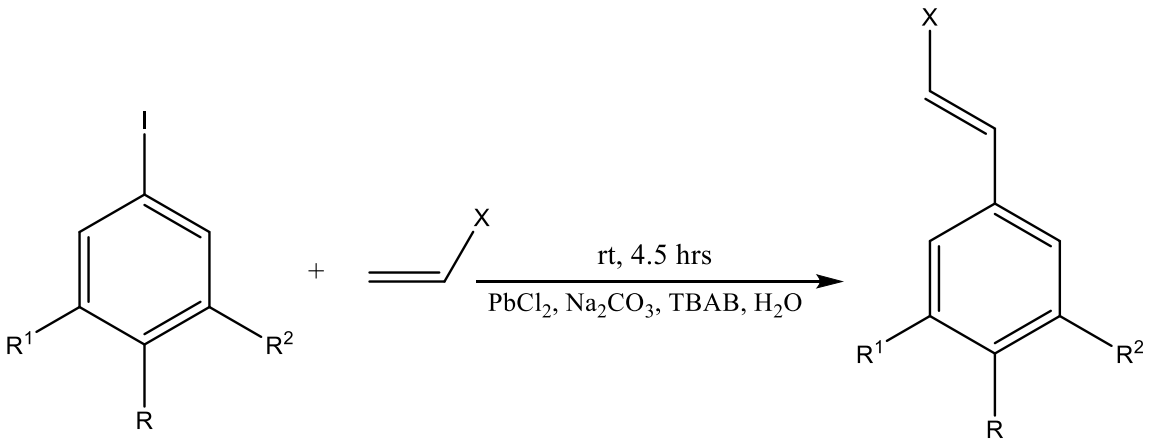


Yield = 43-93%

R= H, OMe, Cl, Br, NHCOMe, or $NO_2$

$R^1$= I, CHO, H

$R^2$= I or H

X= $CO_2$Me, COOH, CN, or Ph

Scheme 6. Synthesis of cinnamic acid derivatives using palladium chloride as a catalyst

### 1.3.4.3. Using Diatomite-Supported Pd Nanoparticles

Solid supported palladium, nickel, gold, and other metals have an important role in the creation of C-C bonds. The method shown in Scheme 7 was used to prepare diatomite-supported palladium nanoparticles.

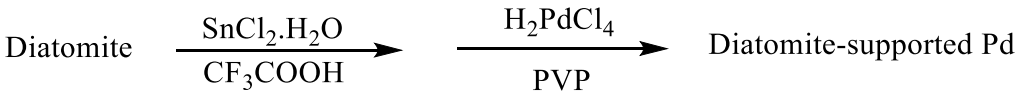


Scheme 7 Preparing method of Diatomite-supported palladium nanoparticles

Pd-nanoparticles prepared in Scheme 7 were used in the reaction of aryl halides and methyl acrylate to produce cinnamic acid and its derivatives in good yield, where NMP (*N*-Methyl -2-pyrrolidone) was used as a solvent and triethylamine was used as a base as shown in Scheme 8.[69,74,75]

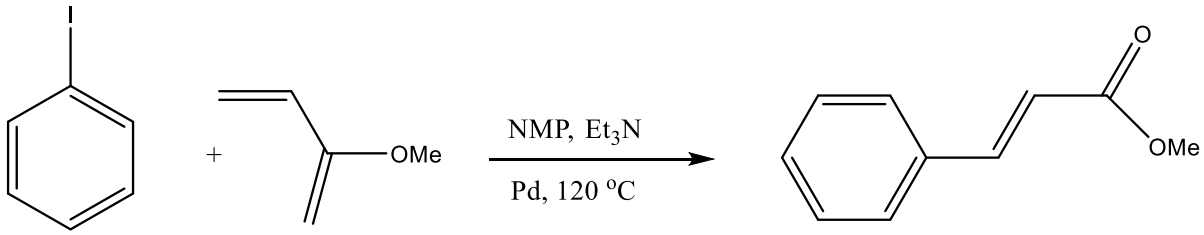


Scheme 8. Synthesis of cinnamic acid derivatives using Diatomite-Supported Pd Nanoparticles

### 1.3.4.4. Claisen–Schmidt Condensations

A different of (*E*)-cinnamic acid derivatives are produced in good yields using Claisen–Schmidt condensation as shown in Scheme 9. Claisen-Schmidt condensation reaction Scheme 9, the reaction was in the presence of sodium metal and a catalytic amount of methanol with toluene employed as the co-solvent.[11,70,76]

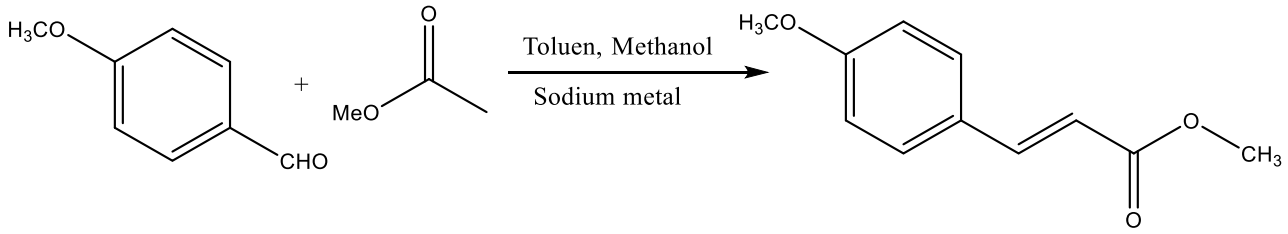


Scheme 9. Claisen-Schmidt condensation reaction.

## 1.4. Synthesis of thiocarbohydrazones and its derivatives

N-heteroaromatic TCHs are generally obtained by a simple condensation reaction of (DHS) with N-heteroaromatic aldehydes and ketones. By controlling the ratio of mol (DHS) to the number of mol aldehydes or ketones in the flask to produce **m-TCHs** or **b-TCHs**. Scheme 10 is shown the synthesis of N-heteroaromatic TCHs as mentioned by *Bozic et al*.[27]

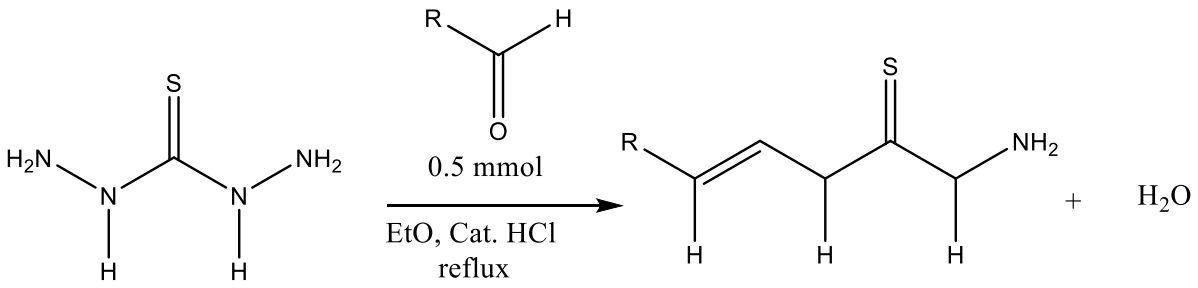


1 mmol

R= 8-quinolinyl, 2-quinolinyl, 8-hydroxy-2-quinolinyl

Scheme 10. Synthesis of N-heteroaromatic thiocarbohydrazones.

Moreover, TCHs derivatives were obtained by the condensation reaction of DHS and appropriate aldehyde, glacial acetic acid used as a catalyst as shown in Scheme 11.[77]

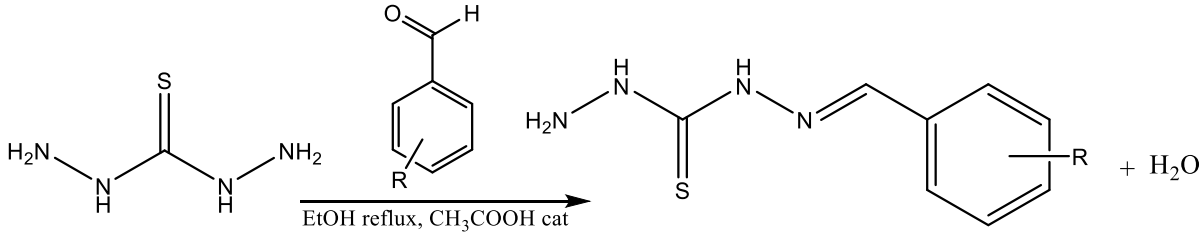


1.0 mmol

R= H, *o/m/p* -OH, *o/m/p* -$CH_3$, *o/m/p* -$NO_2$, *o/m/p* -$OCH_3$, *m/p* -Cl, *m/p* -Br, *p*-F

Scheme 11. Synthesis of TCHs derivatives.

### 1.5. Biological activity

Besides the naturally occurring cinnamic acid derivatives in plants,[78,79] because of a benzene ring and an acrylic acid group, it can be modified to produce synthetic cinnamic acid derivatives.[80] Cinnamic acid and its derivatives have become a source focus for researchers to improve and modify structure due to biological characteristics and its drug-like properties; the addition of effective phytochemical moieties has the ability to have additional or synergistic activity, allowing for the development of multi-effective new derivatives.[81] Cinnamic acids present various pharmacological activities including, antibacterial, neuroprotective, antioxidant, anticancer, anti-inflammatory, antifungal, antidiabetic activities and they have been estimated as multifunctional cholinesterase inhibitors against Alzheimer's disease.[78]

The nature and position of the substituent groups have been linked to the biological activity of several cinnamic acid derivatives. The lack of curative drugs with low reverse side effect profiles to control the growth of cancer, microbial, neurological diseases, and other conditions has prompted research into the development of medicinal molecules based on cinnamic acid and its derivative.[82]

Furthermore, nitrogen and sulfur compounds had a long history in analytical and medical chemistry for several years. A large number of heterocyclic nitrogen and sulfur compounds are of great interest to improve the biological activity of drugs. Significant pharmacological activities of TCHs and their derivatives are the cause of increasing interest in their transformations in order to increase activity.[68]

### 1.5.1. Antioxidant Activity

An antioxidant is defined as enough stable molecule to donate an electron to an exciting free radical and neutralize it, therefore, prevents, or removing the oxidation reactions of other molecules, which remove the intermediate free radicals to break the chain reaction before they interact with the cells.[83–85]

Antioxidants are classified according to defense lines:

- First-line of defense is the preventive antioxidant that prevent the creation of free radicals that resulted in oxidative stress through enzymes, such as catalase (CAT), superoxide dismutase (SOD), glutathione peroxidase (GPx), glutathione reductase, and other kinds of minerals, for example, iron (Fe), manganese (Mn), selenium (Se) and copper (Cu).
- The second-line of defense is a radical-scavenging antioxidant that prevents the production of damage; the most potent scavengers of free radicals are vitamins C and E, uric acid, and flavonoids.
- The third-line of defense is repair and de-novo enzymes that serve to repair damage caused by free radicals on cellular biomolecules such as DNAs, peroxides, oxidized lipids, and proteins to restore cellular functions, besides inhibiting the spread reaction of chain in peroxyl lipid radicals.[86,87]

Free radicals are highly reactive chemical entities (molecules, atoms, or ions) that occur naturally in the human body. Free radicals are neutralized in the body by natural cellular processes or by eating foods. However, oxidative stress might arise if the body is unable to protect itself against the detrimental effects of these reactive species. In modern medicine, finding novel antioxidants is a difficult task. The chemical reaction of free radicals stems from the inclination to couple unpaired electrons at the final energy level of the atom. In most situations, this process is followed by the disturbance of other molecules' stability, and the commencement of uncontrollable chain reactions[88] which lead to the removal of the organism from balance, the appearance of various diseases, both acute and chronic.[89] The fact that free radicals target cell membranes and damage their genetic material which leads to the most harm and caused diseases such as neurological disorders (Parkinson's disease, cerebrovascular damage, Alzheimer's disease, and muscular dystrophy), inflammatory processes (vasculitis and rheumatoid arthritis), cardiovascular disorders (atherosclerosis, hypertension and hypertensive heart disease), respiratory diseases (asthma), various cancers (breast, colorectal, lung, prostate, bladder cancers). fibrosis, pulmonary, cataracts, and pulmonary, depending on the element that is composed of them.[90,91]

Generally, pro-oxidants/oxidants are termed as Reactive Oxygen Species (ROS)/ Reactive Nitrogen Species (RNS). ROS are the most common free radicals generated during reactions. both ROS and RNS are from endogenous sources derivatives such as (endoplasmic reticulum, peroxisomes, mitochondria, phagocytic cells, etc.), also from exogenous sources such as (tobacco, alcohol, smoke, transition metals, heavy metals, pollution, pesticides, industrial solvents, certain drugs like radiation, paracetamol, and halothane). Free radicals may harm a variety of important biological components; such as nucleic acids, proteins, and lipids, disrupting the usual redox balance and causing increased oxidative stress.[90,92]

Reactive Oxygen Species (ROS) which formed from oxygen radicals such as superoxide anion ($O_2^{\bullet-}$), hydroperoxide radical ($HOO^{\bullet}$), hydroxide radical ($HO^{\bullet}$), peroxyl ($RO_2^{\bullet}$), alkoxyl ($RO^{\bullet}$), nitrogen (II) oxide ($NO^{\bullet}$), nitrogen(IV) oxide ($NO2^{\bullet}$) as well as, non-radical compounds like hypochlorous acid (HOCl), hydrogen peroxide ($H_2O_2$), also ozone molecules ($O_3$), etc. which can easily make the ability to react the free radical with a living organism.[92,93]

Reactive Nitrogen Species (RNS) include various species of compounds having a variety of properties. The only matter for belonging to these radicals group is that they are derived from nitric oxide compounds. The most known RNS radical (peroxy-nitrite, $ONOO^-$) is created when $NO^{\bullet}$ radicals react with superoxide $O_2^{\bullet-}$, which results in oxidation, nitroso compound production, or nitration.[94]

Reactive Sulfur Species (RSS) are easily produced from the reaction of thiols with ROS.[95] The most popular kind of ROS is the superoxide radical that is created through breath in the mitochondria during the transfer of electrons from the substrate to oxygen. Another significant radical is the hydroxyl radical, which is formed in biological systems by ionic radiation that causes water molecules to decompose or alkyl hydroperoxide to photolytically decompose.[96]

In the biological system, antioxidants serve to neutralize free radicals by balancing the stability of unpaired electrons and neutralizing the potentially damaging impact of free radicals while leaving more stable radical/radical cationic kinds of antioxidants. Their major antiradical activity is reflected in the release of electrons and their transformation to the radical types.[96] They can make a role as inhibitors of oxidative reactions, which involve free radicals and deactivate the chain reactions of auto-oxidation of the substrate, by solidarity with other antioxidants such as metal ions and chelators of metal ions or by transforming redox-active pro-oxidants (copper and iron derivatives) to other products with more stability, for instance, inhibitors of pro-oxidative enzymes (eg lipoxygenase).[97]

Oxidative stress is caused by a lack of antioxidants or antioxidant enzymes in the body, which can cause cell damage. This has been related to aging as well as a variety of diseases like atherosclerosis, cancer and, diabetes.[89,98] Antioxidants are classified as enzymatic or non-enzymatic based on their method of action. Superoxide dismutase, catalase, and glutathione peroxidase are the most essential enzymatic antioxidants. The processes of converting the superoxide radical through hydrogen peroxide to water are catalyzed by this set of enzymes, moreover, non-enzymatic antioxidants like vitamin E, Vitamin C, glutathione, polyphenols, carotenoids, and others. Within this category of antioxidants, natural and synthetic origins were differentiated. Although the safety of synthetic antioxidants in comparison to natural antioxidants is frequently, debated, natural antioxidants' structures are being altered to increase their efficacy, resulting in molecules that are more active. They are widely applied to extend the shelf life of food, and their main target is to prevent fatty acid oxidation.[96]

### 1.5.2. Determination of the antioxidant mechanism

The understanding mechanism of the antioxidant action is the most important requirement to develop the design to obtain compounds with more biological activity. Free radical scavenging is the most significant antioxidant activity mechanism of compounds. Reactive free radicals follow through three mechanisms to accept hydrogen atoms from antioxidants such as hydrogen atom transfer (HAT), electron transfer followed by proton transfer (SET-PT), and Sequential Proton Loss Electron Transfer (SPLET). Another major antioxidant mechanism is the chelation of $Fe^{2+}$ ions, which reduces the oxidative damage caused by hydroxyl radicals and inhibits the Fenton reaction.[99,100]

#### Modeling of antioxidant mechanisms

In the HAT, the antioxidant compound (M–H) transfers hydrogen atom ($H^{\cdot}$) to reactive radical species ($R^{\cdot}$) via homolytic cleavage of a single bond:

$$M–H + R^{\cdot} \longrightarrow M^{\cdot} + R–H \qquad (1)$$

This process forms a new radical species ($M^{\cdot}$), which is, in the case of good antioxidant compounds, highly stabilized via electronic and resonance effects that diminish its reactivity. The HAT potency of a molecule can be quantified via bond dissociation enthalpy (BDE), which can be determined according to the equation below:

$$BDE = H(H^{\cdot}) + H(M^{\cdot}) – H(M–H) \qquad (2)$$

In equation 2, $H(H^{\cdot})$, $H(M^{\cdot})$ and $H$(M–H) denote the enthalpies of H atom, radical derived from the antioxidant compound, and parent compound, respectively. Potent antioxidants have low BDE values. HAT mechanism is the most common and most widely studied mechanism of antioxidant activities in natural and synthetic antioxidants.

In the single electron transfer (SET) mechanism, antioxidants neutralize R· by electron transfer, forming a closed-shell anion R– which is more stable than parent free radical. Simultaneously, antioxidant converts to radical-cation, which is stabilized by electronic and resonance effects (equation 3).

$$M–H + R^{\cdot} \longrightarrow M–H^{\cdot+} + R^{-} \quad (3)$$

This process is usually accompanied by proton-transfer from the radical cation.

The stabilization of reactive radical species through SET mechanism can be quantified by computing the ionization potential (IP) of a molecule:

$$IP = H(M–H^{\cdot+}) + H(e^{-}) – H(M–H) \quad (4)$$

where $H(M–H^{\cdot+})$ is the enthalpy of radical-cation, and $H(e^{-})$ is the enthalpy of an electron.[101] In general, antioxidants with pronounced SET mechanisms have low IP values that indicate good stability of a radical-cation formed.

(SPLET) is the third common mechanism on how antioxidants scavenge reactive free radicals. This three-step mechanism starts with the dissociation of a proton (equation 5) followed by the transfer of an electron from anion to reactive free radical (equation 6), and neutralization of anion (Equation 7).

$$M–H \longrightarrow M^{-} + H^{+} \quad (5)$$
$$M^{-} + R^{\cdot} \longrightarrow M^{\cdot} + R^{-} \quad (6)$$
$$R^{-} + H^{+} \longrightarrow RH \quad (7)$$

SPLET mechanism can be characterized by proton affinity (PA) calculations, which is the first step of this process (equation 8).

$$PA = H(H^{+}) + H(M^{-}) – H(M–H) \quad (8)$$

The outcome of all three mechanisms (HAT, SET, and SPLET) is the transfer of one H atom from a radical scavenger to a reactive free radical. Quantum chemical calculations, particularly DFT, are very useful for studying these mechanisms and rational design of more potent analogs

**Methods for determining antioxidant activity**

The most common methods used for the examination of antioxidant activity are based on colorimetric measurements. Whereas the mechanism of action is based on the ability to neutralize various kinds of free radicals. The time of reaction and period changes from one method to the other, the modification linked to kind and sample complexity for the antioxidant potential examination as appropriate.[102] The most common in vitro methods used are free radical methods such as $DPPH^{\bullet}$ (2,2-diphenyl-1-picrylhydrazyl), $ABTS^{\bullet+}$ (2,2'-Azino-bis(3-ethylbenzothiazoline-6-sulfonic acid)) and ORAC (Oxygen Radical Absorbance Capacity). In addition, reduction methods such as CUPRAC (Cupric Reducing Antioxidant Capacity), FRAP (Ferric Reduction Antioxidant Power) and TAC (Total Antioxidant Capacity. The methods, used in this dissertation to determine the antioxidant activity of tested compounds, are $DPPH^{\bullet}$, $ABTS^{\bullet+}$, CUPRAC, and TAC. The $DPPH^{\bullet}$ method for evaluating antioxidant activity allows the determination of the pure substance capacity or national product extracts to neutralize an unpaired electron on a hydrogen atom ($DPPH^{\bullet}$) by creating less reactive species. $DPPH^{\bullet}$ is a stable chromogen radical, commercially available with a dark purple color of long-lived organic nitrogen radical. The $DPPH^{\bullet}$ assay is based on the electron donation of antioxidants to neutralize $DPPH^{\bullet}$

radicals. When the tested antioxidant is combined with DPPH$^{\bullet}$ solution, the color changes from dark purple to yellow, which matches the color of hydrazine. This change is measured spectrophotometrically in the wavelength of 515 to 528 nm, and the change of color acts as a signal of the antioxidant efficacy. The inhibitory concentration given in % or $IC_{50}$ value in mM is a quantitative measure of antioxidant activity as determined by the DPPH$^{\bullet}$ method.[103,104] The DPPH$^{\bullet}$ radical is sensitive to light and limited the utilize of reagents to examine the activity of hydrophilic antioxidants because it is dissolved in organic solvents. The ABTS$^{\bullet+}$ method depends on the oxidation of the radical cation (ABTS$^{\bullet+}$) with potassium persulfate. Before starting the assay, the mixture was allowed to stay in a dark place for 12-16 hours at room temperature, a complex chromophore formed blue/green, which shows the reached absorption at 734 nm. The formed ABTS$^{\bullet+}$ in reacting with the examined antioxidant accepts a proton and/or electron from the antioxidant, and changes the blue/green solution to the colorless, which leads to reduced absorbance, this reduction is proportionate to the antioxidant capacity of the examined antioxidant and is used as the inhibitory concentration expressed in% or $IC_{50}$ value expressed in mM as in DPPH$^{\bullet}$.[104,105] The CUPRAC procedure involves the use of copper(II) ions with 2,9-dimethyl-1,10-phenanthroline (neocuproin, NC, eng. Neocuproine) this is lead to a colorless oxidizing reagent which is a complex of copper(II)-neocuproin (Cu(II)-Nc) cation. The reaction of Cu (II)-Nc complex in the oxide reduction with the examined compounds is reduced to copper (I) neocuproin (Cu(I)-Nc), which shows absorption maximum in the wavelength at 450 nm. The reaction condition is performed at pH=7. As result, the color of the mixture solution changes from light blue (Cu(II)-Nc cation) to orange-yellow (Cu(I)-Nc cation). The increasing absorbance of the reaction mixtures in this method indicates an increase in antioxidant capacity. The TAC method is a spectroscopic procedure used for the quantitative determination of antioxidant capacity. The determination is in an acid medium which is the reduction of Mo (VI) to Mo (V) and the following formation of a green phosphomolybdenum complex.[106]

In the past few years, research has increased on applications of cinnamic acids and their antioxidant especially those combining the cinnamoyl moiety with phenolic hydroxyl groups, which exhibit powerful free radical scavenging properties. However, the identification of vitamins A, C, and E as antioxidants gave rise to the realization of the importance of antioxidants in the biochemistry of living organisms.[74,85,107,108] Several studies have been conducted over the past years to determine activities of thiocarbohydrazones derivatives, which showed various biological activities including antioxidant activity.[19,109]

According to a study reported by *Sultan et al.*[110] A group of cinnamic amides compounds were tested as shown in Figure 6. Cinnamic amides with 3,4-dihydroxyphenyl groups including compound (2) (81.88% inhibition), and compound (5) (84.55% inhibition). Likewise, compounds with a 4-hydroxy-3-methoxyphenyl group including cinnamic amides such as compound (3) (82.58% inhibition), and compound (6) (78.94% inhibition), showed high DPPH$^{\bullet}$ scavenging activities compared to L-ascorbic acid with inhibition 84.64% which was used as a positive control. Furthermore, cinnamic amides with the 4-hydroxy group were sensitive to their amino moiety and showed extremely weak to strong DPPH$^{\bullet}$ radical scavenging activity of compound (1) (16.55% inhibition) and compound (4) (3.87% inhibition) *vs.* compound (7) (81.57% inhibition) according to their structure.

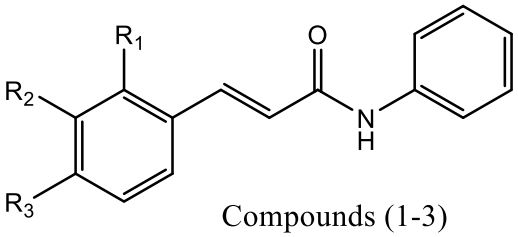


Compounds (1-3)

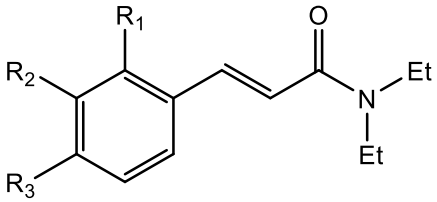


Compounds (4-6)

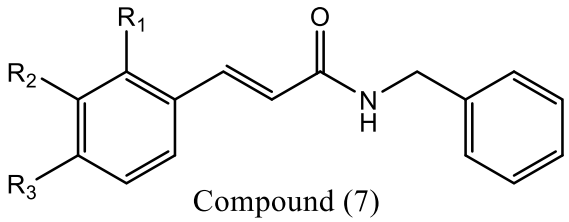


Compound (7)

| Comp | $R_1$ | $R_2$ | $R_3$ |
|---|---|---|---|
| 1 | H | H | OH |
| 2 | H | OH | OH |
| 3 | H | Me | OH |
| 4 | H | H | OH |
| 5 | H | OH | OH |
| 6 | H | Me | OH |
| 7 | H | H | OH |

Figure 6. Radical scavenging activities were determined of cinnamic amides to DPPH•.

*Pal Chinmay et al*. Reported that compound N-(4-fluorophenyl) cinnamamide which were examined have shown a good DPPH• free radical scavenging activity, which inhibited 79% DPPH• scavenging activity at a concentration of 100 μM.[111]

### 1.5.3. Antimicrobial activity

The resistance of microorganisms to antibiotics that have long been used to prevent and treat infectious diseases has recently become an increasing issue and in the danger of losing their efficacy because of the increase in microbial resistance.[112] The strategy of the pharmaceutical industry is reflected in changes to the molecular structure of existing antibiotics in order to improve their activity. This leads to improving new synthesis and testing of antimicrobial substances that will have a sufficiently wide spectrum of action, will not cause resistance, and will have a low probability of causing side effects. Due to the specificity of the structure of bacteria, there are several antibacterial targets, and the most successful agents work on bacterial cell wall construction, protein synthesis, or DNA transcription.[113–116]

Different qualitative and quantitative standardized methods are used to identify the antimicrobial activity of an extract of pure compounds; the most popular testing methods include rapidly automated or both microdilution instrument methods which are commercially available equipment and materials, manual methods that can save money and more flexibility such as disk diffusion and gradient diffusion methods. There are weaknesses and strengths in each method including the accurate method testing that is used to test the organisms. All methods provide qualitatively standardized using the intermediate, resistant or categories susceptible, and some other methods give quantitative results such as minimum inhibitory concentration. In general, recently testing methods determine accurate resistance exams of popular antimicrobial mechanisms.[117–119]

Complex organic structures containing heterocyclic moiety with nitrogen atoms are very important in actual medical chemistry, also representing a good basis for designing and developing new drugs.[120,121] Among different biological activities, it should be highlighted its antimicrobial activity due to a large number of drugs used in everyday practice. Since many bacterial strains have become resistant to antibiotics, it has become a major problem in recent decades. To solve this very complicated situation, the pharmaceutical industry is trying to make changes in the molecular structure of existing antibiotics in order to improve the product's overall efficiency. Therefore, it is necessary to test new antimicrobial substances that will have a sufficiently wide range of applications and effects, and which will not cause side effects in patients. Bacterial cells have a very specific structure because they have several antibacterial targets. The most successful agents act on the

construction of the bacterial cell wall, protein synthesis or replication of deoxyribonucleic acid (DNA) molecules, as well as the transcription of DNA molecules.[120] Activity parameters that determine the susceptibility of bacteria and fungi to existing antimicrobial drugs are Minimal Inhibitory Concentration (MIC) and Minimal Bactericidal Concentration (MBC). MIC is the lowest concentration of antimicrobial agent that inhibits visible growth of microorganisms, while MBC is the lowest concentration that prevents the growth of ≥ 99.9% of microorganisms after subculture of the initial infectious dose in medium without test agent. The antimicrobial activity of the compounds can also be assessed on the basis of the diameter of the inhibition zone if the test is performed by diffusion methods. If the broth is cloudy after the test, the effect of the substance is microbiostatic, and if the broth is clear, the substance has a microbicidal effect.

Cinnamic acids derivatives especially those presence esters and amides groups are the most privileged structural scaffolds in drug discovery and exert various biological effects. Moreover, they are famed for antimicrobial activity, therefore, researchers are looking for increasing the effect of antimicrobial agents more than currently used standard drugs.[122] Several studies for cinnamic acid derivatives have reported significant antifungal, antiviral, and antibacterial activity. Narasimhan and co-workers have reported the antifungal activity against *Aspergillus niger* and *Candida albicans* and antibacterial activity against *Staphylococcus aureus* and *Escherichia coli*, *Bacillus subtilis* (Gram-positive, Gram-negative, respectively). In addition, the authors noted that the presence of halogens in the side chain leads to an increase in the growth inhibitory effect of cinnamic acid whereas the addition of hydroxy groups to the side chain double bond did not enhance the antimicrobial activity.[123,124]

Furthermore, nitrogen-based heterocyclic analogs compounds and **TCH** have a significant role in pharmacology and agriculture which are unique classes among the applied branches of organic chemistry,[125] which have the ability to react with many fundamental metalloenzymes for microbes, whereas the presence of a sulfur atom increase lipophilicity, mostly positively correlated with potency.[126] In recent years, nitrogen and sulfur ligands became one of the main subjects in coordination chemistry,[68] some researchers indicate that the presence of nitrogen and sulfur in the structure give rise to an increase in the antimicrobial activity of the compound, Nitrogen atoms create hydrogen bonds with target proteins, whereas sulfur atoms increase the lipophilicity of compounds. Thus, the permeability of the cell membrane increase where a higher concentration of compound reaches the target.[126,127]

Cinnamic acid derivatives exhibit inhibitory activity against several Gram-negative and Gram-positive bacteria.[3] Several cinnamic acid derivatives (amides, thioesters, and hydrazides) exhibit favorable antimycobacterial activity.[128–131] Cinnamates have been reported to have HIV-1 integrase inhibiting action[132]. Cinnamates and cinnamamides have been shown to exhibit antifungal activities in vitro as well as antiviral activity against viruses from several taxonomic families.[132]

Antibacterial activity of several structures related to cinnamic acid and their derivatives against *B. subtilis* and *E. coli* was studied by Tonari and coworkers, which exhibited that compounds with a substituted phenyl group in ester are more active against *B. subtilis* and *E. colihe*.[132]

#### 1.5.3.1. Methods for determining antimicrobial activity

##### 1.5.3.1.1. Assessment of antibacterial activity

To determine the antibacterial activity of studied compounds, different standardized qualitative and quantitative methods are applicable: diffusion, dilution[133] and combined methods,[134] as well as highly sensitive automated systems (e.g. VITEK 2 system) based on reactions of microorganisms with substrates used for biochemical detection based on their characteristics change. This method is performed by measuring fluorescence at short intervals during incubation with specific reagents.[135] It is possible to test the sensitivity of bacteria to a certain substance by diffusion methods, but only from a qualitative aspect. Unlike diffusion methods, dilution methods are quantitative, because they can be used to determine the minimum inhibition concentration, i.e. MIC, of tested samples.

#### 1.5.3.1.2. Assessment of antimycobacterial activity

MTT assay is a commonly used colorimetric technique for the estimation of eucaryotic and procaryotic cells viability and proliferation in the population of interest. The principle of the assay relates to the reduction of a yellow tetrazolium salt into formazan crystals by mitochondrial NAD(P)H-dependent oxidoreductase enzymes in living cells.[136] The insoluble formazan crystals are further dissolved using either isopropyl alcohol, sodium dodecyl sulfate, or dimethylsulfoxide and optical density is measured at 520-600 nm using a spectrophotometer. Measured absorbance is proportional to the number of viable, metabolically active cells.

### 1.5.3.2. Application of TCH and Cinnamic acid derivatives as antimicrobial agents

An interesting and attractive class of organic compounds are derivatives that contain cinnamic acid as a structural framework, as they are evidenced as antitumor, anti-inflammatory, antimicrobial, and immunostimulatory agents.[36,123] Due to this use of such building block, it could contribute to the synthesis and development of newly potent antimicrobial agents, and among them cinnamides are the most interesting, where a wide variety of amino terminated compounds, e.g. **m-TCHs**, could react with cinnamic acid or its substituted analogs.[137]

Up to now, no study was published which relates to synthesis of cinnamamide from acid and (**m-TCH**). **m-TCH** are a versatile group of organic compounds which possess a broad range of biological activity, as well as antimycobacterial and antiviral activity.[15,19,25,26,138,139]

A detailed study on antimicrobial activity of twenty two TCH was recently presented.[126] It was shown that studied **m-TCH** and **b-TCH** are valuable pharmacophores useful for the development of new antibiotics which are in line with increased microbial resistance. Studied compounds showed activity against Gram-positive, Gram-negative and fungal strains similar to amikacin and nystatin. Also, results from an alignment of independent 3D QSAR models showed that improvement of activity, with respect to *S. aureus*, could be achieved by a change of methyl with trifluoromethyl group which should contribute to hydrophobicity and the HBA effect increase, as suggested by the model used. on the other hand, the replacement of hydroxyl with methoxy group will decrease the effect of unfavorable hydrogen bonding interactions to increase TCH potency.[126]

Also, a series of **$TCH_{2ap}$** were synthesized and tested as inactivators of iron-dependant enzyme herpes simplex virus (HSV-1) ribonucleotide reductase[16] with better results than the analogous 2-acetylpyridine thiosemicarbazone derivatives. They were also tested for spectrophotometric determination of mercury(II),[140] antimicrobial and mutagenic[141,142] and antioxidant activity.[106,142],,

Therefore, it would be of high interest to conduct a study on the synthesis of cinnamides, which include both **m-CTH** and cinnamic acid pharmacophores to be tested for their biological activity.

## 1.6. Density functional theory (DFT)

Over the years, a DFT model has been developed with the intention to provide a rule to understand and rationalize the geometry and properties of molecules. In the mid-1960s, Kon and Sham[143] published a paper presenting DFT as the most successful method for calculating the electronic structure of compounds.

Nowadays, the DFT is successfully applied to the study of atoms, molecules, solids, liquids, complexes, intermolecular interactions, excited and transient states, mechanisms of chemical reactions, NMR, FTIR and UV spectra, etc. The DFT method offers satisfactory accuracy of the obtained results at a reasonable computing time, which depends on the complexity of the problem under consideration.

The main variable of quantum mechanics (QM) is the wavefunction. It is a mathematical descriptor of a quantum state of an isolated system and provides all necessary data on

“micro(quantum)-objects“. The wavefunction defines the probability of the existence of a particle, e.g. electron, within the defined volume element. In general, the probability of the existence in a certain volume is the “electron density, ρ”. As the electron density and wavefunction are closely related, this method is based on the electron density function (ρ(x, y, z)).[144,145]

The DFT is nowadays the most applicable approach with high success in describing the electronic structure of matter. With the help of DFT, different properties of atoms, molecules, complexes, ions, materials, etc. can be determined very accurately. These properties include, but are not limited to, elements of geometry, magnetic properties, atomization and ionization energy, electrostatic potential, electron affinity, hardness/softness, global electrophilicity index, vibrational frequencies, proton accepting/donating capabilities etc. Some of molecular properties could be graphically presented:
“molecular electrostatic potential maps, local ionization potential maps and LUMO maps”,
which are useful for the visualization of the differences in chemical reactivity.

### 1.6.1. Fundamental aspect

The basics of DFT mathematics are functional. A functional is a function of a function and is denoted as follows

$$y= f(x) \qquad (9)$$

where, the dependent variable (y) depends on one or more single variables.
To understand the DFT theory it is important to introduce the functional denoted as follows

$$y=F[f(x)] \qquad (10)$$

"where the value of y is intrinsically dependent on another function. The first f(x) function becomes the input for the functional, that is, a function of a function. Electron density, ρ(r), is the most important parameter, while the energy of a molecule is a function of the electron density."[146]

Electron density can be determined experimentally by using X-ray or electron diffraction, and the result is a function of only three variables (x, y, z-axis where the variable denotes position of electron) which are not dependent on the dimensions and number of electrons in the molecule. Oppositely, the wavefunction depends on the number of electrons and is a function of 4n-variables, where n is the number of electrons. Therefore, the electron density as a measurable parameter is advantageous over the wavefunction due to better and clearer results obtained by mathematical calculations.[144,145]

The wavefunction is the solution of a well-known *Schrödinger equation* (SE), and it describes all properties of “micro(quantum)-“ objects. The non-relativistic time-independent SE could be presented in the form:

$$\hat{H}\psi = E\psi$$

"where $\hat{H}$ designates the *Hamiltonian.* Hamiltonian is the *operator* of the energy and contains mathematical forms and rules that should be “performed” on the wave function in order to get the energy of the system. Hamiltonian includes potential and kinetic energy terms." [147]

Quantum chemical calculation aims are to provide an accurate description of the electronic structure, physical and chemical properties of molecules. Hamiltonian could be defined for any system but could be explicitly solved only for the most simple, one electron systems. SE does not offer a unique solution, where any solution is given by a discrete value of energy (quantum). The lowest energy solution is called the ground state and other solutions are known as excited states.

The DFT calculation is directed to finding the value of the functional F, and always includes several approximations to make the computations feasible. As a result of a huge number of possible

approximations, a plethora of DFT methods are in use nowadays. The time necessary for appropriate calculation is dependent on the size of the molecule and the limitations introduced by the method applied. For the achievement of greater accuracy, longer computational times are required.

Proper selection of the function as well as additional calculations, by the inclusion of the solvation effect, basis set, and functional adjustment/selection, or application of zero point energy corrections can improve the quality of the obtained results. The main drawbacks,[148] of the DFT method are: self-interaction error,[149] medium to long range correlation errors[150] and the tendency to ignore the effects of dispersion forces.[151] The electron density is related to the wavefunction *via* the equation.

$$\rho(\mathbf{r})=\sum_{i=1}^{n} n|\Psi_i|^2 \tag{11}$$

The DFT method is based on two theorems, given by Hoenberg and Kohn[152]:

*"-The ground-state energy from Schrödinger's equation is a unique functional of the electron density, and*

*- The electron density that minimizes the energy of the overall functional is the true electron density corresponding to the full solution of the Schrödinger equation"*

as well as on a set of equations derived by Kohn and Sham,[153] applicable to real systems and studies of chemical reactions.

Kohn and Sham explained that the definition of exact electron density could be done by solving a set of one-electron equations, given in the form:

$$\rho(\mathbf{r})=\sum_{i} |\Psi_i(\mathbf{r})|^2 \tag{12}$$

Ψi represents populated either atomic or molecular orbitals so-called Kohn and Sham orbitals.

Kohn and Sham suggest that the exact kinetic energy of an electron of a non-interacting system is calculated using the same electron density as a real, interacting system, with non-interacting electrons moving in the field of the effective potential of other electrons. They suggest a mathematical simplified mathematical model for electron density in correlation to the energy of molecules:

$$E[\rho]=T_{Hartree}[\rho]+E_{ext}[\rho]+E_{Coul}[\rho]+E_{XC}[\rho] \tag{13}$$

which describes the contribution of Hartree (Couloumb) potentials generated by the nucleui, attraction between the electrons and the nucleui ($E_{ext}$), electron-electron repulsions ($E_{coul}$), electron exchange and correlation energy ($E_{xc}$).

$$E_{DFT}[\rho] = T[\rho] + E_{ne}[\rho] + J[\rho] + E_{xc}[\rho] \tag{14}$$

"where E is the energy, T is the kinetic energy of the electrons, $E_{ne}$ is the nuclear-electron attraction (Coulombic) energy, J is the electron-electron repulsive (Coulombic) energy, and $E_{xc}$ is the electron electron exchange-correlation energy."[146]

Minimization of the energy functional gives Kohn and Sham's equations:

$$\left[-\frac{\hbar^2}{2m}\nabla^2+V_{eff}(\mathbf{r})\right]\Psi_i(\mathbf{r})=\varepsilon_i\Psi_i(\mathbf{r}) \tag{15}$$

$$V_{eff}(\mathbf{r})=V_{ext}(\mathbf{r})+V_H(\mathbf{r})+V_{XC}(\mathbf{r}) \tag{16}$$

$$n(\boldsymbol{r}) = \sum_{i} |\Psi_i(\boldsymbol{r})|^2 \tag{17}$$

$$V_{xc}=\frac{\delta E_{xc}}{\delta\rho(\mathbf{r})} \tag{18}$$

KS equations could be solved by an iterative procedure using the self-consistent field method as the effective $V_{eff}$ potential is dependent on $n$(r) and Ψ(r), respectively. From the calculated values of eigen-energies and eigen-functions of the ground state, the total energy, vibrational properties of molecules and charge density of molecules could be derived.

### 1.6.2. Approximate functional

The further development of DFT is focused on examining the performance of existing functions aimed at improving the part of the change/correlation $E_{xc}$ within the Kohn-Sham method. Based on the theoretical assumptions on which they are based, approximate functionals can be divided into: Local Density Approximation (LDA), Generalized-Gradient Approximation (GGA), meta-GGA hybrid functional, hybrid functional (Hybrid Functional) and double hybrid functional. LDAs are the least widely used in computational chemistry.
$E_{xc}$ is calculated under the assumption that the system behaves locally as a uniform electronic gas, i.e.:

$$E_{xc} = \int \rho\,(\boldsymbol{r})\varepsilon_{xc}^{LDA}\big(\rho(\boldsymbol{r})\big) \tag{19}$$

where $\varepsilon_{xc}^{LDA}(\rho)$ is the exchange-correlation energy of one electron of a homogeneous gas with density $\rho$. The second class of functionals, which have a much greater application in computational chemistry and give better results in relation, are functionals based on the approximation of the generalized gradient. In this approximation, the change-correlation function depends on both the value of the electron densities and its gradient:

$$E_{xc}= \int \rho\,(\mathbf{r})\varepsilon_{xc}^{GGA}\big(\rho(\mathbf{r}),\nabla\rho(\mathbf{r})\big)d\mathbf{r} \tag{20}$$

The expression $\varepsilon_{xc}^{GGA}$ in GGA is not unique, so there are numerous functionals based on the generalized gradient approximation. They are used in the calculation of molecules in the solid state because they give precise geometries. Meta-GGA functionalities increase flexibility by adding KS kinetic energy density ($(\tau_{KS})$ to the electron density obtained by summing gradients. The best known and most commonly used GGA functionalities are PW91,[154] PBE[155] and BLYP.[156]

$$E_{xc}= \int \rho\,(\mathbf{r})\varepsilon_{xc}^{GGA}\left(\rho(\mathbf{r}),\nabla\rho(\mathbf{r}),\nabla^2\rho(\mathbf{r}),\tau_{KS}(\mathbf{r})\right)d\mathbf{r} \tag{21}$$

$$\tau_{KS}(\mathbf{r})=-\frac{1}{2}\sum_{i}|\nabla_i(\mathbf{r})| \tag{22}$$

Due to the increased flexibility, meta-GGA functionalities are more accurate when calculating the properties of molecules compared to GGA and LDA functionalities. Hybrid functionalities use Hartree-Fox modifications and require more computing time. Hartree-Fock introduced changes in the energy of KS orbitals to Beke[157] in order to improve the thermochemical properties of molecules. Hartree-Fox changes are represented by the formula:

$$E_{xc}[\rho]= \int_0^1 \left( \langle \sum_{i>j} r_{ij}^{-1} \rangle_\lambda - J\left[\rho^\lambda\right] \right) d\lambda = \int_0^1 U_{xc}^\lambda d\lambda \tag{23}$$

The value of the parameter $\lambda = 0$ represents an uninteracting KS system, while $\lambda = 1$ represents a real system. Hybrid functionals use KS orbitals that are represented by basic Gaussian-type

functions. In addition to the Gaussian function, a numerical base function is used, which is in fact a table of values that the orbital wave function has at many points around the nucleus. The best known hybrid functionalities are B3LYP[158], TPSSh, PBE1PBE and M06[159].

### 1.6.3. Basis set

Basic sets[144] represents a set of vectors that define the space in which a problem is observed and solved. It is very important to choose the right basis set in relation to the desired accuracy, because this greatly affects the length of the calculation. From the point of view of molecular orbitals, these are mathematical functions. The method of a linear combination of atomic orbitals (LCAO) is a method by which molecular orbitals are represented as a linear combination of basic functions.
Some of DFT methods are as follows, with a description of their preferential area of use:
1. Hartree-Fock Slater (HFS) functional, Hartree-Fock with local density approximation exchange
2. Vosko, Wilks, and Nusair (VWN), Local Density Approximation (emphasis on electron correlation approximation).
3. Becke correlation functional; Lee, Yang, Parr electron exchange functional (BYP), Gradient-corrected LDA functional, particularly accurate for metal-organic compounds, calculation of charge density on atoms in molecules.
4. Becke 3-term correlation functional; Lee, Yang, and Parr exchange functional (B3YP), Hybrid DFT, the best for model chemistry of organic compounds, especially B3LYP/6-31G*, reaction chemistry, calculation of charge density on atoms in molecules.
5. Perdew 1986 functional (P86), Gradient-corrected LDA functional.
6. Becke 3-term correlation functional; Perdew correlation term, (P3P86), Hybrid DFT.
7. Modified Perdew-Wang one parameter hybrid for kinetics (MPW1K), Hybrid DFT.
All methods are not acceptable for the system that includes weak hydrogen bonding interactions.

### 1.6.4. Molecular descriptors

Molecular descriptors represent the quantities whose numerical values describe a certain physico-chemical property. There is a large number of molecular descriptors, and some of them are HOMO and LUMO orbital energies, their difference ($E_{g\text{ap}}$ energy), thermodynamical parameters of molecules, etc.

### 1.6.5. Geometry optimization

Optimization of the ground state geometry of a particular molecular structure can be easily accomplished because there are carefully tuned algorithms for finding the minimum at the potential energy surface. These mimima are characterized by the absence of imaginary (negative) vibrational frequencies.[160] Geometries optimized by the DFT method in most cases agree well with experimental results,[161] although the agreement of the results is closely related to the initial geometry. For the compounds where the optimization of geometry could be based on the crystallographic data input, the optimization result give more accurate geometries of the studied compounds.[147]
Compounds containing imino groups,[162] hydrazone[163] and cinnamic acid moiety were the subject of many studies with a large part devoted to quantum chemical calculation. Symmetrical Imino hydrazone was already presented[27], while asymmetrical ones were less thoroughly studied. The electronic and geometrical/structural properties, biological and antioxidant activity of cinnamamides have not been studied so far using quantum chemical calculations.

## 1.7. Anticancer activity

### 1.7.1. Characteristics of cell cultures used in the study

During this research, the biological activity of the tested compounds was initially evaluated on five commercial cell lines isolated from patients with different types of malignancy: human non-microcellular lung adenocarcinoma (A549, ATCC® CCL-185™), human breast adenocarcinoma (MCF-77, ATCC® HTB-22™), human colon adenocarcinoma (LoVo, ATCC® CCL-229™), human pancreatic adenocarcinoma (AsPC-1, ATCC® CRL-1682™), and human ovarian adenocarcinoma (SkOV-3, ATCC® HTB-77™). Potential toxicity was determined on a healthy culture of human epidermal skin keratinocytes (HaCaT, CLS, Cat. No. 300493) and hepatocellular adenocarcinoma (HepG-2, ATCC® HB-8065™). All cell cultures are of medium to highly differentiate epithelial origin, and in laboratory conditions those form a monolayer on the surface of the plastic dish where cells are either grown or treated. The exception is LoVo cells, which to a certain extent are also in suspension.

Aside from being originated from different tissues, every cell line has been derived from a distinctive individual (contains a particular genotype), was caused by a different mutation (i.e. possesses a set of diverse biomolecular dysfunctions in relation to healthy tissues). Also, each of them has a different length of the mitotic cycle (doubling time, the time required for the initial number of cells to double), which is not in direct relation to their malignant potential. For example, A549 cells have the shortest mitotic cycle of 20 hours,[164] while the time required for Mcf-7, SkOV-3, and LoVo cell multiplication is 24, 36, and 37 hours,[165–167] whereas the number of HaCaT cells doubles within the timeframe of 28 hours.[168]

### 1.7.2. Principles of vital dyes application to determine the number of live cells

During this research, several methods were used to discriminate living cells in the observed population. Discrimination is achieved by the application of so-called vital colors, which for various reasons specifically color either vital cells or cells in some form of cell death. Each vital dye was applied only to cells that have not been previously fixed, i.e. to cells whose selective membrane permeability has not been altered by some chemical treatment (for example 70% alcohol, triton X100, and others).

#### Trypan blue

Trypan blue is a diazo dye, whose negatively charged molecule cannot enter a cell which plasma membrane is not damaged.[169] Cells with the damaged membrane (cells in necrosis) are seen under the microscope as intensively blue. Trypan blue will not stain cells in apoptosis, independently of whether those are in early or advanced phases of apoptotic death. For these reasons, cells in the advanced stages of apoptosis can be discerned only according to their specific morphology, while those in the early stage of apoptotic death cannot be discriminated in relation to vital cells.

#### Calcein acetoxymethil (Calcein AM)

Calcein AM (CAM) is a non-fluorescent compound that passively enters cells. As long as acetoxymethyl ester is intact, the probe is not fluorogenic. In live cells, CAM undergoes the enzymatic transformation by non-specific esterases and becomes a fluorophore that can be seen within green emission spectrum (excitation/emission 322/435 nm).[170] Therefore, live cells and those in early phases of apoptosis and necrosis are seen as green in the observed sample.

**Propidium iodide**

Like CAM, propidium iodide (PI) fluoresces very faintly, but after binding to nucleic acids, especially by intercalation into double-helix DNA, its fluorescence is enhanced more than 30 times.[120] The maximum excitation and emission wavelength for PI is 535 nm and 617 nm. It has recently been proven that PI can enter a vital cell by endocytosis that forms vesicles located along the inner side of the plasma membrane.[171] In these vesicles, PI is stored and prevented to interact with nucleic acids, which makes it undetected.

Simultaneous staining with CAM and PI allows visual discrimination of apoptotic and necrotic death in the observed samples. Due to the damaged integrity of the plasma membrane, cells that die in necrosis are stained with both fluorescent colors with smudged red-yellow reflection. Unlike them, vital cells and cells in early apoptosis are stained only by CAM and fluoresce intensely green. Apoptotic bodies, which are result of advanced stages of apoptotic death, are staied only with PI and are seen as intensively red, clearly demarcated spheroidal bodies in the visual field.[172]

**Annexin V**

Annexin V is a phospholipid by a structure that binds with high affinity to phosphatidylserine. Phosphatidylserine is located on the inner side of the plasma membrane in a vital cells, but with the cell entering apoptosis it relocates on its outer side and makes apoptotic cell to become "visible" for macrophages. This sequence of events in the tissue of a living organism allows for the dying cell to be eliminated by the immune system without causing consequences for the surrounding cells.

Staining of the examined sample with Annexin V and PI provides a clear discrimination between living cells (non-stained), and those in the early phase of apoptosis (Annexin V single-stained) or in the early phase of necrosis (PI single-stained).[173] Cells stained with both fluorescent markers are found in the later stages of cell death, whereby discrimination between late apoptosis and necrosis can be determined subsequently by determining the presence of cells in the sub-G0/G1 area.

### 1.7.3. Basic differences between types of cell death

Mammalian cells that are exposed to irreparable damage can activate one of the many cascading pathways that will unequivocally lead to their death.[174] When a cellular homeostasis is compromised, the sequence of events that starts by an initial intracellular signal that is further mutually propagated by well-coordinated molecular mechanisms is called Regulated Cell Death (RCD). Unlike RCD, there is Accidental Cell Death (ACD), which arises due to severely impaired integrity of a cell either by physical, chemical, or mechanical stimulus. While the progression of ACD is completely uncontrolled, RCD can be modulated to some extent, not only by inhibiting the transmission of signals that lead to the end of the process but also by increasing the adaptive capacity of a cell to respond to stress. While necrosis is the outcome of any ACD, regardless of its cause, RCD is divided into three basic groups: (1) apoptosis; (2) autophagy; (3) necrosis, i.e. cell death due to altered mitochondrial Permeability (Mitochondrial Permeability Transition (MPT) -driven necrosis) - MPT necrosis.

Necrosis, regardless of whether it originated as ACD or RCD, is a form of cell death implying a loss of cell membrane integrity with the consequently uncontrolled release of intracellular contents. In a living organism, necrosis can have different repercussions depending in which tissue/organ cells are dying in necrosis, as well as whether is it just about a small, well-localized necrotic focus or is a process that leads to the mass release of intracellular contents into systemic circulation. Therefore, in the case of a small localized focus, necrosis can only lead to damage of the surrounding tissue with consequent scar formation, while necrosis is a large scale can lead to malfunction to distant tissues and organs, such as acute renal failure.[175] Apoptosis, on the other hand, is a form of cell death where cell disintegrates in an organized manner, by forming so-called apoptotic bodies. Apoptotic bodies in

the organism are removed by white blood cells via the process of phagocytosis, so that apoptotic cell death does not lead to local either systemic consequences. Healthy tissue cells always die in apoptosis except when they are severely damaged by physical or chemical factors. Drugs used in the therapy of malignant diseases stimulate apoptotic death when applied to cells in laboratory conditions, while the same drugs at the level of malignant tissue mainly lead to necrosis. This different outcomr is conditioned primarily by the lower partial oxygen pressure in the tumor mass, so the cells in the tumor mass create energy by a less efficient glycolysis process, instead of oxidative phosphorylation. Considering apoptotic death is an energy-dependent process, malignant cells within the tissue mass are not able to carry out apoptosis to its very end, and majority of them will finish in necrosis instead in advanced stages of apoptosis. For those reasons, experimental drugs that in preclinical investigation induce apoptosis in a dominant percentage are selected for further evaluation.

### 1.7.4. Determination of cell distribution within phases of mitotic division

Cell division is a highly organized and controlled process that enables duplication of genetic materials and organelles with subsequent reorganization mother cell into two daughter cells. Control of this process includes regulation of cell growth signals as well as preservation of genetic integrity.[176] The cell undergoes four phases of the cell cycle during division: G0/G1, S, G2, and M. Commercial cell cultures, either are malignant or not, belong to the so-called immortalized models, i.e. populations with almost unlimited ability to divide.

Changes in cell-cycle distribution of treated cells during the mitotic cycle can provide information on the phase of cell death at which treated cells are stopped, and can also indicate the phase of cell death at which the process targeted by the test subject has a vital role.

When cells are accumulated at the G2/M phase with concurrent significantly reduced percentage at the S and G0/G1 phases serves as an information that investigated compound interferes with some of the processes at the final phase when the dividing spindle is formed and chromosomes are in process of separation. Accumulation of cells in the S phase indicates that the compound most likely interferes with the process of DNA replication, while their accumulation in the G0/G1 phase is the least informative in the context of a potential intracellular target. In addition, within the mitotic division, exist two main control points at which cell integrity is control by clearly precise intracellular mechanisms before it continues to divide.[177] The first control point is at the end of the G1 phase and before the cells entry the S phase (G1-to-S checkpoint), and the second is at the end of the S phase before the cell enters the final phase of division (S-to-G2 checkpoint). There are different feedback networks in the cell which mutually exchange information about the functional status of each segment that plays a certain role in the process of mitotic division and cell homeostasis. If serious DNA damage occurre, or the activity of an enzyme with an important role in chromosome replication is suppressed by an external agent, feedback mechanisms will be activated and the cell will be held at the G1-to-S control point level, prevented from continuing the division. Cells will be kept at this checkpoint as long as reparation mechanisms need to repair caused damage, and if repair is not possible, a cell will be introduced into apoptosis. This scenario will be seen as an increase in percentage of cells at the G0/G1 and S phase with strikingly decreased percentage of cells at the G2/M phase. If the external agent caused damage that the control mechanisms could not recognize before cell entered mitotic division, cell accumulation will be occurred during the S phase, with a significantly lower percentage of cells in the G0/G1 and G2/M phases. When cells manage to pass through the phase of chromosomal division, but impairment has to be repaired in order cell could divide into two fully functional daughter cells, the division is going to be retained at the S-to-G2 control point. As in the case of the G1-to-S checkpoint, if it is not possible to repair the injury, cell will enter apoptotic death.

Control and reparation mechanisms impeccably operate only in healthy cells, whereas in malignantly transformed cells some of them become ineffective.[178] Drugs with a well-defined mechanism of action, such as cisplatin, provoke different stagnation by phase of mitotic division in

the different malignant cell lines, because each malignancy has the unique loss of function in controlling and repairing mechanisms. For those reasons, the rearrangement of malignant cells by stages of mitotic division should be interpreted primarily as an illustration of the reaction to the applied compound, rather than being used as reliable information about compound's potential mechanism of activity.

### 1.7.5. Determination of caspase pathway activation by test compounds

Apoptosis can be initiated by a large number of different causes, but from a moment of its initiation, the rest of the process is highly organized and based on signal propagation over a well-established series of biomolecular interactions (cascades).[179] The most prominent role in apoptotic signal propagation have caspase pathways, which are divided into two basic pathways: external and internal.[180,181] Each of these two cascade pathways has a particular way of initiation, but in both cases mitochondria are the final determination.

The first step in the cascade of the external caspase pathway is the activation of caspase 8, which may be triggered either by stimulation of receptors on the cell membrane by various cytokines, or by endoplasmic reticulum stress. Initiation of the internal caspase pathway starts with activation of caspase 9 due to significantly affected bioenergetic or structural homeostasis of the cell. Also, the internal and extern pathways can co-activate each other. By structure, caspases belong to the endoprotease family and are synthesized in the cell as inactive monomer molecules. For their activation is necessary to dimerize with another identical molecule (homodimerization), which as a consequence makes their catalytic center available for interaction with substrate molecules.

### 1.7.6. Determination of the ability of test compounds to initiate the generation of superoxide radicals in mitochondria

A significant number of drugs in use for cancer treatment operate over generation of reactive oxygen species (ROS) that leads to chromosomal damage of malignant cells.[182,183] Mitochondria are the main source of ROS in the cell, wherein the superoxide anion ($^{\bullet}O_2^-$) being the first in a series of aroused ROS products.[184,185] Mitochondrial superoxide dismutase (MnSOD, SOD2) is the first line of cellular defense from increased production of $^{\bullet}O_2^-$, and is in charge for its rapid conversion to less aggressive hydrogen peroxide. The role of SOD2 is of crucial significance for cellular homeostasis because it directly protects the integrity of the oxidative chain and the synthesis of adenosine-3-phosphate (ATP). In the case of overwhelming $^{\bullet}O_2^-$ production that SOD2 is not able to effectively neutralize, the anion is exported to the cytoplasm via voltage-dependent mitochondrial channels, where it is afterward converting partly into hydrogen peroxide and partly into a highly reactive hydroxyl radical ($^{\bullet}OH$).[186] Unlike peroxide, which participates in regulation of numerous physiological processes, $^{\bullet}OH$ oxidizes the lipid structures, while intermediates of this reaction cause damage of the cellular DNA.[187] It has been proven that malignant tumors have decreased ability to defend from increased ROS production compared to healthy tissues.[188] The same phenomenon was established in cells of numerous malignant cell cultures, making them particularly sensitive to compounds with the ability to generate $^{\bullet}O_2^-$ production.[189]

### 1.7.7. Testing the influence of the tested compounds on the migratory activity of malignant cells

The basic characteristics of malignant tumors are genetic instability associated with mutations in various genes, together with the ability of malignant cells to metastasize from the primary tumor mass to distant tissues and organs.[190] Metastatic ability is the main reason for the lethal outcome of malignant disease, which is a very complex process that includes cytoskeletal dynamics with an expression of adhesive and proteolytic enzymes. The first step during this process is invasion when

cells break through the basement membrane of the primary tumor mass and migrate through the extracellular Matrix (ECM) into the surrounding tissues. There are more different laboratory tests that are used to determine the migratory potential of malignant cells, as well as to examine the influence of the investigated drug on this process. However, none of these laboratory methods is comprehensive enough to fully mimic such a complex operation.[191] Therefore, these tests can primarily detect the cytoskeletal dynamics and the influence of the tested compounds on it, whereas the real resistance of ECM to cell movement, influence of tissue hypoxia and chemoattractants as stimulating forces are practically impossible to imitate in a single laboratory model.

### 1.7.8. Investigation of potential toxic activity in a human keratinocyte and hepatocellular models

The biggest problem during the treatment of malignant diseases is a narrow therapeutic index, i.e. the non-selective activity on tumor mass with toxicity toward healthy tissues and organs. The true extent and severity of unwanted effects of new drugs can be determined during only in clinical trials. As part of preclinical testing, different cell models can be used to evaluate potential toxicity, but none of them can provide a reliable assessment of the expected side effects. In order to provide at least a preliminary estimation of whether compounds in this investigation have ability to target malignant cells while sparing healthy ones, we selected two cell culture models: healthy skin epidermal keratinocytes (HaCaT) and hepatocellular adenocarcinoma (HepG-2) cells. The reason for choosing the HaCaT culture relies on the fact that these cells is the most dominant cell type constituting epidermis, thus playing multiple roles essential in skin defense and repair.[192] Skin is the largest organ in the human body, and one of the most commonly damaged tissues during chemotherapy.[193] Although HepG-2 cells were originated from liver malignant tumor, those are previously well established as a reliable model for evaluation of hepatotoxicity.[194] Considering that liver is the main laboratory in the human body responsible for metabolic transformation and excretion of drugs, it was logical to include this model for assessment of investigated drugs' toxicity profile.

## 2. Experimental part

### 2.1. Chemicals, equipments and laboratory plastic

All chemicals, solvents, and reagents were of analytical grade and were used as received without further purification. Cinnamic acid and their derivatives (3-chlorocinnamic, 4-chlorocinnamic, 4-methoxycinnamic, 3-Hydroxycinnamic, Ferulic and Caffeic acid), diisopropylethylamine, 1-[*Bis*(dimethylamino)methylene]-1*H*-1,2,3-triazolo[4,5-*b*]pyridinium 3-oxid hexafluorophosphate (HATU) and thionyl chloride were purchased from Fluka AG – Chemische and Sigma-Aldrich. 2-Formylpyridine, salicylaldehyde, and 2-acetylpyridine were obtained from Sigma-Aldrich. Methanol, ethyl acetate, hexane, dimethylformamide (DMF) and dimethyl sulfoxide (DMSO) were obtained from Fisher Chemical, 8-hydroxy-2-quinolinecarboxaldehyde was supplied by Acros, while iron(II) sulfate×7$H_2O$ and iron(III) nitrate×9$H_2O$ were supplied by Merck. All chemicals and reagents were of analytical grade and used as received. Thiocarbohydrazide (98%) was obtained from Acros Organics (BVBA, Geel, Belgium).

For biological investigations, Rifampicin (RIF), glycerol, Tween 80, 3-(4,5-dimethylthiazol-2-yl)-2,5-diphenyltetrazolium bromide (MTT), sodium dodecyl sulfate (SDS), DMSO, Calcein AM (CAM), propidium iodide (PI), ethylenediaminetetraacetic acid (EDTA), and ribonuclease A (RNase A) were purchased from Sigma-Aldrich, CaspGLOW$^{TM}$ fluorescein active caspase-8 staining kit and CaspGLOW$^{TM}$ red active caspase-9 staining kit from BioVision, MitoSox Red from ThermoFisher Scientific, GenoType MTBC and GenoType MTBDRplus assays from Hain Lifescience, Isoniazid (INH) from Supelco, Middlebrook 7H9 broth medium from Liofilchem, ADC Enrichment from Difco, Dulbecco's Modified Eagle's Medium (DMEM) from Dominique Dutscher, fetal bovine serum (FBS) from Life Technologies, penicillin-streptomycin (Pen-Strep) from Gibco, trypsin-EDTA from

BioWest, Annexin V-FITC from Immuno Tools. Equipment used includes Celigo® imaging cytometer (Cyntellect), Guava® easyCyte 12HT Benchtop flow microcapillary cytometer (Millipore), and Multiscan™ Microplate Reader (ThermoFisher Scientific). Software packages used for data analysis were InCyte® software (Millipore), TScratch software (CSElab), and Prism 8 (GraphPad Software). 96 flat bottom well plates were purchased from Corning® Costar® and Thermo Scientific, while Millex-SV 5.0 µm filters from Millipore.

### 2.2. Synthesis of m-TCH and b-TCH

Monothiocarbohydrazones (**m-TCH**) were synthesized following literature method.[195] Condensation of thiocarbohydrazide (DHS) and corresponding aldehydes/ketone was performed as shown in (Scheme 12). 2.35 mmol of (2-Formylpyridine, Salicylaldehyde, 8-Hydroxyquinoline-2-carbaldehyde or 2-Acetylpyridine) was added to the hot solution of thiocarbonohydrazide (DHS) (4.7 mmol DHS in 40 mL ethanol), a drop of concentrated hydrochloric acid was added as catalytic. The solution was heated at 80 C˚ for 3 hours, cooled and precipitate was isolated by filtration and rinsed with cold ethanol. In an analogous manner **b-TCH** was synthesized, using 2.1:1 molar ratio of aldehyde/ketone: DHS.

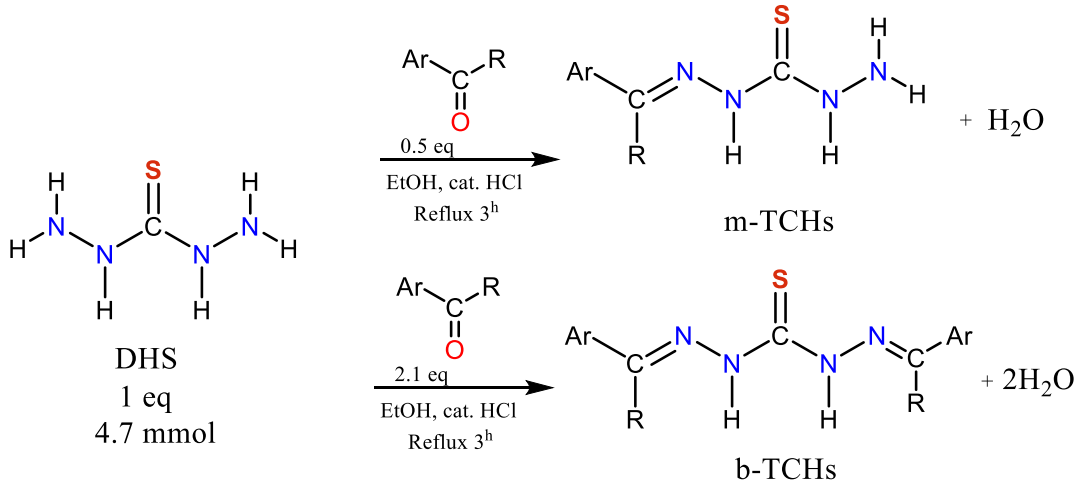


Scheme 12. Synthesis pathways of **m-TCH** and **b-TCH**

Table 1. List of synthesized compounds

| Compound | Ar | R |
|---|---|---|
| **m-TCH$_{2fp}$** | 2-Pyridineyl | H |
| **m-TCH$_{sal}$** | 2-Hydroxyphenyl | H |
| **b-TCH$_{sal}$** | 2-Hydroxyphenyl | H |
| **m-TCH$_{8OH2qu}$** | 8-Hydroxy-2-quinolinyl | H |
| **m-TCH$_{2ap}$** | 2-Pyridinyl | $CH_3$ |
| **b-TCH$_{2ap}$** | 2-Pyridinyl | $CH_3$ |

The compounds **m-TCH$_{sal}$**,[196] **b-TCH$_{sal}$**,[197] **m-TCH$_{2ap}$**[198] and **b-TCH$_{2ap}$**[26] (Scheme 12) was published earlier. Purity and structure were confirmed by NMR data and elemental analysis. Even **m-TCH$_{sal}$** and **m-TCH$_{2ap}$** were published without full data on their characterization. Synthesis and characterization of **m-TCH$_{8OH2qu}$** and **m-TCH$_{2fp}$** were given in recent literature.[195]

### 2.3. General procedure for the synthesis of cinnamamides

Cinnamides were synthesized by coupling of cinnamoyl chlorides with the synthesized **m-TCH**, method (a), or using coupling agents HATU/DIPEA, as it is given in Scheme 13. Method (a): Cinnamoyl chlorides and **m-TCH** were prepared according to the previously published

procedures.[126,199,200,21] In the first step, cinnamic acid derivatives were transformed into acid chlorides using $SOCl_2$ in large excess (30 eq., 27mmol). The reaction vessel was cooled during the dropwise addition of $SOCl_2$ using an ice bath, and then stirred under reflux for 5 hours. After the completion of the reaction, the excess of thionyl chloride was removed under a vacuum. The solid residue was washed with DMF and used without further purification. Into a prepared solution of synthesized cinnamoyl/ 3-chlorocinnammoyl, 4-chlorocinnamoyl, or 4-methoxycinnamoyl chloride in DMF was added DMF solution (2 mL) of 0.82 mmol of appropriate **m-TCH** in a dropwise manner. The mixture was heated at 40 ˚C for 24 h, and the precipitate was isolated by filtration. The washing solution was mixed with 20 mL of cold distilled water to provide further product crystallization. A new crop of precipitate was filtered and raw material was crystallized from ethyl acetate, while **4-ClCimTCH$_{2ap}$** was recrystallized from methanol.

Method **(b)** was used for synthesis of **3-OHCimTCHs, CafTCHs, and FerTCHs**, using HATU-DIPEA as a coupling reagent. In an ice bath, (2 eq, 0.8 mmol) of DIPEA was added to the (1 eq, 0.4 mmol) of 3-Hydroxycinnamic, Caffeic, or Ferulic acid and stirred for 10 minutes followed by (1.15 eq, 0.45 mmol) of HATU, then (1.1 eq, 0.48 mmol) of **m-TCH** was added to the flask. The mixture was stirred at room temperature for 5 hours and then 40 ml of cold distilled water was added for further product crystallization. The precipitate was filtered, 3-OHCimTCH purified from EtAc. CAfTCHs and FerTCHs were crystallized from a mixture of (DCM: Methanol, 90:10).

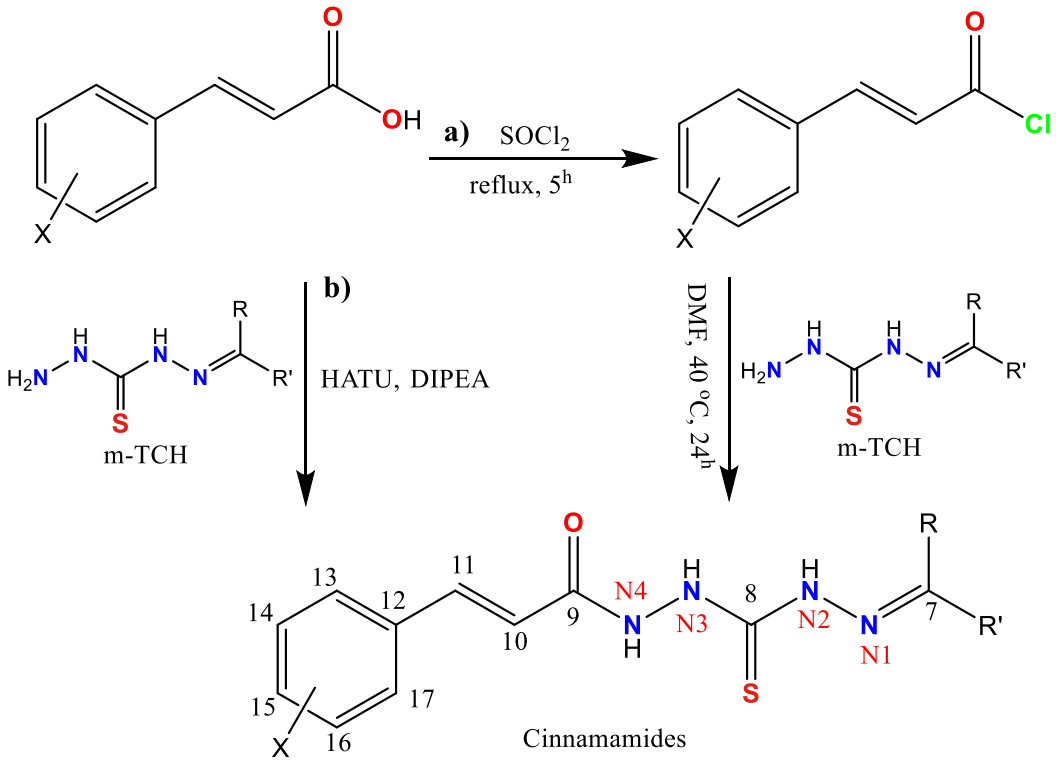


Scheme 13. Synthetic route of Cinnamamides (with numeration used in NMR analysis).

Table 2. List of synthesized Cinnamamides

| Compound | X | R | R’ |
|---|---|---|---|
| $CimTCH_{2fp}$ | H | H | 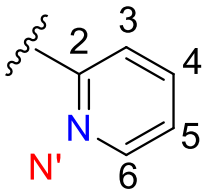 |
| $3\text{-}ClCIMTCH_{2fp}$ | 3-Cl | | |
| $4\text{-}ClCimTCH_{2fp}$ | 4-Cl | | |
| $4\text{-}MeOCimTCH_{2fp}$ | $4\text{-}OCH_3$ | | |
| $3\text{-}OHCimTCH_{2fp}$ | 3-OH | | |
| $CafTCH_{2fp}$ | 3,4-di-OH | | |
| $FerTCH_{2fp}$ | 3-MeO, 4-OH | | |
| $CimTCH_{sal}$ | H | H | 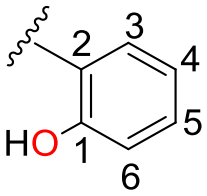 |
| $3\text{-}ClCIMTCH_{sal}$ | 3-Cl | | |
| $4\text{-}ClCimTCH_{sal}$ | 4-Cl | | |
| $4\text{-}MeOCimTCH_{sal}$ | $4\text{-}OCH_3$ | | |
| $3\text{-}OHCimTCH_{sal}$ | 3-OH | | |
| $CafTCH_{sal}$ | 3,4-di-OH | | |
| $FerTCH_{sal}$ | 3-MeO, 4-OH | | |
| $CimTCH_{8OH2q}$ | H | H | 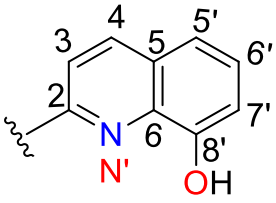 |
| $3\text{-}ClCIMTCH_{8OH2q}$ | 3-Cl | | |
| $4\text{-}ClCimTCH_{8OH2qu}$ | 4-Cl | | |
| $4\text{-}MeOCimTCH_{8OH2qu}$ | $4\text{-}OCH_3$ | | |
| $3\text{-}OHCimTCH_{8OH2q}$ | 3-OH | | |
| $CimTCH_{2ap}$ | H | $CH_3$ | 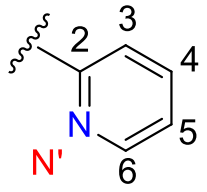 |
| $3\text{-}ClCIMTCH_{2ap}$ | 3-Cl | | |
| $4\text{-}ClCimTCH_{2ap}$ | 4-Cl | | |
| $4\text{-}MeOCimTCH_{2ap}$ | $4\text{-}OCH_3$ | | |
| $3\text{-}OHCimTCH_{2ap}$ | 3-OH | | |

### 2.3.1. Characterization methods

Full data on characterization methods used was given in recent publication:[198]
"The melting points of synthesized compounds were determined on a Stuart digital SMP-30 melting point apparatus. Elemental analyses (C, H, and N) were performed by the standard micro-methods using an ELEMENTAR VARIO ELIII C.H.N.S.O analyzer. ATR-FTIR spectra were obtained on a Thermo Scientific™ Nicolet™ iS™ 10 (Thermo Scientific USA) spectrometer with a Smart iTX™ accessory. Infrared (IR) spectra were obtained on a Thermo Scientific™ Nicolet™ iS1010 spectrometer. $^{1}H$ and $^{13}C$ characterization spectra were recorded on a Bruker Avance III 500 spectrometer equipped with a broad-band direct probe. The spectra were recorded at room temperature in DMSO-$d_6$. Chemical shifts are given on the δ scale relative to tetramethylsilane (TMS), as an internal standard for $^{1}H$ and $^{13}C$. Coupling constants (*J*) were expressed in Hz. Abbreviations used for NMR spectra: s, singlet; d, doublet; dd, doublet of doublets; t, triplet; m, multiple; and br. m. ovlp. (broad multiplet overlapping). 1D ($^{1}H$ and $^{13}C$) and 2D (COSY, NOESY, $^{1}H$–$^{13}C$ HSQC and $^{1}H$–$^{13}C$ HMBC) spectra of studied compounds are shown in (Figure 48- Figure 110) in Appendix. UV-Vis spectrophotometer Shimadzu 1800 was used for the determination of antioxidant activities of synthesized compounds and stability constant."

## 2.4. Determination of antioxidative potential

The antioxidant potential of cinnamamides was determined by free radical scavenging ability which was assessed by $DPPH^{\bullet}$, $ABTS^{\bullet+}$, CUPRAC and TAC method.

### 2.4.1. Free radical scavenging antioxidant assay ($DPPH^{\bullet}$)

The $DPPH^{\bullet}$ radical scavenging activity of cinnamides was quantified according to the method of *Blois*[201] and *Jiang et al*. [202] with suitable modifications. Briefly, the reaction mixture of cinnamamides with different concentrations was prepared and incubated in the dark for 30 min at room temperature and absorbance was measured at 517 nm. The scavenging activity was calculated using the equation (24)

$$\text{Scavenging activity } (\%) = \frac{(A_{control} - A_{sample})}{A_{control}} \times 100 \qquad (24)$$

Where $A_{sample}$ and $A_{control}$ indicate the absorbance of $DPPH^{\bullet}$ at 517nm in the sample and control solution. The $IC_{50}$ values were determined using a graph of scavenging activity *versus* sample concentrations. $IC_{50}$ for synthesized compounds was calculated based on the percentage of $DPPH^{\bullet}$ scavenged using Ascorbic acid as a reference.

### 2.4.2. $ABTS^{\bullet+}$ radical scavenging assay

The procedure was followed by method of *Erel* [203] with some modifications. The working solution was prepared from 7 mmol of $ABTS^{\bullet+}$ solution and 2.45 mmol of potassium persulfate. The mixture was kept at room temperature in a dark place for 12-16 h before use. Then, the $ABTS^{\bullet+}$ solution was diluted to reach an absorbance of 0.706 ± 0.02 units at 734 nm, and after it was added to the serial of cinnanamides with different concentrations. After standing for 30 min in the dark the absorbance was measured at 734 nm. Ascorbic acid was used as standard.

### 2.4.3. Total antioxidant capacity (TAC)

TAC activity was determined according to the method given by *Prieto. et a*l,[204] The cinnamamides were dissolved in methanol and combined with a reagent (sulfuric acid, sodium phosphate, and ammonium molybdate). The tubes were incubated for 90 min at 95°C in a thermal block then decrease to ambient temperature. Absorbance was recorded at 695 nm, and results expressed in relation to Ascorbic acid.

### 2.4.4. Cupric reducing antioxidant power (CUPRAC)

CUPRAC was carried out as described by *Cekic et al*[205] with some modifications. Briefly, cinnamamides (0.15625 mmol) were added to the solution consisting of 10 mmol $CuCl_2.2H_2O$, 7.5mmol Neocuprion and 1 mol $NH_4Ac$ at PH 7, and after absorbance was measured at 450 nm after incubating 30 minutes at room temperature.

The results on antioxidant activities are given in Table 3.

Table 3. Antioxidant activity of cinnamamides

| | Compound | DPPH$^{\bullet(*)}$ $IC_{50}$ mM | ABTS$^{\bullet+}$ $IC_{50}$ mM | CUPRAC 1 mM | TAC mg/mL |
|---|---|---|---|---|---|
| 1 | **CimTCH$_{2fp}$** | 0.1812 | 0.0926 | 3.7126 | 0.708 |
| 2 | **CimTCH$_{sal}$** | 0.1054 | 0.0751 | 2.1933 | 0.648 |
| 3 | **CimTCH$_{8OH2qu}$** | 0.0651 | 0.0724 | 1.2339 | 0.413 |
| 4 | **CimTCH$_{2ap}$** | 0.2218 | 0.1342 | 2.9709 | 0.625 |
| 5 | **3-ClCimTCH$_{2fp}$** | 0.1284 | 0.0802 | 3.1202 | 0.707 |
| 6 | **3-ClCimTCH$_{sal}$** | 0.1073 | 0.0906 | 1.9910 | 0.484 |
| 7 | **3-ClCimTCH$_{8OH2qu}$** | 0.0842 | 0.0751 | 3.0432 | 0.684 |
| 8 | **3-ClCimTCH$_{2ap}$** | 0.2130 | 0.1338 | 3.4688 | 0.773 |
| 9 | **4-ClCimTCH$_{2fp}$** | 0.2202 | 0.0672 | 6.1914 | 0.747 |
| 10 | **4-ClCimTCH$_{sal}$** | 0.0822 | 0.0866 | 4.6182 | 0.552 |
| 11 | **4-ClCimTCH$_{8OH2qu}$** | 0.0514 | 0.0505 | 2.2963 | 0.913 |
| 12 | **4-ClCimTCH$_{2ap}$** | 0.2632 | 0.0695 | 3.4253 | 1.180 |
| 13 | **4-MeOCimTCH$_{2fp}$** | 0.1210 | 0.0736 | 3.7306 | 0.640 |
| 14 | **4-MeOCimTCH$_{sal}$** | 0.0916 | 0.0663 | 2.4499 | 0.634 |
| 15 | **4-MeOCimTCH$_{8OH2qu}$** | 0.2097 | 0.0518 | 2.6989 | 0.563 |
| 16 | **4-MeOCimTCH$_{2ap}$** | 0.2184 | 0.1136 | 3.8618 | 0.786 |

**(*) $IC_{50}$ (mM) for compounds: 3-OHCimTCH$_{2fp}$**= 0.14789, **3-OHCimTCH$_{sal}$**= 0.09944, **3-OHCimTCH$_{8OH2q}$**= 0.13485, **3-OHCimTCH$_{2ap}$**= 0.22203, **CafTCH$_{2fp}$**= 0.13535, **CafTCH$_{sal}$**= 0.10714, **FerTCH$_{2fp}$**= 0.06466, **FerTCH$_{sal}$**= 0.08474.

DPPH test highlighted compounds with phenolic –OH group **3-OHCimTCH$_{2fp}$**, **3-OHCimTCH$_{sal}$**, **3-OHCimTCH$_{8OH2q}$**, **CafTCH$_{2fp}$**, **CafTCH$_{sal}$** **FerTCH$_{2fp}$** and **FerTCH$_{sal}$** as the most potent ones, with 2-4 times lower IC50 values compared to non-phenolic congeners.

## 2.5. Antimicrobial activity

### 2.5.1. Assessment of antibacterial activity

A stock solution of Cinnamamides, dissolved in distilled water (50 mg/mL), were used for assessment of their antimicrobial activity. Antibacterial activity was performed according to the standard broth dilution assay, given by the National Committee for Clinical Laboratory Standards (M07-A8) for bacteria.[206] Serial dilutions of tested compounds were prepared and added to bacterial cultures. The highest used concentration was 500 μg/mL. Bacterial growth was determinig optical density, and minimal concentrations of compounds required to inhibit 50% of bacterial growth after 24h at 37 $^{o}$C ($MIC_{50}$) were determined. Testing was performed using *Enterococcus cloacae* ATCC13047, *Staphylococcus aureus* NCTC 6571, *Klebsiella pneumoniae* ATCC 13883, *Acinetobacter baumannii* ATCC 19606, *Pseudomonas aeruginosa* NCTC 10662, and *Escherichia coli* ATCC 1175 strain.

### 2.5.2. Assessment of antimycobacterial activity

The methodology has been previously described in details.[200] Briefly, the investigation was organised on three *Mtb* strains that were selected from a panel of 25 randomly chosen clinical isolates according to detection of mutations known as associated to resistance to INH and RIF by means of GenoType MTBDRplus.[207,208] The selected strains were:

1. *Mtb-InhRif-S* strain that is sensitive to both drugs;
2. *Mtb-Inh-R* strain that is resistant to INH but sensitive to RIF;

3. *Mtb-Rif-R* strain that is resistant to RIF but sensitive to INH.
Colonies of selected strains were transferred to fully supplemented 7H9 broth medium and single cell suspensions were established using Millex-SV filters. Suspensions were left to grow for a week, when their densities were adjusted using McFarland standard as recommended previously.[209] Bacilli of selected strains were seeded in 96 well plates (in 0.1 mL of supplemented broth medium per well), after INH, RIF and investigated compounds were added to final concentrations from 0.03-100 μM. Evaluation of anti-*Mtb* activity has been performed after six days of incubation by means of MTT assay. Survival of treated bacilli was computed in relation to non-treated samples according to the previously defined formula.[210] $MIC_{90}$ was defined as the lowest concentration that reduced viability of treated strain by 90 % or more.

### 2.6. Samples preparation for UV-measurements for water induced isomerization

A stock solutions of cinnamamides were prepared in DMSO. The working solutions were prepared by diluting the defined volume of stock solution and water, and diluted with DMSO to obtain V(DMSO)/V($H_2O$) solvents ratio of 4:1 (Figure 9).[211] Concentration of cinnamamide was $5 \times 10^{-5}$ mol $L^{-1}$.

### 2.7. Quantum chemical study for mTCHs and dTCHs

The methodology has been previously described in details[200]
"The initial geometry of each isomeric form was obtained using MMFF94 force field.[212] Afterward, a conformational search was performed using AMMP program[213] and Vega ZZ 3.1.0 GUI.[214] Boltzman jump search parameters were used, while all flexible torsions were rotated by 15°. The dielectric constant was set to 78.4 (water) and other settings were retained at default values. The lowest-energy conformer of each form was additionally optimized using DFT with B3LYP functional and 6-311++G(d,p) basis set. Non-specific solvent effects were simulated using the water IEF-PCM model. Frequency calculations were performed in order to obtain zero-point corrected energies and other thermodynamic parameters. No imaginary vibrational frequencies were present in the optimized geometries, confirming that the geometry reported represents the minimum on the potential energy surface. The absorption spectra are simulated using time-dependent DFT method with CAM-B3LYP functional[215] and the same basis set as for geometry optimization, while solvent effects were simulated using IEF-PCM model of DMSO. Gauge independent atomic orbital (GIAO) method[216] was used for predicting the NMR chemical shifts of diastereoisomers in DMSO. The rotational barrier was calculated by stepwise rotation around $C_2$-$C_7$ bond by 20 º and geometry optimization of each rotamer at DFT/$\omega$B97XD/6-311g(d,p) level to account for dispersion interactions.[217] All calculations were performed in Gaussian 09."[218]

### 2.8. 3D-QSAR model

To elucidate the relationship between the structure of cinnamamides and their antibacterial activity toward *A. baumanii* we developed an alignment-independent 3D QSAR model in Pentacle 1.06 software.[219,220] The $MIC_{50}$ values (Table 3) were converted into $-\log MIC_{50}$ and used as a dependent variable. The initial geometries of compounds were generated using MMFF94 force field,[212] and further refined using the PM7 semi-empirical quantum chemical method,[221] implemented in MOPAC2016.[222,223] The convergence criteria were increased by a factor of 100 using PRECISE keyword, and MMOK was applied for the correct treatment of the amide bond. The .sdf database of the optimized structures was prepared in Vega ZZ 3.2.0[214] and imported in Pentacle. The ionization state was set to pH 7.4, and all compounds at this pH were neutral.

Molecular interaction fields (MIFs)[224] were computed for 4 GRID chemical probes that map different pharmacophoric features of the molecules: DRY probe for mapping the favorable

hydrophobic sites on the molecule, O probe for binding to HBD sites, N1 probe for mapping HBA features, and TIP probe that accounts for the molecule shape.[225] The grid spacing was set to 0.4, and other settings for MIF computations were kept at default values. The program takes the matrix of interaction energies (IE) and converts it into a set of variables, where each variable represents the maximum product of two IE at the defined distance. The most relevant positions for each MIF type were extracted using the AMANDA discretization algorithm,[226] and the selected hot-spots were encoded into GRIND descriptors using the maximum auto- and cross-correlation (MACC2) algorithm. After the application of one cycle of fractional factorial design (FFD) for the removal of redundant variables, 388 variables were retained in the model. The partial least square (PLS) mathematical model was applied for establishing a correlation between the biological activity and GRIND descriptors.[227]
In all Figures, variables positively correlated with the potency are shown as red lines, while inversely correlated variables are colored in blue.

### 2.9. Determination of stability constants of cinnamamides with $Fe^{2+}$ and $Fe^{3+}$ ion

A stock solutions of $FeSO_4x7H_2O$ and $Fe(NO_3)_3x9H_2O$ ($1.0 \times 10^{-2}$ mol $dm^{-3}$) and cinnamamides ($2.0 \times 10^{-4}$ mol $dm^{-3}$) were prepared in deionized water and DMSO, respectively. Stock solutions of cinnamamides were diluted with DMSO to the $\lambda_{max}$ absorbance in the range 0.5 - 0.6. The procedure, given by *Momidi et al*., was followed.[228] Briefly, an aliquot of 2μL of stock solution was combined with 3 mL of working solution. After homogenization the UV spectra were recorded until equilibrium was reached.

### 2.10. Assays for determination of anticancer activity

#### 2.10.1. Cell cultures and preparation of compounds

The methodology has been previously described in details.[200] All cell lines used in this investigation were maintained in high glucose DMEM medium supplemented with 10 % FBS and 1 % Pen-Strep. Incubations have been performed at 37 °C in a humidified atmosphere containing 5 % (v/v) $CO_2$. Compounds were initially dissolved in DMSO at 20 mM and stored at 4 °C, whereas working dilutions have been prepared using DMEM full medium immediately before each experiment.

#### 2.10.2. Cell viability assessment by CAM/PI dual staining

The methodology has been previously described in details.[200] Briefly, cells were seeded in 96 well plates (0.1 mL per well) a day before experiment. Investigated compounds were added at concentrations from 30-100 μM, and left for 24 hours on cells. At the end of incubation, CAM ($0.5 \times 10^{-3}$ gr/mL) and PI ($1 \times 10^{-6}$ gr/mL) were added to each well. Plates were left for 30 minutes at room temperature in dark, after cells were analysed on Celigo® imaging cytometer using green and red fluorescence. The percentage of cell survival was estimated in respect to none treated control samples.

#### 2.10.3. Percentages of cell death evaluation by Annexin V and PI staining

Methodology has been previously described in details.[200] Briefly, cells were seeded in 96 well plates (0.1 mL per well) a day before the experiment. Investigated compounds were added at concentrations from 1-100 μM, and left for 24 hours on cells. After incubation was over, cells were detached from the bottom of wells by trypsin treatment, and Annexin V (3 μL) and PI ($1 \times 10^{-6}$ g/mL in PBS) were added to each well. Cells were analysed on Guava® flow cytometer using InCyte® software, and classified as following:

1. Non-stained - viable cells;
2. Annexin V single-stained - cells in an early phase of apoptotic death;
3. PI single-stained - cells in an early phase of necrotic death;
4. Annexin V/PI stained - cells in advanced phases of death.

Percentages of all stained cells were summarized and plotted against corresponding concentrations in Prism software, after concentration-response curves were plotted using either a sigmoidal or biphasic model. $CdC_{50}$ was compouted as the concentration that triggered death in 50 % of treated cells.

### 2.10.4. Percentages of cells in sub-G0/G1 area

The methodology has been previously described in details.[200] Briefly, residual cells after Annexin V/PI reading were fixed in 70 % ethanol overnight at 4ºC. On the next day, ethanol was discarded, and cells were treated with RNAse (0.5 x $10^{-6}$ g/mL in PBS) at 37ºC for 1 h. When incubation was over, PI was added (1 × $10^{-6}$ g/mL in PBS), and cells were left at room temperature in dark till analysis. Cells were analysed on Guava® flow cytometer using InCyte® software.

### 2.10.5. Distribution of cells within phases of mitotic division

Methodology has been previously described in details.[200] Briefly, cells were seeded in 96 well plates (0.1 mL per well) a day before the experiment. Investigated compounds were added at concentrations from 1-100 µM, and left for 12 hours on cells. After incubation was over, cells were detached from the bottom of wells by trypsin treatment fixed in 70 % ethanol overnight at 4ºC. On the next day, ethanol was discarded, and cells were treated with RNAse and stained with PI as is described in *2.5.4*. Cells were analysed on Guava® flow cytometer using InCyte® software.

### 2.10.6. Percentages of cells with activated caspase-8 or/and caspase-9

The methodology has been previously described in details.[200] Briefly, cells were seeded in 96 well plates (0.1 mL per well) a day before the experiment. Investigated compounds were added at a concentration of 50 µM, and left for 6 hours on cells. After incubation was over, cells were detached from the bottom of wells by trypsin treatment and stained for detection of active caspase-8 and active caspase-9 according to the instruction of the manufacturer. Cells were analysed on Guava® flow cytometer using InCyte® software. Acquired data were assessed for statistical significance between treated and none treated samples using an unpaired *t*-test with Welch's correction.

### 2.10.7. Percentages of cells positive for superoxide radical ($^{\bullet}O_2^-$) generation in mitochondria

The methodology has been previously described in details.[200] Breifly, cells were seeded in 96 well plates (0.1 mL per well) a day before the experiment. Investigated compounds were added at a concentration of 50 µM, and left or 6 hours on cells. After incubation was over, cells were detached from the bottom of wells by trypsin treatment and stained with MitoSox Red according to the instruction of the manufacturer. Cells were analysed on Guava® flow cytometer using InCyte® software, and classified according to the following parameters:

1. Percentage of cells with amplified $^{\bullet}O_2^-$ generation;
2. Mean fluorescent intensity (MFI, correlates to the average flow of $^{\bullet}O_2^-$ per cell in $^{\bullet}O_2^-$-positive subpopulation), expressed in arbitrary units [AU].

Acquired MFI data were assessed for statistical significance using the Kruskal-Wallis test with an unpaired *t*-test with Welch's correction as a post-test.

### 2.10.8. Assessment of compounds' ability to impact motility of treated cells

The methodology has been previously described in details.[200]. Briefly, cells were seeded in 96 well plates (0.1 mL per well), and left for several days to form confluency. A day before the experiment, full DMEM medium was changed with FBS-free DMEM and cells were incubated for another 18 hours. A scratch in a confluent monolayer was made, cells were stained with CAM and recorded on Celigo® cytometer, followed by FBS-free DMEM removal and addition of investigated compounds prepared in DMEM with 1 % FBS. Cells were incubated with investigated compounds for 24 hours, when CAM staining and Celigo® imaging were repeated. TScratch software was used to compare scratch area between day 0 and day 1 (24 hours) of treatment, and presented as % of open wound area. Acquired data were assessed for statistical significance using Kruskal-Wallis test and unpaired t-test with Welch's correction.

## 2.11. Characterization of cinnamides

*N*'-((*E*)-2-(pyridin-2-ylmethylene)hydrazinecarbonothioyl)cinnamohydrazide **(CimTCH$_{2fp}$)**
The compound was obtained as a white powder (69% yield), mp 205-206 ˚C. Formula: $C_{16}H_{15}N_5OS$ (*Mw* =325.10 g mol$^{-1}$): Calculated: C, 59.06; H, 4.65; N, 21.52; S, 9.85%; Found: C, 59.01; H, 4.59; N, 21.46; S, 9.78 %. IR-ATR (cm$^{-1}$): C=S (1283.80), C=N (1628.54), C=O (1673.25), NH (3180.70), NH amide (3250.17). $^1$H NMR (400 MHz, DMSO-$d_6$, $\delta$ (ppm)): 12.04 (*s*, H-N$_2$, 1H), 10.47 (*s*, H-N$_3$, 1H), 10.30 (*s*, H-N$_4$, 1H), 8.60 (*d*, H–C$_6$, $^3J_{6,5}$ = 4.3 Hz 1H), 8.40 (*d*, H-C$_3$, $^3J_{3,4}$ = 8.0 Hz, 1H), 8.15(*s*, H-C$_7$, 1H), 7.87 (*td*, H-C$_4$, $^3J_{4,3}$ = 7.8 Hz, $^3J_{4,5}$ = 1.2 Hz, 1H), 7.64 (*d*, H-C$_{13}$ = H-C$_{17}$, $^3J_{13,14}$ = $^3J_{17,16}$ = 6.7 Hz, 2H), 7.59 (*d*, H-C$_{11}$, $^3J_{11,10}$ = 15.9 Hz, 1H), 7.48 – 7.37 (*m*, H-C$_{14}$= H-C$_{16}$, H-C$_{15}$, H-C$_5$, 4H), 6.78 (*d*, H-C$_{10}$, $^3J_{10,11}$ = 15.9 Hz, 1H). $^{13}$C NMR (101 MHz, DMSO-$d_6$, $\delta$ (ppm)): 179.26 (C$_8$), 164.60 (C$_9$), 153.65 (C$_2$), 149.84 (C$_6$), 143.99 (C$_7$), 140.69 (C$_{11}$), 136.98 (C$_4$), 135.08 (C$_{12}$), 130.30 (C$_{14}$ = C$_{16}$), 129.49 (C$_{15}$), 128.18 (C$_{13}$=C$_{17}$), 124.73 (C$_5$), 120.93 (C$_3$), 120.11 (C$_{10}$).

*N*'-((*E*)-2-(2-hydroxybenzylidene)hydrazinecarbonothioyl)cinnamohydrazide **(CimTCH$_{sal}$)**
The compound was obtained as a white powder (86% yield), mp 197-200 ˚C. Formula: $C_{17}H_{16}N_4O_2S$ (*Mw* =340.10 g mol$^{-1}$): Calculated: C, 59.98; H, 4.74; N, 16.46; S, 9.42 %; Found: C, 53.33; H, 3.80; N, 19.35; S, 8.79 %. IR-ATR (cm$^{-1}$): C=S (1276.27), C=N (1628.56), C=O (1667.33), NH (3257.87), NH amide (3333.85). $^1$H NMR (400 MHz, DMSO-$d_6$, $\delta$ (ppm)): 11.77 (*s*, H-N$_2$, 1H), 10.25 (*s*, H-N$_3$, C-OH, 2H), 9.93 (*s*, H-N$_4$, 1H), 8.44(*s*, H-C$_7$, 1H), 8.05 (*d*, H–C$_6$, $^3J_{6,5}$= 5.6 Hz, 1H), 7.63 (d, H-C$_{17}$ = H-C$_{13}$, $^3J_{13,14}$ = $^3J_{17,16}$ = 7.1 Hz, 2H), 7.58 (*d*, 1H, H-C$_{11}$, $^3J_{11,10}$ = 15.9 Hz), 7.49 – 7.38 (*m*, H-C$_{15}$, H-C$_{14}$=H-C$_{16}$, 3H), 7,25 (*t*, H–C$_4$, *J* = 7.6 Hz, 1H,), 6,90 (*d*, H–C3, $^3J_{3,4}$ = 8.2 Hz, 1H), 6,85 (*t*, H–C$_5$, *J* = 7.5 Hz, 1H), 6.78 (*d*, H-C$_{10}$, $^3J_{10,11}$ = 15.8 Hz, 1H,). $^{13}$C NMR (101 MHz, DMSO-$d_6$, $\delta$ (ppm)): 178.66 (C$_8$), 164.55 (C$_9$), 157.06 (C$_1$), 140.55 (C$_7$), 135.09 (C$_{11}$), 131.78 (C$_{12}$), 130.28 (C$_5$), 129.50 (C$_{15}$), 128.24 (C$_{14}$ = C$_{16}$), 128.16 (C$_{13}$ = C$_{17}$), 127.47 (C$_3$), 120.67 (C$_{10}$), 120.19 (C$_6$), 119.69 (C$_4$), 116.60 (C$_2$).

*N*'-((*E*)-2-((8-hydroxyquinolin-2-yl)methylene)hydrazinecarbonothioyl)cinnamohydrazide **(CimTCH$_{8OH2qu}$)**
The compound was obtained as a very slight yellow powder (88% yield), mp 204-206 ˚C. Formula $C_{20}H_{17}N_5O_2S$ (*Mw* =391.11 g mol$^{-1}$): Calculated: C, 61.37; H, 4.38; N, 17.89; S, 8.19%; Found: C, 61.30; H, 4.29; N, 17.79; S, 8.11%. IR-ATR (cm$^{-1}$): C=S (1270.12), C=N (1629.74), C=O (1668.25), NH (3166.72), NH amide (3298.26). $^1$H NMR (400 MHz, DMSO-$d_6$, $\delta$ (ppm)): 12.30 (*s*, H-N$_2$, 1H), 10.63 (*s*, H-N$_3$, 1H), 10.38 (*s*, H-N$_4$, 1H), 9.94 (*s*, OH, 1H), 8.56 (*d*, H–C$_3$, $^3J_{3,4}$ = 8,7 Hz, 1H), 8.33 (*d*, H–C$_4$, H–C$_7$, *J* = 7.7 Hz, 2H), 7.66 (*d*, H-C$_{13}$ = H-C$_{17}$, $^3J_{13,14}$ = $^3J_{17,16}$ = 7.2 Hz, 2H), 7.61 (*d*, H-C$_{11}$, $^3J_{11,10}$ = 15.9 Hz, 1H), 7.49 – 7.38 (*m*, H-C$_{14}$= H-C$_{16}$, H-C$_{15}$, H-C$_{5'}$, H-C$_{6'}$, 5H), 7.12 (*d*, H–C$_{7'}$, $^3J_{7',6'}$ = 7,4 Hz, 1H), 6.80 (*d*, H-C$_{10}$, $^3J_{10,11}$ = 15.9 Hz, 1H). $^{13}$C NMR (101 MHz, DMSO-$d_6$, $\delta$ (ppm)):

179.32 ($C_8$), 164.67 ($C_9$), 153.97 ($C_{8'}$), 152.12 ($C_2$), 143.85 ($C_7$), 140.76 ($C_{11}$), 138.68 ($C_6$), 136.64 ($C_4$), 135.03 ($C_{12}$), 130.35 ($C_{14}$ = $C_{16}$), 129.52 ($C_{15}$), 129.34 ($C_{6'}$), 128.70 ($C_5$), 128.21 ($C_{13}$=$C_{17}$), 120.03 ($C_{10}$), 119.08 ($C_3$), 118.23($C_{5'}$), 112.64 ($C_{7'}$).

*N*'-((*E*)-2-(1-(pyridin-2-yl)ethylidene)hydrazinecarbonothioyl)cinnamohydrazide **(CimTCH$_{2ap}$)**
The compound was obtained as a white powder (79 % yield), mp 170-173 ˚C. Anal: $C_{17}H_{17}N_5OS$ (*Mw* =339.12 g mol$^{-1}$): Calculated: C, 60.16; H, 5.05; N, 20.63; S, 9.45%; Found: C, 60.06; H, 4.98; N, 20.53; S, 9.35%. IR-ATR (cm$^{-1}$): C=S (1205.48), C=N (1615.58), C=O (1668.84), NH(3174.88), NH amide (3300.70). $^1$H NMR (400 MHz, DMSO-$d_6$, $\delta$ (ppm)): 10.80 (*s*, H-$N_2$, 1H), 10.30-10.42 (*br.m.ovlp*., H-$N_3$, H-$N_4$, 2H), 8.61 (*dd*, H–$C_6$, $^3J_{6,5}$ =4.8 Hz, $^3J_{6,4}$ =0.7 Hz, 1H), 8.56 (*d*, H-$C_3$, $^3J_{3,4}$ = 8.1 Hz, 1H), 7.83 (*td*, H-$C_4$, $^3J_{4,3}$ = 8.1 Hz, $^4J_{4,5}$ = 1.7 Hz, 1H), 7.64 (*d*, H-$C_{13}$ = H-$C_{17}$, $^3J_{13,14}$ = $^3J_{17,16}$ = 6.7 Hz, 2H), 7.59 (*d*, H-$C_{11}$, $^3J_{11,10}$ = 15.9 Hz, 1H), 7.47 – 7.39 (*m*, H-$C_{14}$= H-$C_{16}$, H-$C_{15}$, H-$C_5$, 4H), 6.80 (*d*, H-$C_{10}$, $^3J_{10,11}$ = 15.9 Hz, 1H), 2.44 (s, H-$C_{methyl}$, 3H). $^{13}$C NMR (101 MHz, DMSO-$d_6$, $\delta$ (ppm)): 179.70 ($C_8$), 164.44 ($C_9$), 154.96 ($C_2$), 148.96 ($C_6$), 144.39 ($C_7$), 140.66 ($C_{11}$), 136.79 ($C_4$), 130.31 ($C_{15}$), 129.51 ($C_{14}$ = $C_{16}$), 128.66 ($C_{12}$), 128.18 ($C_{13}$=$C_{17}$), 124.59 ($C_5$), 121.65 ($C_3$), 120.22 ($C_{10}$), 12.531($C_{methyl}$).

(*E*)-3-(3-chlorophenyl)-*N*'-((*E*)-2-(pyridin-2-ylmethylene)hydrazinecarbonothioyl)acrylohydrazide **(3-ClCimTCH$_{2fp}$)**
The compound was obtained as a beige powder (72% yield), mp 212-215 ˚C. Formula: $C_{16}H_{14}ClN_5OS$ (*Mw* =359.06 g mol$^{-1}$): Calculated: C, 53.41; H, 3.92; N, 19.46; S, 8.91%; Found: C, 53.39; H, 3.88; N, 19.40; S, 8.85%. IR-ATR (cm$^{-1}$): C=S (1289.58), C=N (1631.97), C=O (1677.01), NH (3177.54), NH amide (3253.67). $^1$H NMR (400 MHz, DMSO-$d_6$, δ (ppm)): 12.10 (s, H-$N_2$, 1H), 10.52 (s, H-$N_3$, 1H), 10.35 (s, H-$N_4$, 1H), 8.59 (d, H–$C_6$, $^3J_{6,5}$= 4.6 Hz, 1H), 8.41 (d, H-$C_3$, $^3J_{3,4}$ = 7.8 Hz, 1H), 8.14 (s, H-$C_7$, 1H), 7.86 (t, H-$C_4$, $^3J_{4,3}$ = 7.8 Hz, 1H), 7.73 (s, H-$C_{17}$, 1H), 7.65 – 7.61 (m, H-$C_{14}$, 1H), 7.58 (d, H-$C_{11}$, $^3J_{11,10}$ = 15.9 Hz, 1H), 7.49 (d, H-$C_{13}$, H-$C_{15}$, $^3J_{13,14}$ = $^3J_{15,14}$ = 4.5 Hz, 2H), 7,41 (m, H–$C_5$, 1H), 6.83 (d, H-$C_{10}$, $^3J_{10,11}$ = 15.9 Hz, 1H). $^{13}$C NMR (101 MHz, DMSO-$d_6$, δ (ppm)): 179.20 ($C_8$), 164.29 ($C_9$), 153.61 ($C_2$), 149.86 ($C_6$), 144.02 ($C_7$), 139.21 ($C_{11}$), 137.33 ($C_{12}$), 137.01 ($C_4$), 134.22 ($C_{16}$), 131.33 ($C_{15}$), 129.95 ($C_{13}$), 127.99 ($C_{17}$), 126.58 ($C_{14}$), 124.77 ($C_5$), 121.72 ($C_{10}$), 120.93 ($C_3$).

(*E*)-3-(3-chlorophenyl)-*N*'-((*E*)-2-(2-hydroxybenzylidene)hydrazinecarbonothioyl)acrylohydrazide **(3-ClCimTCH$_{sal}$)**
The compound was obtained as a beige powder (79% yield), mp 191-194 ˚C. Formula: $C_{17}H_{15}ClN_4O_2S$ (*Mw* =374.06 g mol$^{-1}$): Calculated: C, 54.47; H, 4.03; N, 14.95; S, 8.55%; Found: C, 54.38; H, 3.98; N, 14.87; S, 8.50%. IR-ATR (cm$^{-1}$): C=S (1267.48), C=N (1632.39), C=O (1670.34), NH(3182.42), NH amide (3345.63). $^1$H NMR (400 MHz, DMSO-$d_6$, $\delta$ (ppm)): 11.80 (*s*, H-$N_2$, 1H), 10.27 (*s*, H-$N_3$, $C_1$-OH, 2H), 9.95 (*s*, H-$N_4$, 1H), 8.44 (*s*, H-$C_7$, 1H), 8.06 (d, H–$C_6$, $^3J_{6,5}$= 6.1 Hz, 1H), 7.71 (s, H-$C_{17}$, 1H), 7.61 (dd, H-$C_{14}$, *J* = 4.9 Hz, 1H), 7.57 (d, H-$C_{11}$, $^3J_{11,10}$ = 15.9 Hz, 1H), 7.55-7.48 (m, H-$C_{13}$, H-$C_{15}$, 2H), 7,25 (t, H–$C_4$, $^3J_{4,3}$=$^3J_{4,5}$ = 7.7 Hz, 1H), 6.90 (d, H-$C_3$, *J* = 8.2 Hz, 1H), 6,85 (t, H–$C_5$, $^3J_{5,4}$=$^3J_{5,6}$ = 6.0 Hz, 1H), 6.82 (d, H–$C_{10}$, $^3J_{10,11}$ = 15.9 Hz, 1H,). $^{13}$C NMR (101 MHz, DMSO-$d_6$, $\delta$ (ppm)): 178.54 ($C_8$), 164.19 ($C_9$), 157.10 ($C_1$), 141.07 ($C_7$), 139.03 ($C_{11}$), 137.41 ($C_{12}$), 134.23 ($C_{16}$), 131.79 ($C_4$), 131.31 ($C_{13}$), 129.89 ($C_{15}$), 127.91 ($C_{17}$), 127.51 ($C_6$), 126.56 ($C_{14}$), 121.90 ($C_{10}$), 120.65 ($C_2$), 119.70 ($C_5$), 116,64 ($C_3$).

(*E*)-3-(3-chlorophenyl)-*N*'-((*E*)-2-((8-hydroxyquinolin-2-yl)methylene)hydrazinecarbonothioyl)acrylohydrazide **(3-ClCimTCH$_{9PH2qu}$)**
The compound was obtained as a beige powder (72% yield), mp 183.5-186 ˚C. Formula: $C_{20}H_{16}ClN_5O_2S$ (*Mw* =425.07 g mol$^{-1}$): Calculated: C, 56.40; H, 3.79; N, 16.44; S, 7.53%; Found: C, 56.31; H, 3.69; N, 16.36; S, 7.45%. IR-ATR (cm$^{-1}$): C=S (1219.42), C=N (1633.96), C=O (1669.11), NH (3207.77), NH amide (3353.15). $^1$H NMR (400 MHz, DMSO-$d_6$, $\delta$ (ppm)): 12.27 (s, H-$N_2$, 1H), 10.60 (s, H-$N_3$, 1H), 10.37 (s, H-$N_4$, 1H), 9.86 (s, $C_{8'}$-OH, 1H), 8.55 (d, H–$C_3$, $^3J_{3,4}$ = 8.7 Hz, 1H),

8.35-8.30 (m, H–$C_4$, H–$C_7$, 2H), 7.73 (s, H-$C_{17}$, 1H), 7.64 (d, H-$C_{14}$ $^3J_{13,14}$ = 2.9 Hz, 1H), 7.60 (d, H-$C_{11}$, $^3J_{11,10}$ = 16.0 Hz, 1H), 7.51 – 7.38 (m, H-$C_{13}$, H-$C_{15}$, H-$C_{5'}$, H-$C_{6'}$, 4H), 7.12 (dd, H–$C_{7'}$, $^3J_{7',6'}$ = 7.4, $^3J_{7',5'}$ = 1.1 Hz, 1H), 6.86 (d, H-$C_{10}$, $^3J_{10,11}$ = 16.0 Hz, 1H). $^{13}$C NMR (101 MHz, DMSO-$d_6$, $\delta$ (ppm)): 179.30 ($C_8$), 164.32 ($C_9$), 153.95 ($C_{8'}$), 152.11 ($C_2$), 143.89 ($C_7$), 139.20 ($C_{11}$), 138.69 ($C_6$), 137.38 ($C_{12}$), 136.62 ($C_4$), 134.23 ($C_{16}$), 131.32 ($C_{15}$), 129.93 ($C_{13}$), 129.33 ($C_{6'}$), 128.69($C_5$), 127.95($C_{17}$), 126.61 ($C_{14}$), 121.81 ($C_{10}$), 119.09 ($C_3$), 118.23 ($C_{5'}$), 112.61($C_{7'}$).

(*E*)-3-(3-chlorophenyl)-*N*'-((*E*)-2-(1-(pyridin-2-yl)ethylidene)hydrazinecarbonothioyl) acrylohydrazide **(3-ClCimTCH$_{2ap}$)**

The compound was obtained as a beige powder (63% yield), mp 179-181.5 ˚C. Formula: $C_{17}H_{16}ClN_5OS$ (*Mw* =373.08 g mol$^{-1}$): Calculated: C, 54.62; H, 4.31; N, 18.73; S, 8.58%; Found: C, 54.52; H, 4.21; N, 18.63; S, 8.48%. IR-ATR (cm$^{-1}$): C=S (1205.48), C=N (1629.31), C=O (1674.29), NH (3124.03), NH amide (3382.11). $^1$H NMR (400 MHz, DMSO-$d_6$, $\delta$ (ppm)): 10.81 (s, H-$N_2$, 1H), 10.37-10.41 (br.m.ovlp., H-$N_3$, H-$N_4$, 2H), 8.61 (d, H–$C_6$, $^3J_{6,5}$ =4.3 Hz, 1H), 8.55 (d, H-$C_3$, $^3J_{3,4}$ = 8.1 Hz, 1H), 7.83 (t, H-$C_4$, $^3J_{4,3}$ =$^3J_{4,5}$ = 7.1 Hz, 1H), 7.72 (s, H-$C_{17}$,1H), 7.64-7.61 (m, H-$C_{14}$, 1H), 7.58 (d, H-$C_{11}$, $^3J_{11,10}$ = 16.0 Hz, 1H), 7.48 (d, H-$C_{13}$= H-$C_{15}$, $^3J_{13,14}$=$^3J_{15,14}$ = 4.4vHz, 2H), 7,41 (т, H–$C_5$, 1H), 6.86 (d, H-$C_{11}$, $^3J_{11,10}$ = 16.0 Hz, 1H), 2.44 (s, H-$C_{methyl}$, 3H). $^{13}$C NMR (101 MHz, DMSO-$d_6$, $\delta$ (ppm)): 179.68 ($C_8$), 164.08 ($C_9$), 154.96 ($C_2$), 150.05 ($C_6$), 148.95 ($C_7$), 139.12 ($C_{11}$), 137.39 ($C_{12}$), 136.79 ($C_4$), 134.23 ($C_{16}$), 131.32 ($C_{15}$), 129.91 ($C_{13}$), 127.92 ($C_{17}$), 126.58 ($C_{14}$), 124.59 ($C_5$), 121.82 ($C_{10}$), 121.64 ($C_3$), 12.72 ($C_{methyl}$).

**(***E*)-3-(4-chlorophenyl)-*N*'-((*E*)-2-(pyridin-2-ylmethylene)hydrazinecarbonothioyl) acrylohydrazide **(4-ClCimTCH$_{2fp}$)**

The compound was obtained as a beige powder (79% yield), mp 217-219 ˚C. Formula: $C_{16}H_{14}ClN_5OS$ (*Mw* =359.06 g mol$^{-1}$): Calculated: C, 53.41; H, 3.92; N, 19.46; S, 8.91%; Found: C, 53.34; H, 3.87; N, 19.41; S, 8.86%. IR-ATR (cm$^{-1}$): C=S (1282.53), C=N (1628.00), C=O (1667.33), NH (3173.63), NH amide (3368.47). $^1$H NMR (400 MHz, DMSO-$d_6$, $\delta$ (ppm)): 12.06 (s, H-$N_2$, 1H), 10.49 (s, H-$N_3$, 1H), 10.34 (s, H-$N_4$, 1H), 8.59 (d, H–$C_6$, $^3J_{6,5}$= 4.8 Hz, 1H), 8.40 (d, H-$C_3$, $^3J_{3,4}$= 8 Hz, 1H) 8.14 (s, H-$C_7$, 1H), 7.87 (t, H-$C_4$, $^3J_{4,3}$= $^3J_{4,5}$ = 7.9 Hz, 1H), 7.67 (d, H-$C_{13}$, H-$C_{17}$, $^3J_{13,14}$= $^3J_{17,16}$ = 8.2 Hz, 2H), 7.59 (d, H-$C_{11}$, $^3J_{11,10}$ = 15.8 Hz, 1H), 7.51 (d, H-$C_{14}$, H-$C_{16}$, $^3J_{14,13}$= $^3J_{16,17}$ = 8.1 Hz, 2H,), 7,40 (t, H–$C_4$, $^3J_{4,3}$=$^3J_{4,5}$ = 6.3 Hz, 1H,), 6.78 (d, H-$C_{10}$, $^3J_{10,11}$ = 15.8 Hz, 1H). $^{13}$C NMR (101 MHz, DMSO-$d_6$, $\delta$ (ppm)): 179.26 ($C_8$), 164.42 ($C_9$), 153.61 ($C_2$), 149.82 ($C_6$), 144.00 ($C_7$), 139.37 ($C_{11}$), 137.02 ($C_4$), 134.75 ($C_{12}$), 134.03 ($C_{15}$), 129.90 ($C_{13}$, $C_{17}$), 129.53 ($C_{14}$, $C_{16}$), 124.74 ($C_5$), 120.96 ($C_3$), 120.89 ($C_{10}$).

(*E*)-3-(4-chlorophenyl)-*N*'-((*E*)-2-(2-hydroxybenzylidene)hydrazinecarbonothioyl) acrylohydrazide **(4-ClCimTCH$_{sal}$)**

The compound was obtained as a white powder (77% yield), mp 197-199 ˚C. Formula: $C_{17}H_{15}ClN_4O_2S$ (*Mw* =374.06 g mol$^{-1}$): Calculated: C, 54.47; H, 4.03; N, 14.95; S, 8.55%; Found: C, 54.39; H, 3.96; N, 14.85; S, 8.47%. IR-ATR (cm$^{-1}$): C=S (1226.23), C=N (1631.60), C=O (1669.99), NH (3178.32), NH amide (3301.54). $^1$H NMR (400 MHz, DMSO-$d_6$, $\delta$ (ppm)): 11.77 (s, H-$N_2$, 1H), 10.26 (s, H-$N_3$, $C_1$-OH, 2H), 9.94 (s, H-$N_4$, 1H), 8.44(s, H-$C_7$, 1H), 8.04 (d, H–$C_6$, $^3J_{6,5}$= 5.7 Hz, 1H), 7.66 (d, H-$C_{13}$= H-$C_{17}$, $^3J_{13,14}$ =$^3J_{17,16}$=8.5 Hz, 2H), 7.57 (d, H-$C_{11}$, $^3J_{11,10}$ = 15.9 Hz, 1H), 7.51 (d, H-$C_{14}$=H-$C_{16}$, $^3J_{14,13}$ =$^3J_{16,17}$=8.4 Hz 2H), 7,25 (t, H–$C_4$, $^3J_{4,3}$=$^3J_{4,5}$ = 7.7 Hz, 1H), 6.90 (d, H–$C_3$, $^3J_{3,4}$ = 8.2 Hz, 1H), 6,85 (t, H–$C_5$, $^3J_{5,6}$=$^3J_{5,4}$ = 7.5 Hz, 1H), 6.78 (d, H-$C_{10}$, $^3J_{10,11}$ = 15.9 Hz, 1H). $^{13}$C NMR (101 MHz, DMSO-$d_6$, $\delta$ (ppm)): 178.59 ($C_8$), 164.35 ($C_9$), 157.13 ($C_1$), 141.09 ($C_7$), 139.23 ($C_{11}$), 134.72 ($C_{12}$), 134.07 ($C_{15}$), 131.79 ($C_4$), 130.38 ($C_{14}$ = $C_{16}$),129.87 ($C_{13}$ = $C_{17}$), 129.53 ($C_6$), 121.00 ($C_{10}$), 120.54 ($C_2$), 119.70 ($C_5$), 116.70 ($C_3$).

(*E*)-3-(4-chlorophenyl)-*N*'-((Z)-2-((8-hydroxyquinolin-2-yl)methylene)hydrazinecarbonothioyl)acrylohydrazide **(4-ClCimTCH$_{8OH2qu}$)**

The compound was obtained as a beige powder (80% yield), mp 207-209 ˚C. Formula: $C_{20}H_{16}ClN_5O_2S$ (*Mw* =425.07 g mol-1): Calculated: C, 56.40; H, 3.79; N, 16.44; S, 7.53%; Found: C, 56.30; H, 3.70; N, 16.34; S, 7.42%. IR-ATR (cm$^{-1}$): C=S (1236.93), C=N (1633.02), C=O (1670.86), NH (3166.49), NH amide (3309.46). $^1$H NMR (400 MHz, DMSO-$d_6$, $\delta$ (ppm)): 12.28 (s, H-N$_2$, 1H), 10.62 (s, H-N$_3$, 1H), 10.39 (s, H-N$_4$, 1H), 9.89 (s, C$_{8'}$-OH, 1H), 8.56 (d, H–C$_3$, $^3J_{3,4}$ = 8.8 Hz, 1H), 8.37-8.30 (m, H–C$_4$, H–C$_9$, 2H), 7.68 (d, H-C$_{13}$ = H-C$_{17}$, $^3J_{13,14}$ = $^3J_{17,16}$ = 8.5 Hz, 2H), 7.60 (d, H-C$_{11}$, $^3J_{11,10}$ = 15.9 Hz, 1H), 7.52 (d, H-C$_{14}$= H-C$_{16}$, $^3J_{14,13}$ = $^3J_{16,17}$ = 8.5 Hz, 2H), 7.40 (d, H-C$_{5'}$, H-C$_{6'}$, 2H), 7.12 (d, H–C$_{7'}$, $^3J_{7',6'}$ = 7.5 Hz, 1H), 6.81 (d, H-C$_{10}$, $^3J_{10,11}$ = 15.9 Hz, 1H). $^{13}$C NMR (101 MHz, DMSO-$d_6$, $\delta$ (ppm)): 179.33 (C$_8$), 164.49 (C$_9$), 153.95 (C$_{8'}$), 152.11 (C$_2$), 143.89 (C$_7$), 139.42 (C$_{11}$), 138.68 (C$_6$), 136.63 (C$_4$), 134.76 (C$_{12}$), 134.01 (C$_{15}$), 129.93 (C$_{13}$ = C$_{17}$), 129.54 (C$_{14}$=C$_{16}$), 129.34 (C$_5$), 128.70 (C$_{6'}$), 120.85 (C$_{10}$), 119.08 (C$_3$), 118.24(C$_{5'}$), 112.63 (C$_{7'}$).

(*E*)-3-(4-chlorophenyl)-*N*'-((*Z*)-2-(1-(pyridin-2-yl)ethylidene)hydrazinecarbonothioyl) acrylohydrazide **(4-ClCimTCH$_{2ap}$)**

The compound was obtained as a beige powder (69% yield), mp 185.5-187.5 ˚C. Formula: $C_{17}H_{16}ClN_5OS$ (*Mw* =373.08 g mol$^{-1}$): Calculated: C, 54.62; H, 4.31; N, 18.73; S, 8.58%; Found: C, 54.52; H, 4.21; N, 18.63; S, 8.49%. IR-ATR (cm$^{-1}$): C=S (1233.48), C=N (1614.81), C=O (1667.26), NH (3178.47), NH amide (3303.21). $^1$H NMR (400 MHz, DMSO-$d_6$, $\delta$ (ppm)): 10.79 (s, H-N$_2$, 1H), 10.38 (s, H-N$_4$, H-N$_5$, 2H), 8.60 (s, H–C$_6$, 1H), 8.55 (d, H-C$_3$, $^3J_{3,4}$ = 7.8 Hz, 1H), 7.83 (t, H-C$_4$, $^3J_{4,3}$=$^3J_{4,5}$ = 7.8 Hz, 1H), 7.67 (d, H-C$_{13}$ = H-C$_{17}$, $^3J_{13,14}$ = $^3J_{17,16}$ = 7.9 Hz, 2H), 7.59 (d, H-C$_{11}$, $^3J_{11,10}$ = 15.8 Hz, 1H), 7.52 (d, H-C$_{14}$= H-C$_{16}$, $^3J_{14,13}$ = $^3J_{16,17}$ = 7.9 Hz, 2H),7.45-7.39 (m, H-C$_5$, 1H) 6.81 (d, H-C$_{10}$, $^3J_{10,11}$ = 15.8 Hz, 1H,), 2.45 (s, H-C$_{methyl}$,, 3H). $^{13}$C NMR (101 MHz, DMSO-$d_6$, $\delta$ (ppm)): 179.72 (C$_8$), 164.23 (C$_9$), 154.98 (C$_2$), 150.03 (C$_6$), 148.96 (C$_7$), 139.31 (C$_{11}$), 136.78 (C$_4$), 134.73 (C$_{12}$), 134.01 (C$_{15}$), 129.88 (C$_{13}$ = C$_{17}$), 129.53 (C$_{14}$=C$_{16}$), 124.57 (C$_5$), 121.63 (C$_{10}$), 120.93 (C$_3$), 12.70 (C$_{methyl}$).

(*E*)-3-(4-methoxyphenyl)-*N*'-((*Z*)-2-(pyridin-2-ylmethylene)hydrazinecarbonothioyl) acrylohydrazide **(4-MeOCimTCH$_{2fp}$)**

The compound was obtained as a curcuma coloured powder, 66% yield, mp 184-185 C˚. Formula: $C_{17}H_{17}N_5O_2S$ (Mw =355.11 g mol$^{-1}$): Calculated: C, 57.45; H, 4.82; N, 19.71; S, 9.02%; Found: C, 57.38; H, 4.77; N, 19.66; S, 9.00 %. ATR-FTIR ($\nu$/cm$^{-1}$): C=S (1285), C=N (1625.94), C=O (1662), NH (3164), NH Amide (3385). $^1$H NMR (400 MHz, DMSO-d$_6$, $\delta$ (ppm)): 12.04 (s, H-N$_2$, 1H), 10.46 (s, H-N$_3$, 1H), 10.21 (s, H-N$_4$, 1H), 8.59 (d, H–C$_6$, 3J$_{6,5}$= 4.5 Hz, 1H), 8.41 (d, H-C$_3$, $^3$J$_{3,4}$=7.9 Hz, 1H), 8.14 (s, H-C$_7$, 1H), 7.96-7.74 (m, H-C$_4$, 1H), 7.59 (d, H-C$_{13}$=H-C$_{17}$, $^3$J$_{13,14}$=$^3$J$_{17,16}$ = 8.7 Hz, 2H), 7.53 (d, H-C$_{10}$, J=15.8 Hz, 1H), 7.43-7.36 (m, H-C$_5$, 1H), 7.01 (d,H-C$_{14}$=H-C$_{16}$, $^3$J$_{14,13}$= $^3$J$_{16,17}$= 8.7 Hz, 2H), 6.63 (d, 1H, H-C$_{11}$, J=15.8 Hz), 3.81 (s,3H, H-OCH$_3$). $^{13}$C NMR (101 MHz, DMSO-d$_6$, δ (ppm)): 179.27 (C$_8$), 164.95 (C$_9$), 161.10 (C$_{15}$), 153.63 (C$_2$), 149.82 (C$_6$), 143.85 (C$_7$), 140.41 (C$_{10}$), 137.02 (C$_4$), 129.83 (C$_{13}$= C$_{17}$), 127.64 (C$_{12}$), 124.73 (C$_5$), 120.94 (C$_3$), 117.48 (C$_{11}$), 114.95 (C$_{14}$=C$_{16}$), 55.77 (C$_{18}$).

(*E*)-3-(4-methoxyphenyl)-*N*'-((*E*)-2-(2-hydroxybenzylidene)hydrazinecarbonothioyl) acrylohydrazide **(4-MeOCimTCH$_{sal}$)**

The compound was obtained as a white powder, 84% yield, mp 193-195 C˚. Formula: $C_{18}H_{18}N_4O_3S$ (Mw =370.11 g mol$^{-1}$): Calculated: C, 58.36; H, 4.90; N, 15.13; S, 8.65 %; Found: : C, 58.28; H, 4.81; N, 15.05; S, 8.55 %. ATR-FTIR ($\nu$/cm$^{-1}$): C=S (1253), C=N (1624), C=O(1657), NH(3230), NH Amide(3307). 1H NMR (400 MHz, DMSO-d$_6$, $\delta$ (ppm)): 11.75 (s, H-N$_1$, 1H), 10.22 (s, H-N$_2$ 1H), 10.14 (s, C$_1$-OH, 1H), 9.93 (s, H-N$_3$, 1H), 8.44 (s, H-C$_7$, 1H), 8.05 (d, H–C$_6$, $^3J_{6,5}$= 6.2 Hz, 1H), 7.58 (d, H-C$_{17}$ = H-C$_{13}$, J=8.6Hz, 2H), 7.52 (d, H-C$_{11}$, *J*=15.9 Hz, 1H), 7.25 (t, H-C$_4$, *J*=7.6Hz, 1H), 7.01 (d, H–C$_{14}$, H-C$_{16}$, *J*= 8.6 Hz, 2H), 6,89 (d, H–C$_3$, *J*=8.2 Hz, 1H), 6,85 (t, H–C$_5$, $^3J_{5,6}$ = $^3J_{4,5}$=7.4

Hz, 1H), 6.62 (d, H-$C_{10}$, *J*=15.8 Hz, 1H), 3.81 (s, H-$C_{18}$, 3H). 13C NMR (101 MHz, DMSO-d6, δ (ppm)): 178.82 ($C_8$), 167.68 ($C_9$), 161.11 ($C_{15}$), 157.06 ($C_1$), 140.85 ($C_7$), 140.28 ($C_{11}$), 131.78 ($C_4$), 129.80 ($C_{13}$ = $C_{17}$), 127.85 ($C_{12}$), 127.65 ($C_3$), 127.51 ($C_6$), 120.62 ($C_2$), 119,62 ($C_5$), 117,60 ($C_{10}$), 116.6 ($C_3$), 114.97 ($C_{14}$=$C_{16}$), 55.75 ($C_{18}$)

(*E*)-3-(4-methoxyphenyl)-*N*'-((*Z*)-2-((8-hydroxyquinolin-2-yl)methylene)hydrazinecarbonothioyl) acrylohydrazide **(4-MeOCimTCH$_{8OH2qu}$)**
The compound was obtained as white powder, 72% yield, mp 206.5-209 C°. Formula: $C_{21}H_{19}N_5O_3S$ (Mw =421.12 g mol$^{-1}$): Calculated: C, 59.84; H, 4.54; N, 16.62; S, 7.61 %; Found: C, 59.74; H, 4.46; N, 16.53; S, 7.54%. ATR-FTIR ($\nu$/cm$^{-1}$): C=S (1234), C=N (1631), C=O (1668), NH (3157), NH Amide (3308). 1H NMR (400 MHz, DMSO-$d_6$, δ (ppm)): 12.24 (s, H-$N_2$, 1H), 10.57 (s, H-$N_3$, 1H), 10.24 (s, H-$N_4$, 1H), 9.85 (s, OH, 1H), 8.55 (d, H–$C_3$, $^3J_{3,4}$ = 8.8 Hz, 1H), 8.24-8.40 (br.m.ovlp. H–$C_4$, H–$C_7$, 2H,), 7.60 (d, H-$C_{13}$=H-$C_{17}$, $^3J_{13,14}$ = $^3J_{17,16}$ = 8.7 Hz, 2H), 7.55 (d, H-$C_{11}$, J=15.8 Hz, 1H), 7.45 (d, H-C6', $^3J_{6,7}$=7.6 Hz, 1H), 7.40 (dd, H-C5', $3J_{5,6}$=8.0 Hz, $4J_{5,7}$=1.1 Hz, 1H), 7.12 (dd, H–$C_{7'}$, $^3J_{7,6}$=7.6 Hz, $^3J_{7,5}$=1.1 Hz, 1H), 7.02 (d, H-$C_{14}$=H-$C_{16}$, $^3J_{14,13}$=$^3J_{16,17}$=8.7 Hz, 2H) 6.65 (d, H-$C_{10}$, J=15.8 Hz, 1H), 3.81 (s, H-$OCH_3$, 3H). 13C NMR (101 MHz, DMSO-$d_6$, δ (ppm)): 179.29 ($C_8$), 165.00 ($C_9$), 161.12 ($C_{15}$), 153.94 ($C_{8'}$), 152.14 ($C_2$), 143.80 ($C_7$), 140.44 ($C_{11}$), 138.69 ($C_6$), 136.62 ($C_4$), 129.83 ($C_{13}$=$C_{17}$), 129.32 ($C_{12}$), 128.67 ($C_{6'}$), 127.67 ($C_5$), 119.10 ($C_3$), 118.23 ($C_{5'}$), 117.54 ($C_{10}$), 114.96 ($C_{14}$=$C_{16}$), 112.60 ($C_{7'}$), 55.78 ($C_{18}$).

(*E*)-3-(4-methoxyphenyl)-*N*'-((*E*)-2-(1-(pyridin-2-yl)ethylidene)hydrazinecarbonothioyl) acrylohydrazide **(4-MeOCimTCH$_{2ap}$)**
The compound was obtained as beige powder, 74% yield, mp 180.5-183 C°. Formula: $C_{18}H_{19}N_5O_2S$ (Mw =369.13 g mol$^{-1}$): Calculated: C, 58.52; H, 5.18; N, 18.96; S, 8.68 %; Found: C, 58.43; H, 5.09; N, 18.86; S, 8.58%. ATR-FTIR ($\nu$/cm$^{-1}$): C=S (1252), C=N (1616), C=O (1663), NH (3176), NH Amide (3303). 1H NMR (400 MHz, DMSO-$d_6$, δ (ppm)): 10.77 (s, H-$N_2$, 1H), 10.37 (s, H-$N_3$, 1H), 10.25 (s, H-$N_4$, 1H), 8.61(d, H-$C_6$, J=4.1 Hz, 1H), 8.55 (d, H-$C_3$, J= 8.1 Hz, 1H) 7.82 (dd, H-$C_4$, J= 11.5, 4.1 Hz, 1H), 7.59 (d, H-$C_{13}$, H-$C_{17}$, J= 8.6 Hz, 2H), 7.54 (d, H-$C_{11}$, J= 15.8 Hz, 1H) 7.45-7.38 (m, H-$C_5$, 1H) 7.01 (d, H-$C_{14}$, H-$C_{16}$, J=8.6 Hz, 2H) 6.65 (d, H-$C_{10}$, J= 15.8 Hz, 1H) 3.81 (s, H-$C_{18}$, 3H), 2.44 (s, H-$C_{7'}$, 3H). 13C NMR (101 MHz, DMSO-$d_6$, δ (ppm)): 179.74 ($C_8$), 164.76 ($C_9$), 161.10 ($C_{15}$), 154.98 ($C_2$), 149.93 ($C_7$), 148.95 ($C_6$), 140.36 ($C_{11}$), 136.78 ($C_4$), 129.81 ($C_{13}$ = $C_{17}$), 127.68 ($C_{12}$), 124.57 ($C_5$), 121.63 ($C_3$), 117.55 ($C_{10}$), 114.96 ($C_{14}$=$C_{16}$), 55.78 ($C_{18}$), 12.68 ($C_{7'}$).

(*E*)-3-(3-hydroxyphenyl)-*N*'-(2-((*E*)-pyridin-2-ylmethylene)hydrazine-1-carbonothioyl)acrylohydrazide (**3-OHCimTCH$_{2fp}$**)
The compound was obtained as beige powder, 68 % yield, mp 215-217 C°. Formula: $C_{16}H_{15}N_5O_2S$ (Mw =341.09 g mol$^{-1}$): Calculated: C, 56.29; H, 4.43; N, 20.51; S, 9.39% ; Found: C, 56.19; H, 4.33; N, 20.41; S, 9.30%. ATR-FTIR ($\nu$/cm$^{-1}$): C=S (1217.96), C=N (1630.02), C=O (1676.87), NH (3126.36), NH Amide (3316.33). $^1$H NMR (400 MHz, DMSO-$d_6$, δ (ppm)): 12.06 (s, H-$N_2$, 1H), 10.48 (s, H-OH-$C_{16}$, 1H), 10.31 (s, H-$N_3$, 1H), 9.64 (s, H-$N_4$, 1H), 8.59 (d, H–$C_6$, $^3J_{6,5}$= 4.6 Hz, 1H), 8.40 (d, H-$C_7$, 1H), 8.14 (s, H-$C_3$, $^3J_{3,4}$ = 7.8 Hz, 1H), 7.86 (t, H-$C_4$, $^3J_{4,3}$ = 7.8 Hz, 1H), 7,49 (d, H–$C_5$, 1H), 7.40 (dd, H-$C_{11}$, $^3J_{11,10}$ = 15.9 Hz, 1H), 7.25 (t, H-$C_{14}$, 1H) 7.04 (m, H-$C_{13}$, -H-$C_{10}$, 2H), 6.83 (dd, H-$C_{15}$, 1H), 6.70 (d, H-$C_{17}$, 1H). $^{13}$C NMR (101 MHz, DMSO-$d_6$, δ (ppm)): 179.28 ($C_8$), 164.64 ($C_9$), 158.23 ($C_{16}$), 153.63 ($C_2$), 149.85 ($C_7$), 143.99 ($C_6$), 140.90 ($C_{11}$), 137.00 ($C_3$), 136.31 ($C_{12}$), 130.52 ($C_{14}$), 124.75 ($C_5$), 120.94 ($C_{13}$), 119.83 ($C_4$), 119.46 ($C_{10}$), 117.59 ($C_{17}$), 114.21 ($C_{15}$).

*N*'-(2-((*E*)-2-hydroxybenzylidene)hydrazine-1-carbonothioyl)cinnamohydrazide (**3-OHCimTCH$_{sal}$**)
The compound was obtained as beige powder, 61 % yield, mp 191-193 C°. Formula: $C_{17}H_{16}N_4O_3S$ (*Mw* =356.09 g mol$^{-1}$): Calculated: C, 57.29; H, 4.53; N, 15.72; S, 9.00 % ; Found: : C, 57.20; H, 4.43; N, 15.63; S, 8.93 %. ATR-FTIR ($\nu$/cm$^{-1}$): C=S (1232.54), C=N (1620.80), C=O (1660.98), NH(3162.58), NH Amide(3330.78). $^1$H NMR (400 MHz, DMSO) δ 11.75 (s, H-$N_2$, 1H), 10.22 (s, H-

N3, 1H), 9.93 (s, H-$N_4$ 1H), 9.61 (s, H-OH-$C_{16}$, 1H), 8.43 (d, H-$C_7$, *J* = 8.1 Hz, 1H), 8.04 (s, H-$C_{17}$, H-$C_{13}$, 1H), 7.47 (d, $C_3$, *J* = 15.8 Hz, 1H), 7.24 (m,H-$C_{16}$, H-$C_{14}$, 2H), 7.07 – 6.97 (m, H-$C_{15}$, H-$C_{11}$, 2H), 6.95 – 6.77 (m, H-$C_6$, H-$C_5$, H-$C_4$, 3H), 6.68 (d, H-$C_{10}$ J = 15.9 Hz, 1H). $^{13}$C NMR (101 MHz, DMSO-$d_6$, δ (ppm)): 179.58 ($C_8$), 169.25 ($C_9$), 157.06 ($C_6$), 140.55 ($C_7$), 135.09 ($C_{11}$), 131.78 ($C_{12}$), 130.28 ($C_4$), 129.50 ($C_{16}$ = $C_{14}$), 128.33 ($C_{17}$ = $C_{13}$), 127.53 ($C_{15}$), 120.67 ($C_3$), 120,35 ($C_4$), 119,62 ($C_{10}$), 117.99 ($C_2$). 115.21 ($C_5$).

(*E*)-3-(3-hydroxyphenyl)-*N'*-(2-((*E*)-(8-hydroxyquinolin-2-yl)methylene)hydrazine-1-carbonothioyl)acrylohydrazide (**3-OHCimTCH$_{8OH2qu}$**)

The compound was obtained as Yellow to brown powder, 62% yield, mp 194-196 C˚. Formula: $C_{20}H_{17}N_5O_3S$ (Mw =407.11 g mol-1): Calculated: C, 58.96; H, 4.21; N, 17.19; S, 7.87 %; Found: C, 58.86; H, 4.12; N, 17.09; S, 7.78%. ATR-FTIR ($\nu$/cm$^{-1}$): C=S(1224.51), C=N(1629.62), C=O(1667.79), NH(3159.45), NH Amide (3330.58). $^1$H NMR (400 MHz, DMSO) δ 12.28 (d, H-$N_2$ 1H), 10.60 (d, H-$N_3$, 1H), 10.35 (d, H-$N_4$, 1H), 9.89 (s, H-OH-$C_{8'}$, 1H), 9.65 (d, H-OH-$C_{16}$, 1H), 8.55 (q, H-$C_4$, *J* = 5.7, 3.6 Hz, 1H), 8.33 (dt, H-$C_7$, H-$C_3$ *J* = 8.4, 4.3 Hz, 2H), 7.47 (ddd, H-$C_{5'}$, H-$C_{6'}$, H-$C_{11}$, *J* = 27.1, 17.3, 8.0 Hz, 3H), 7.26 (q, H-$C_{14}$ *J* = 8.0 Hz, 1H), 7.18 – 6.96 (m, H-$C_{13}$, H-$C_{15}$, H-$C_{10}$, 3H), 6.84 (m, H-$C_{7'}$, 1H), 6.72 (m, H-$C_{17}$ 1H). $^{13}$C NMR (101 MHz, DMSO-$d_6$, δ (ppm)): 179.36 ($C_8$), 164.32 ($C_9$), 164.68 ($C_{8'}$), 1153.93 ($C_{16}$), 152.11 ($C_2$), 143.84 ($C_7$), 140.93 ($C_{11}$), 138.66 ($C_6$), 136.66 ($C_4$), 136.32 ($C_{15}$), 130.52 ($C_5$), 129.34 ($C_{14}$), 128.7 ($C_{6'}$), 119.84 ($C_{13}$), 119.47 ($C_3$), 119.09 ($C_{10}$), 118.24 ($C_{5'}$), 117.60 ($C_{17}$), 114.22 ($C_{15}$), 112.63 ($C_{7'}$).

*(*E)-3-(3-hydroxyphenyl)-N'-(2-((E)-1-(pyridin-2-yl)ethylidene)hydrazine-1-carbonothioyl)acrylohydrazide (**3-OHTCHCim$_{2ap}$**)

The compound was obtained as beige powder, 62% yield, mp 204-205.5 C˚. Formula: $C_{17}H_{17}N_5O_2S$ (Mw =355.11 g mol-1): Calculated: C, 57.45; H, 4.82; N, 19.71; S, 9.02 %; Found: C, 57.35; H, 4.72; N, 19.61; S, 8.92%. ATR-FTIR ($\nu$/cm$^{-1}$): C=S(1214.68), C=N(1623.14), C=O(1660.23), NH(3204.53), NH Amide (3308.88). $^1$H NMR (400 MHz, DMSO) δ 10.79 (s,H-$N_2$, 1H), 10.36 (d, br.m.ovlp., H-$N_3$, H-$N_4$ *J* = 13.8 Hz, 2H), 9.64 (s, H-OH-$C_{16}$, 1H), 8.58 (dd, H-$C_3$, H-$C_6$, *J* = 21.9, 6.5 Hz, 2H), 7.83 (m, H-$C_4$, 1H), 7.54 – 7.37 (m, H-$C_5$, H-$C_{11}$, 2H), 7.25 (t, H-$C_{14}$ *J* = 7.8 Hz, 1H), 7.04 (m, H-$C_{13}$, 1H), 6.83 (d, H-$C_{10}$, *J* = 8.1 Hz, 1H), 6.72 (d, $C_{17}$, *J* = 15.8 Hz, 1H), 2.44 (s, H-$C_{nethoxy}$ 3H). $^{13}$C NMR (101 MHz, DMSO-$d_6$, δ (ppm)): 179.75 ($C_8$), 164.44 ($C_9$), 158.23 ($C_{16}$), 154.99 ($C_2$), 150.01 ($C_6$), 148.96 ($C_7$), 140.84 ($C_{11}$), 136.78 ($C_4$), 136.36 ($C_{12}$), 130.51 ($C_{14}$), 124.58 ($C_5$), 121.63 ($C_3$), 119.90 ($C_{13}$), 119.44 ($C_{10}$), 117.56 ($C_{17}$), 114.2 ($C_{15}$), 12.70 ($C_{Methoxy}$).

(*E*)-3-(4-hydroxy-3-methoxyphenyl)-*N'*-(2-((*E*)-pyridin-2-ylmethylene)hydrazine-1-carbonothioyl)acrylohydrazide (**FerTCH$_{2fp}$**)

The compound was obtained as orange powder, 69% yield, mp 202-204 C˚. Formula: $C_{16}H_{15}N_5O_3S$ (Mw =375.09 g mol$^{-1}$): Calculated: C, 53.77; H, 4.23; N, 19.60; S, 8.97% ; Found: C, 53.67; H, 4.13; N, 19.50; S, 8.87%. ATR-FTIR (ν/cm$^{-1}$): C=S (1251.51), C=N (1630.72), C=O (1662.45), NH (3137.04), NH Amide (3348.35). $^1$H NMR (400 MHz, DMSO-$d_6$, δ (ppm)): 12.03 (s, H-$N_2$, 1H), 10.45 (s, H-$N_3$, 1H), 10.13 (s H-OH-$C_{15}$ 1H) 9.52 (s, H-$N_4$, 1H), 8.59 (d, H–$C_6$, $^3J_{6,5}$= 4.5 Hz, 1H), 8.45 (m, H-$C_7$, 1H) 8.14 (s, H-$C_3$, $^3J_{3,4}$=7.9 Hz, 1H), 7.99 (ddd, H-$C_4$, 1H), 7.86 (t, H-$C_5$, 1H), 7.40 (t, H-$C_{11}$, J=15.8 Hz 1H), 7.21 (d,H-$C_{15}$1H), 7.08 (dd, H-$C_{14}$, 1H), 6.85 (m, H-$C_{10}$, J=15.8 Hz, 1H), 6.60 (d, H-$C_{13}$, 1H), 3.84 (d, H-$OCH_3$, 3H). $^{13}$C NMR (1101 MHz, DMSO-d6, δ (ppm)): 178.06 ($C_8$), 165.09 ($C_9$), 149.12 ($C_2$), 148.38 ($C_{16}$), 141.42 ($C_{15}$), 131.90 ($C_{11}$), 127.75 ($C_5$), 126.56 ($C_{12}$), 122.33 ($C_{13}$), 120.66 ($C_3$), 119.63 ($C_{14}$), 116.86 ($C_4$), 116.76 ($C_{10}$), 116.61 ($C_7$), 116.10 ($C_6$), 111.43 ($C_{17}$), 56.06 (C-$_{Methoxy}$).

(*E*)-3-(4-hydroxy-3-methoxyphenyl)-*N'*-(2-((*E*)-2-hydroxybenzylidene)hydrazine-1-carbonothioyl)acrylohydrazide (**FerTCH$_{sal}$**)

The compound was obtained as a slight green powder, 63% yield, mp 180-182 C°. Formula:$C_{18}H_{18}N_4O_4S$ (Mw =386.10 g mol$^{-1}$): Calculated: C, 55.95; H, 4.70; N, 14.50; S, 8.30 %; Found: C, 55.85; H, 4.61; N, 14.41; S, 8.20 %. ATR-FTIR (ν/cm$^{-1}$): C=S (1254.40), C=N (1621.16), C=O (1659.61), NH(3274.41), NH Amide(3339.87). $^1$H NMR (400 MHz, DMSO-d$_6$, δ (ppm)): 11.75 (s, H-N$_2$, 1H), 10.07 (s, H-N$_3$, 1H) 9.96 (s, H-OH-C$_{16}$-H-C$_1$, 2H), 9.52 (s, H-OHC$_{15}$ ), 9.52 8.43 (s, H-N$_4$ 1H), 8.05 (d, H-C$_7$, 1H), 7.47 (m, H-C$_{11}$, J=15.9 Hz, 1H), 7.22 (m, H–C$_3$-C$_5$, 2H), 6.87 (dd, H–C$_{13}$-C$_{14}$-C$_6$-C$_4$, 4H), 6.59 (d, H-C$_{12}$1H) 6.83 (s, H-OCH$_3$, 1H). 13C NMR (1101 MHz, DMSO-d6, δ (ppm)): 178.00 (C$_8$), 165.04 (C$_9$), 149.12 (C$_1$), 148.35 (C$_{16}$), 140.96 (C$_{15}$), 131.76 (C$_{11}$), 127.51 (C$_5$), 126.63 (C$_{12}$), 123.97 (C$_2$), 122.20 (C$_{13}$), 120.70 (C$_3$), 119.69 (C$_{14}$), 116.91 (C$_4$), 116.82 (C$_{10}$), 116.63 (C$_7$), 116.23 (C$_6$), 111.59 (C$_{17}$), 56.07 (C-$_{Methoxy}$).

(*E*)-3-(3,4-dihydroxyphenyl)-*N'*-(2-((*E*)-2-hydroxybenzylidene)hydrazine-1-carbonothioyl)acrylohydrazide (**CafTCH$_{2fp}$**)

The compound was obtained as orange powder, 59% yield, mp 206-209 C°. Formula: $C_{16}H_{15}N_5O_3S$ (Mw =375.09 g mol$^{-1}$): Calculated: C, 53.77; H, 4.23; N, 19.60; S, 8.97% ; Found: C, 53.67; H, 4.13; N, 19.50; S, 8.87%. ATR-FTIR (ν/cm$^{-1}$): C=S (1251.51), C=N (1630.72), C=O (1662.45), NH (3137.04), NH Amide (3348.35). $^1$H NMR (400 MHz, DMSO-d$_6$, δ (ppm)): 12.03 (s, H-N$_2$, 1H), 10.44 (s, H-N$_3$, 1H), 10.17 (s, H-N$_4$, 1H), 9.44 (s H-OH-C$_{16}$ 1H), 9.21 (s, H-OH-C$_{15}$ 1H), 8.59 (d, H–C$_6$, $^3$J$_{6,5}$= 4.5 Hz, 1H), 8.40 (d, H-C$_3$, $^3$J$_{3,4}$=7.9 Hz, 1H), 8.14 (s, H-C$_7$, 1H), 7.86 (t, H-C$_4$, 1H), 7.40 (t, H-C$_5$- H-C$_{17}$ 2H), 7.03 (s, H-C$_{11}$, J=15.8 Hz 1H), 6.92 (d, H-C$_{10}$, J=15.8 Hz, 1H), 6.78 (d, H-C$_{14}$, 1H), 6.48 (d, H-C$_{16}$, 1H). $^{13}$C NMR (101 MHz, DMSO-d$_6$, δ (ppm)): 179.32 (C$_8$), 165.11 (C$_9$), 153.65 (C$_2$), 149.83 (C$_{15}$), 148.21 (C$_{16}$), 146.10 (C$_7$), 143.91 (C$_{11}$), 141.19 (C$_5$), 136.99 (C$_{12}$), 126.58 (C$_3$), 124.72 (C$_{13}$), 121.33 (C$_4$), 120.94 (C$_6$), 116.30 (C$_{10}$), 114.34 (C$_{14}$-C$_{17}$).

(*E*)-3-(3,4-dihydroxyphenyl)-*N'*-(2-((*E*)-pyridin-2-ylmethylene)hydrazine-1 carbonothioyl)acrylohydrazide (**CafTCH$_{sal}$**)

The compound was obtained as beige powder, 57% yield, mp 199-203 C°. Formula: $C_{17}H_{16}N_4O_4S$ (Mw =372.09 g mol$^{-1}$): Calculated: C, 54.83; H, 4.33; N, 15.05; S, 8.61 % ; Found: : C, 54.74; H, 4.23; N, 14.97; S, 8.51 %. ATR-FTIR (ν/cm$^{-1}$): C=S (1264.34), C=N (1615.69), C=O (1651.67), NH(3253.92), NH Amide(3343.23). $^1$H NMR (400 MHz, DMSO-d$_6$, δ (ppm)): 12.20 (s, H-N$_2$, 1H), 10.63 (s, H-N$_3$, 1H), 10.56 (s, H-N$_4$, 1H),9.45 (s H-C-OH-C$_1$, 1H) 9.25 (s H-OH-C$_{16,}$ 1H), 9.13 (s, H-OH-C$_{15}$ 1H), 8.63 (d, H–C$_6$, $^3$J$_{6,5}$= 4.5 Hz, 1H), 8.44 (d, H-C$_3$, $^3$J$_{3,4}$=7.9 Hz, 1H), 8.18 (s, H-C$_7$, 1H), 7.89 (t, H-C$_4$, 1H), 7.48 (t, H-C$_5$-C$_{17}$ 1H), 7.08 (s, H-C$_{11}$, J=15.8 Hz 1H), 6.96 (d, H-C$_{10}$, J=15.8 Hz, 1H), 6.75 (d, H-C$_{14}$, 1H), 6.46 (d, H-C$_{13}$, 1H). $^{13}$C NMR (101 MHz, DMSO-d$_6$, δ (ppm)): 179.34 (C$_8$), 165.16 (C$_9$), 153.67 (C$_1$), 149.84 (C$_{15}$), 148.28 (C$_{16}$), 146.14 (C$_7$), 143.881 (C$_{11}$), 141.15 (C$_5$), 137.08 (C$_{12}$), 126.61 (C$_3$), 124.76 (C$_{13}$), 121.35 (C$_4$), 120.94 (C$_6$), 116.38 (C$_{10}$-C$_2$), 114.41 (C$_{14}$-C$_{17}$).

## 3. Results and discussion

### 3.1. The structure and isomerism of thiocarbohydrazones in a solution

To study the solution structure, conformational preferences, and isomerism of cinnamic acid hydrazides, we first synthesized a series of four TCHs (Figure 7) and studied their properties. The conclusions gained from these experiments will serve as a basis for the elucidation of structural effects of more complex cinnamic acid hydrazides.

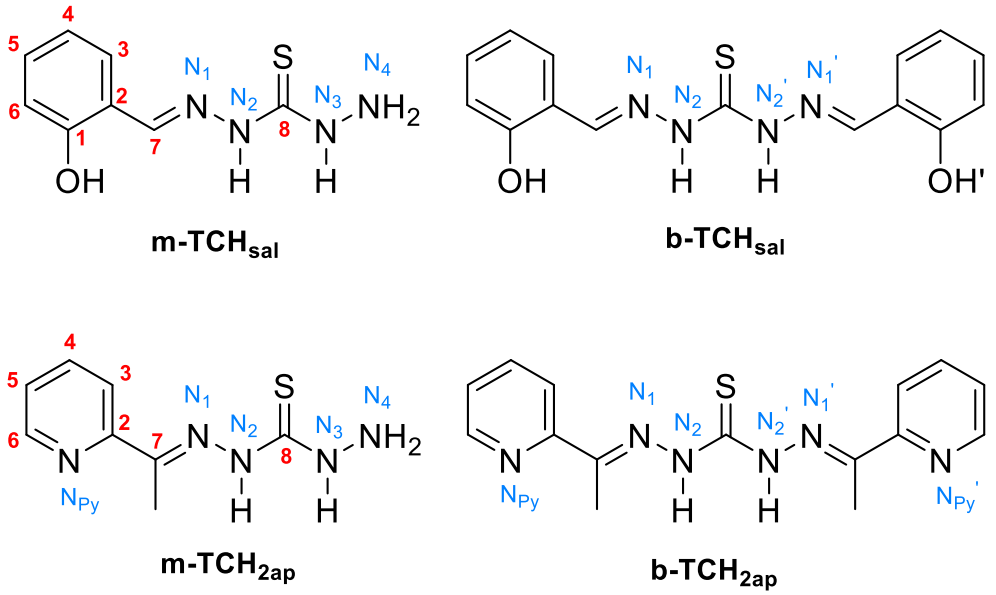


Figure 7. The structure of **m-TCHs** and **b-TCHs** along with corresponding atom numbering scheme

The (**m-TCH**) **m-TCH$_{sal}$** and **m-TCH$_{2ap}$** were obtained by mixing 2.35 mmol of salicylaldehyde or 2-acetylpyridine with 40 mL of a hot solution of 4.7 mmol of (DHS) in ethanol and adding the catalytic amount of concentrated HCl. The mixture was heated under reflux for 3 hours, and after cooling to room temperature the precipitate was filtered and rinsed with ice-cold ethanol. To synthesize **b-TCHs**, 2.1 eq. of carbonyl compound were combined with 1 eq. of DHS and the same procedure was applied (Scheme 14).

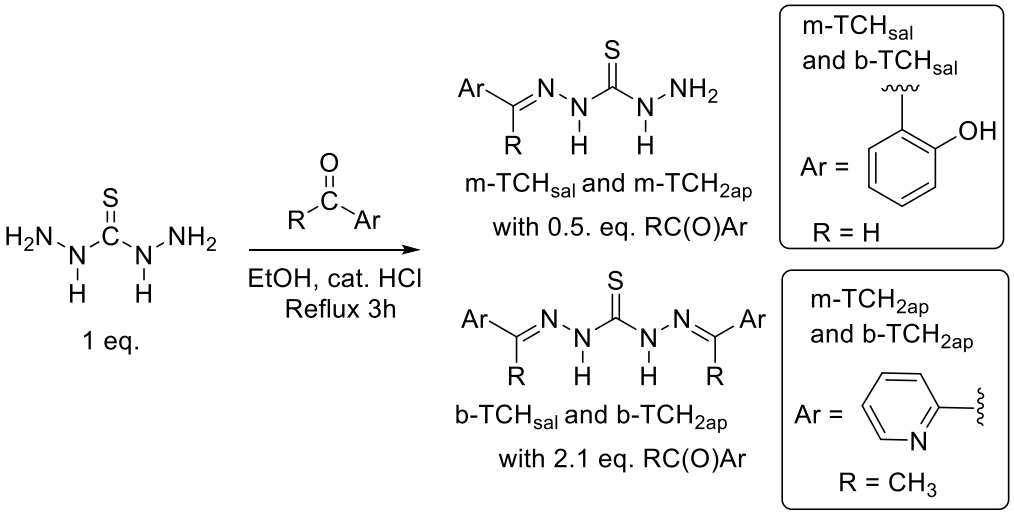


Scheme 14. The synthesis of **m-TCHs** and **b-TCHs**

The contribution of *E* and *Z* isomers of **m-TCH$_{sal}$** in solution was revealed from NMR spectra.
[(2-hydroxyphenyl)methylene]carbonothioic dihydrazide **(m-TCH$_{sal}$)**
Yellow solid (76 %); Melting point 186-187°C; IR (KBr, cm$^{-1}$) $\nu_{max}$: 3452s (OH), 3196s ($NH_2$), 3069m (NH), 2999w ($CH_{aryl}$), 1483s (amide II), 1282vs (C=S); Anal. Calc. For $C_8H_{10}N_4OS$ (210.06 g mol$^{-1}$): C, 45.70; H, 4.79; N, 26.65; S, 15,25 %, Found: C, 45.66; H, 4.77; N, 26.45; S, 15,18 %. The solvent for recrystallization: methanol. *E*:*Z Isomers ratio (81:19).*
*Isomer E*: $^1$H NMR (500 MHz, DMSO-$d_6$, $\delta$ ppm): 4.85 (s, 2H, $H_2$–$N_4$); 6.77-6.92 (*m*, 2H, H–$C_4$, H–$C_6$); 7.20 (*t*, 1H, H–$C_5$, $^3J_{5,6}$ = 6.3 Hz); 7.98 (*d*, 1H, H–$C_3$, $^3J_{3,4}$ = 6.5 Hz); 8.33 (s, 1H, H–$C_7$); 9.73 (*s*, 1H, H-$C_1$(OH)); 9.85 (*s*, 1H, H–$N_3$,); 11.35 (s, 1H, H–$N_2$). $^{13}$C NMR (126 MHz, DMSO-$d_6$, $\delta$ ppm,

TMS): 116.06 ($C_6$); 119.28 ($C_4$); 120.36 ($C_2$); 127.20 ($C_3$); 130.96 ($C_5$); 139.81 ($C_7$); 156.29 ($C_1$); 175.91 ($C_8$); $^{15}$N NMR (DMSO-$d_6$ at 298 K): 96.22 ($N_4$); 133.27 ($N_3$); 166.38 ($N_2$); 310.74 ($N_1$).
*Isomer Z*: $^1$H NMR (500 MHz, DMSO-$d_6$, $\delta$ ppm): 4.85 (s, 2H, $H_2$–$N_4$); 6.77-6.92 (*m*, 2H, H–$C_4$, H–$C_6$); 7.26-7.35 (*m*, 1H, H–$C_3$, H-$C_5$); 8.62 (s, 1H, H–$C_7$); 9.28-9.61 ((br.m.ovlp. 2H, H–$N_3$, H-$C_1$(OH)); 11.78 (s, 1H, H–$N_2$). $^{13}$C NMR (126 MHz, DMSO-$d_6$, $\delta$ ppm, TMS): 116.06 ($C_6$); 119.28 ($C_4$); 129.25 ($C_2$); 130.30 ($C_5$); 127.61($C_3$); 147.57 ($C_7$); 155.14 ($C_1$); 171.68 ($C_8$) (Figure 10).

The *E*-isomer of **m-TCH$_{2ap}$** was dominant in the solution, while the presence of thione/thiol isomerism was observed from NMR data.
*E*-[1-(2-pyridinyl)ethylidene]carbonothioic dihydrazide **(m-TCH$_{2ap}$)**
Yellow solid (88 %); Melting point 179-181ºC; IR (KBr, cm$^{-1}$) $\nu_{max}$: 3265s ($NH_2$), 3166m (NH), 3000w ($CH_{aryl}$), 1500vs (amide II), 1235s (C=S); Anal.Calc. For $C_8H_{11}N_5S$ (209.27 g mol$^{-1}$): C, 45.91; H, 5.30; N, 33.47; S, 15.32 %, Found: C, 45.82; H, 5.21; N, 33.32; S, 15.41 %. The solvent for recrystallization: ethanol. *Thione/Thiol form ratio (97:3)*
*Thione form:* $^1$H NMR (500 MHz, DMSO-$d_6$, $\delta$ ppm): 2.38 (s, 3H, $CH_3$); 4.98 (s, 2H, H–$N_4$); 7.36 (dd, 1H, H–$C_5$); 7.78 (td, 1H, H–$C_4$, $^3J_{4,3}$ =8.1 Hz ); 8.50 – 8.59 (*m*, 2H, H–$C_3$, H–$C_6$); 9.95 (s, 1H, H-$N_3$); 10.30 (s, 1H, H–$N_2$); $^{13}$C NMR (126 MHz, DMSO-$d_6$, $\delta$ ppm, TMS): 12.46 ($CH_3$); 121.55 ($C_3$); 124.28 ($C_5$); 136.71 ($C_4$); 148.72 ($C_7$); 148.81 ($C_6$); 155.20 ($C_2$); 176.68 ($C_8$); $^{15}$N NMR (DMSO-$d_6$, $\delta$ ppm): 72.47 ($N_4$); 136.01 ($N_3$); 162.31 ($N_2$); 310.70 ($N_{Ar}$); 313.11 (N1).
*Thiol form*: $^1$H NMR (500 MHz, DMSO-$d_6$, $\delta$ ppm): 2.37 (3H, $CH_3$); 4.98 (2H, H–$N_4$); 7.58 (1H, H–$C_5$); 8.08 (1H, H–$C_4$, $^3J_{4,3}$ =8.1 Hz); 8.77 (2H, H–$C_3$, H–$C_6$); 9.54 (s, 1H, H–$N_3$), 14.14 (s, 1H, H–S); $^{13}$C NMR (126 MHz, DMSO-$d_6$, $\delta$ ppm, TMS): 23.74 ($CH_3$); 121.74 ($C_3$); 123.35 ($C_5$); 137.28 ($C_4$); 148.27 ($C_7$); 149.33 ($C_6$); 159.93 ($C_2$); 171.97 ($C_8$) (Figure 8).

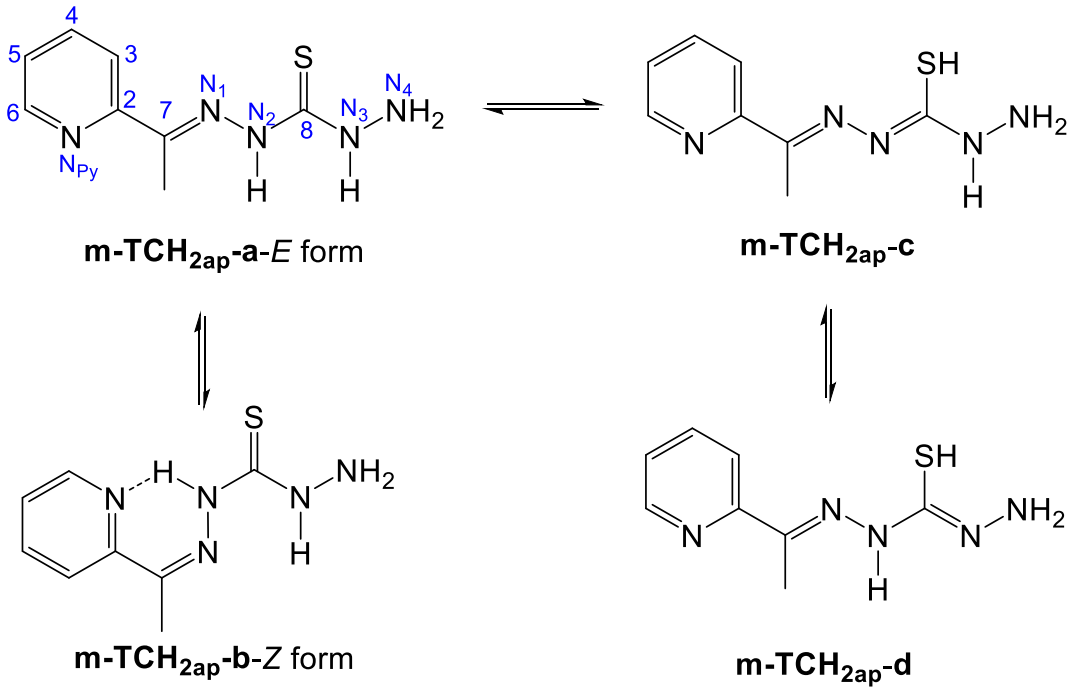


Figure 8. The plausible scheme for thione/thiol tautomerism and *E/Z* isomerism of **m-TCH$_{2ap}$**, along with the atom numeration

The synthesis of compounds **b-TCH$_{sal}$** and **b-TCH$_{2ap}$** is already described in the literature, so we only report their NMR data required for studying the isomerism.

2,2'-bis[(2-hydroxyphenyl)methylene]carbonothioic dihydrazide **(b-TCH$_{sal}$)**
$^{1}$H NMR (500 MHz, DMSO-$d_6$, $\delta$ ppm): 6.94 (*s*, 4H, H–C$_4$, H–C$_6$, H–C$_{4'}$, H–C$_{6'}$); 7.31 (*s*, 2H, H–C$_5$, H–C$_{5'}$); 7.43 (*s*, 1H, H–C$_{3'}$); 8.10 (*s*, 1H, H–C$_3$); 8.53 (*s*, 1H, H–C$_{7'}$); 8.79 (*s*, 1H, H–C$_7$); 10.06 (*s*, 1H, H-C$_{1'}$(OH)); 11.65 (*s*, 1H, H-C$_1$(OH)); 11.92 (s, 1H, H–N$_{2'}$); 12.10 (s, 1H, H–N$_2$). $^{13}$C NMR (126 MHz, DMSO-$d_6$, $\delta$ ppm, TMS): 116.72 (C$_{6'}$); 117.08 (C$_6$); 118.86 (C$_{2'}$);119.68 (C$_4$=C$_{4'}$); 120.49 (C$_2$); 127.46 (C$_{3'}$); 130.97 (C$_3$); 131.69 (C$_{5'}$); 132.01 (C$_5$); 141.59 (C$_{7'}$); 149.87 (C$_7$); 157.29 (C$_{1'}$); 157.53 (C$_1$); 175.86 (C$_8$).

2,2'-bis[1-(2-pyridinyl)ethylidene]carbonothioic dihydrazide **(b-TCH$_{2ap}$)**
*Thione/Thiol form ratio (85*:*15).Thione form*: $^{1}$H NMR (500 MHz, DMSO-$d_6$, $\delta$ ppm): 2.49 (*s*, 6H, CH$_3$´= CH$_3$); 7.45 (*dd*, 2H, H–C$_{5'}$ = C$_5$); 7.88-7.94 (*m*, 2H, H–C$_{4'}$ = C$_4$); 8.20 (*d*, 2H, H–C$_{3'}$ = H–C$_3$ );8.64 (*d*, 2H, H–C$_{6'}$ = H–C$_6$ ); 11.10 (s, 2H, H–N$_{2'}$ = N$_2$); $^{13}$C NMR (126 MHz, DMSO-$d_6$, $\delta$ ppm, TMS): 13.04 (CH$_3$´ = CH$_3$); 124.76 (C$_5$ = C$_{5'}$); 137.28 (C$_4$ = C$_{4'}$); 120.88 (C$_3$ = C$_{3'}$); 149.23 (C$_6$ = C$_{6'}$); 155.11 (C$_2$ = C$_{2'}$); 176.25 (C$_8$). *Thiol form*: $^{1}$H NMR (500 MHz, DMSO-$d_6$, $\delta$ ppm): 2.47 (*d*, 6H, CH$_3$´, CH$_3$); 7.50 (*t*, 1H, H–C$_{5'}$); 7.58 (*t*, 1H, C$_5$); 7.85-7.88 (*m*, 1H, H–C$_{4'}$); 8.00 (*t*, 1H, H–C$_4$); 8.11 (*t*, 2H, H–C$_{3'}$= C$_3$); 8.57 (*d*, 1H, H–C$_{6'}$); 8.67 (*d*, 1H, C$_6$); 10.98 (s, 1H, H–N$_2$), 15.41 (s, 1H, H–S); $^{13}$C NMR (126 MHz, DMSO-$d_6$, $\delta$ ppm, TMS): 22.83 (CH$_3$´ = CH$_3$); 124.84, 125.51 (C$_5$, C$_{5'}$); 125.31, 137.25 (C$_4$, C$_{4'}$); 139.11 (C$_3$ = C$_{3'}$); 148.14, 149,44 (C$_6$ , C$_{6'}$); 152.70 (C$_2$ = C$_{2'}$); 177.54 (C$_8$).

*E/Z* isomerism on C=N bond influences pharmacodynamics of Schiff bases as well as their metal chelating properties.[229] Moreover, thione/thiol isomerism is also important for pharmacokinetics and pharmacodynamics of biologically active compounds as it significantly changes the adsorption, distribution, metabolism, excretion, and toxicity (ADMET) properties and hydrogen-bonding preferences that drive the interactions with biological targets.[230]

In this dissertation, the solution structure of **m-TCH$_{sal}$, m-TCH$_{2ap}$, b-TCH$_{sal}$** and **b-TCH$_{2ap}$** was determined in DMSO/water mixtures using a variety of spectroscopic techniques, and the conclusions were supported by quantum chemical calculations. Different spectroscopic methods are applicable for the analysis of tautomeric equilibria. The absorption coefficients of isomers/tautomers are different, so UV-Vis spectroscopy could be utilized for studying the solvent-induced isomerism.[231] In case of structurally similar hydrazones derived from 2-(5-thioxo-4,5-dihydro-1,3,4-thiadiazol-2-ylthio)acetohydrazide, it was shown that the percentage of two conformers (*anti* and *syn*) in solution is clearly influenced by the strength of intramolecular hydrogen bond (IHB), which can be disrupted with the addition of water inducing conformational isomerism.[232] The light-induced changes are also observable using UV-Vis spectroscopy. For example, *E/Z* photoisomerization of pyridine-substituted semicarbazide Schiff bases is accompanied by batochromic shift in the absorption peak.[233,234] Moreover, the addition of water induces the conversion of thionamide into thiolimine (thione to thiol) tautomer.[235]

To study the water-induced isomerism, the UV-Vis spectra of compounds **m-TCH$_{sal}$**, **b-TCH$_{sal}$**, **m-TCH$_{2ap}$** and **b-TCH$_{2ap}$** were acquired in both DMSO and DMSO/water systems. The changes in peak intensity and wavelength clearly indicate water-induced *E* to *Z* isomerization or shift in thione-thiol equilibrium (Figure 9).

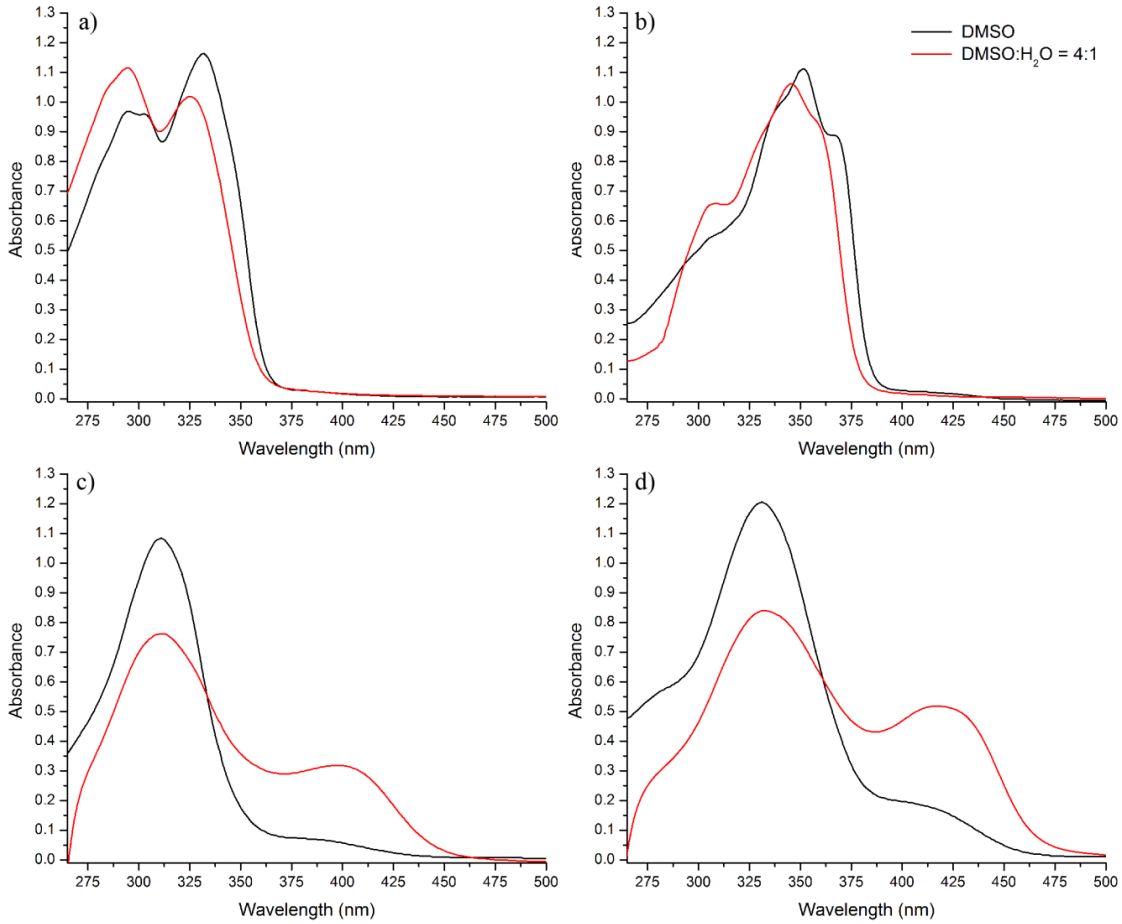


Figure 9. The water-induced UV-Vis spectra changes of: a) **m-TCH$_{sal}$**; b) **b-TCH$_{sal}$**; c) **m-TCH$_{2ap}$**; and d) **b-TCH$_{2ap}$** in DMSO

Previous studies revealed that the tautomeric equilibrium shift toward thiolimine form is accompanied by the occurrence of absorption peak at ~400 nm [235], while *E*/*Z* isomerization leads to similar effects in UV-Vis spectrum, i.e. red-shift of $\lambda_{max}$ [233,234]. Therefore, it is hard to describe the observed intensity increase of the peak at ~425 nm (Figure 9 c and d) to the one of these two effects.

To explain which of two phenomena occurs, we performed $^{1}$H NMR experiments. A typical downfield signal of thiolimine SH proton at ~15 ppm [236] was not observed in NMR spectra of **m-TCH$_{sal}$** and **m-TCH$_{2ap}$** (Figure 11 and Figure 14) which excluded the presence of thione/thiol tautomerism in mono- and bis-salicylaldehyde TCHs (**b-TCH$_{sal}$**). As a summary of UV-Vis and NMR results, we conclude that water induces *E*/*Z* isomerization in a DMSO solution of **m-TCH$_{sal}$** and **m-TCH$_{2ap}$**.

To gain more details on the mechanism of *E*/*Z* isomerization, we hypothesize that water addition in DMSO solution destabilize the ground state of **m-TCH$_{sal}$** by disrupting the IHB and reduce the height of energy barrier required for isomerization (Figure 10).

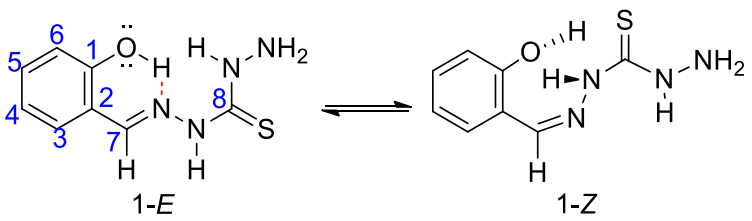


Figure 10. The *E*/*Z* isomerization scheme of **m-TCH$_{sal}$** along with atom numeration

Further evidences are gained from the analysis of $^{1}$H NMR spectrum of **m-TCH$_{sal}$** (Figure 11) The intensity of the peak at 11.73 ppm, ascribed to *Z*-isomer, increases with water addition, while the intensity of the peak at 11.37 ppm, assigned to *E*-isomer, decreases. The water addition into DMSO solution of **m-TCH$_{sal}$** causes a change of *E* and *Z* isomers ratio from 81:19 to 21:79. A previous study showed that the chemical shift of $N_2$-H proton of thiosemicarbazones, a structurally similar compounds, are downfield by 0.22 ppm upon light-induced *E*/*Z* isomerization.[233]

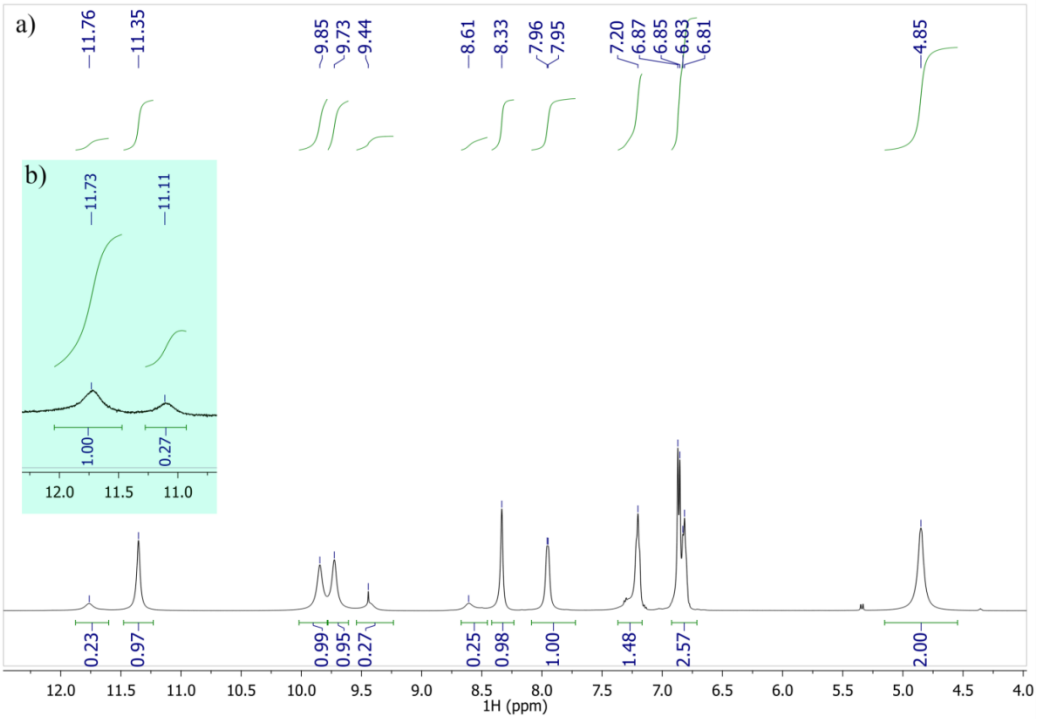


Figure 11. a) $^{1}$H NMR spectrum of **m-TCH$_{sal}$**; b) The change in the ratio of *E*- and *Z*- isomers after water addition in DMSO-$d_6$

The preference of **m-TCH$_{sal}$** toward *E*-configuration was elucidated from 2D NOESY spectrum, evidenced by through-space connectivity of H-atoms at $C_7$/$C_3$ and $OH$/$N_3$-$H$ (Figure 12).

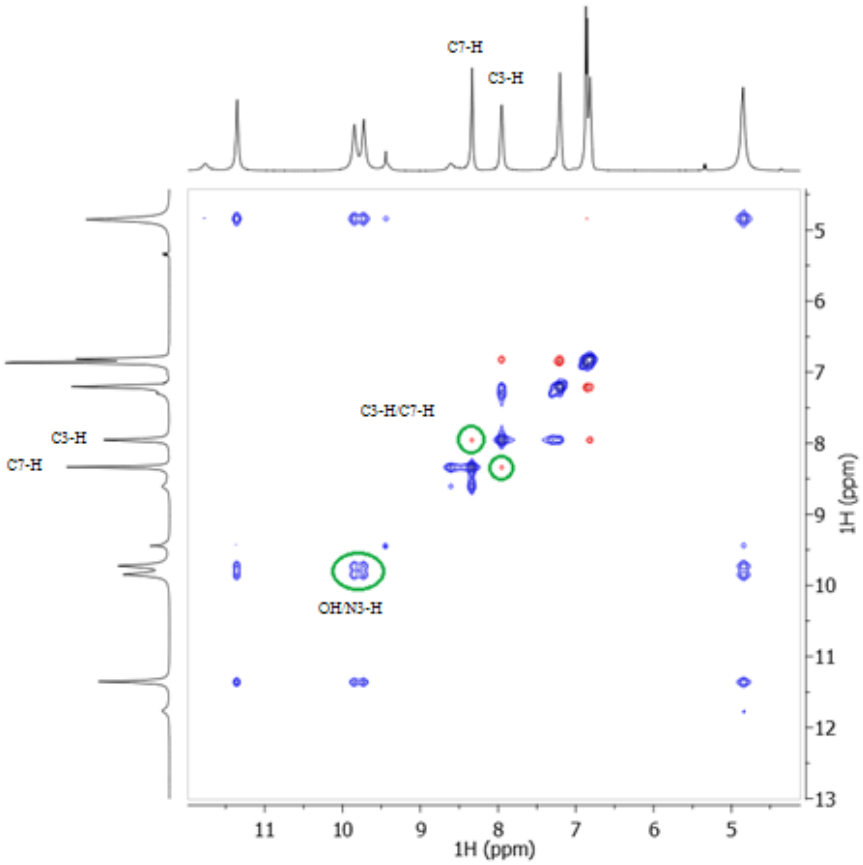


Figure 12. The NOESY spectrum of **m-TCH$_{sal}$**; solvent – DMSO-$d_6$

Two separated $^1$H NMR signals of H-atoms on hydrazide and imine N were observed for **b-TCH$_{sal}$** (Figure 14) although one may expect only one signal for such a symmetrical 2D structure. Similar separation of NH signals was observed for structurally similar symmetric bis(hydrazones).[26] Water causes small changes in the absorption spectrum of **b-TCH$_{sal}$** (Figure 9 b) and merges two $^1$H NMR signals of $N_2$-H and $N_2$'-H at 12.10 and 11.92 ppm (Figure 14 b) To explain this phenomenon, we computed $^1$H NMR spectra for (*E*,*E*)-, (*E*,*Z*)- and (*Z*,*Z*)-forms of **b-TCH$_{sal}$** using the gauge independent atomic orbital (GIAO) method. [216] The results (Figure 13) show that the chemical shifts of $N_2$-H and $N_2$'-H for (*E*,*E*)-isomer differ by 0.97 ppm, and this difference ($\Delta_\delta$) drops to 0.17 ppm after isomerization to (*E*,*Z*)-form. Finally, full isomerization to (*Z*,*Z*)-isomer results in a symmetrical structure with $\Delta_\delta$ = 0.01 ppm. According to that, the experimentally found fusion of N-H peaks (Figure 14) could be assigned to *E*-to-*Z* isomerism.

The thorough NMR analysis of a solution of **b-TCH$_{sal}$** in DMSO reveals that the compound was found to be in both (*E*,*Z*)-isomer, whereas the water addition cause the equilibrium shifting to (*Z*,*Z*)-form. The addition of low amount of water, which is always present in a hydroscopic solvents such as DMSO, might initiate isomerism from **b-TCH$_{sal}$**-(*E*,*E*) to **b-TCH$_{sal}$**-(*E*,*Z*). This claim is confirmed by $^{13}$C NMR data for **b-TCH$_{sal}$** that show two signals from olefinic C atoms (Figure 15) indicating the presence of two diastereomeric carbazone groups and the existence of **b-TCH$_{sal}$**-(*E*,*Z*) isomer in an investigated system. Additional confirmation of geometric preferences of **b-TCH$_{sal}$** was obtained from NOESY spectrum (Figure 16), as connectivity between H atoms at $N_2$ and $N_2$' is only possible for (*E*,*Z*) and (*Z*,*Z*)-isomers.

| | | Atom | Chemical shift, ppm |
|---|---|---|---|
| **b-TCH$_{sal}$** -(*E*,*E*) | 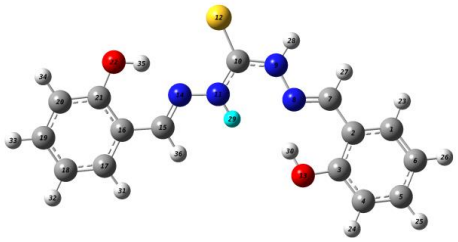 | N2-H | 9.40 |
| | | N2`-H | 8.43 |
| **b-TCH$_{sal}$** -(*E*,*Z*) | 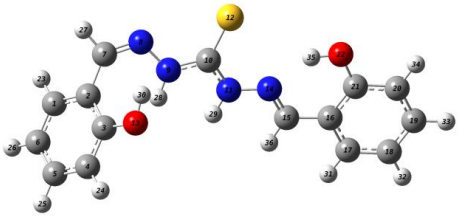 | Atom | Chemical shift, ppm |
| | | N2-H | 8.21 |
| | | N2`-H | 8.38 |
| **b-TCH$_{sal}$** -(*Z*,*Z*) | 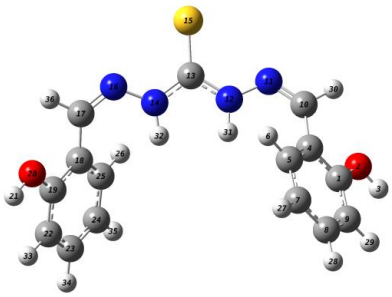 | Atom | Chemical shift, ppm |
| | | N2-H | 8.96 |
| | | N2`-H | 8.97 |

Figure 13. The GIAO/B3LYP-6-311G++(d,p) $^{1}$H NMR shifts for (*E*,*E*)-, (*E*,*Z*)- and (*Z*,*Z*)-isomers of **b-TCH$_{sal}$**. Effects of the solvent was simulated with IEF-PCM model of DMSO.

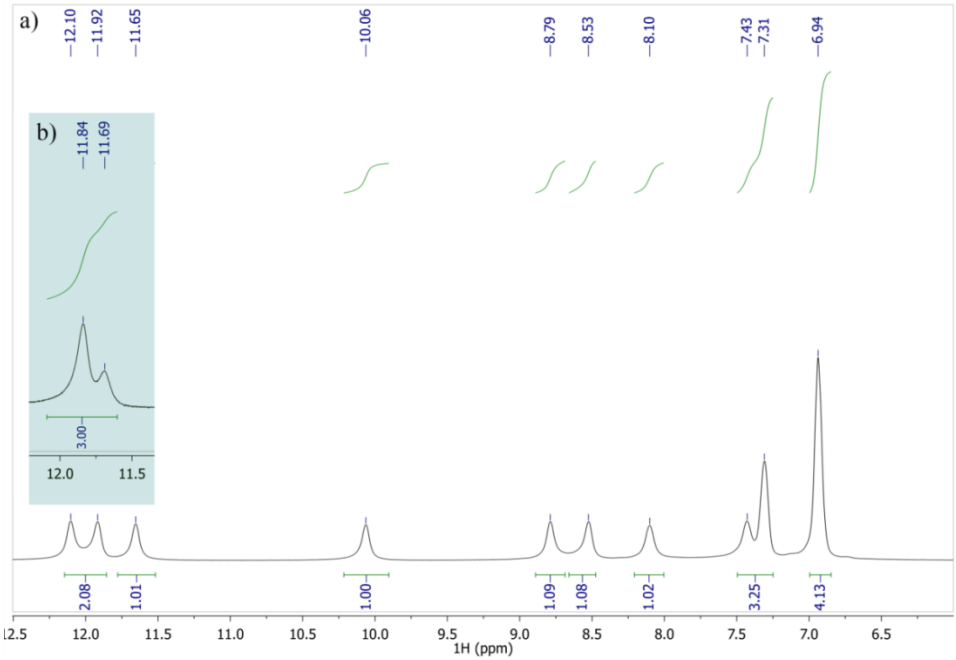


Figure 14. a). $^{1}$H NMR spectrum of **b-TCH$_{sal}$** in DMSO-$d_6$; b). The change in the intensity of overlapped $N_2$-H and $N_2$`-H signals

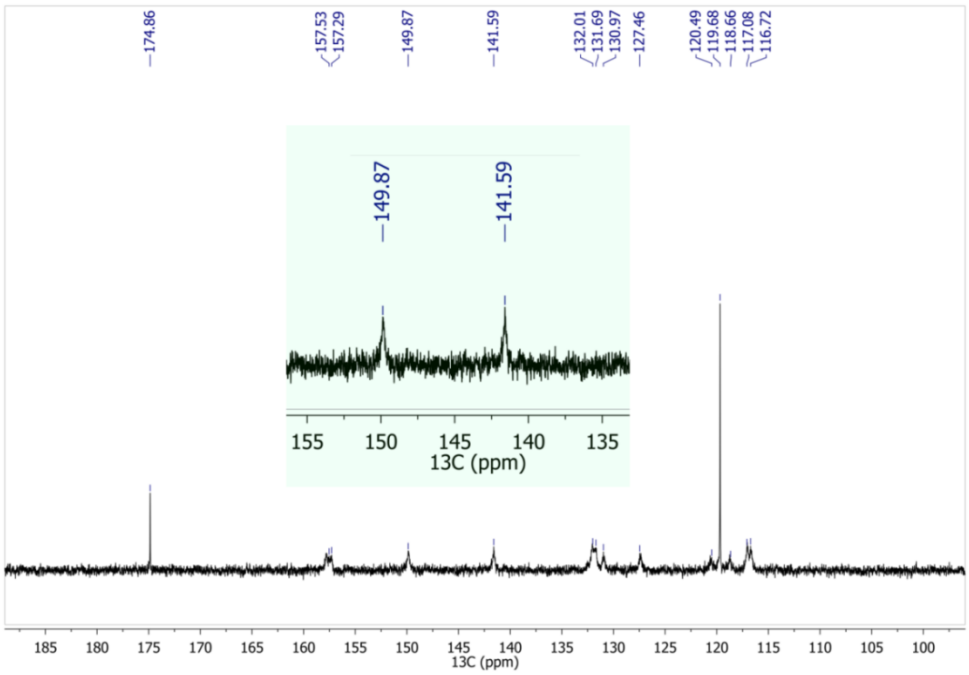


Figure 15. $^{13}$C NMR spectrum of **b-TCH$_{sal}$**; solvent - DMSO-$d_6$

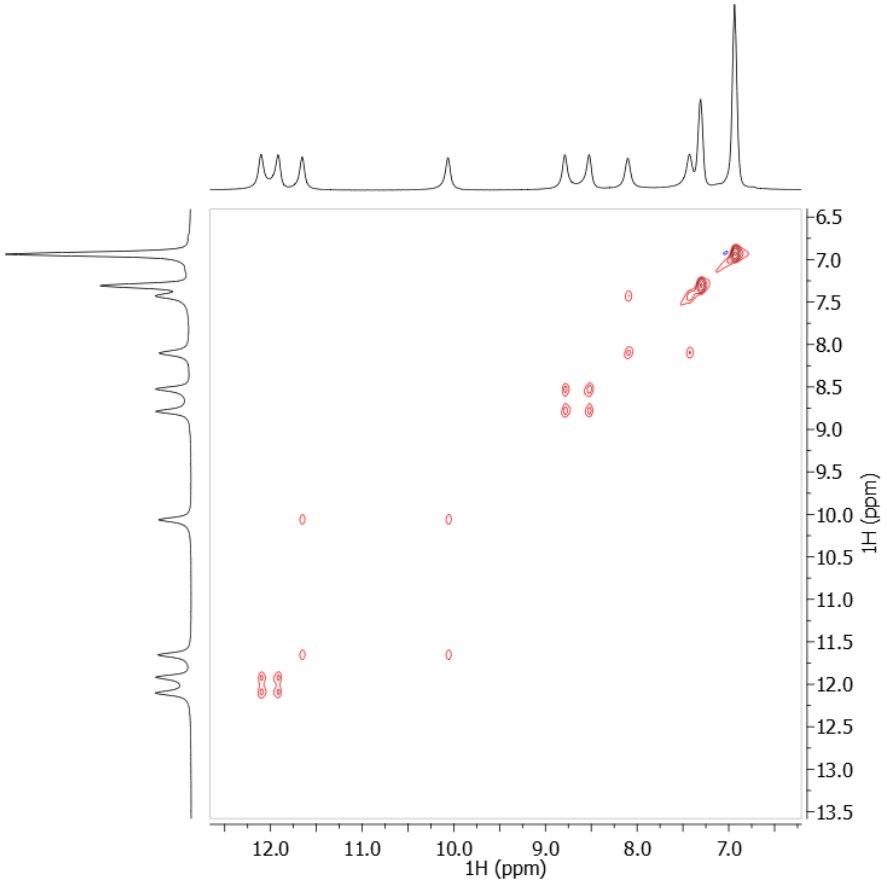


Figure 16. The NOESY spectrum of **b-TCH$_{sal}$** in DMSO-$d_6$

Compared to compound **b-TCH$_{sal}$**, **b-TCH$_{2ap}$** shows different structural preferences in a solution although both molecules are **bis-TCHs**. According to the results of $^{13}$C NMR spectrum (Figure 17), no diastereomeric C atoms were observed. Moreover, $^{1}$H NMR data of **b-TCH$_{2ap}$** indicate a fully symmetric structure of a molecule (Figure 18). This can be explained by the restricted flexibility of

**b-TCH$_{2ap}$** that increases the energy barrier for *E*/*Z* isomerization due to the presence of methyl group at $C_7$, which results in the more abundant symmetric configuration.[26]

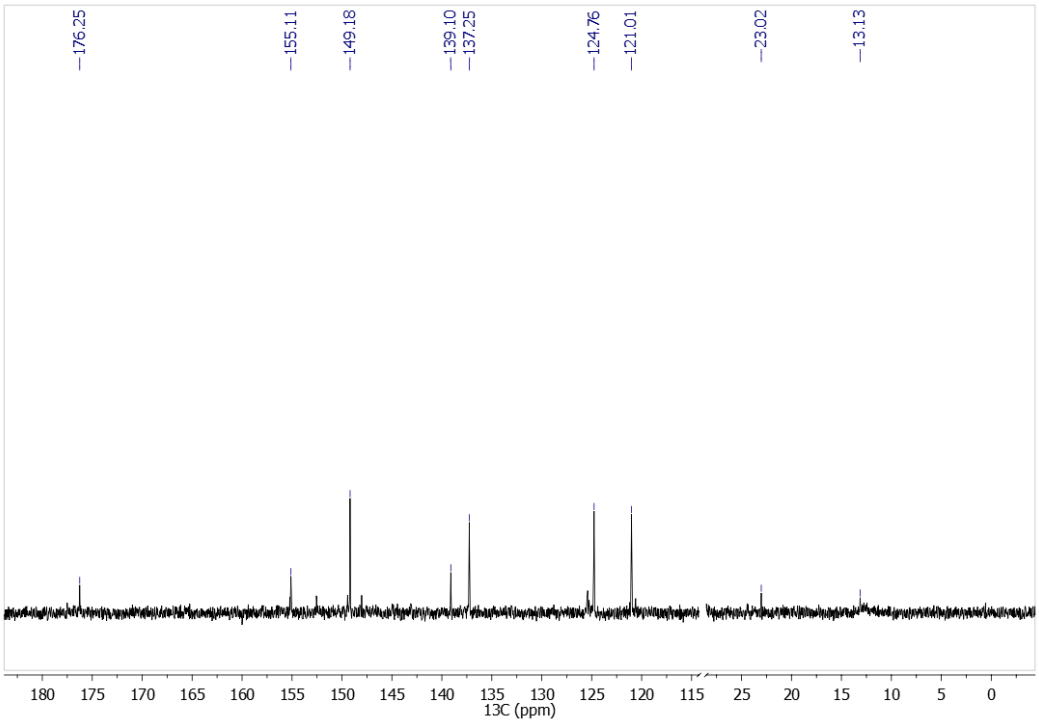


Figure 17. $^{13}$C NMR spectrum of **b-TCH$_{2ap}$** in DMSO-$d_6$

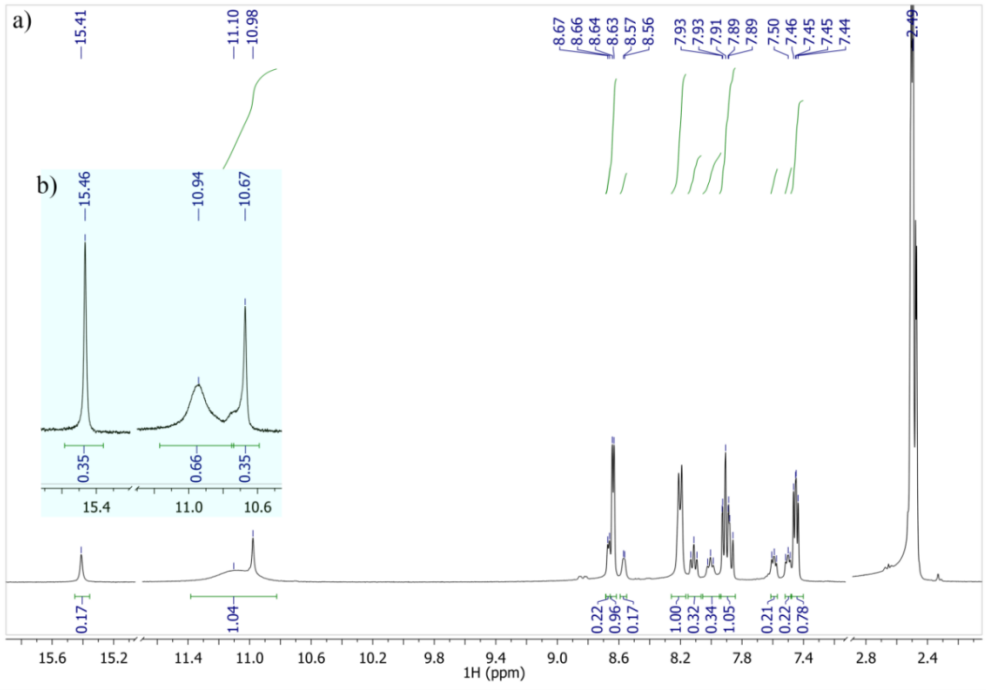


Figure 18. $^1$H NMR spectrum of **b-TCH$_{2ap}$**; b) The inset of $^1$H NMR spectrum of **b-TCH$_{2ap}$** in DMSO-$d_6$/water mixture that show increased intensity of S-H signal.

Contrary to compounds **m-TCH$_{sal}$** and **b-TCH$_{sal}$** that undergo *E*/*Z* isomerism, the water addition in DMSO solution of **m-TCH$_{2ap}$** and **b-TCH$_{2ap}$** induces thione to thiol tautomerism. This was revealed from the increased intensity of NMR signal at 14.14 and 15.41 ppm (Figure 18 and Figure 14) which is typical for thiolimine –SH proton [235,236]. The all-*E* configuration of compounds **m-TCH$_{2ap}$** and **b-TCH$_{2ap}$** is deduced from NOESY cross-peak of –$CH_3$ groups and $N_2$-H atoms

(Figure 20), as well as the absence of through-space correlations between -$CH_3$ and $C_3$-H expected for *Z*-forms (**m-TCH$_{2ap}$-b-*Z*** form, Figure 8).

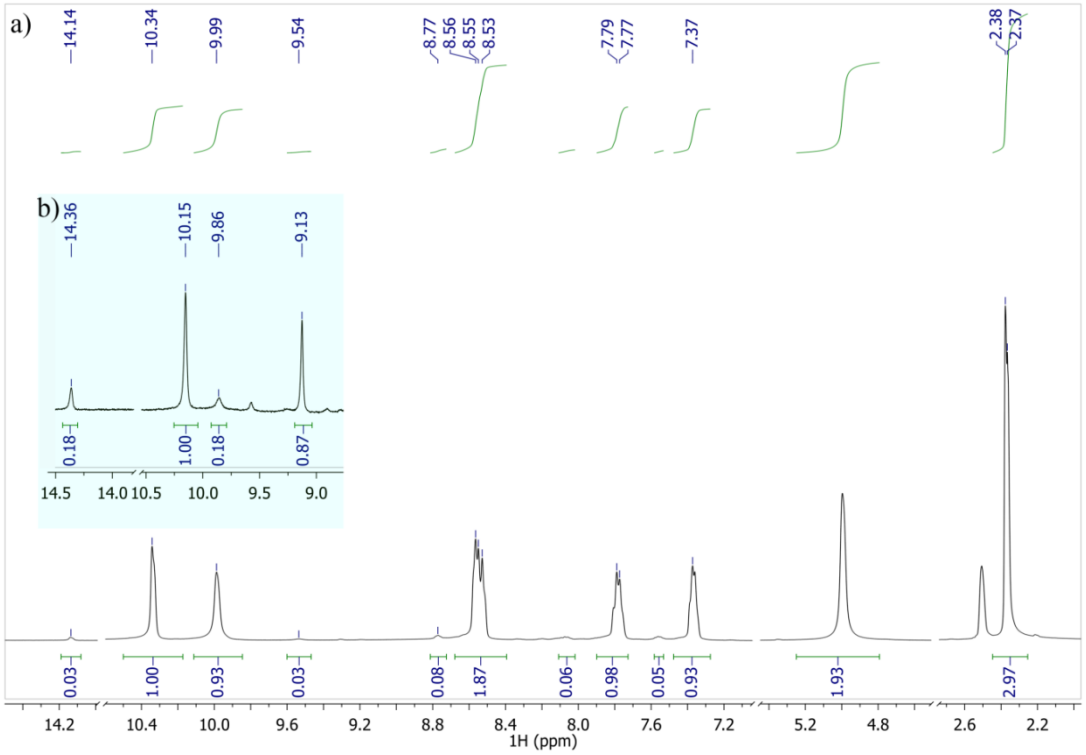


Figure 19. $^1$H NMR spectrum of **m-TCH$_{2ap}$** in DMSO-$d_6$; b) The magnified part of NMR spectrum showing the increased intensities of S-H and N-H peaks

Concerning the mechanism of *E*-to-*Z* isomerism, there are two main reaction routes: (1 torsional mode around azomethine bond, and 2) *in plane* inversion via transition state having a linear geometry with *sp* hybridized N atom.[237] Analogy with the isomerism of azobenzene suggests that the torsional pathway is the most likely an isomerization mechanism of TCHs.[237,238] Taking into account that steric effects hinder the torsional *E*/*Z* isomerism, we can explain the trends in TCHs, where **m-TCH$_{sal}$** and **b-TCH$_{sal}$** undergo *E*-to-*Z* isomerism while sterically more demanding **m-TCH$_{2ap}$** and **b-TCH$_{2ap}$** lack this phenomenon.

The proportion of thiol form in thione/thiol equilibrium of **m-TCH$_{2ap}$** and **b-TCH$_{2ap}$** increased with the addition of water, as revealed from the increase in corresponding $^1$H NMR peaks from 0.17 to 0.35 for **b-TCH$_{2ap}$** (Figure 18), and from 0.03 to 0.18 for **m-TCH$_{2ap}$** (Figure 19). Moreover, the intensity of absorption peak of compound **m-TCH$_{2ap}$** located at 400 nm increases (Figure 9 c), and the same effect is observed at 425 nm for **b-TCH$_{2ap}$** (Figure 9 d). This result is supported by quantum-chemical prediction of the absorption spectrum. Using time-dependent DFT calculations, we calculated the UV-Vis spectrum of **b-TCH$_{2ap}$** (Figure 21). The maximum of the absorption of thiolimine form is shifted batochromically by 19.7 nm in relation to thioneamime, and the new absorption peak was found at ~270 nm.

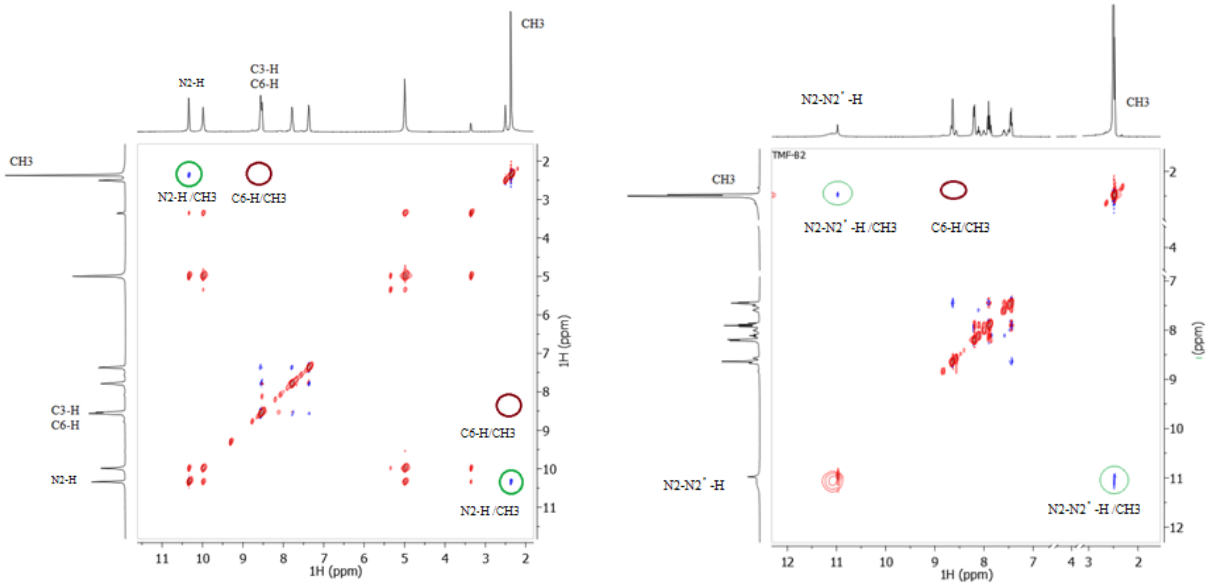


Figure 20. NOESY spectrum of **m-TCH$_{2ap}$** (left) and **b-TCH$_{2ap}$** (right); solvent: DMSO-$d_6$.

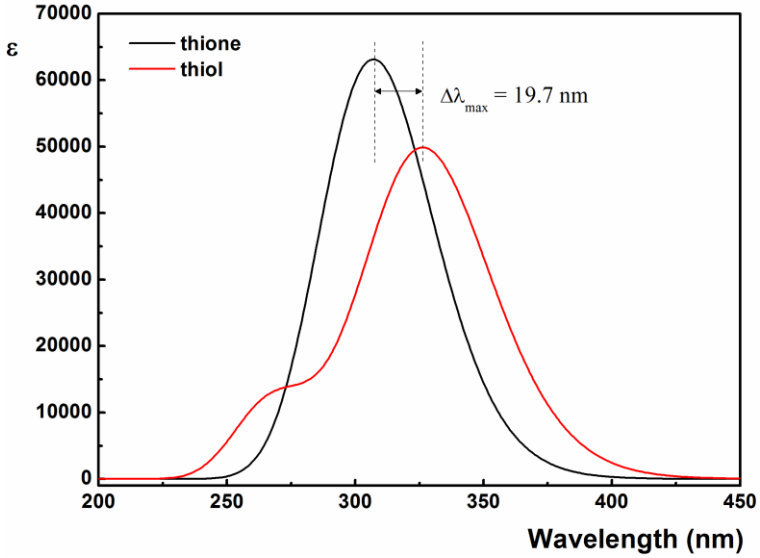


Figure 21. The calculated UV-Vis spectra of two tautomeric forms of **b-TCH$_{2ap}$**

The relative proportion of thiolimine form for **m-TCH$_{2ap}$** and **b-TCH$_{2ap}$** is deduced from the NMR peak intensities. The thioneamine:thiolimine ratio for compound **b-TCH$_{2ap}$** (1:0.35) is higher compared to **3** (1:0.18). This result can be explained by strong hydrogen bonding between solute and solvent, which dominate over IHB in pseudo-6-membered ring of 3-*Z* form (**m-TCH$_{2ap}$**-b-*Z*, Figure 8). Previous study revealed that the strong IHB in (*Z*)-bis(2-pyridyl)hydrazones results in $^1$H NMR signal at around 15 ppm,[239] but the peak at similar chemical shift observed in NMR spectra of **m-TCH$_{2ap}$** and **b-TCH$_{2ap}$** originates from thiolimine –SH.

The influence of steric hindrance imposed by methyl group in compound **m-TCH$_{2ap}$** (2-acetylpyridine TCH) on the strength of IHB was studied by computing the rotational barrier height for the rotation of 2-pyridyl substituent around thiocarbohydrazide chain. This barrier was compared with sterically less demanding 2-formylpyridyl derivative, and a hypothetical 4-acetylpyridine derivative lacking N atom that forms IHB. The stepwise rotation around $C_2$-$C_7$ bond (Figure 7) was performed and the relative energies of these three compounds were monitored (Figure 22).

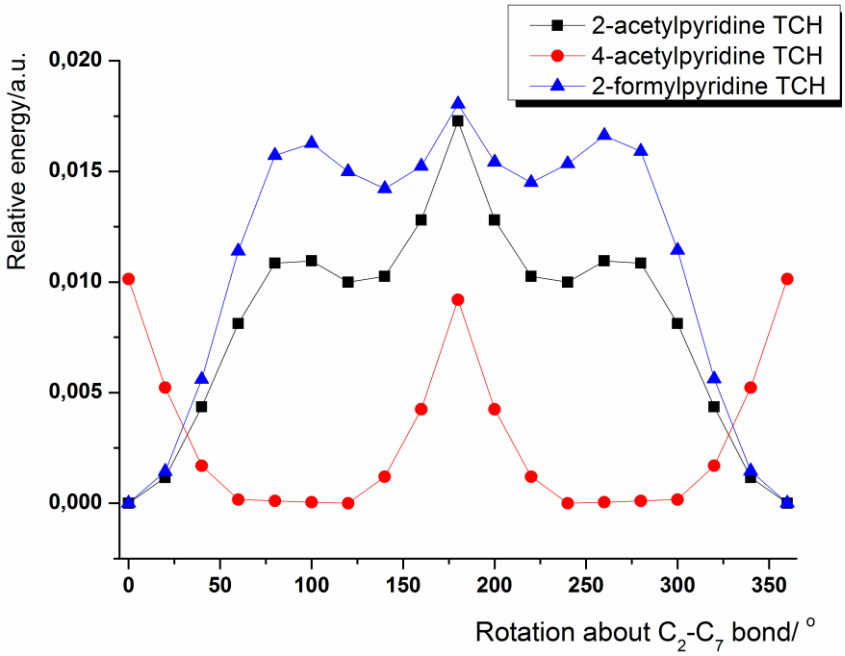


Figure 22. The relative energy of **m-TCH$_{2ap}$** and two structurally similar compounds vs. the rotation around $C_2$-$C_7$ bond by 15°

Starting from a fully planar structure (rotation angle 0°), 2-formylpyridine and 2-acetylpyridine derivatives were more stable than 4-acetylpyridine TCH due to the formation of IHB. Rotation for 60$^o$ sets the 4-acetylpyridine derivative into *gauche* conformation with minimized steric repulsions and a minimum potential energy. The energies of rotamers at local maximum at ~90° indicate the relative strength of IHB, as this interaction is broken in this conformation. The higher energy of 2-formylpyridine TCH suggests that it takes more energy to impair IHB in this structure, so we conclude that the steric hindrance in **m-TCH$_{2ap}$** diminishes the strength of IHB. At a global maximum (180$^o$ rotation), both derivatives with N atom in ortho position have similar relative energy as higher steric effect participation to the rotational barrier in **m-TCH$_{2ap}$** compensates weaker contribution of IHB effect. These results corroborate previous findings for (*Z*)-(2-pyridinyl) based carbonic dihydrazide, where the substitution of azomethine H atom with methyl group reduces the IHB strength.[80]

### 3.2. Isomerism of cinnamic acid hydrazides

Our previous study revealed that salicylaldehyde TCH (**m-TCH$_{sal}$**, Figure 7) undergo *E*-to-*Z* isomerism upon the addition of water due to disruption of IHB, while 2-acetylpiridine TCH (**m-TCH$_{2ap}$**, Figure 7) is prone to thioneamine-thiolimine tautomerism[15]. Cinnamic acid may also undergo *E*/*Z* isomerism. However, the literature describes that lower-energy *E*-isomer is present in over 99% of cinnamic acid derivatives.[240,241] Taking into account these findings, we aimed to elucidate the solution structure of more complex cinnamic acid hydrazides.

The configurational and conformational preferences of cinnamamide which are given in Scheme 13 are studied using 1D ($^1$H, $^{13}$C) and 2D NMR spectroscopy techniques (COSY, NOESY, $^1$H-$^{13}$C HSQC, and $^1$H-$^{13}$C HMBC). The representative spectra are shown in this dissertation (Figure 48 - Figure 110), while all spectra can be found in Supplementary material.

**Several examples of 1D spectra and explanations of some typical peaks**

The NOESY spectra proved as particularly useful for determining the configuration of azomethine C=N bond. The through-space coupling of $N_2$-H atoms with H- or $CH_3$- from azomethine C7 position suggests the *E*-configuration of cinnamic acid hydrazides (Figure 23).

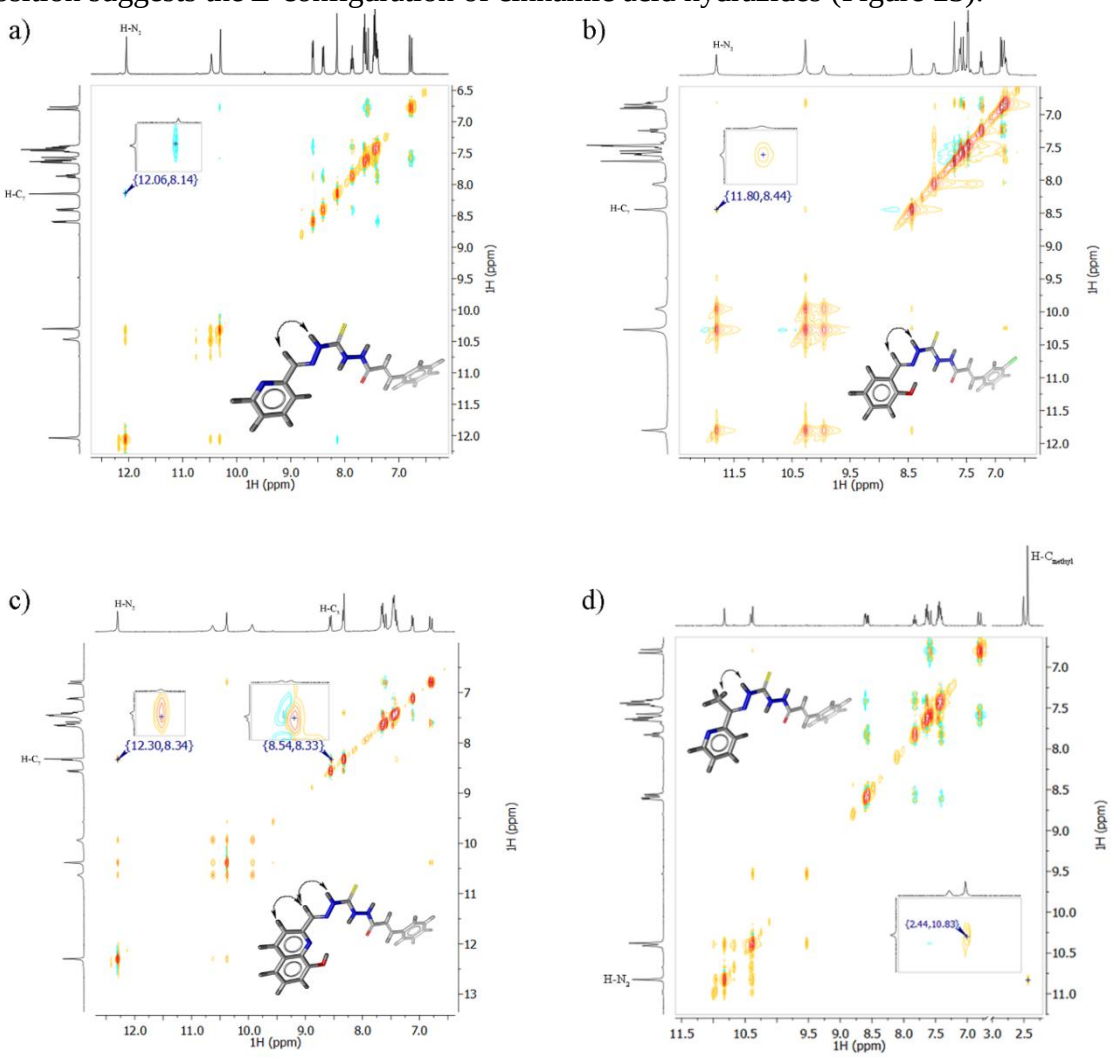


Figure 23. The NOESY spectra of a) **CimTCH$_{2fp}$**; b) **3-ClCimTCH$_{sal}$**; c) **CimTCH$_{8OH2qu}$**, and d) **CimTCH$_{2fp}$**

Furthermore, the configuration of cinnamoyl *α,β*-unsaturated moiety was assessed from the coupling constants ($^3J_{HH}$) of vicinal H atoms at ~ 6.80 ppm and ~7.60 ppm. The high value for $^3J_{HH}$ (15.9 Hz) suggests the *E*-configuration of C=C bond, which agrees with the geometric preferences previously described in the literature.[240,241] Therefore, the (*E*,*E*)-isomer is the most represented form of cinnamamides in a solution.

The relative stability of *E*- and *Z*- isomers around azomethine C=N bond are studied using quantum chemical geometry optimizations at the DFT level, employing ωB97xD functional and 6-31+G(d,p) basis set, in the gas phase. The absolute energies of pairs of isomers and the relative stability are given in Table 4.

Table 4. The relative stability of *E* and *Z*-isomers at azomethine bond of cinnamides. Cinnamic acid part is modelled as *E*-form. Energies are computed on DFT/ ωB97xD/6-31+G(d,p) level in gas phase.

| Comp. | $E_{E\text{-}isomer}$, a.u. | $E_{Z\text{-}isomer}$, a.u. | ΔE, kcal/mol |
|---|---|---|---|
| **CimTCH$_{2fp}$** | -1365.5676 | -1365.5709 | 2.06 |
| **CimTCH$_{sal}$** | -1424.7450 | -1424.7233 | -13.59 |
| **CimTCH$_{8OH2qu}$** | -1594.3792 | -1594.3793 | 0.10 |
| **CimTCH$_{2ap}$** | -1404.8815 | -1404.8818 | 0.18 |
| **3-ClCimTCH$_{2fp}$** | -1825.1465 | -1825.1500 | 2.20 |
| **3-ClCimTCH$_{sal}$** | -1884.3239 | -1884.3021 | -13.68 |
| **3-ClCimTCH$_{8OH2qu}$** | -2053.9580 | -2053.9583 | 0.21 |
| **3-ClCimTCH$_{2ap}$** | -1864.4605 | -1864.4610 | 0.36 |
| **4-ClCimTCH$_{2fp}$** | -1825.1468 | -1825.1503 | 2.18 |
| **4-ClCimTCH$_{sal}$** | -1884.3243 | -1884.3026 | -13.59 |
| **4-ClCimTCH$_{8OH2qu}$** | -2053.9584 | -2053.9588 | 0.24 |
| **4-ClCimTCH$_{2ap}$** | -1864.4608 | -1864.4613 | 0.31 |

The results indicate strong preferences of **TCH$_{sal}$** cinnamamides toward *E*-configuration, with high energy difference (~13 kcal/mol) originating from strong IHB between –OH group and $N_2$-H atom. This stabilizing interaction has been reported in the literature.[80] However, geometric preferences of other compounds do not follow the experimental results. 2-Pydiryl derivatives exhibit ~ 2 kcal/mol more stable *Z*-configuration, while other compounds show almost negligible energy differences between two forms. The observed discrepancy between the experimental differences in isomeric preferences of cinnamamides are given in Scheme 13 be ascribed to the lack of explicit modeling of solvation effects, which could impair the IHB that is responsible for stabilization of *Z*-isomers in the gas phase.

### 3.3. The impact of structural isomerism of thiocarbohydrazones antioxidant capacity

The literature describes several powerful antioxidants containing thione group such as ergothioneine [242] and thiosemicarbazones.[243,244] In this dissertation, the antioxidant capacity of mono- and bis-thiocarbohydrazones (Figure 7) was studied using DPPH$^{\cdot}$ assay, following the procedure given in the Experimental section. According to the results given in Table 5, mono- and bis-TCHs derived from salicylaldehyde (**m-TCH$_{sal}$** and **b-TCH$_{sal}$**) were effective scavengers of 2,2-diphenyl-1-picrylhydrazyl radical compared to compounds **m-TCH$_{2ap}$** and **b-TCH$_{2ap}$**. This trend is expected as it is well-known that the existence of phenolic –OH groups potentiate the antioxidant properties of TCHs.[27]

Table 5. Antioxidant capacity of **m-TCH$_{sal}$**, **b-TCH$_{sal}$**, **m-TCH$_{2ap}$** and **b-TCH$_{2ap}$** in DPPH· test

| | $IC_{50}$, mM | |
|---|---|---|
| | DMSO | DMSO:$H_2O$ = 4:1 |
| **m-TCH$_{sal}$** | 0.15 | 0.083 |
| **b-TCH$_{sal}$** | 0.13 | 0.078 |
| **m-TCH$_{2ap}$** | 0.24 | 0.11 |
| **b-TCH$_{2ap}$** | 0.67 | 0.13 |
| Ascorbic acid | 0.11 | 0.21 |

It was interesting to observe the significant decrease in $IC_{50}$ values, i.e. increase in the antioxidant capacity of **m-TCH$_s$ and b-TCHs**, when 20% water was added in the DMSO solution of 2,2-diphenyl-1-picrylhydrazyl radical (DPPH$^{\cdot}$). For comparison, the addition of water diminished the antioxidant potency of ascorbic acid. We hypothesized that the water-induced

isomerism/tautomerism of mono- and bis-TCHs increases the antioxidant activity, but we didn't find literature reports on the exact mechanisms that explain this phenomenon.

To gain insights into details on how water-induced effects potentiate TCHs as antioxidant, we submitted studied **m-TCH$_s$ and b-TCHs** to quantum chemical calculations of electronic structure and bond dissociation enthalpies (BDE). The radical scavenging potency of a molecule (Mol–H) is correlated with the energy required to transfer a hydrogen atom (one proton + one electron) to the reactive radical species. In DPPH$^{\cdot}$ assay, this transfer occurs from Mol-H to DPPH$^{\cdot}$:

$$M–H + DPPH^{\cdot} \longrightarrow M^{\cdot} + DPPH_2 \qquad (25)$$

This overall process can proceed via three main mechanisms: HAT (equation 1), SET (equation 3), and SPLET (equation 5-7). Among them, HAT is the most common and the most studied mechanism of radical scavenging activity of small organic molecules (SOMs). The HAT is characterized by bond dissociation enthalpy (BDE) of a molecule, where the X-H bond (X = O, N, S) with the lowest BDE is the one that transfers the H atom to the free radical. According to equation 2, the stabilization of radical M$^{\cdot}$ via IHB, resonance, and conjugation decreases the BDE values and improves antioxidant capacity. [245]

The geometry optimization of *E*- and *Z*-isomers of both tautomers thione and thiol form of **m-TCH$_{sal}$** and **m-TCH$_{2ap}$** compound (DFT/B3LYP/6-311++G(d,p) level and PCM solvation model of water) revealed relative stability of isomers/tautomers. It has to be stressed that the results obtained (Figure 24 - Figure 25) may be useful only for comparison as PCM model does not include real solvent-solute interactions which may significantly influence the energy barrier for isomerism/tautomerism.

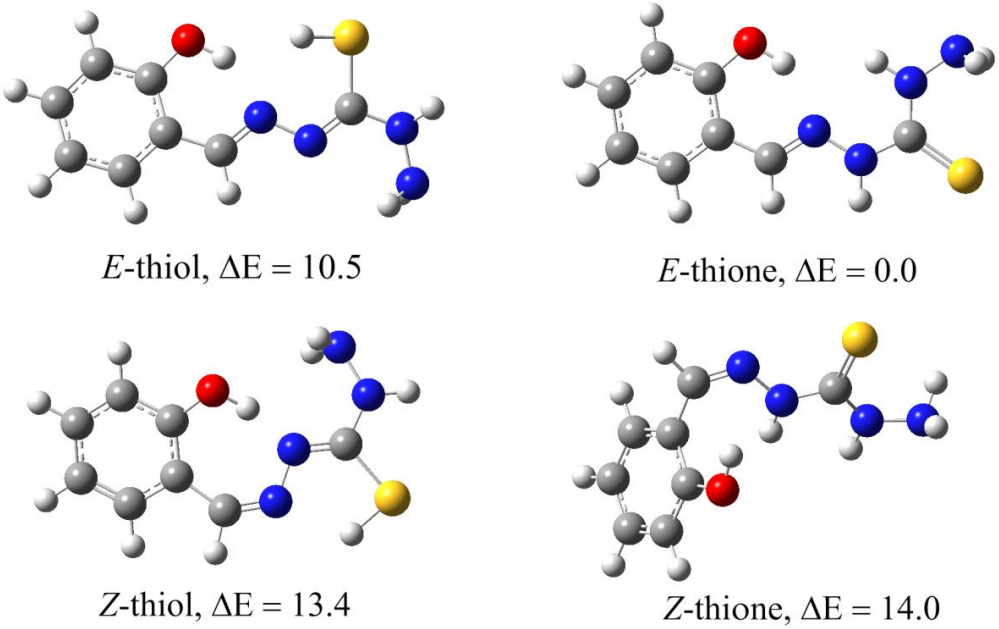


Figure 24. The relative stability of *E*- and *Z*- isomers for thione/thiol tautomers of **m-TCH$_{sal}$** given in kcal/mol relative to the lowest-energy form (*E*-thione)

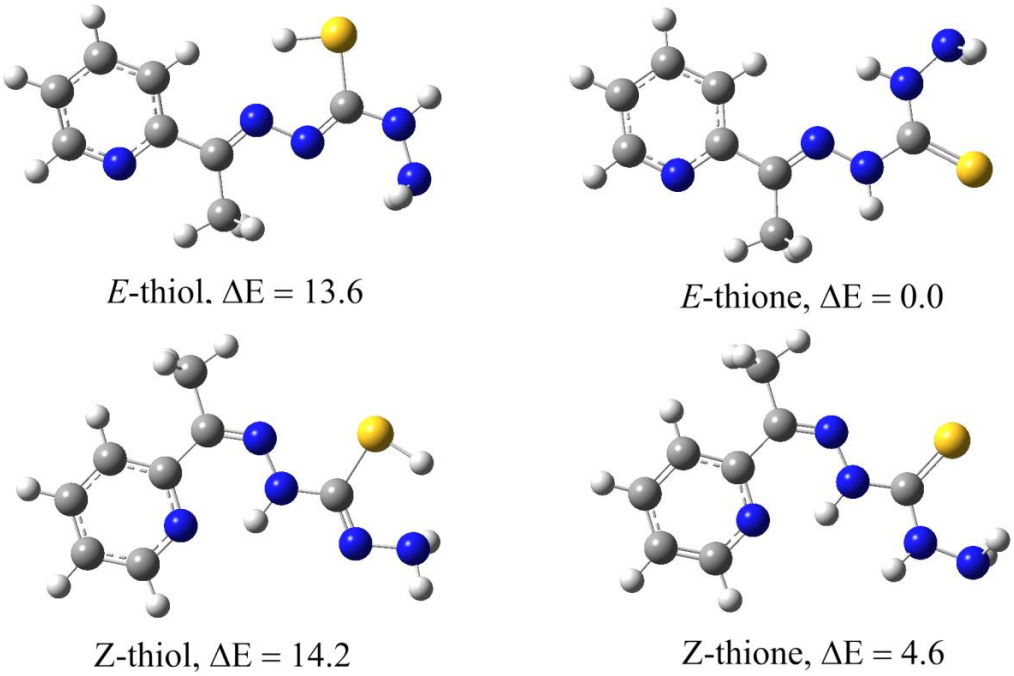


Figure 25. The relative stability of *E*- and *Z*- isomers for thione/thiol tautomers of **m-TCH$_{2ap}$** given in kcal/mol relative to the lowest-energy form (*E*-thione) Figs 24 and 25 to one (a and b)

The *E*-thione isomer was the most stable form of **m-TCH$_{sal}$** is a simulated aqueous environment (Figure 24). This form is stabilized by IHB between ortho-hydroxyl group and $N_1$ atom. Conversion into *Z*-isomer breaks this interaction, resulting in 14.0 kcal/mol less stable form. The *E*-thione isomer also appeared as the most stable one for compound **m-TCH$_{2ap}$**. However, IHB between $N_2$-H and $N_{Py}$ (for atom labeling see Figure 7) stabilizes *Z*-form to some extent and reduces the energy difference between *E* and *Z* forms to 4.6 kcal/mol (Figure 25).

The observed geometric isomerism of **m-TCH$_{sal}$** (Figure 9 and Figure 11) and increased antioxidant capacity in DPPH$^{\cdot}$ assay upon the addition of water (Table 4) opened an interesting research question. Aiming to discover whether the appearance of *Z*-isomer facilitates the HAT process from **m-TCH$_{sal}$** to reactive DPPH$^{\cdot}$ radical, we calculated BDEs for several bonds of two geometric isomers of **1**-thione tautomer. According to the results given in Table 5, $N_3$-H and $N_2$-H atoms of **m-TCH$_{sal}$** -*Z*-isomer show 3-5 kcal/mol lower BDEs compared to *E*-form. On the other hand, BDE of terminal $N_4$-H atom is not influenced by isomerism. The largest difference was observed for phenolic –OH group, and the process of *E*-to-*Z* isomerisation decreases BDE for 11 kcal/mol due to disruption of IHB that destabilizes the ground state and facilitates HAT from –OH to reactive free radical.

Table 6. The ZPE-corrected energy, enthalpy, BDEs, and the extent of radical spin delocalization of isomers of **m-TCH$_{sal}$**, **b-TCH$_{sal}$, m-TCH$_{2ap}$** and **b-TCH$_{2ap}$.**

| | *E*, Hartree* | *H*, Hartree | BDE (kcal/mol) | % of spin delocalized |
|---|---|---|---|---|
| ***m-TCH$_{sal}$-E*** | -1003.280812 | -1003.266216 | | |
| ***m-TCH$_{sal}$-E*** O· | -1002.645219 | -1002.630606 | 85.14 | 68.5 |
| ***m-TCH$_{sal}$-E*** $N_2$· | -1002.643755 | -1002.630212 | 85.39 | 53.9 |
| ***m-TCH$_{sal}$-E*** $N_3$· | -1002.661405 | -1002.647469 | 74.56 | 65.2 |
| ***m-TCH$_{sal}$ -E*** $N_4$· | -1002.651313 | -1002.637514 | 80.81 | 22.1 |
| ***m-TCH$_{sal}$-Z*** | -1003.258467 | -1003.243658 | | |
| ***m-TCH$_{sal}$-Z*** O· | -1002.639390 | -1002.625150 | 74.41 | 70.9 |
| ***m-TCH$_{sal}$-Z*** $N_2$· | -1002.629226 | -1002.615147 | 80.69 | 51.7 |
| ***m-TCH$_{sal}$-Z*** $N_3$· | -1002.644748 | -1002.630488 | 71.06 | 64.1 |
| ***m-TCH$_{sal}$-Z*** $N_4$· | -1002.630368 | -1002.616346 | 79.94 | 24.1 |
| ***b-TCH$_{sal}$-(E,E)*** | -1347.665656 | -1347.645320 | | |
| ***b-TCH$_{sal}$-(E,E)*** O· | -1347.024326 | -1347.003802 | 88.85 | 67.0 |
| ***b-TCH$_{sal}$-(E,E)*** N· | -1347.031306 | -1347.011300 | 84.15 | 54.8 |
| ***b-TCH$_{sal}$-(Z,Z)*** | -1347.629283 | -1347.608459 | | |
| ***b-TCH$_{sal}$-(Z,Z)*** O· | -1346.998695 | -1346.978125 | 81.83 | 66.1 |
| ***b-TCH$_{sal}$-(Z,Z)*** N· | -1347.003122 | -1346.982485 | 79.10 | 55.0 |
| ***m-TCH$_{2ap}$-thione*** | -983.385815 | -983.370732 | | |
| ***m-TCH$_{2ap}$-thione*** $N_2$· | -982.746778 | -982.731858 | 87.19 | 51.5 |
| ***m-TCH$_{2ap}$-thione*** $N_3$· | -982.762078 | -982.747400 | 77.44 | 65.7 |
| ***m-TCH$_{2ap}$-thione*** $N_4$· | -982.757113 | -982.742808 | 80.32 | 23.1 |
| ***m-TCH$_{2ap}$-thiol*** | -983.366585 | -983.351654 | | |
| ***m-TCH$_{2ap}$-thiol*** S· | -982.733342 | -982.718097 | 80.68 | 20.6 |
| ***m-TCH$_{2ap}$-thiol*** $N_3$· | -982.749506 | -982.734528 | 70.54 | 63.5 |
| ***m-TCH$_{2ap}$-thiol*** $N_4$· | -982.738845 | -982.723987 | 77.23 | 26.8 |
| ***b-TCH$_{2ap}$-thione*** | -1307.871753 | -1307.850203 | | |
| ***b-TCH$_{2ap}$-thione*** $N_2$· | -1307.233272 | -1307.211542 | 87.06 | 57.0 |
| ***b-TCH$_{2ap}$-thiol*** | -1307.852979 | -1307.830817 | | |
| ***b-TCH$_{2ap}$-thiol*** S· | -1307.222336 | -1307.200584 | 81.77 | 18.2 |
| ***b-TCH$_{2ap}$-thiol*** $N_2$· | -1307.225046 | -1307.202900 | 80.32 | 52.2 |

* Energies are ZPE-corrected

The same trend was observed for bis-salicylaldehyde TCH, **b-TCH$_{sal}$**, where isomerism from *E,E* to *Z-Z* favors the HAT from O-H and $N_3$-H by ~7 and 5 kcal/mol, respectively (Table 5).

As an addition to the % of spin density delocalized, we plotted the spin density distribution (SDD) maps to visualize the extent of spin delocalization. In general, more delocalized SDD means more stabilized radical species, and corresponding reactive center has lower BDE and greater HAT potency. As can be seen from Figure 26, **m-TCH$_{sal}$-*Z*** and **b-TCH$_{sal}$-(*Z,Z*)** isomers have more delocalized SDD, which is in accordance with higher potency induced by isomerism.

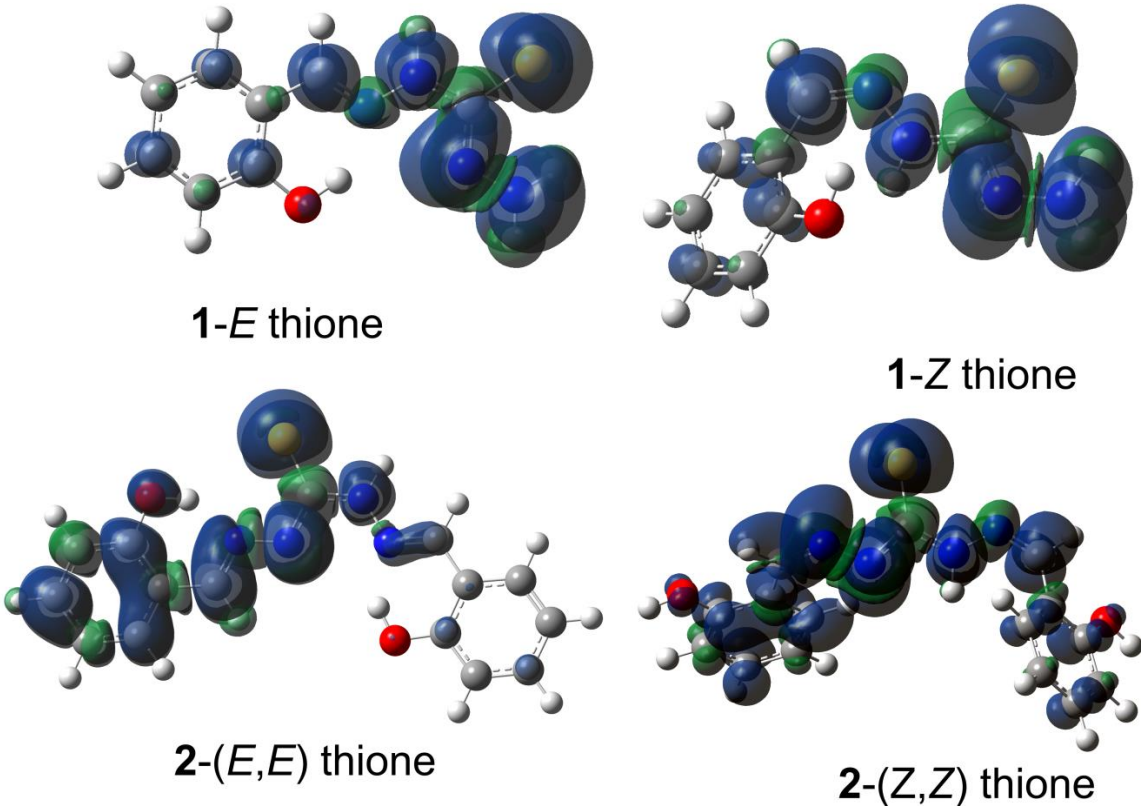


Figure 26. SDD for lowest-energy radical forms of **m-TCH$_{sal}$** and **b-TCH$_{sal}$**

Furthermore, we aimed to investigate the mechanisms of how the thione/thiol tautomerism changes the antioxidant capacity of **m-TCH$_{2ap}$**. Using the same methodology as for **m-TCH$_{sal}$** and **b-TCH$_{sal}$**, we computed BDEs of several probable HAT sites for thionimine and thiolamine isomers of **m-TCH$_{2ap}$** -*E*. As shown in Table 5, the formation of thiol form decreases lowest-energy BDE by 7 kcal/mol the, which explains the trend in experimental values of the radical scavenging activities.

The –SH center formed by water-induced tautomerism appears as the likely site for HAT and DPPH· neutralization. However, BDEs computed (Table 5) reveal that the –$N_3$-H is a more active HAT center with BDE lower for 10 kcal/mol. In the case of bis-derivative **b-TCH$_{2ap}$**, tautomerism from (*E*,*E*)-thione to (*E*,*E*)- thiol decreases the BDE of –$N_2$-H by ~7 kcal/mol and results in the active site with similar BDE as –SH atom (81.77 kcal/mol). As **b-TCH$_{2ap}$** exhibited the most striking increase in radical scavenging activity upon isomerism (5-fold increase, Table 4), we hypothesize that the formation of two reactive sites with similar potencies jointly increases the antioxidant capacity of **b-TCH$_{2ap}$**. In addition, SDD of thiol form of **m-TCH$_{2ap}$** and **b-TCH$_{2ap}$** is delocalized over the entire molecule and contributes to radical stabilization, which results in higher antioxidant activities (Figure 27).

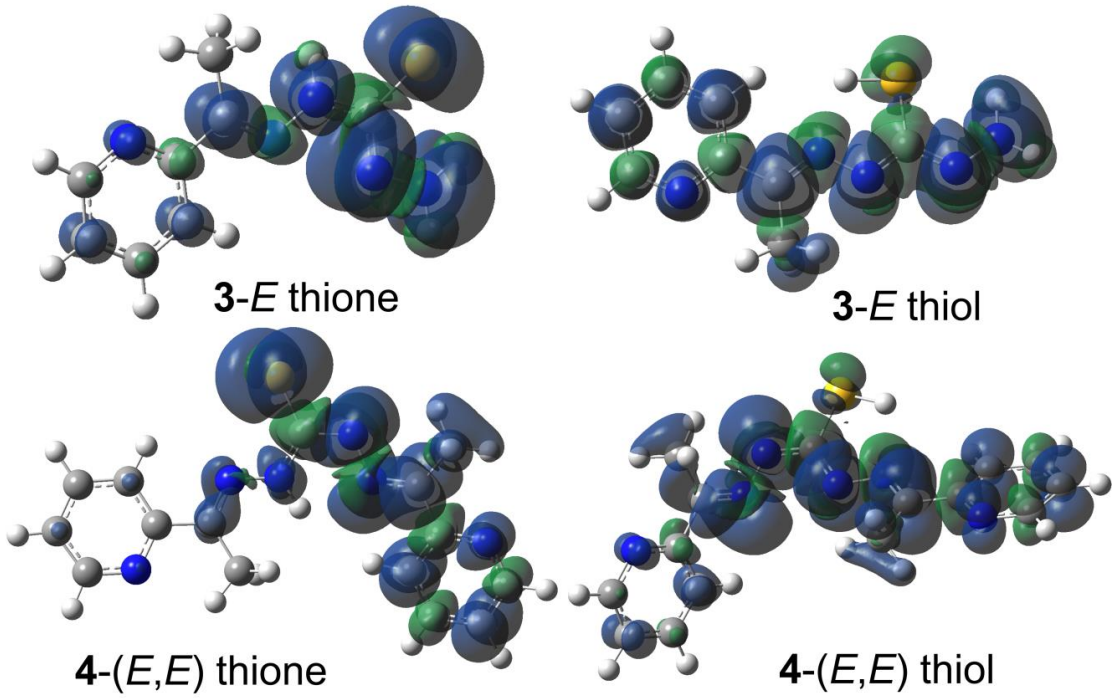


Figure 27. SDD of **m-TCH$_{2ap}$-*E*** radical from $N_3$–H and **b-TCH$_{2ap}$-(*E*,*E*)** radical formed by hydrogen abstraction from $N_2$–H bond.

### 3.4. Investigation of anticancer activity

A compound performs anticancer activity if it can either inhibit the unlimited and uncontrolled capacity of malignant cells to divide, or can induce their death. There are many drugs for the treatment of cancer patients that are using different strategies to cease the growth of cancer mass, with the ultimate goal toward cancer cell eradication. Each cancer drug had been thoroughly tested for years before becoming approved for application in oncology, while the indication for the majority of them is narrowed to certain tumor types.[246] Unwanted side effects of cancer therapy are common, where some of those may significantly impair the quality of a patient's life, or even lead to discontinuation of treatment.

Although there are various ways to impede stamina of cancer cell, this investigation was aimed to evaluate do our compounds have some properties among the most important for a successful anticancer drugs: (1) ability to induce death of cancer cells; (2) ability to reduce the mobility of cancer cells; (3) lack of activity on healthy cells.

#### 3.4.1. Testing compounds' ability to induce death of cancer cells

At the very beginning of the study on anticancer activity, it was necessary to determine which malignant phenotype is the most susceptible to the treatment with investigated compounds. Subsequently, attention was assigned to assessment of cell death modalities and the key intracellular mechanisms associated with the cell death outcome.

##### 3.4.1.1. Investigated compounds revealed the highest activity against human lung adenocarcinoma cells

Several human cancer cell lines were chosen as representatives of the top 20 most common malignancies according to the global statistical report.[247] Compounds were added on cells in a

concentration range from 30-100 μM, and evaluation of their effect was performed after 24 h using a fast screening method of Calcein AM (CAM) and propidium iodide (PI) dual staining. As it can be seen in Table 7, lung adenocarcinoma cells (A549) are the most susceptible to the treatments. Survival of A549 cells were reduced for more than 50 % by seven out of twelve investigated compounds, while **3-ClCimTCH$_{sal}$** and **4-ClCimTCH$_{8OH2qu}$** were highly efficient in two and three applied concentrations, respectfully. Ovarian adenocarcinoma cells (SkOV-3) were affected by the treatment of five compounds, but only **3-ClCimTCH$_{sal}$** and **4-ClCimTCH$_{8OH2qu}$** reduced their viability for more than 50 %. Although colorectal adenocarcinoma cells (LoVo) responded to the treatment with four compounds, **4-ClCimTCH$_{8OH2qu}$** was the one with notable activity. Furthermore, only compounds **3-ClCimTCH$_{sal}$** and **4-ClCimTCH$_{8OH2qu}$** significantly reduced population of breast adenocarcinoma cells (MCF7), whereas pancreatic adenocarcinoma cells (AsPC1) remained unaffected by any of tested treatments.

Compounds **CimTCH$_{2ap}$**, **3-ClCimTCH$_{2fp}$**, and **3-ClCimTCH$_{8OH2qu}$** had no activity on any of treated cell lines. Compounds **CimTCH$_{2fp}$**, **3-ClCimTCH$_{2ap}$**, **4-ClCimTCH$_{2fp}$**, and **4-ClCimTCH$_{2ap}$** declined survival of A549 cells only, whereas **CimTCH$_{sal}$** and **4-ClCimTCH$_{sal}$** impacted vitality of SkOV-3 and LoVo cells as well. Finally, **3-ClCimTCH$_{sal}$** and **4-ClCimTCH$_{8OH2qu}$** showed the highest activity. According to results presented in Table 7, investigation of cell death modalities has been continued on compounds **3-ClCimTCH$_{sal}$** and **4-ClCimTCH$_{sal}$** in A549 cells.

Table 7. Effects of investigated compounds on cell survival after 24 hours of treatment, expressed as percentage of viable treated cells in respect to corresponding none treated controls. Numbers are the mean ± SD of three replicates from independent experiments. Shaded areas mark outcomes with ≤ 50 % of cell survival that is considered as favorable activity.

| Compound | Concentration [μM] | LoVo cells | SkOV-3 cells | A549 cells | MCF-7 cells | AsPC1 cells |
|---|---|---|---|---|---|---|
| **CimTCH$_{2fp}$** | 100 | –* | – | 49±7 | – | – |
| | 75 | – | – | 58±6 | – | – |
| | 50 | – | – | 64±3 | – | – |
| | 30 | – | – | 67±1 | – | – |
| **CimTCH$_{sal}$** | 100 | 75±5 | 67±9 | 48±4 | – | – |
| | 75 | 81±2 | 71±2 | 56±1 | – | – |
| | 50 | 82±2 | 73±1 | 63±2 | – | – |
| | 30 | 83±1 | 79±8 | 84±3 | – | – |
| **CimTCH$_{8OH2qu}$** | 100 | – | 65±5 | 48±4 | – | – |
| | 75 | – | 75±1 | 56±4 | – | – |
| | 50 | – | 79±4 | 60±3 | – | – |
| | 30 | – | 84±3 | 70±6 | – | – |
| **CimTCH$_{2ap}$** | 100 | – | – | – | – | – |
| | 75 | – | – | – | – | – |
| | 50 | – | – | – | – | – |
| | 30 | – | – | – | – | – |
| **3-ClCimTCH$_{2fp}$** | 100 | – | – | – | – | – |
| | 75 | – | – | – | – | – |
| | 50 | – | – | – | – | – |
| | 30 | – | – | – | – | – |
| **3-ClCimTCH$_{sal}$** | 100 | 64±3 | 21±8 | 39±3 | 48±3 | – |
| | 75 | 69±3 | 79±9 | 46±4 | 71±8 | – |
| | 50 | 79±8 | 78±9 | 53±1 | 75±1 | – |
| | 30 | 91±2 | 90±9 | 65±3 | 86±3 | – |
| **3-ClCimTCH$_{8OH2qu}$** | 100 | – | – | – | – | – |
| | 75 | – | – | – | – | – |
| | 50 | – | – | – | – | – |
| | 30 | – | – | – | – | – |

Table 7 continued

| | | | | | | |
|---|---|---|---|---|---|---|
| **3-ClCimTCH$_{2ap}$** | 100 | – | – | 48±2 | – | – |
| | 75 | – | – | 70±2 | – | – |
| | 50 | – | – | 73±9 | – | – |
| | 30 | – | – | 85±3 | – | – |
| **4-ClCimTCH$_{2fp}$** | 100 | – | – | 50±5 | – | – |
| | 75 | – | – | 65±1 | – | – |
| | 50 | – | – | 76±5 | – | – |
| | 30 | – | – | 80±6 | – | – |
| **4-ClCimTCH$_{sal}$** | 100 | 57±2 | 72±5 | 58±6 | – | – |
| | 75 | 62±1 | 72±6 | 69±1 | – | – |
| | 50 | 67±4 | 77±2 | 63±5 | – | – |
| | 30 | 72±1 | 77±5 | 80±4 | – | – |
| **4-ClCimTCH$_{8OH2qu}$** | 100 | 43±5 | 43±3 | 38±2 | 35±3 | – |
| | 75 | 70±2 | 95±6 | 46±3 | 84±6 | – |
| | 50 | 76±4 | 91±2 | 50±1 | 82±8 | – |
| | 30 | 83±2 | 90±4 | 53±1 | 85±2 | – |
| **4-ClCimTCH$_{2ap}$** | 100 | – | – | 57±2 | – | – |
| | 75 | – | – | 60±4 | – | – |
| | 50 | – | – | 73±6 | – | – |
| | 30 | – | – | 75±1 | – | – |

* ≥ 90 % of cell survival.

### 3.4.1.2. Compounds 3-ClCimTCH$_{sal}$ and 4-ClCimTCH$_{8OH2qu}$ induce apoptotic death in A549 cells

The Nomenclature Committee on Cell Death listed multiple cell death types in relation to intracellular mechanisms that orchestrate various cell death pathways.[174] Although the underlying molecular interactions may be different between cell death types, their final outcome emerges either as apoptotic or necrotic morphology. Annexin V/PI dual staining and Sub-G0/G1 analysis were carried out after 24 h incubation of A549 cells with **3-ClCimTCH$_{sal}$** and **4-ClCimTCH$_{sal}$** in order to define the exact frequency of cell death, as well as whether morphology of dead cells has hallmarks common to apoptosis or necrosis.

Results of Annexin V/PI staining clearly shows that early necrosis (PI single-stained cells) was a rare event in all analyzed samples within a range from 1-100 μM (Figure 28). On the other hand, frequencies of Annexin V single stained cells (early apoptosis) and double-stained cells (advanced phases of death) increase concentration-dependently due to the A549 cells treatment with either of investigated compounds. After Annexin V/PI analysis, the same cell samples were fixed in ethanol and day later assessed for Sub-G0/G1 events. Chromosomal cleavage into nucleosomal and oligonucleosomal fragments is a feature typical for advanced stages of apoptotic death. Those fragments appear as sub-diploid cells in FL2-area histogram, beneath diploid cells at the G0/G1 phase of mitotic division.[248,249] It is clearly obvious that percentages of cells at the Sub-G0/G1 area (Figure 29) strongly correlate with percentages of double-stained cells in Figure 28. This result serves as indubitable confirmation that both, **3-ClCimTCH$_{sal}$** and **4-ClCimTCH$_{8OH2qu}$**, trigger apoptotic death in A549 cells.

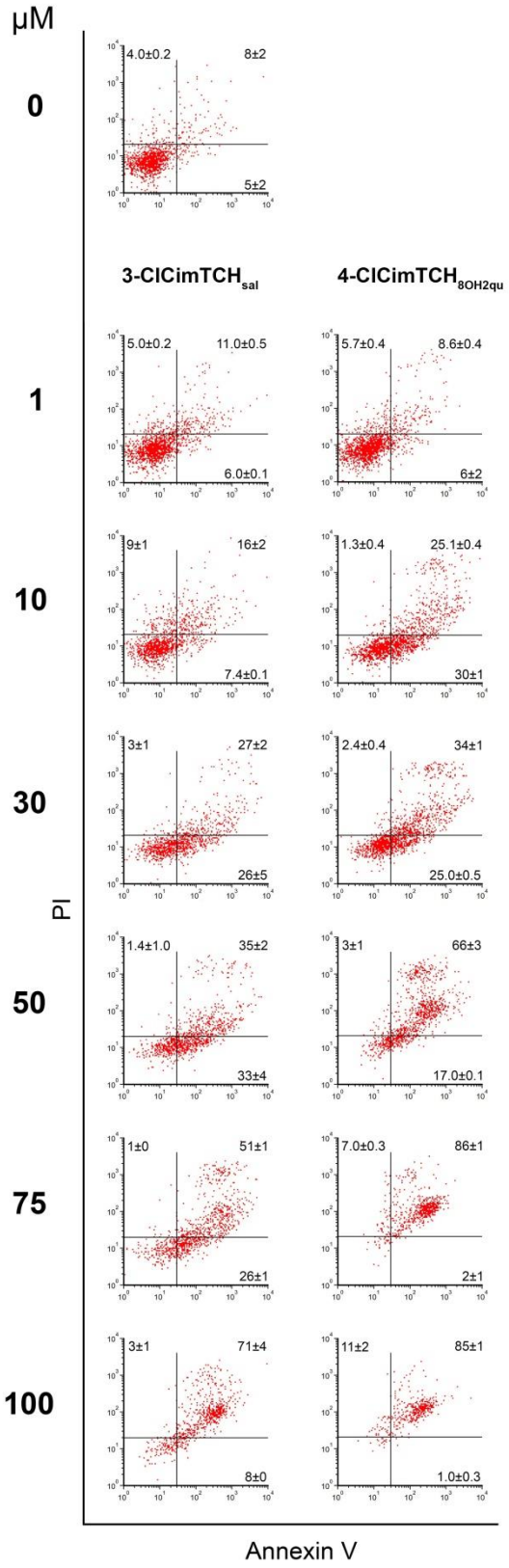


Figure 28 . Results of Annexin V/PI staining shown as representative pictures and the mean ± SD percentages of two replicates from independent experiments.

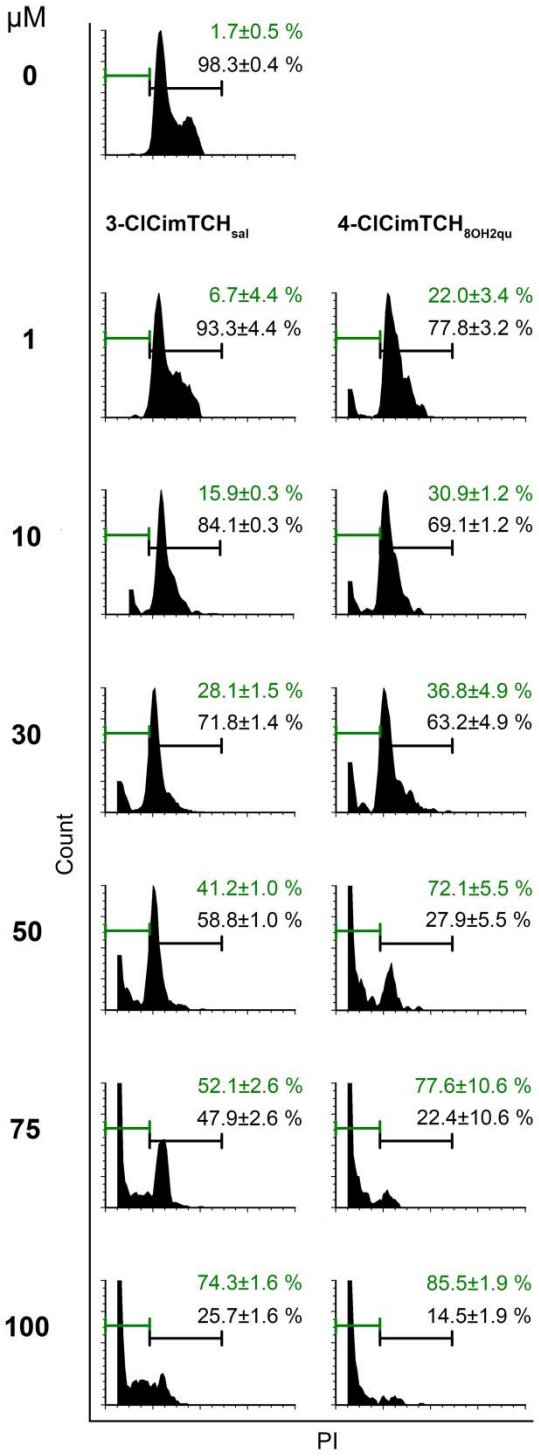


Figure 29. Frequences of cells in advanced phases of apoptotic death (population in Sub-G0/G1area, gated with green) compared to percentages of live dividing cells (gated with black), expressed as the mean ± SD of two replicates from independent experiments.

Contrary to CAM/PI staining, Annexin V/PI method provides more precise information regarding incidence of cell death induced by the particular treatment. Summed percentages of all cells stained with Annexin V and/or PI for each sample were plotted against particular concentrations of **3-ClCimTCH$_{sal}$** resulted in a nicely contoured sigmoidal curve whose exponential phase is plotted between 10-100 μM (Figure 30 A). The same data handling for the results gained after treatment with **4-ClCimTCH$_{8OH2qu}$** defines a straight line, which signified that five-parameter sigmoidal equation is not the adequate mathematical model to define concentration-response relationship for this

compound. Instead, biphasic model perfectly fits with experimental results (Figure 30 B), also indicating on possibility that **4-ClCimTCH$_{8OH2qu}$** may exhibit a concentration-dependent shift in the mechanism of its pro-apoptotic activity.

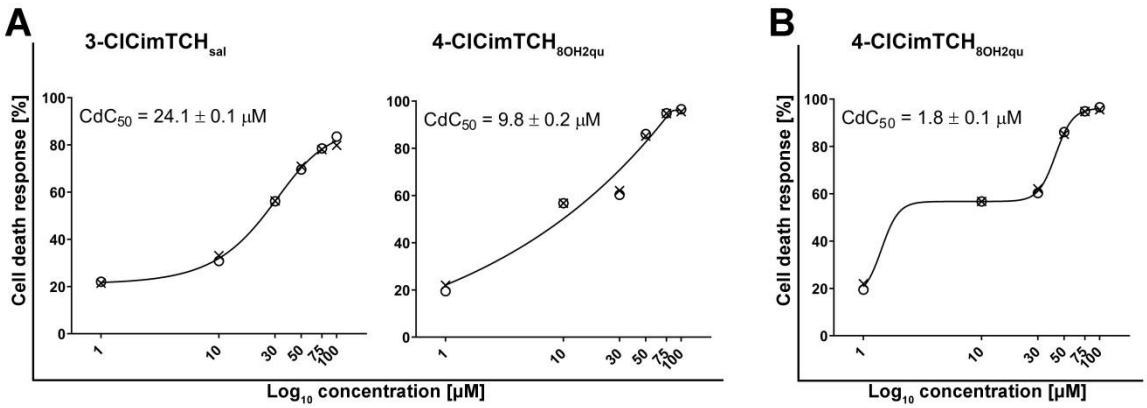


Figure 30. Curves describing relationship between applied concentrations and gained cell death responses. $CdC_{50}$ is computed concentration that induce death in 50 % of treated cells (the mean ± SD from two independent replicates).

### 3.4.1.3. Compounds 3-ClCimTCH$_{sal}$ and 4-ClCimTCH$_{8OH2qu}$ induce arrest of A549 cells at the G1 phase of mitotic division

Analysis of cell cycle distribution of treated cells in respect to non-treated population provides insight on which phase of mitotic division has been disrupted by the applied treatment. Such information serves as an indication of how the treatment with **3-ClCimTCH$_{sal}$** and **4-ClCimTCH$_{8OH2qu}$** interfered homeostasis of A549 cells so harshly that led them to apoptotic death. Comparison of cells frequencies along phases of mitotic cycle between treated samples does not reveal any particular difference (Figure 31). Both compounds initially induce slight aggregation of treated cells at the S phase, which at higher concentrations (30 μM of **3-ClCimTCH$_{sal}$** and 10 μM of **4-ClCimTCH$_{8OH2qu}$**) progress toward cell accumulation at the G1-to-S check point, and finally ended with the division arrest at the G1 phase (50 μM of **3-ClCimTCH$_{sal}$** and 30 μM of **4-ClCimTCH$_{8OH2qu}$**). Those changes strongly indicate that both compounds caused difficulties during DNA replication process that aggravated with an increase of applied concentration. Initially, cellular repairing mechanisms prolonged duration of the S phase that is seen as cell accumulation, then control feedback signaling induced delay in mitotic division at the G1-to-S check point, and finally prevented cells to start the division by arresting them at the G0/G1 phase. The distinction between concentrations of **3-ClCimTCH$_{sal}$** and **4-ClCimTCH$_{8OH2qu}$** at which those compounds induce same cell cycle changes corresponds with the difference in intensity of apoptotic response in Figure 28 and Figure 29. Finally, this analysis did not provide any information regarding a possible concentration-dependent shift in the mechanism of **4-ClCimTCH$_{8OH2qu}$** pro-apoptotic activity that is indicated by concentration-response curve in Figure 30 B.

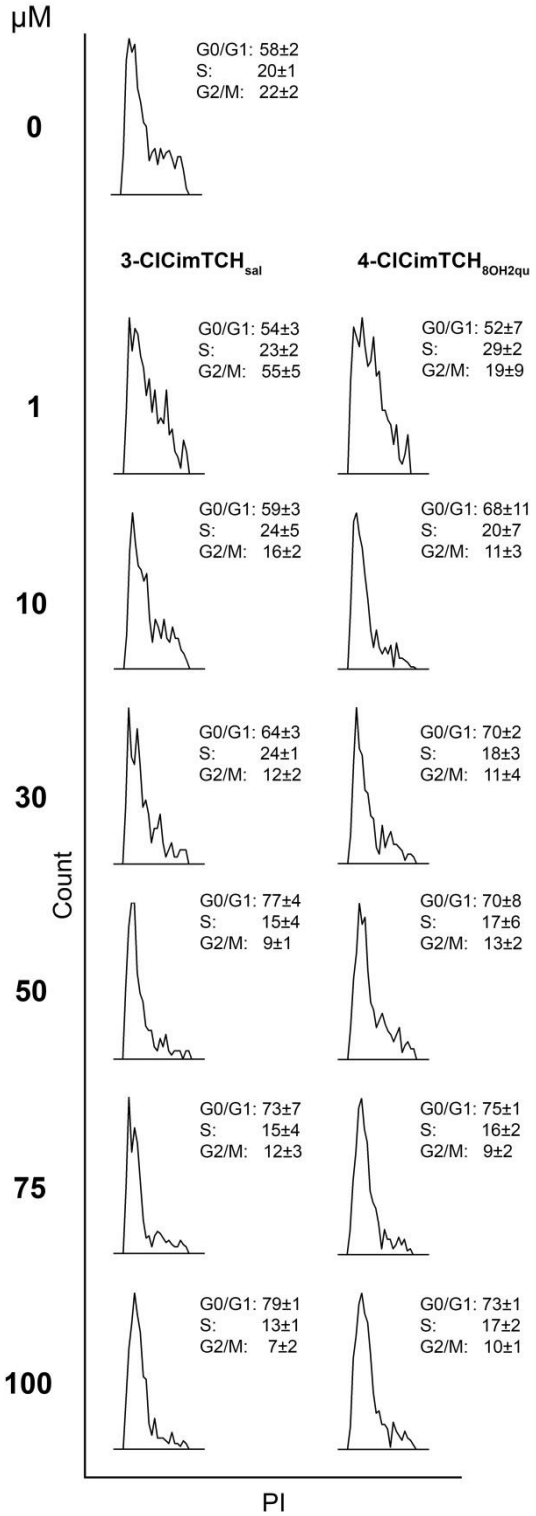


Figure 31. Distribution of cells along phases of cellular division recorded after 12 hours of treatment with investigated compounds, expressed as the mean ± SD from two independent replicates.

### 3.4.1.4. Compounds 3-ClCimTCH$_{sal}$ and 4-ClCimTCH$_{8OH2qu}$ induce activation of intrinsic caspase pathway

To afford additional perspective regarding intracellular developments, patterns of intrinsic and extrinsic apoptotic pathways activation were monitored after 6 h of treatment, with compounds **3-ClCimTCH$_{sal}$** and **4-ClCimTCH$_{8OH2qu}$** added at 50 μM. At this chosen concentration both compounds induced arrested mitotic division of A549 cells at the G0/G1 phase (Figure 31), while short incubation time should provide insight in initial course of intracellular developments before apoptosis became massive event in treated samples. It is strikingly evident that both compounds arose significantly strong activation of caspase-9 (Figure 32), which is a key enzyme in the intrinsic apoptotic cascade that initiates due to significant intracellular homeostasis distress. Significant cross-talk activation of caspase-8 is present only in cells subjected to **4-ClCimTCH$_{8OH2qu}$**, but this is a common interaction between two caspase cascades and in the current settings correlates with more vigorous activity of **4-ClCimTCH$_{8OH2qu}$** compared to **3-ClCimTCH$_{sal}$** (Figure 28). The result of caspase activation in treated A549 cells additionally suggests that mechanisms which underlie pro-apoptotic activity of investigated compounds may be quite similar or even the same, while **4-ClCimTCH$_{8OH2qu}$** tends to be more efficient than **3-ClCimTCH$_{sal}$**.

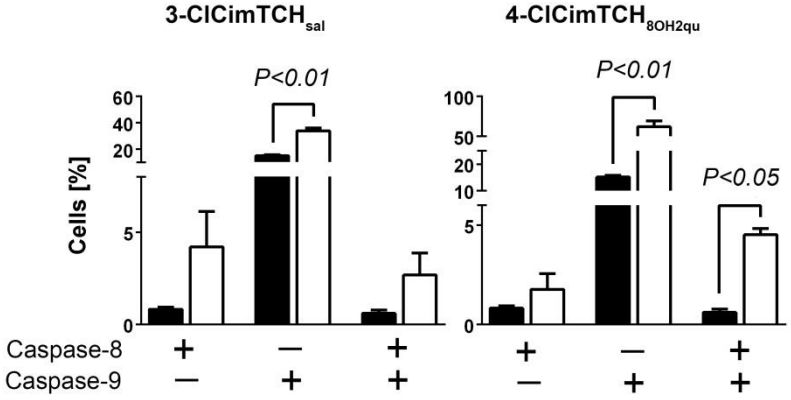


Figure 32. Frequency of cells with activated caspase-8, caspase-9, or both, in control samples (black bars) and samples subjected to investigated compounds at 50 μM over 6 hours (white bars). Statistical assessment was performed using unpaired t-test with Welch's correction comparing treated to control populations.

### 3.4.1.5. Compound 4-ClCimTCH$_{8OH2qu}$ is a strong inducer of mitochondrial superoxide anion production

The A549 cells were exposed to **3-ClCimTCH$_{sal}$** and **4-ClCimTCH$_{8OH2qu}$** at the same concentration and time of incubation as for the evaluation of caspase activation. The assessment of mitochondrial superoxide anion production ($^{\bullet}O_2^-$) revealed first pivotal difference in mechanism of activity between those two compounds. As it is presented in (Figure 33A) treatment with compound **3-ClCimTCH$_{sal}$** only slightly raised the percentage of cells with increased production of $^{\bullet}O_2^-$ compared to non-treated control. On the contrary, population of $^{\bullet}O_2^-$-producing cells was enhanced 14 times in the samples subjected to **4-ClCimTCH$_{8OH2qu}$** in respect to control. In addition, compound **4-ClCimTCH$_{8OH2qu}$** has the ability to cause statistically significant accumulation of $^{\bullet}O_2^-$ in mitochondria of A549 cells (Figure 33 B) which indicates that mitochondrial (manganese) superoxide dismutase (SOD2), as the enzyme responsible for $^{\bullet}O_2^-$ conversion to hydrogen peroxide, could not efficiently respond to overwhelming flow of $^{\bullet}O_2^-$ production. It has been previously confirmed that SOD2 in A549 cells is well expressed and its basic activity is on the level of healthy tissue,[250] which

is not the case with other malignant phenotypes used in this investigation.[189] Considering those facts, further studies are necessary to demonstrate whether $^{\bullet}O_2^-$ production by **4-ClCimTCH$_{8OH2qu}$** has a critical role in its pro-apoptotic effect in A549 cells, as well as does this compound undergoes an intracellular transformation that creates a product with more powerful pro-oxidant activity in A549 cells compared to other tested malignant models.

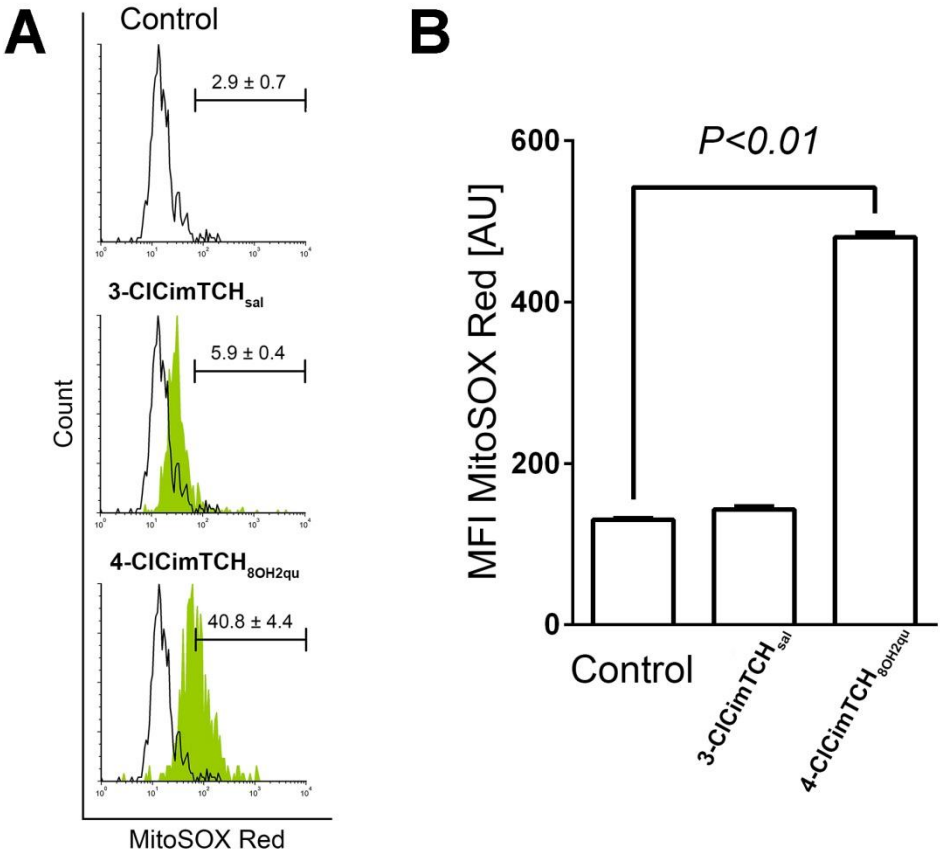


Figure 33. (A) Percentages of cells positive for superoxide ($^{\bullet}O_2^-$) production after incubation with investigated compounds at 50 µM during 6 hours, expressed as the mean ± SD of three replicates from independent experiments. (B) MFI values for $^{\bullet}O_2^-$-positive subpopulations computed of data obtained from three independent replicates. Statistical assessment was performed using the Kruskal-Wallis test with unpaired t-test with Welch's correction as post-test

### 3.5. Testing compounds' ability to reduce mobility of A549 cells

The ability of malignant cells to migrate is one of the decisive mechanisms responsible for cancer metastasis. In order to exam whether compounds **3-ClCimTCH$_{sal}$** and **4-ClCimTCH$_{8OH2qu}$** can interfere with A549 cell mobility, both compounds had been applied in low concentrations for 24 h. Assessment was performed by comparing a surface of wound area between images made just before investigated compounds were added with those recorded at the end of incubation (Figure 34 A). In non-treated control samples, cells were migrating by momentum typical for the investigated phenotype, and 83.2 ± 4.3 % of initial wounds were left uncovered over 24 h (Figure 34 B). In samples exposed to **4-ClCimTCH$_{8OH2qu}$**, a basic motion momentum of cells has been decelerated, thus remaining wound areas were 90.2 ± 5.3 % and 91.5 ± 2.1 % at 1 and 10 µM of **4-ClCimTCH$_{8OH2qu}$**, respectively. However, minimal migration was seen in the samples treated with compound **3-ClCimTCH$_{sal}$**, which at 1 µM was more effective with 97.6 ± 2.3 % of open wound area and 95.7 ± 1.8 % and 10 µM. Both concentrations of **3-ClCimTCH$_{sal}$** achieved statistically significant inhibition of A549 cell migration, and therefore confirmed that this compound has a potential to interfere progression of lung cancer in multiple ways.

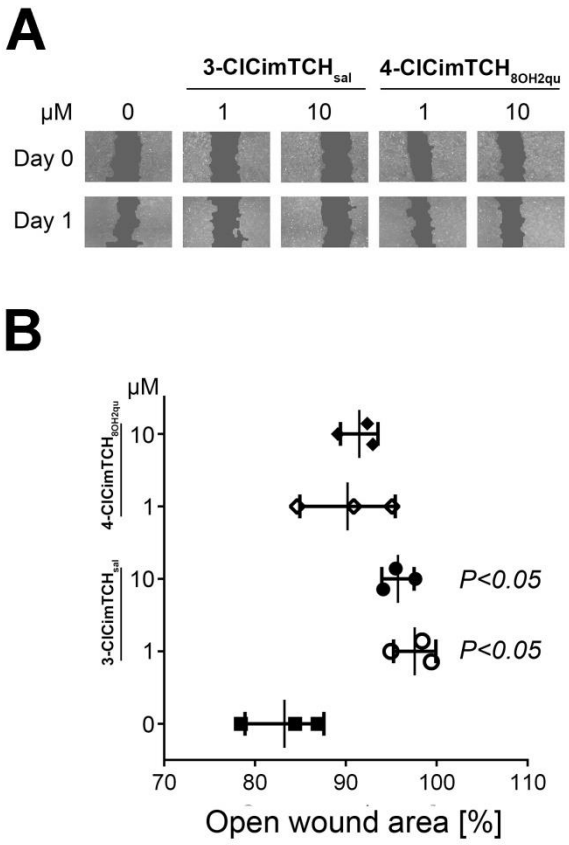


Figure 34. (A) Images of scratch assay on Day 0 and Day 1 (24 hours of incubation with investigated treatments). (B) Percentages of open wound area computed by TScratch software. Statistical assessment was performed by Kruskal-Wallis test and unpaired t-test with Welch's correction.

### 3.6. Testing compounds' ability to induce death in healthy cell lines

Non-selective activity of anticancer drugs toward malignant tissue is the main cause of side effects that in some cases may seriously compromise patients' quality of life, can lead to treatment restriction or even withdrawal. Pharmacokinetic properties of the drug, which can be thoroughly examined only in early clinical studies, have a decisive role in its toxicological profile. Therefore, although results of *in vitro* tests on healthy cell lines should be considered as implicative, those can be strongly indicative whether investigated compound operates in a way that may be harmful for non-malignant tissues. In this investigation, human keratinocytes (HaCaT) and hepatocellular adenocarcinoma cell line (HepG2) were treated with **3-ClCimTCH$_{sal}$** and **4-ClCimTCH$_{8OH2qu}$** at the same concentrations and for the same incubation time as A549 cells. As it can be seen in (Figure 35), compound **4-ClCimTCH$_{8OH2qu}$** revealed more activity on HaCaT and HepG2 cells than against A549 cell line. This result demonstrates that it can be expected of **4-ClCimTCH$_{8OH2qu}$** to induce serious unwanted effects if is applied to men. On the contrary, **3-ClCimTCH$_{sal}$** had only mild activity on HaCat cell line, while HepG2 cells were not affected by the treatment. It can be concluded that **3-ClCimTCH$_{sal}$** has a certain degree of selectivity toward malignant cells, which is a favorable quality that supports further studies of this compound for anticancer treatment.

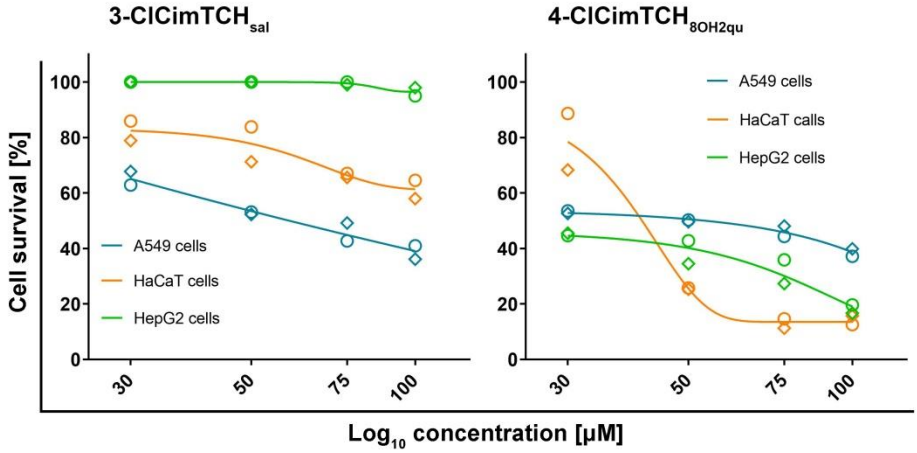


Figure 35. Curves describing relationship between applied concentrations and cell survival. Data for A549 cells in both graphs correspond to those presented in Table 7.

### 3.7. Structure-activity relationship

The IR spectra of studied compounds display all absorption bands characteristic for the amide bond, 4-methoxy cinnamic acid residue and TCH moiety. A strong absorption band at 1616-1631 $cm^{-1}$ is assigned to the azomethine ν(C=N) stretching vibration. Bands in the range 1622-1668 $cm^{-1}$ and 3303-3385 $cm^{-1}$ are assigned to the ν(C=O) and ν(-N-H) stretching vibrations of the amide group, respectively. Also, the absence of the ν(S-H) stretching with the presence of the peak at 1234-1258 $cm^{-1}$, which originate from ν(C=S) vibrations prove the existence of these compounds for thione form in solid state.

$^{1}$H NMR spectra show three single peaks at *δ* 9.93-12.24, assigned to the N-H protons, with the singlet from –OH proton at δ 9.93 and 9.85 found for **4-MeOCimTCH$_{sal}$** and **4-MeOCimTCH$_{8OH2qu}$,** respectively. A singlet at δ 8.14-8.44, found for compounds **4-MeOCimTCH$_{2fp}$, 4-MeOCimTCH$_{sal}$, and 4-MeOCimTCH$_{8OH2qu}$,** originates from azomethine (-CH=N) proton. **4-MeOCimTCH$_{2ap}$** have a singlet at δ 2.44 from azomethine methyl group protons. Characteristic doublet peaks from olefinic protons of cinnamic acid are present at δ 6.62-6.65 and 7.52-7.59 in all spectra. The coupling constant value $^{3}J_{HH}$ of 15.9 Hz indicates existence of pure *E*-isomers, considering *α,β*-unsaturated structure in the cinnamic acid part.[241,251]

Results from $^{13}$C NMR spectra also confirmed the structure and purity of synthesized compounds. The most prominent observed NMR signals are following: thione carbon (C=S) at 179.90-179.27 ppm, carbonyl carbon (C=O) at 164.95-164.44 ppm and azomethine carbon (C=N) at 144.39-140.55 ppm. Unsaturated olefinic carbons appear at 140.76-135.09 and 120.67-120.03 ppm. The peak at 157.13-157.06 ppm and 153.97-153.95 ppm are assigned to the hydroxyl carbon (C-OH) present in **4-MeOCimTCH$_{sal}$** and **4-MeOCimTCH$_{8OH2qu}$,** respectively.

With the intention to improve the antibacterial activity of newly synthesized compounds the substituted cinnamic acid with chloro and methoxy group in *para* position was selected. According to previous study and results from structure-activity analysis these groups are recognized as a crucial factor which contributes to increasing of antimicrobial activity.[137,252] It was explained that "the ability to acquire resistance to antibacterial drugs is not distributed evenly throughout all bacteria. Infectious Disease Society of America (IDSA) identified six species as especially dangerous pathogens responsible for life-threatening nosocomial infections throughout the world[253] and named them as ″ESKAPE″ pathogens, which is an acronym for *Enterococcus faecium*, *Staphylococcus aureus*, *Klebsiella pneumoniae*, *Acinetobacter baumannii*, *Pseudomonas aeruginosa* and *Enterobacter species.* Especially dangerous and ranked as one of the top priority is *A. baumannii* since it is the most common bacteria in intensive care units with a high mortality rate, due to its ability

to produce biofilms on various surfaces and develop resistance to all currently available antibiotics.[254,255]"

Regarding anti-*Mtb* activity (Figure 37- Figure 39, Table 9), the least efficiency was achieved by the treatment compound **CimTCH$_{sal}$**. Replacement of 2-hydroxyphenyl group in **CimTCH$_{sal}$** with 2-pyridyl ring (compound **CimTCH$_{2fp}$**) didn't notably enhance anti-*Mtb* potential, but did by additional inclusion of methyl group at C7 position as it is in compound **CimTCH$_{2ap}$**. However, **CimTCH$_{8OH2qu}$** which is endowed with 8-hydroxy-2-quinolyl ring was the one with capacity to diminish survival of treated *Mtb* in all treated strains. Further introduction of chlorine in 3- or 4- position to phenyl ring resulted in differently altered activity compared to parental compound. This structural manipulation to **CimTCH$_{8OH2qu}$** drastically reduced activity of both of its chlorine analogues, whereas no particular improvement was seen for **3-ClCimTCH$_{sal}$** and **4-ClCimTCH$_{sal}$** compared to **CimTCH$_{sal}$.** On the contrary, 3-chlorine analogue of **CimTCH$_{2ap}$** (**3-ClCimTCH$_{2ap}$**) and 4-chlorine analogue of **CimTCH$_{2fp}$** (**4-ClCimTCH$_{2fp}$**) were more successful than their parental compounds (Figure 39), achieving MIC$_{90}$ in *Mtb-Inh-R* strain (Table 9).

### 3.7.1. Antimicrobial activity

#### 3.7.1.1. Results on antibacterial activity

Bacteria from the "ESKAPE" group are pathogens related to widespread infections in humans, which effect a large number of mortality. These pathogens are resistant to common drugs/antibiotics, or they could acquire resistance what creates pressure to constantly develop new drugs. The antibacterial activity of synthesized compounds (Table 8) against six microorganisms (*Enterococcus cloacae* ATCC13047, *Staphylococcus aureus* NCTC 6571, *Klebsiella pneumoniae* ATCC 13883, *Acinetobacter baumannii* ATCC 19606, *Pseudomonas aeruginosa* NCTC 10662, and *Escherichia coli* ATCC 1175) was tested. Some investigated compounds (**CimTCH$_{2fp}$**, **CimTCH$_{2ap}$**, **4-ClCimTCH$_{8OH2qu}$**, **4-ClCimTCH$_{2ap}$**, **4-MeOCimTCH$_{2fp}$** and **4-MeOCimTCH$_{2ap}$**) showed appreciable antibacterial activity to all strains used, while all compounds showed significant activity against *A. baumannii*. Obtained activities are similar to usually used antibiotics in practice.[256] The activities, given as minimum inhibitory concentration necessary to inhibit the growth of 50% of organisms (MIC$_{50}$), are given in Table 8.

Table 8. Minimun inhibitory concentration MIC$_{50}$ (μmol/L) of compounds

| Compound | *E.cloacae* ATCC 13047 | *P. aeruginosa* NCTC 10662 | *K. pneumoniae* ATCC 3883 | *S. aureus* NCTC 6571 | *A. baumannii* ATCC 19606 | *E. coli* ATCC 1175 |
|---|---|---|---|---|---|---|
| **CimTCH$_{2fp}$** | 46.1 | 122.9 | 24.6 | 15.4 | 30 | 62.5 |
| **CimTCH$_{sal}$** | + | + | + | + | 183.6 | + |
| **CimTCH$_{8OH2qu}$** | + | + | + | + | 19.3 | + |
| **CimTCH$_{2ap}$** | 58.9 | + | 117.8 | 58.9 | 11.5 | 15.6 |
| **4-ClCimTCH$_{2fp}$** | + | + | + | + | 21.7 | + |
| **4-ClCimTCH$_{sal}$** | 53.4 | 106.7 | + | + | 53.4 | + |
| **4-ClCimTCH$_{8OH2qu}$** | 47.0 | 70.4 | 93.6 | 70.4 | 46.9 | + |
| **4-ClCimTCH$_{2ap}$** | 40.1 | 53.5 | 53.5 | 53.5 | 10.4 | 31.25 |
| **4-MeOCimTCH$_{2fp}$** | 168.8 | 281.4 | 196.9 | 140.7 | 10.9 | 31.25 |
| **4-MeOCimTCH$_{sal}$** | + | + | + | + | 168.7 | + |
| **4-MeOCimTCH$_{8OH2qu}$** | + | + | + | + | 18.5 | + |
| **4-MeOCimTCH$_{2ap}$** | 108.3 | + | 81.2 | 54.1 | 27.1 | 31.25 |

(+) indicates growth of microorganism

The results from Table 8 indicate on large variability of MIC$_{50}$ values obtained in the range from 0.4 to 196.9 μM. Among all tested bacteria *A. baumannii* showed the highest sensitivity to all studied compounds. Regardless to the wide range of MIC$_{50}$ values (Table 8) appropriate conclusion and the

structure-activity relationship could be established. Compounds with salicylic moiety and for all types of cinnamic acid residues showed low or no activity against tested bacteria. Other compounds showed better significant activities which means that the presence of heterocyclic ring (quinoline or pyridine) highlights the significance of nitrogen atom/aromaticity in the compound to acquire higher activity. Such a conclusion is in accordance with the literature findings.[257] In general, compounds with pyridine ring, preferentially those with 2-acetyl pyridine residue (**CimTCH$_{2ap}$, 4-ClCimTCH$_{2ap}$ and 4-MeOCimTCH$_{2ap}$**) are the most potent.

In regard to *A. baumannii* good activity showed compound with 4-chlorocinnamoyl moiety and 2-formylpyridine and 2-acetylpyridine residue.

The hybrid of *p*-chloro cinnamic acid and MTCH of acetyl pyridine (**4-ClCimTCH$_{2ap}$**) is particularly active compound with the $MIC_{50}$ = 10.4 μM against *A. baumannii*.

These values are approximately 2 to 4 folds higher than the most of commonly used β-lactam antibiotics,[256] even 20-40 folds higher than for cefalosporins[258] and 5-8 folds higher than for carbapenems –as one of the most important antibiotics used for the treatment of *A. baumanni*.[259]

Individually cinnamic acid showed weak antibacterial activity[3], while **m-TCHs** also display weak to moderate activity,[260,261] what imply that synthesized compound offer appropriate synergism of the two pharmacophores connected by an amide bond. In order to understand the relation between obtained activities and structural properties of studied compounds an alignment-independent 3D QSAR model based on molecular interaction fields was applied.

This approach provides basic information on the effect of the present pharmacophore to obtained activity, which is essential to the development of a new drug of higher potency.

### 3.7.1.2. Investigation of anti-*Mtb* activity

In order to assess whether investigated compounds can impact survival abilities of *Mtb*, the investigation has been organized on three selected strains isolated from clinical samples. Selection of strains was performed on the basis of their genotyping sensitivity or resistance to INH and RIF as follows (Figure 36):

(1) *Mtb-InhRif-S* is the strain without mutations confirmed to be associated with resistance to any of these two drugs;

(2) *Mtb-Inh-R* is the strain harboring S315T mutation in *katG* gene associated with resistance to INH;

(3) *Mtb-Rif-R* is the strain with S531L mutation in *rpoB* gene accountable for resistance to RIF.

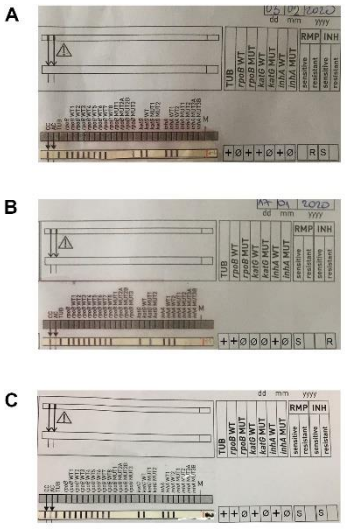


Figure 36. Profiles of *Mtb* strains obtained by the GenoType MTBDRplus assy (A) *Mtb-Rif-R,* (B) *Mtb-Inh-R,* and (C) *Mtb-InhRif-S.* CC – Conjugate Control; AC – Amplifiation Control; TUB –

*Mycobacterium tuberculosis* complex; *rpoB, katG, inhA* – locus control zones; *rpoB* WT1-8 – *rpoB* wild type probes 1-8 (codons 505-533); *rpoB* MUT1-3 – *rpoB* mutation probes (MUT1 - D516V; MUT2A - H526Y; MUT2B - H526D; MUT3 - S531L); *katG WT* – *katG* wild type *probe* (codon 315); *katG* MUT1-2 – *katG* mutation probes (MUT1 - S315T1); *inhA* WT1-2 – *inhA* wild type probes (nucleic acid positions -15, -16, -8); *inhA* MUT1-3 – *inhA* mutation probes (MUT1 - C15T; MUT2 - A16G; MUT3A - T8C; MUT3B - T8A); RMP – rifampicin; INH – isoniazid; R – resistant; S – sensitive.

Anti-*Mtb* activity has been determined as minimal inhibitory concentration (MIC), with INH and RIF as positive control treatments. Concentration-response curves are presented in Figure 37 - Figure 39, while MIC values are shown in Table 9.

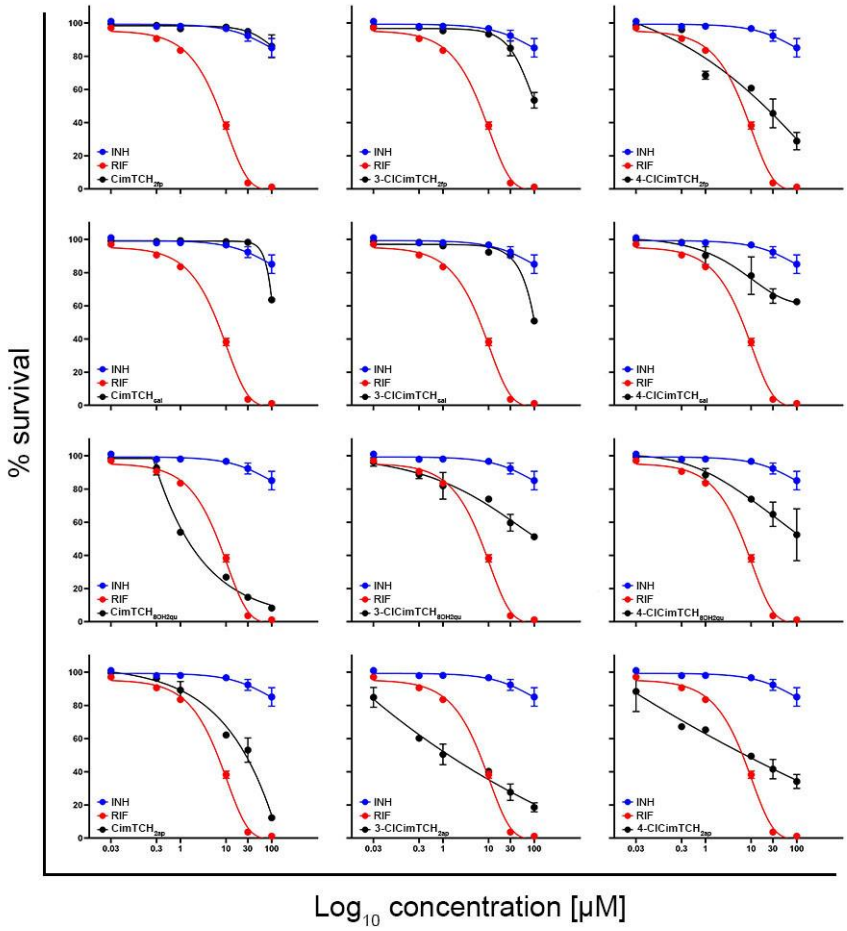


Figure 37. Curves describing relationship between applied concentrations and survival of *Mtb-InhRif-S* strain treated with INH, REF, and investigated compounds.

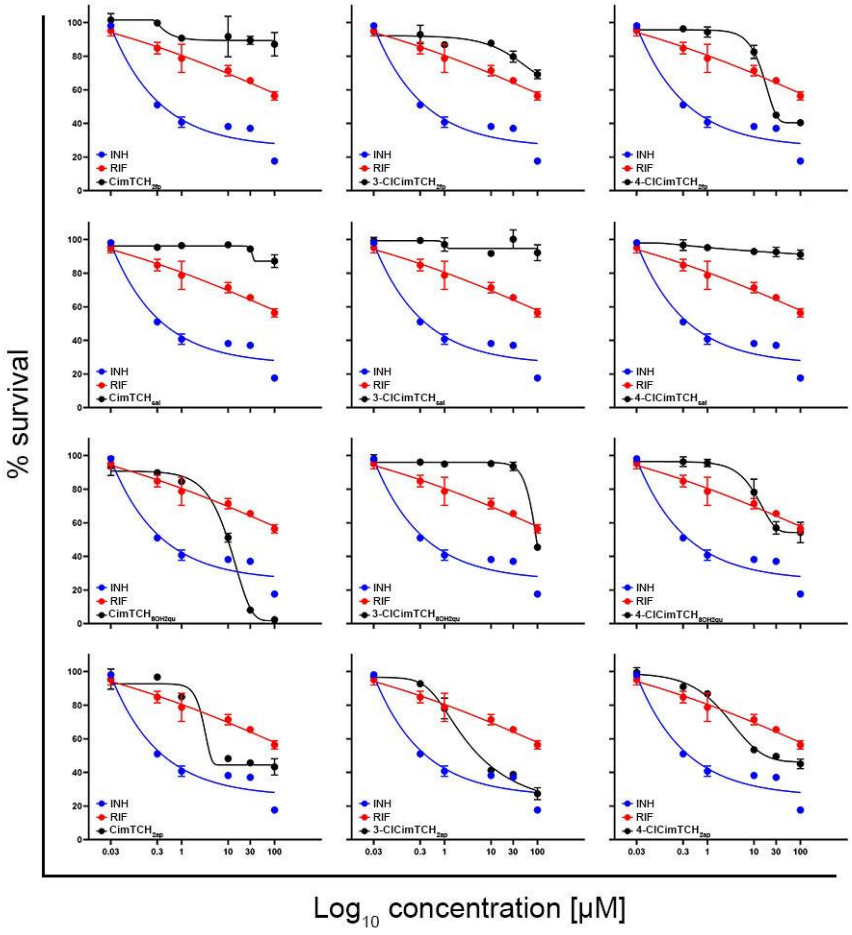


Figure 38. Curves describing relationship between applied concentrations and survival of *Mtb-Rif-R* strain treated with INH, REF, and investigated compounds.

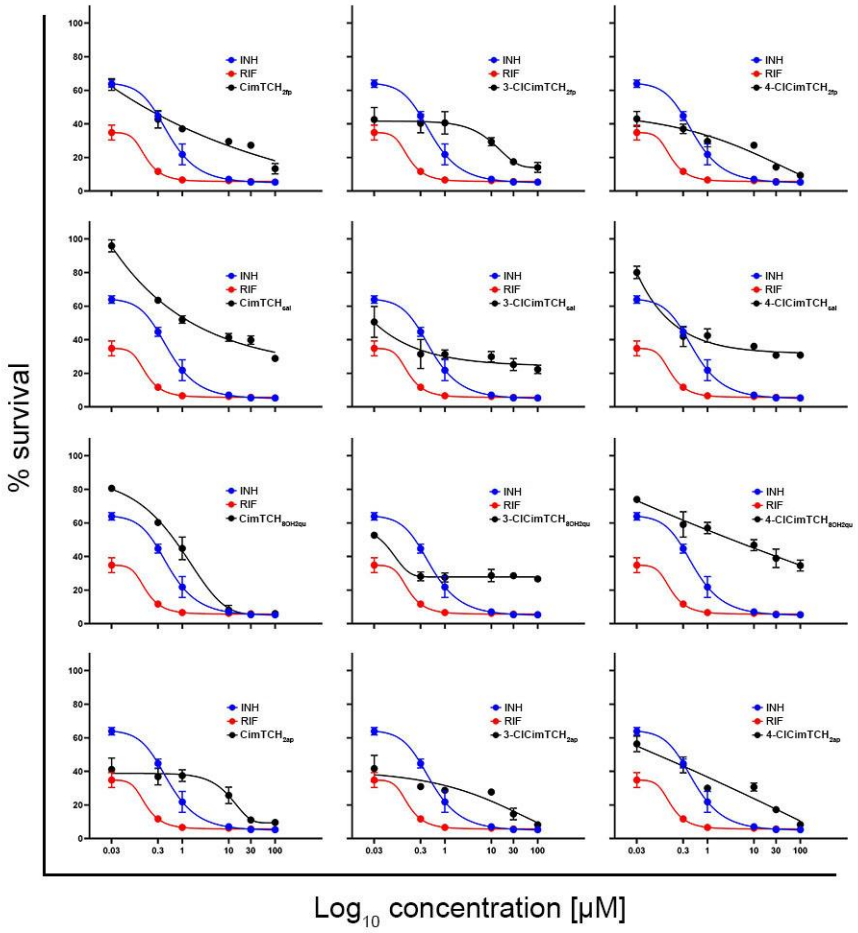


Figure 39. Curves describing relationship between applied concentrations and survival of *Mtb-Inh*-R strain treated with INH, REF, and investigated compounds.

Table 9**.** Minimal inhibitory concentrations (MIC) determined by means of MTT assay for investigated compounds with isoniazid (INH) and rifampicin (RIF) as reference drugs after six days of incubation on selected *Mtb* strains.

| | **Treatment [µM]** | | | | | |
|---|---|---|---|---|---|---|
| **Strains** | INH | RIF | $CimTCH_{8OH2qu}$ | $CimTCH_{2ap}$ | $3\text{-}ClCimTCH_{2ap}$ | $4\text{-}ClCimTCH_{2fp}$ |
| *Mtb-InhRif-S* | /* | 26 | 92 | / | / | / |
| *Mtb-Rif-R* | / | / | 30 | / | / | / |
| *Mtb-Inh-R* | 4 | 2 | 10 | 42 | 90 | 88 |

* - not determined in the range of applied concentrations.

Results acquired by MTT assay illustrate phenotypic sensitivity of the treated *Mtb* strains, which in terms of INH and RIF activities reveal a notable degree of discrepancy compared to the outcomes of genotype testing. As it can be seen in Figure 37 and Table 9, RIF achieved a high MIC value while INH did not affect the vitality of *Mtb-InhRif-S* strain that was confirmed for lacking mutations related to resistance to either of drugs (Figure 36). In RIF resistant *Mtb-Rif-R* strain, INH was more effective, but none of these two treatments attained 90 % of *Mtb* growth inhibition (Figure 38 and Table 9). In *Mtb-Inh-R* strain, MIC value gained by RIF is only one that correlates with literature data reported for wild type $H_{37}Rv$ strain, whereas MIC for INH is about 5 times higher than in $H_{37}Rv$ and it correlates with detected mutation.[128,262] Described genotypic-phenotypic

inconsistencies have been noted by other authors,[263–265] and a possible explanation is the emanation of mutation on other gene regions that cannot be detected by GenoType MTBDR plus test.

Investigated compounds revealed strain-dependent capacity to reduce viability of treated bacilli. The most susceptible strain was *Mtb-Inh-R*, where four out of twelve compounds reduced *Mtb* survival for more than 90 % (Figure 39 and Table 9). The same four, **CimTCH$_{8OH2qu}$**, **CimTCH$_{2ap}$**, **3-ClCimTCH$_{2ap}$**, **4-ClCimTCH$_{2fp}$**, were the most effective in other two strains as well. However, while **CimTCH$_{8OH2qu}$** in *Mtb-Rif-R* achieved MIC value, compounds **CimTCH$_{2ap}$**, **3-ClCimTCH$_{2ap}$** and **4-ClCimTCH$_{2fp}$** decreased population of *Mtb* from 50 - 70% (Figure 38). Similar results were acquired by the treatment of *Mtb-InhRif-S* strain, but compared to *Mtb-Rif-R*, activities of **CimTCH$_{2ap}$**, **3-ClCimTCH$_{2ap}$** and **4-ClCimTCH$_{2fp}$** were higher while MIC value of **CimTCH$_{8OH2qu}$** was above those in other two strains (Figure 37 and Table 2). Overall, compound **CimTCH$_{8OH2qu}$** is only the one that successfully reduced the viability of *Mtb* bacilli in all three treated strains that were not fulfilled with either INH or RIF.

#### 3.7.1.3. Compounds with confirmed anti-*Mtb* activity do not affect survival of HepG-2 cells

Hepatotoxicity is the major and serious side effect of tuberculosis treatment with INH.[266] It was previously published that INH significantly compromized vitality of HepG-2 cells that were used as a reliable model for evaluation of hepatotoxic potential.[262]. In order to evaluate whether compounds that demonstrated anti-*Mtb* activity may also harm hepatocytes, HepG-2 cells were treated with **CimTCH$_{8OH2qu}$**, **CimTCH$_{2ap}$**, **3-ClCimTCH$_{2ap}$** and **4-ClCimTCH$_{2fp}$** for 24 h and viability of treated cells was assessed by the means of CAM/PI dual staining. As it can be seen in Figure 40 - Figure 43 none of those compounds induced cell death of HepG-2 cells.

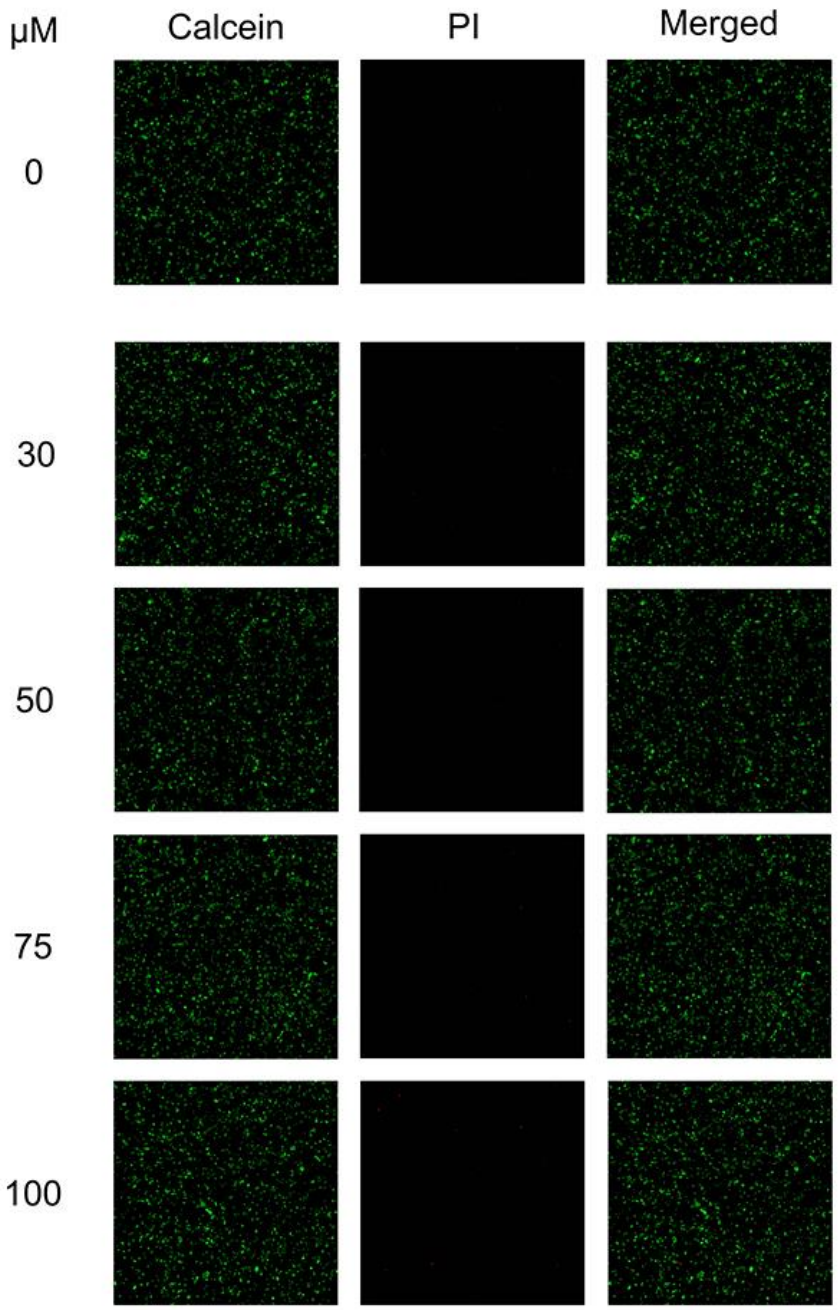


Figure 40 Images of HepG-2 cells stained with CAM/PI after 24 hours treatment with **$CimTCH_{8OH2qu}$.**

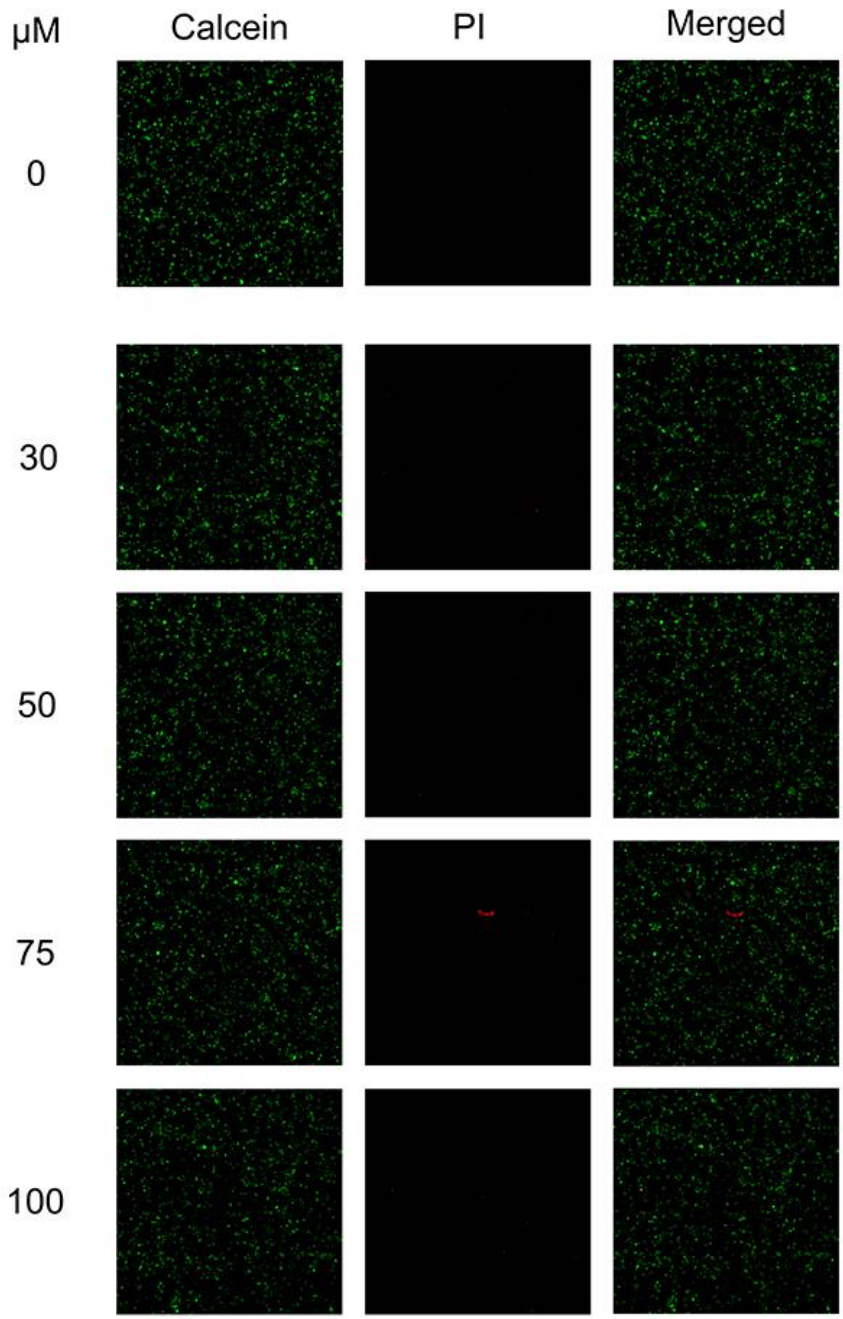


Figure 41. Images of HepG-2 cells stained with CAM/PI after 24 hours treatment with **$CimTCH_{2ap}$**.

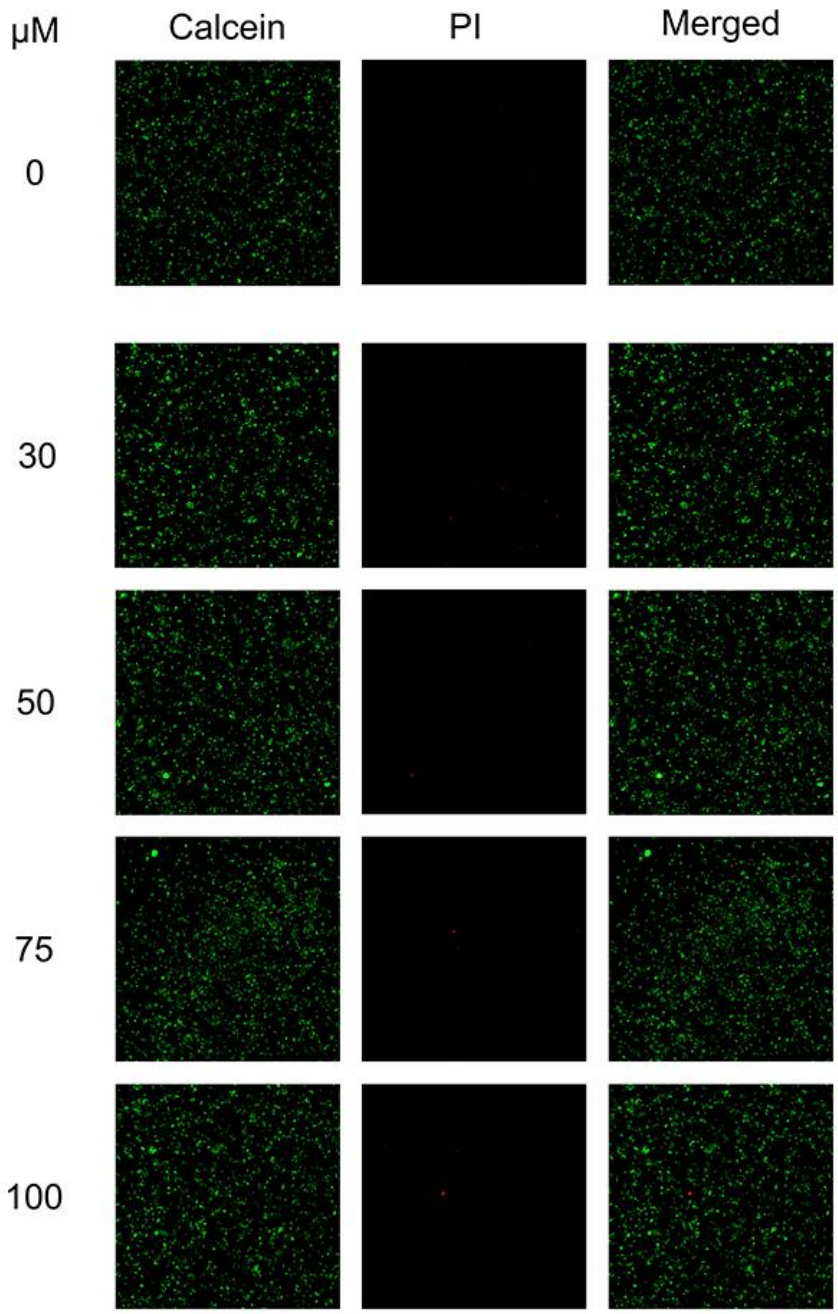


Figure 42. Images of HepG-2 cells stained with CAM/PI after 24 hours treatment with **3-ClCimTCH$_{2ap}$**

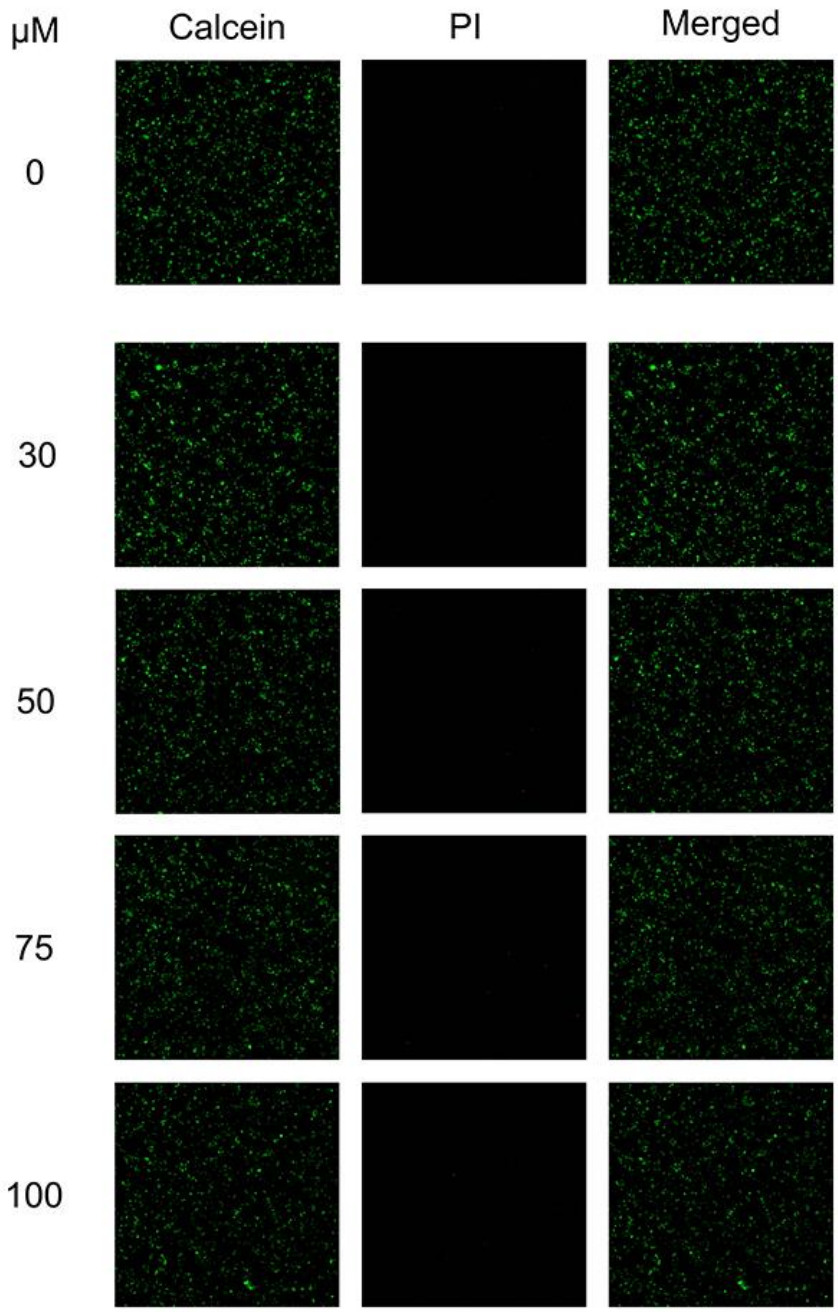


Figure 43. Images of HepG-2 cells stained with CAM/PI after 24 hours treatment with **4-ClCimTCH$_{2fp}$**.

### 3.7.2. 3D QSAR model

The "four-component principal component analysis (PCA) model derived from the FFD-filtered set of variables explained 77.72% of the initial X sum of squares ($SSX_{acc}$) and 64.81% of their variance ($VarX_{acc}$)" are given in Table 10.

Table 10. The statistical data of the four-component PCA model for the set of 388 GRIND descriptors

| PC | SSX | $SSX_{acc}$ | VarX | $VarX_{acc}$ |
|---|---|---|---|---|
| 1 | 28.33 | 28.33 | 21.06 | 21.06 |
| 2 | 20.00 | 48.33 | 15.63 | 36.69 |
| 3 | 16.33 | 64.67 | 14.54 | 51.23 |
| 4 | 13.06 | 77.72 | 13.58 | 64.81 |

In the forthcoming step PLS model, used for the investigation of pharmacophoric structure properties significant for the antibacterial activity of cinnamamides with respect to *A. baumanii*, was developed. The parameters obtained by statistical validation of the developed model for three cross-validation procedures "(leave-one-out - LOO, leave-two-out - LTO, and random groups - RG)" are given in Table 11. It is not of high value to separate such a relatively small set (12 cinnamamides) into training and test set, as RG cross-validation basically provides the same information on the predictivity of the model.

Table 11. The statistics of the PLS model for two latent variables (LV) after one FFD cycle and application of 3 cross-validation (CV) procedures: LOO, LTO, and RG. The other CV parameters were FFD-LV = 2, 20% of dummy variables, 20 randomization cycles, and 3 random groups.

| Component | $SSX_{acc}$ | SDEC | SDEP | $r^2_{acc}$ | $q^2_{acc}$ |
|---|---|---|---|---|---|
| 2 LV (LOO) | 43.36 | 0.11 | 0.57 | 0.93 | 0.65 |
| 2 LV (LTO) | 42.33 | 0.11 | 0.61 | 0.93 | 0.60 |
| 2 LV (RG) | 41.71 | 0.10 | 0.65 | 0.94 | 0.54 |

The 2 LV model, after application of the LOO CV method, was interpreted in the next step. The coefficients obtained from PLS plot (Figure 44) showed the distribution of the variables in 10 blocks and their relative impact on the antimicrobial potency of the cinnamamides. The most significant variables that differentiate potent from less potent cinnamamides are given by sequential numbers. The appropriate corresponding LV coefficients obtained for calculated variables are presented in Table 12.

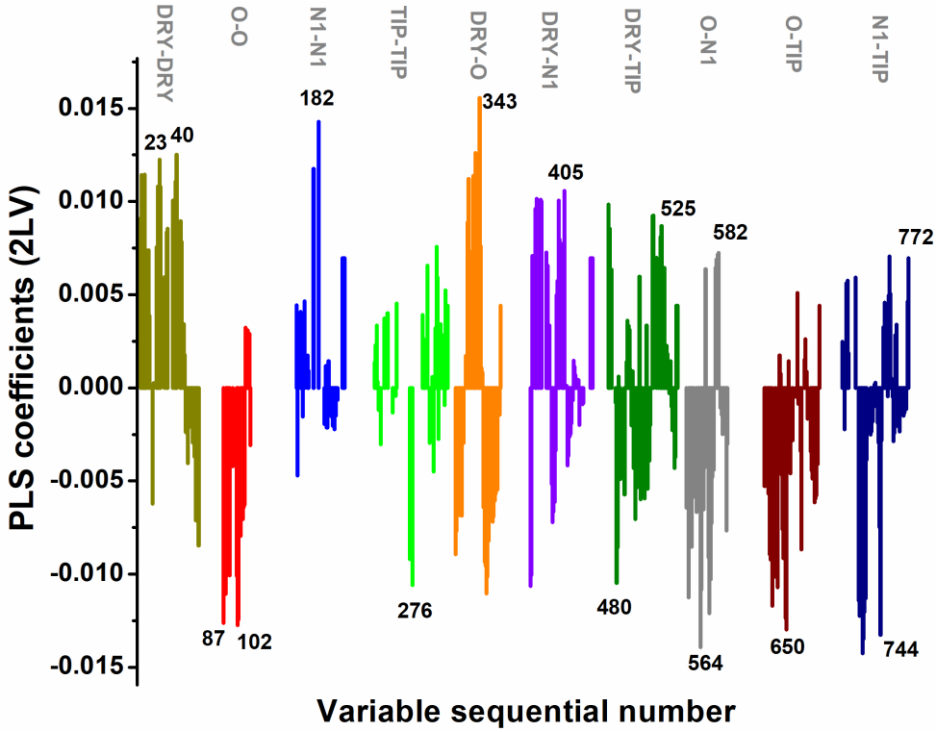


Figure 44. PLS coefficients plot for 2LV model

DRY-DRY autocorrelograms gave the indication on the existence of two groups having hydrophobic character at distances up to 15 Å with positive influence to increased antibacterial activity, while, on the other hand, higher spatial separation of hydrophobic hotspots contribute to negative correlation with the antimicrobial potential. O-O correlograms showed that the two groups with HBD properties, at distances from 3 to 10 Å, also showed a negative correlation with the antimicrobial potential of cinnamides. Oppositely, the existence of two groups with HBD properties which showed interaction with N1 probes at various distances (N1-N1 probe block) positively

contributes on antimicrobial potential. The TIP-TIP probe block showed very intensive variables at 13-14 Å and contribute to decrease of antimicrobial potency, and in that way dictate discrimination of cinnamides with respect to the shape/dimensions. Obtained results from DRY-O cross-correlograms, the optimal distance between the group with HBD properties and a hydrophobic hotspot is approximately 10 Å, as obtained by the value of variable 343. The most of variables from the block of DRY-N1 variable contribute to increases of the activity with respect to *A. baumanii* and differentiate the cinnamamides on the basis of their potency. DRY-TIP variable block provides data on the optimal distance between structural fragments with hydrophobic character and molecule edge. The most of variables at the distance higher than 16 Å gave a positive correlation with antibacterial activity. The high intensity of O-N1 variables with negative values of PLS coefficients asserts the negative effect of the presence of salicylaldehyde residue to the antimicrobial activity. The variables at higher distances (~ 11Å) define the optimal distance between groups with HBD and HBA properteis. The variables from the block of O-TIP probe gave a mainly negative correlation with the antimicrobial activity, which, in line with that, indicate the negative influence of the presence of *ortho*-OH group to potency. The results for the block of N1-TIP probe determine the optimal distance between group with HBA properties and molecule edge. Also, variables at the distance less than 14 Å showed a negative correlation, and longer variables exist only in the most active cinnamamides.

The structural fragments closely related with all variables significant for the interpretation of the developed model are given in Figure 45 and Figure 46. Also, the corresponding LV coefficients are given in Table 12. The overview of selected variables, which have a pronounced influence on the developed 3D QSAR model is listed in Table 13.

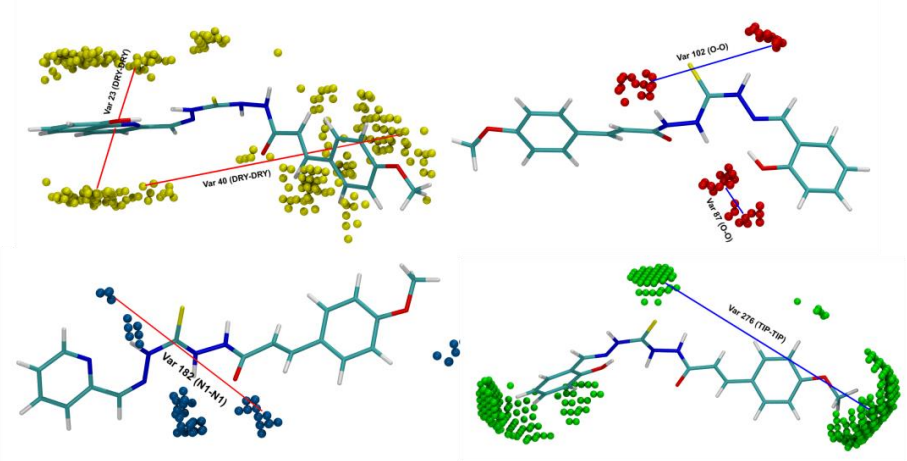


Figure 45. The structural fragments associated with GRIND variables derived from auto-correlograms depicted on **4-MeOCimTCH$_{8OH2qu}$** (for DRY-DRY), **4-MeOCimTCH$_{sal}$** (for O-O and TIP-TIP), and **4-MeOCimTCH$_{2fp}$** (for N1-N1)

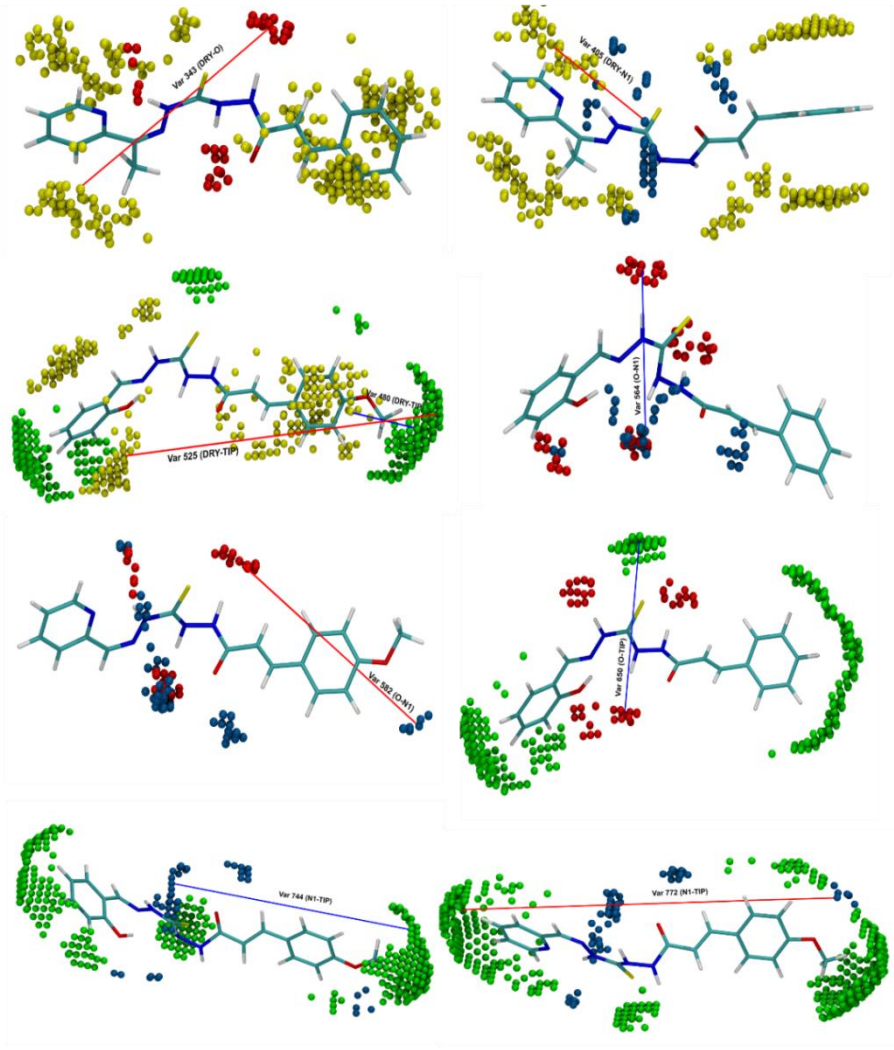


Figure 46. The structural motif associated with GRIND variables derived from MIF cross-correlogram.

Table 12. The list of compounds ordered according to descending potency against *A. baumanii*, the list of most important variables, and the LV coefficients associated with them. The sign in brackets denotes a positive or negative correlation with the potency for a given variable.

| | | **LV coefficients** | | | | | | | | | | | | | | |
|---|---|---|---|---|---|---|---|---|---|---|---|---|---|---|---|---|
| | | **23 (+)** | **40 (+)** | **87 (–)** | **102 (–)** | **182 (+)** | **276 (–)** | **343 (+)** | **405 (+)** | **480 (–)** | **525 (+)** | **564 (–)** | **582 (+)** | **650 (–)** | **744 (–)** | **772 (+)** |
| **Compounds** | **3-ClCimTCH$_{2ap}$** | 0.440 | 0.548 | 0 | 0.422 | 0.581 | 0.248 | 0.609 | 0.687 | 0.286 | 0.695 | 0.711 | 0 | 0.368 | 0.607 | 0 |
| | **4-ClCimTCH$_{2fp}$** | 0.411 | 0.505 | 0 | 0.422 | 0.713 | 0.281 | 0.639 | 0.737 | 0.289 | 0.666 | 0.758 | 0.554 | 0.405 | 0.590 | 0.395 |
| | **CimTCH$_{2ap}$** | 0.408 | 0.550 | 0 | 0.406 | 0.687 | 0.183 | 0.652 | 0.790 | 0.317 | 0.534 | 0.677 | 0 | 0.456 | 0.612 | 0 |
| | **4-ClCimTHC$_{8OH2qu}$** | 0.478 | 0.505 | 0 | 0.450 | 0.718 | 0.101 | 0.635 | 0.754 | 0.336 | 0.744 | 0.705 | 0.579 | 0.352 | 0.680 | 0 |
| | **CimTCH$_{8OH2qu}$** | 0.478 | 0.550 | 0 | 0.449 | 0.663 | 0.102 | 0.609 | 0.701 | 0.236 | 0.463 | 0.708 | 0.545 | 0.388 | 0.579 | 0 |
| | **3-ClCimTCH$_{2afp}$** | 0.430 | 0.531 | 0 | 0.434 | 0.614 | 0.232 | 0.607 | 0.675 | 0.298 | 0.682 | 0.685 | 0 | 0.406 | 0.664 | 0 |
| | **4-ClCimTCH$_{2afp}$** | 0.390 | 0.505 | 0 | 0.420 | 0.696 | 0.203 | 0.573 | 0.786 | 0.297 | 0.719 | 0.770 | 0.429 | 0.401 | 0.705 | 0 |
| | **CimTCH$_{2fp}$** | 0.402 | 0.523 | 0 | 0.407 | 0.721 | 0.188 | 0.547 | 0.736 | 0.260 | 0.465 | 0.761 | 0 | 0.406 | 0.584 | 0 |
| | **3-ClCimTCH$_{8OH2qu}$** | 0.476 | 0.515 | 0 | 0.426 | 0.650 | 0.134 | 0.612 | 0.619 | 0.311 | 0.721 | 0.734 | 0.432 | 0.460 | 0.659 | 0 |
| | **3-ClCimTCH$_{sal}$** | 0.365 | 0.488 | 0.441 | 0.615 | 0.457 | 0.511 | 0.558 | 0.456 | 0.361 | 0.452 | 0.701 | 0 | 0.557 | 0.623 | 0 |
| | **4-ClCimTCH$_{sal}$** | 0.327 | 0.448 | 0.424 | 0.612 | 0 | 0.430 | 0.521 | 0.599 | 0.377 | 0.467 | 0.847 | 0 | 0.547 | 0.744 | 0 |
| | **CimTCH$_{sal}$** | 0.309 | 0.482 | 0.391 | 0.606 | 0 | 0.502 | 0.521 | 0.583 | 0.372 | 0.425 | 0.877 | 0 | 0.539 | 0.761 | 0 |

Table 13. “The overview of several variables having the highest influence on the developed 3D QSAR model”

| Probe block | Variable Nº | Distance (Å) | Impact | Regions, comments |
|---|---|---|---|---|
| DRY-DRY | 23 | 7.36 - 7.68 | + | “Positively correlated with potency, more pronounced in more potent compounds. It distinguishes derivatives **CimTCH$_{sal}$/ 3-ClCimTCH$_{sal}$/ 4-ClCimTCH$_{sal}$** from **CimTCH$_{2fp}$/ 3-ClCimTCH$_{2fp}$/ 4-ClCimTCH$_{2fp}$, CimTCH$_{8OH2qu}$/ 3-ClCimTCH$_{8OH2qu}$/ 4-ClCimTCH$_{8OH2qu}$,** and **CimTCH$_{2ap}$/ 3-CimTCH$_{2ap}$/ 4-CimTCH$_{2ap}$.** Variable is located within two hydrophobic hotspots on (TCH) moiety.” |
| DRY-DRY | 40 | 12.80 - 13.12 | + | “This variable shows similar trends in the influence on the potency and its expression. It is located between two hydrophobic hotspots on the cinnamic acid and TCH moieties.” |
| O-O | 87 | 2.88 - 3.20 | – | “Expressed only in the least potent compounds. One node is located on the *ortho*-hydroxy group of salicylaldehyde moiety and the other is near $N_3$–H atom. It highlights the negative influence of the *ortho*-hydroxy group on the interaction of compounds bearing salicylic moiety within the virtual receptor site.” |
| O-O | 102 | 7.68 - 8.00 | – | “This variable maps two HBD groups, and is most pronounced in the least potent salicylic derivatives.” |
| N1-N1 | 182 | 8.32 - 8.64 | + | “The optimum distance between two HBA groups. One node is positioned on carbonyl oxygen atom, and the second one is on *ortho*-nitrogen atom of pyridyl moiety or 8–hydroxy group of **CimTCH$_{8OH2qu}$/ 3-ClCimTCH$_{8OH2qu}$/ 4-ClCimTCH$_{8OH2qu}$** moiety. This variable discriminates more potent **CimTCH$_{2fp}$/ 3-ClCimTCH$_{2fp}$/ 4-ClCimTCH$_{2fp}$, CimTCH$_{8OH2qu}$/ 3-ClCimTCH$_{8OH2qu}$/ 4-ClCimTCH$_{8OH2qu}$, CimTCH$_{2ap}$/ 3-CimTCH$_{2ap}$/ 4-CimTCH$_{2ap}$** and from less potent **CimTCH$_{sal}$/ 3-ClCimTCH$_{sal}$/ 4-ClCimTCH$_{sal}$** derivatives. It highlights the importance of *ortho*-pyridyl moiety for the potency toward *A. baumanii.”* |
| TIP-TIP | 276 | 13.44 - 13.76 | – | “This variable encodes shape features negatively correlated with the potency. It is more expressed in less potent compounds. One node is located on the thione S atom, and the other one represents the molecule edge around the cinnamoyl phenyl ring. The highest variable values (VV) are obtained for methoxy-substituted derivatives, which indicate its negative influence on potency.” |
| DRY-O | 343 | 9.92 - 10.24 | + | “Represents favorable distance between hydrophobic moiety and HBD group. O probe node is located around $N_4$–H and the DRY probe is positioned close to the center of the aromatic ring on TCH moiety. Discriminates compounds according to potency, as more potent compounds have larger VV (Table 12).” |
| DRY-N1 | 405 | 4.80 - 5.12 | + | “Represents optimum distance between HBA group, which is a carbonyl O atom in the most potent compounds, and hydrophobic hotspot positioned at the aromatic ring of TCH moiety. The variable is better expressed in more potent compounds (Table 12).” |
| DRY-TIP | 480 | 3.84 - 4.16 | – | “This variable suggests the negative influence of para-methoxy phenyl moiety on the potency. Also, the thione S atom as a center of TIP probe is associated with DRY probe node around 2-hydroxy phenyl group in several least potent derivatives (Table 12).” |

| Probe block | Variable Nº | Distance (Å) | Impact | Regions, comments |
|---|---|---|---|---|
| DRY-TIP | 525 | 18.24 - 18.56 | + | "The presence of hydrophobic group at a large distance from the molecule edge is positively correlated with potency. This variable is generally more expressed in more potent compounds (Table 12), and *p*-chloro and *p*-methoxy cinnamic acid are the groups that positively contribute to the variable values." |
| O-N1 | 564 | 5.76 - 6.08 | – | "The distance between HBD (*ortho*-hydroxy group) and HBA ($N_2$-H). The highest VV are observed for the two least potent compounds, **CimTCH$_{sal}$** and **4-ClCimTCH$_{sal}$**." |
| O-N1 | 582 | 11.52 - 11.84 | + | Highlights the positive influence of 8-hydroxy-2-quinoline moiety on biological activity. O probe node is located near 8-hydroxy group while N1 probe is centered at carbonyl O atom. |
| O-TIP | 650 | 8.32 - 8.64 | – | "The distance between molecule edge, which is S atom in the compounds having the highest VV, and the HBD probe which is 2-hydroxy group in **CimTCH$_{sal}$**, **3-ClCimTCH$_{sal}$** and **4-ClCimTCH$_{sal}$** derivatives." |
| N1-TIP | 744 | 13.44 - 13.76 | – | "The unfavorable distance between HBA group and molecule edge. Better expressed in the less potent compounds (Table 12)." |
| N1-TIP | 772 | 22.40 - 22.72 | + | "This variable is expressed only in **4-ClCimTCH$_{2fp}$**, highlighting the importance of methoxy group O atom as HBA and the molecule edge at the large distances on the opposite side of the molecule."[273] |

### 3.7.3. Rationalization of the mechanism of antimicrobial activity versus iron chelating ability

It was found interesting that highest activity of studied compounds with respect to *A. baumannii*, and the fact that among the all tested gram-negative bacteria, it has the fewest and smallest porin channels.[267] Thus it is a substantial goal to rationalize the relation between structure and high potency of synthesized compounds toward *A. baumannii* and give some additional facts to the poorly known mechanism of action and high ability to acquire resistance genes. It was explained that "mechanisms of developing resistance are various and include low permeability of the outer membrane, up-regulation of the efflux system or alteration of penicillin-bonding proteins and porins.[267] Smith and coworkers have identified genes enabling *A. baumannii* to metabolize ferulates and other hydroxycinnamates.[268] Those cinnamic acid analogs are metabolized by intracellular enzymes encoded by *hca* gene, which means that bacteria developed an uptake system for such compounds. Considering these features of *A. baumannii*, it could be expected that, due to the structural similarity, cinnamic acid moieties of synthesized compounds are recognized by this uptake system. Accordingly, the molecule passes through a poorly permeable outer membrane and enters the cell. Once, when reduced entry has been defeated and the molecule penetrates the cell, it can manifest its antibacterial activity."

The literature reports on strategies of design and synthesis of new and effective drugs are limited in number, but the findings are encouraging and interesting. Since the growth and replication of pathogen are strictly dependent on their ability to utilize iron, one promising strategy suggests that iron uptake could be a key target for design of antimicrobials for treating infections.[269] Those quotations were previously confirmed for gram-negative aerobic *A. baumanni*.[270] and *MTB*.[271] Based on the structure of synthesized compounds and the presence of several potential donor sites in the molecule as ligands and coordinate with metal ions.[272,68] Harington et al. affirmed that the antimicrobial activity is related to the affinity of the molecule for binding iron.[273] On those grounds, we have performed additional studies and tested the affinity of cinnamamides to $Fe^{2+}$ and $Fe^{3+}$ ions, and the stability of formed complexes. The results are given in Table 14. Also, for the most stable **3-ClCimTCH$_{2ap}$**, corresponding UV spectra and the dependence of the absorbance difference on the molar ratio of metal and compound are shown in Figure 47.

Table 14. Stability constants of cinnamic acid hydrazide complexes with $Fe^{2+}$ and $Fe^{3+}$ ions.

| Compound | **$K_s$ ($Fe^{2+}$)** | **$K_s$ ($Fe^{3+}$)** |
|---|---|---|
| **CimTCH$_{2fp}$** | $1.11\cdot10^{9}$ | $2.99\cdot10^{8}$ |
| **CimTCH$_{sal}$** | $4.29\cdot10^{8}$ | $1.67\cdot10^{7}$ |
| **CimTCH$_{8OH2qu}$** | $4.89\cdot10^{9}$ | $5.47\cdot10^{8}$ |
| **CimTCH$_{2ap}$** | $6.91\cdot10^{9}$ | $1.91\cdot10^{9}$ |
| **3-ClCimTCH$_{2fp}$** | $1.3\cdot10^{9}$ | $4.8\ 10^{9}$ |
| **3-ClCimTCH$_{sal}$** | $4.0\cdot10^{8}$ | $1.2\cdot10^{9}$ |
| **3-ClCimTCH$_{8OH2qu}$** | $4.9\cdot10^{8}$ | $3.5\ 10^{9}$ |
| **3-ClCimTCH$_{2ap}$** | $1.7\cdot10^{9}$ | $5.4\cdot10^{9}$ |
| **4-ClCimTCH$_{2fp}$** | $3.40\cdot10^{9}$ | $3.85\cdot10^{9}$ |
| **4-ClCimTCH$_{sal}$** | $1.50\cdot10^{9}$ | $1.2\cdot10^{9}$ |
| **4-ClCimTCH$_{8OH2qu}$** | $1.85\cdot10^{9}$ | $5.1\cdot10^{9}$ |
| **4-ClCimTCH$_{2ap}$** | $2.80\cdot10^{9}$ | $2.5\cdot10^{9}$ |
| **4-MeOCimTCH$_{2fp}$** | $7.71\cdot10^{8}$ | $1.1\cdot10^{9}$ |
| **4-MeOCimTCH$_{sal}$** | $2.88\cdot10^{8}$ | $3.3\cdot10^{8}$ |
| **4-MeOCimTCH$_{8OH2qu}$** | $6.16\cdot10^{8}$ | $1.71\cdot10^{9}$ |
| **4-MeOCimTCH$_{2ap}$** | $4.54\cdot10^{8}$ | $1.9\cdot10^{9}$ |

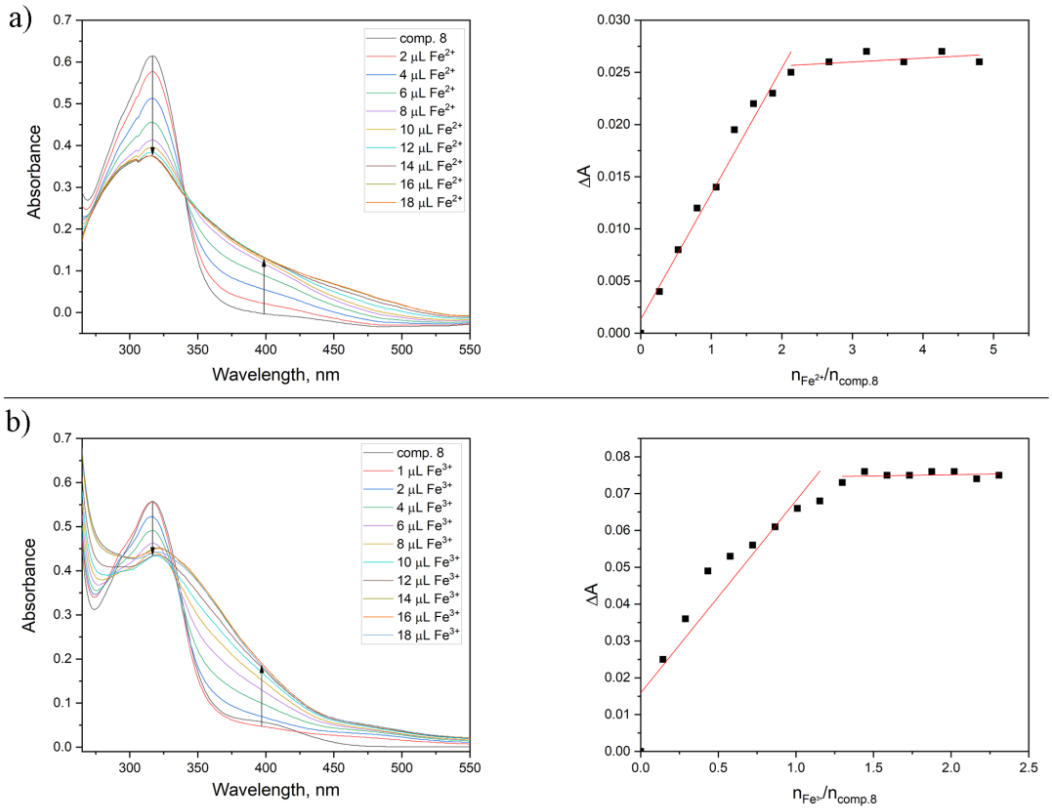


Figure 47. UV-Vis spectra and the plots of absorbance change versus metal/compound ratio for **4-ClCimTCH$_{2ap}$** for the formation of complexes with a) $Fe^{2+}$ and b) $Fe^{3+}$ ions

Synthesized cinnamic acid derivatives form 1:1 (ML) or 1:2 ($ML_2$) types of complexes with iron. According to the calculated stability constant Ks values in the range $10^7 – 10^9$ (Table 14) it is evident that all compounds create stable complexes with iron. The presented approach is not sufficient to attain a deeper understanding of the mechanism of antibacterial activity but it gave a conclusion on the important role of the binding capability of the studied compound since the stability constants follow a similar trend to activity change against *A. baumannii*. The highest values of stability constants were obtained with 4-chloro cinnamic acid derivatives, while the lowest was obtained with amides containing salicylic moiety. Lower chelating ability of these compounds is closely related to strong intramolecular hydrogen bonding,[15] while compound with the pyridine ring provides such spatial arrangement having the highest ability to coordinate iron thus forming stable complexes with Ks of $10^9$.

## 4. Conclusion

Two series of compounds were synthesized, the first series were synthesized **TCH** using DHS in the reaction of Salicylaldehyde and 2-Acetylpyridine. mono- and bis, in the second series of compounds were synthesized cinnamic acid amides in the reaction of cinnamic, 3-chlorocinnamic, 4-chlorocinnamic, 4-methoxycinnamic, 3-hydroxycinnamic, ferulic and caffeic acid and **m-TCH**, and used in an antioxidant, antimicrobial, and anticancer activity study.

For the first series main goals were related to the study of the effect of configurational isomerization and thione/thiole tautomerization on antioxidative activity change based on experimental data and theoretical calculations. Higher antioxidative activities of **m-TCH$_{sal}$** and **b-TCH$_{sal}$** compounds are highly affected by the presence and availability of hydroxyl groups which contribute that these compounds are better radical scavengers than ones with 2-acetylpyridine fragment, i.e. **m-TCH$_{2ap}$** and **b-TCH$_{2ap}$**. The hydrogen bond donating/accepting capability of introduced water disturb the intramolecular hydrogen bond in *E* form of **m-TCH$_{sal}$** what facilitates *E* to *Z* isomerization around $C_2$-$C_7$ bond. The significance of the strength of intramolecular hydrogen bond (IHB) was evaluated by calculation of energetic demand for rotation around $C_2$-$C_7$ bond **m-TCH$_{2ap}$**, **m-TCH$_{2fp}$** and **m-TCH$_{2fp}$** at DFT/$\omega$B97XD/6-311g(d,p) level of theory. It was found that a higher quantum of energy input must be involved to perform IHB beak up in **m-TCH$_{2fp}$**, while oppositely is true for **m-TCH$_{2ap}$** due to higher steric interference. The presence of "free" phenolic in *Z* isomer of **m-TCH$_{sal}$** contributes to lowering of BDE for 11 kcal/mol. More effective electron spin delocalization is observed in both *Z* isomers of **m-TCH$_{sal}$** and **b-TCH$_{sal}$**. The relative stability of *E*- and *Z*-isomers of both thione and thiol tautomers of compounds **m-TCH$_{sal}$** and **m-TCH$_{2ap}$** was calculated using DFT/B3LYP/6-311++G(d,p) level and IEF-PCM for water modeling.

On the other hand, water addition to DMSO solution of **m-TCH$_{2ap}$** and **b-TCH$_{2ap}$** leads to thione/thiol tautomerism of both compounds. Extent of these processes was followed from shifting of UV-Vis maxima to higher wavelength ("red shift") and a "deshielded" $^1$H NMR signal of thiol proton. The thione/thiol transformation induced by water addition is of higher significance for **b-TCH$_{2ap}$** (*E* form of thione:thiol was found to be at 1:0.35 ratio) than in **m-TCH$_{2ap}$** (1:0.18). The increased contribution of thiol form in equilibrium is correlative with the better radical scavenging activity. Thus, the presence of labile N-H and –S-H bond, the results from spin density distribution maps calculation for thione and thiol radical, are in accordance with determined antioxidative activity. The presented results indicate the significance of the structural characteristics of TCH in solution and solute/solvent interactions which are of the highest importance in a future study of structure-activity relationships of TCH or other compounds able to respond to solvent influences by geometry adaptation. Cinnamides based on 3-hydroxycinnamic, Caffeic and Ferulic acid was used in a comparative antioxidative study.

In the second part of this thesis a synthesis of cinnamic acid amides, as structurally similar analogues to isoniazid and anticancer agents 5-HP and 3-AP, was performed from acid chloride of cinnamic, 3-chlorocinnamic and 4-chlorocinnamic acid and **m-TCHs** (**m-TCH$_{2fp}$, m-TCH$_{sal}$, m-TCH$_{8OH2qu}$** and **m-TCH$_{2ap}$**). Also, cinnamamides, based on 3-hydroxycinnamic, with the **m-TCH** were synthesized using HATU coupling agent. Caffec and Ferulic based amides with **m-TCH$_{2fp}$, m-TCH$_{sal}$** were syntheisized in an analogous manner to study their antioxidative potential using DPPH$^{\cdot}$ assay. Presence of phenolic groups Full characterization was obtained by recording 1D ($^1$H and $^{13}$C) and 2D (COSY, NOESY, $^1$H-$^{13}$C HSQC and $^1$H-$^{13}$C HMBC) spectra. Results from $^1$H NMR and 2D NOESY spectra showed that *E,E* isomer dominates in a solution. In the subsequent step assessment of their anti-*Mtb* and anticancer activity was performed.

Results of anticancer testing revealed that compounds **3-ClCimTCH$_{sal}$** and **4-ClCimTCH$_{8OH2qu}$** induce an apoptotic response in A549 cells, where the activity of **4-ClCimTCH$_{8OH2qu}$** was more potent with lower $CdC_{50}$ value compared to **3-ClCimTCH$_{sal}$**. Further examination of cell cycle changes and caspase pathways activation did not show any particular difference between modes of **3-ClCimTCH$_{sal}$** and **4-ClCimTCH$_{8OH2qu}$** activities: each compound affected cell division within the phase of chromosomal replication and activated intrinsic apoptotic pathway. However, compound **4-ClCimTCH$_{8OH2qu}$** displayed a capacity to induce excessive production of mitochondrial $^{\bullet}O_2^-$ in treated A549 cells, which is the feature not seen in samples subjected to **3-ClCimTCH$_{sal}$**. On the other hand, treatment with compound **3-ClCimTCH$_{sal}$** emanated statistically significant suppression of cellular motility, contrary to treatment with **4-ClCimTCH$_{8OH2qu}$**. The breakpoint of the investigation was reached with results of cytotoxic activity on HaCaT and HepG-2 cells, which demonstrated that compound **4-ClCimTCH$_{8OH2qu}$** has an unfavorable toxicity profile. Regarding anti-*Mtb* activity, compound **CimTCH$_{8OH2qu}$** was revealed as competent to reach MIC in all treated strains, thus outperformed both drugs that are standardly in use for a first-line TB treatment. Additionally, **CimTCH$_{8OH2qu}$** didn't affect the vitality of HepG-2 cells which is of particular value considering hepatotoxicity is a limiting feature of INH treatment. The final outcome of this study is that compounds **3-ClCimTCH$_{sal}$** and **CimTCH$_{8OH2qu}$** deserve to be further investigated.

The third part of this thesis was devoted to *in vitro* antimicrobial study of the amide of natural acids: cinnamic, 4-chlorocinnamic and 4-methoxycinnamic acid and **m-TCHs** (**m-TCH$_{2fp}$, m-TCH$_{sal}$, m-TCH$_{8OH2qu}$ and m-TCH$_{2ap}$**) against six microorganisms (*E. cloacae* ATCC13047, *S. aureus* NCTC 6571, *K. pneumoniae* ATCC 13883, *A. baumannii* ATCC 19606, *P. aeruginosa* NCTC 10662, and *E. coli* ATCC 1175). The activity was variable with respect to both bacteria strain and compound tested, and ranged from 10.4 to 196.9 μM. Compounds with salicylic moiety, regardless of the amide fragment, showed very low antimicrobial activity indicating the significance of intramolecular hydrogen bond to control of their activity. It is well known that heterocyclic ring containing compounds (quinoline or pyridine) showed high antimicrobial activity which is confirmed by moderate to high activity of structurally similar tested compounds. All compounds showed good activity with respect to *A. baumannii*. The diversity of the obtained $MIC_{50}$ offered a possibility to establish an appropriate structure-activity relationship using 3D QSAR methodology.

Results of 3D-QSAR analysis indicated on three important structural fragments contributing to activity: two hydrophobic aromatic rings positioned at the opposite ends of cinnamic amide derivatives (cinnamic acids residue and pyridine/quinoline ring from **m-TCH**), and amide bond. It could be supposed that ability of *A. baumannii* to digest and metabolize cinnamic based compounds play a significant role in the high antimicrobial activity observed. Also, it was shown that prevention of *A. baumannii* to use iron in the course of metabolic pathways due to high potential of synthesized compounds to coordinate iron and form stable complexes with the stability constants from $10^8$ to $10^9$ order. In this way, the whole mechanism of antimicrobial activity was not evidenced, but the presented results offer an important premise and base for further investigations. Future design of structural modifications where a combination of exchange of methoxy and hydroxyl, *ortho/meta* substituted derivatives, in both part, cinnamic acid residue and TCH fragment, could provide the compound with high antimicrobial activity.

## 5. References


1. S. Adisakwattana, *Nutrients* **9** (2017) 1–27.
2. M. A. Alam, N. Subhan, H. Hossain, M. Hossain, H. M. Reza, M. M. Rahman, M. O. Ullah, *Nutr. Metab. (Lond).* **13** (2016) 1–13.
3. J. D. Guzman, *Molecules* **19** (2014) 19292–19349.
4. V. Saibabu, Z. Fatima, L. A. Khan, S. Hameed, *Adv. Pharmacol. Sci.* **2015** (2015) 1–10.
5. A. V. Simonyan, *Pharm. Chem. J.* **27** (1993) 92–100.
6. S. Khadem, R. J. Marles, *Molecules* **15** (2010) 7985–8005.
7. P. Sharma, *J. Chem. Pharm. Res.* **3** (2011) 403–423.
8. A. Peperidou, E. Pontiki, D. Hadjipavlou-Litina, E. Voulgari, K. Avgoustakis, *Molecules* **22** (2017) 1–17.
9. M. K. Lee, Y. B. Park, S. S. Moon, S. H. Bok, D. J. Kim, T. Y. Ha, T. S. Jeong, K. S. Jeong, M. S. Choi, *Chem. Biol. Interact.* **170** (2007) 9–19.
10. A. N. Nurfina, M. S. Reksohadiprodjo, H. Timmerman, U. A. Jenie, D. Sugiyanto, H. Van Der Goot, *Eur. J. Med. Chem.* **32** (1997) 321–328.
11. A. Gunia-Krzyżak, K. Słoczyńska, J. Popiół, P. Koczurkiewicz, H. Marona, E. Pękala, *Int. J. Cosmet. Sci.* **40** (2018) 356–366.
12. G. Seelolla, *Med Chem 2014*, **4** (2014) 778–783.
13. B. L. Avinash Nalawade, RekhaNalawade, *IJCRGG* **10** (2017) 553–557.
14. K. M. EL-Mahdy, A. M. El-Kazak, M. Abdel-Megid, M. Seada, O. Farouk, *Acta Chim. Slov* **63** (2016) 18–25.
15. M. H. Assaleh, A. R. Božić, S. Bjelogrlić, M. Milošević, M. Simić, A. D. Marinković, I. N. Cvijetić, *Struct. Chem.* **30** (2019) 2447–2457.
16. M. A. Metwally, M. E. Khalifa, M. Koketsu, *Am. J. Chem.* **2** (2012) 38–51.
17. A. M. Nalawade, R. A. Nalawade, R. V. Shejwal, *Biosci. Discov.* **8** (2017) 274–279.
18. K. Gangarapu, S. Manda, A. Jallapally, S. Thota, S. S. Karki, J. Balzarini, E. De Clercq, H. Tokuda, *Med. Chem. Res.* **23** (2014) 1046–1056.
19. G. Kiran, T. Maneshwar, Y. Rajeshwar, M. Sarangapani, *J. Chem.* **2013** (2013) 1–7.
20. R. Nalawade, A. Nalawade, R. Shejwal, M. Anuse, *Int. J. Eng. Sci. Invent.* **6** (2017) 46–49.
21. T. E. S. Ali, *J. Sulfur Chem.* **30** (2009) 611–647.
22. S. Pospisilova, J. Kos, H. Michnova, I. Kapustikova, T. Strharsky, M. Oravec, A. M. Moricz, J. Bakonyi, T. Kauerova, P. Kollar, A. Cizek, J. Jampilek, *Int. J. Mol. Sci.* **19** (2018) 1–25.
23. M. Shebl, H. S. Seleem, B. A. El-Shetary, *Spectrochim. Acta - Part A Mol. Biomol. Spectrosc.* **75** (2010) 428–436.
24. A. P. Liesen, T. M. De Aquino, C. S. Carvalho, V. T. Lima, J. M. De Araújo, J. G. De Lima, A. R. De Faria, E. J. T. De Melo, A. J. Alves, E. W. Alves, A. Q. Alves, A. J. S. Góes, *Eur. J. Med. Chem.* **45** (2010) 3685–3691.
25. L. Srividya, A. R. N. Reddy, *Asian J. Biol. Sci.* **10** (2017) 126–129.
26. K. H. M. Ebrahim Tehrani, F. Kobarfard, P. Azerang, M. Mehravar, Z. Soleimani, G. Ghavami, S. Sardari, *Iran. J. Pharm. Res.* **12** (2013) 331–346.
27. A. Božić, A. Marinković, S. Bjelogrlić, T. R. Todorović, I. N. Cvijetić, I. Novaković, C. D. Muller, N. R. Filipović, *RSC Adv.* **6** (2016) 104763–104781.
28. A. A. A. Abu-Hussen, A. A. A. Emara, *J. Coord. Chem.* **57** (2004) 973–987.
29. T. A. Blumenkopf, J. A. Harrington, C. S. Koble, D. D. Bankston, R. W. Morrison, E. C. Bigham, V. L. Styles, T. Spector, *J. Med. Chem.* **35** (1992) 2306–2314.

30. S. Adsule, V. Barve, D. Chen, F. Ahmed, Q. P. Dou, S. Padhye, F. H. Sarkar, *J. Med. Chem.* **49** (2006) 7242–7246.
31. Q. Ba, M. Hao, H. Huang, J. Hou, S. Ge, Z. Zhang, J. Yin, R. Chu, H. Jiang, F. Wang, K. Chen, H. Liu, H. Wang, *Clin. Cancer Res.* **17** (2011) 7625–7633.
32. M. Serda, D. S. Kalinowski, A. Mrozek-Wilczkiewicz, R. Musiol, A. Szurko, A. Ratuszna, N. Pantarat, Z. Kovacevic, A. M. Merlot, D. R. Richardson, J. Polanski, *Bioorganic Med. Chem. Lett.* **22** (2012) 5527–5531.
33. H. Huang, Q. Chen, X. Ku, L. Meng, L. Lin, X. Wang, C. Zhu, Y. Wang, Z. Chen, M. Li, H. Jiang, K. Chen, J. Ding, H. Liu, *J. Med. Chem.* **53** (2010) 3048–3064.
34. F. Bisceglie, A. Musiari, S. Pinelli, R. Alinovi, I. Menozzi, E. Polverini, P. Tarasconi, M. Tavone, G. Pelosi, *J. Inorg. Biochem.* **152** (2015) 10–19.
35. F. A. French, E. J. Blanz, S. C. Shaddix, R. W. Brockman, *J. Med. Chem.* **17** (1974) 172–181.
36. P. De, M. Baltas, F. Bedos-Belval, *Curr. Med. Chem.* **18** (2011) 1672–1703.
37. R. A. Dixon, J. Barros, *Open Biol.* **9** (2019) 1–14.
38. R. Shuab, R. Lone, K. K. Koul, *Acta Physiol. Plant.* **38** (2016) 1–9.
39. A. Parthasarathy, P. J. Cross, R. C. J. Dobson, L. E. Adams, M. A. Savka, A. O. Hudson, *Front. Mol. Biosci.* **29** (2018) 1–30.
40. V. Tzin, G. Galili, *Arab. B.* **8** (2010) 1–18.
41. P. Feduraev, L. Skrypnik, A. Riabova, A. Pungin, E. Tokupova, P. Maslennikov, G. Chupakhina, *Plants* **9** (2020) 1–19.
42. S. Metsämuuronen, H. Sirén, *Phytochem Rev* **18** (2019) 623–664.
43. Z. Li, C. Zhao, X. Zhao, Y. Xia, X. Sun, W. Xie, Y. Ye, X. Lu, G. Xu, *Anal Chem* **90** (2018) 14321–14330.
44. H. Peng, T. Yang, B. D. Whitaker, F. Trouth, L. Shangguan, W. Dong, W. M. Jurick, *Hortic. Res.* **3** (2016) 1–9.
45. D. M. Macoy, W. Y. Kim, S. Y. Lee, M. G. Kim, *J. Plant Biol* **58** (2015) 156–163.
46. P. J. Facchini, J. Hagel, K. G. Zulak, *Can. J. Bot* **80** (2002) 577–589.
47. R. J. Robbins, *J. Agric. Food Chem* **51** (2003) 2866–2887.
48. L. Drage, *Bmj* **1** (1905) 927–928.
49. B. Zhu, B. Shang, Y. Li, Y. Zhen, *Mol. Med. Rep.* **13** (2016) 4159–4166.
50. A. Lozynskyi, B. Zimenkovsky, R. Lesyk, *Sci. Pharm.* **82** (2014) 723–733.
51. A. Jitareanu, G. Tataringa, *Res. J. Chem. Sci. Res. J. Chem. Sci* **3** (2013) 2231–606.
52. K. Takao, K. Toda, T. Saito, Y. Sugita, *Chem. Pharm. Bull.* **65** (2017) 1020–1027.
53. S. B. Nimse, D. Pal, A. Mazumder, R. Mazumder, *J. Chem.* **2015** (2015) 1–6.
54. S. Mahesh, K. C. Tang, M. Raj, *Molecules* **23** (2018) 1–43.
55. A. R. Nunes, Í. G. P. Vieira, D. B. Queiroz, A. L. A. B. Leal, S. Maia Morais, D. F. Muniz, J. T. Calixto-Junior, H. D. M. Coutinho, *Adv. Pharmacol. Sci.* **2018** (2018) 1–9.
56. L. C. Cefali, J. A. Ataide, P. Moriel, M. A. Foglio, P. G. Mazzola, *Int. J. Cosmet. Sci.* **38** (2016) 346–353.
57. R. Jansen, U. Osterwalder, S. Q. Wang, M. Burnett, H. W. Lim, *JAM ACAD DERMATOL* **69** (2013) 867.e1-867.e14.
58. C. Xu, X. Zeng, Z. Yang, H. Ji, *Polymers (Basel).* **13** (2021) 1–17.
59. J. van Overbeek, R. Blondeau, V. Horne, *Am. J. Bot.* **38** (1951) 589–595.
60. W. Steenackers, P. Klíma, M. Quareshy, I. Cesarino, R. P. Kumpf, S. Corneillie, P. Araújo, T. Viaene, G. Goeminne, M. K. Nowack, K. Ljung, J. Friml, J. J. Blakeslee, O. Novák, E. Zažímalová, R. Napier, W. Boerjan, B. Vanholme, *Plant Physiol.* **173** (2017) 552–565.
61. W. Steenackers, I. El Houari, A. Baekelandt, K. Witvrouw, S. Dhondt, O. Leroux, N. Gonzalez, S. Corneillie, I. Cesarino, D. Inzé, W. Boerjan, B. Vanholme, *J. Exp. Bot.* **70**

(2019) 6293–6304.
62. M. Rychlicka, A. Rot, A. Gliszczyńska, *Foods* **10** (2021) 1–13.
63. K. Yagi, N. Ohishi, *I Nutr. Sci. Vitaminol,,* **25** (1979) 127–130.
64. S. Mathew, T. E. Abraham, *Crit. Rev. Biotechnol.* **24** (2004) 59–83.
65. A. Rezaei, J. Varshosaz, M. Fesharaki, A. Farhang, S. M. Jafari, *Int. J. Nanomedicine* **14** (2019) 4589–4599.
66. K. M. Monteiro Espíndola, R. G. Ferreira, L. E. Mosquera Narvaez, A. C. Rocha Silva Rosario, A. H. Machado Da Silva, A. G. Bispo Silva, A. P. Oliveira Vieira, M. Chagas Monteiro, *Front. Oncol.* **9** (2019) 1–10.
67. A. I. Kobelev, E. E. Stepanova, M. V. Dmitriev, A. N. Maslivets, *Russ. J. Org. Chem.* **55** (2019) 1013–1018.
68. C. Bonaccorso, T. Marzo, D. La Mendola, *Pharmaceuticals* **13** (2020) 1–19.
69. N. Kumar, A. Parle, *Pharma Innov. J.* **8** (2019) 580–595.
70. M. Asif, M. Imran, *Prog. Chem. Biochem. Res.* **2** (2019) 192–210.
71. P. M. Pawar, K. J. Jarag, G. S. Shankarling, *Green Chem.* **13** (2011) 2130–2134.
72. G. S. Lee, A. Widjaja, Y. H. Ju, *Biotechnol. Lett.* **28** (2006) 581–585.
73. Z. Zhang, Z. Zha, C. Gan, C. Pan, Y. Zhou, Z. Wang, M. M. Zhou, *J. Org. Chem* **71** (2006) 4339–4342.
74. A. B. A. P. K. MONICA RESHI, R.K. KAUL, *Internat. J. Med. Sci* **6** (2013) 14–22.
75. Z. Zhang, Z. Wang, *J. Org. Chem* **71** (2006) 7485–7487.
76. M. Hatsuda, T. Kuroda, M. Seki, *Synth. Commun.* **33** (2003) 427–434.
77. G. S. Mrđan, G. G. Vastag, D. Škorić, M. M. Radanović, T. Verbić, M. K. Milčić, I. N. Stojiljković, O. S. Marković, B. M. Matijević, *Struct. Chem.* **32** (2021) 1231–1245.
78. J. S. Lan, J. W. Hou, Y. Liu, Y. Ding, Y. Zhang, L. Li, T. Zhang, *J. Enzyme Inhib. Med. Chem.* **32** (2017) 776–788.
79. B. Watanabe, S. Nishitani, T. Koeduka, *J Label Compd Radiopharm* **64** (2021) 403–416.
80. A. R. Božić, N. R. Filipović, T. Verbić, M. K. Milčić, T. R. Todorović, I. N. Cvijetić, O. R. Klisurić, M. M. Radišić, A. D. Marinković, *Arab. J. Chem.* **13** (2020) 932–953.
81. W. X. Zhang, H. Wang, H. R. Cui, W. B. Guo, F. Zhou, D. S. Cai, B. Xu, X. H. Jia, X. M. Huang, Y. Q. Yang, H. S. Chen, J. C. Qi, P. L. Wang, H. M. Lei, *Eur. J. Med. Chem.* **183** (2019) 1–16.
82. N. Ruwizhi, B. A. Aderibigbe, *Int. J. Mol. Sci.* **21** (2020) 1–36.
83. M. and H.A., & M. M. Yousse, *Alex. J. Fd. Sci. Technol.* **11** (2014) 31–42.
84. M. Victoria Urquiza-Martínez, B. Fenton Navarro, *Free Radicals Antioxidants* **6** (2016) 1–12.
85. V. Lobo, A. Patil, A. Phatak, N. Chandra, *Pharmacogn. Rev.* **4** (2010) 118–126.
86. Z. Haida, M. Hakiman, *Food Sci Nutr* **7** (2019) 1555–1563.
87. S. George, H. Abrahamse, *Antioxidants* **9** (2020) 1–21.
88. H. Sies, *Exp. Physiol.* **82** (1997) 291–295.
89. L. A. Pham-Huy, H. He, C. Pham-Huy, *Int J Biomed Sci* **4** (2008) 89–96.
90. A. Phaniendra, D. B. Jestadi, L. Periyasamy, *Indian J. Clin. Biochem.* **30** (2015) 11–26.
91. M. D. Milošević, *Univ. BELGRADE* **DOCTORAL D** (2021) 1–202.
92. G. A. Engwa, *Phytochem. - Source Antioxidants Role Dis. Prev.* **4** (2018) 49–73.
93. S. Biswas, R. Das, E. R. Banerjee, *AIMS Biophys.* **4** (2017) 596–614.
94. R. P. Patel, J. McAndrew, H. Sellak, C. R. White, H. Jo, B. A. Freeman, V. M. Darley-Usmar, *Biochim. Biophys. Acta - Bioenerg.* **1411** (1999) 385–400.
95. M. C. H. Gruhlke, A. J. Slusarenko, *Plant Physiol. Biochem.* **59** (2012) 98–107.
96. M. Valko, M. Izakovic, M. Mazur, C. J. Rhodes, J. Telser, *Mol. Cell. Biochem.* **266** (2004) 37–56.

97. M. Sharifi-Rad, N. V. Anil Kumar, P. Zucca, E. M. Varoni, L. Dini, E. Panzarini, J. Rajkovic, P. V. Tsouh Fokou, E. Azzini, I. Peluso, A. Prakash Mishra, M. Nigam, Y. El Rayess, M. El Beyrouthy, L. Polito, M. Iriti, N. Martins, M. Martorell, A. O. Docea, W. N. Setzer, D. Calina, W. C. Cho, J. Sharifi-Rad, *Front. Physiol.* **11** (2020) 1–21.
98. P. Krishnamurthy, A. Wadhwani, *Antioxid. Enzym.* **1** (2012) 3–18.
99. A. Galano, *J. Mex. Chem. Soc* **59** (2017) 231–262.
100. Z. Zhao, *Aging Med.* **2** (2019) 82–87.
101. Z. Marković, J. Tošović, D. Milenković, S. Marković, *Comput. Theor. Chem.* **1077** (2016) 11–17.
102. I. G. Munteanu, C. Apetrei, *Int. J. Mol. Sci* **22** (2021) 1–30.
103. F. Shahidi, Y. Zhong, *J. Funct. Foods* **18** (2015) 757–781.
104. E. Bendary, R. R. Francis, H. M. G. Ali, M. I. Sarwat, S. El Hady, *Ann. Agric. Sci.* **58** (2013) 173–181.
105. A. Floegel, D. O. Kim, S. J. Chung, S. I. Koo, O. K. Chun, *J. Food Compos. Anal.* **24** (2011) 1043–1048.
106. M. N. Alam, N. J. Bristi, M. Rafiquzzaman, *Saudi Pharm. J.* **21** (2013) 143–152.
107. H. A. MATTILL, *Annu. Rev. Biochem.* **16** (1947) 177–192.
108. R. H. Liu, J. Finley, *J. Agric. Food Chem.* **53** (2005) 4311–4314.
109. T. K. Bakır, J. B. Lawag, *Res. Chem. Intermed.* **46** (2020) 2541–2557.
110. S. Ullah, D. Kang, S. Lee, M. Ikram, C. Park, Y. Park, S. Yoon, P. Chun, H. R. Moon, *Eur. J. Med. Chem.* **161** (2019) 78–92.
111. C. Pal, Department, *Chem. Biol. Interface* **11** (2021) 40–47.
112. M. Balouiri, M. Sadiki, S. K. Ibnsouda, *J. Pharm. Anal.* **6** (2016) 71–79.
113. E. Power, *Clin. Microbiol. Infect.* **12** (2006) 25–34.
114. E. P. Abraham, *Compr. Biochem.* **11** (1963) 181–224.
115. T. M. Belete, *Hum. Microbiome J.* **11** (2019) 100052.
116. B. Spellberg, M. Blaser, R. J. Guidos, H. W. Boucher, J. S. Bradley, B. I. Eisenstein, D. Gerding, R. Lynfield, L. B. Reller, J. Rex, D. Schwartz, E. Septimus, F. C. Tenover, D. N. Gilbert, *Clin. Infect. Dis.* **52** (2011) 397–428.
117. T. Ahmed, S. Baidya, B. C. Sharma, M. Malek, K. K. Das, M. Acharjee, S. K. Munshi, R. Noor, *Asian J. Microbiol. Biotechnol. Environ. Sci.* **15** (2013) 655–660.
118. M. A. Pfaller, D. J. Diekema, S. A. Messer, L. Boyken, R. J. Hollis, *J. Clin. Microbiol.* **41** (2003) 1440–1446.
119. J. H. Jorgensen, M. J. Ferraro, *Clin. Infect. Dis.* **49** (2009) 1749–1755.
120. J. Ren, T. C. Jenkins, J. B. Chaires, *Biochemistry* **39** (2000) 8439–8447.
121. B. A. Haughton, M. P. Patel, J. P. Livesey, *Ann. R. Coll. Surg. Engl.* **95** (2013) 532–534.
122. Z. Zhao, H. Song, J. Xie, T. Liu, X. Zhao, X. Chen, X. He, S. Wu, Y. Zhang, X. Zheng, *Eur. J. Med. Chem.* **173** (2019) 213–227.
123. B. Narasimhan, D. Belsare, D. Pharande, V. Mourya, A. Dhake, *Eur. J. Med. Chem.* **39** (2004) 827–834.
124. B. . Jacob, H. Baba, J. O. Oluwadiya, *Niger. J. Pharm. Res.* **16** (2020) 1–8.
125. G. Serban, O. Stanasel, E. Serban, S. Bota, *Drug Des. Devel. Ther.* **12** (2018) 1545–1566.
126. A. R. Božić, S. K. Bjelogrlić, I. T. Novaković, N. R. Filipović, P. M. Petrović, A. D. Marinković, T. R. Todorović, I. N. Cvijetić, *Chem. Sel.* **3** (2018) 2215–2221.
127. T. Nasr, S. Bondock, S. Eid, *Eur. J. Med. Chem.* **84** (2014) 491–504.
128. P. De, G. Koumba Yoya, P. Constant, F. Bedos-Belval, H. Duran, N. Saffon, M. Daffé, M. Baltas, *J. Med. Chem.* **54** (2011) 1449–1461.
129. Prithwiraj De, Florence Bedos-Belval, Corinne Vanucci-Bacque, Michel Baltas, *Curr.*

*Org. Chem.* **16** (2012) 747–768.
130. M. D. Kakwani, P. Suryavanshi, M. Ray, M. G. R. Rajan, S. Majee, A. Samad, P. Devarajan, M. S. Degani, *Bioorg. Med. Chem. Lett.* **21** (2011) 1997–1999.
131. C. V. J. B. G. Cátia Teixeira, F. Martins, *Molecules* **25** (2020) 1–11.
132. M. Sova, *Mini-Reviews Med. Chem.* **12** (2012) 749–767.
133. N. Vaou, E. Stavropoulou, C. Voidarou, C. Tsigalou, E. Bezirtzoglou, *Microorganisms* **9** (2021) 1–28.
134. L. F. Joyce, J. Downes, K. Stockman, J. H. Andrew, *J. CLIN. MICROBIOL.* **30** (1992) 2709–2713.
135. T. K. W. Ling, Z. K. Liu, A. F. B. Cheng, *J. Clin. Microbiol.* **41** (2003) 4705–4707.
136. S. P. Langdon, *Cancer Cell Cult.* **731** (2003) 237–245.
137. N. Gaikwad, S. Nanduri, Y. V. Madhavi, *Eur. J. Med. Chem.* **181** (2019) 111561.
138. M. T. Gabr, N. S. El-gohary, E. R. El-bendary, M. M. El-kerdawy, N. Ni, *Eur. J. Med. Chem.* **128** (2017) 36–44.
139. D. Raffa, B. Maggio, F. Plescia, S. Cascioferro, S. Plescia, M. V. Raimondi, G. Daidone, M. Tolomeo, S. Grimaudo, A. Di Cristina, R. M. Pipitone, R. Bai, E. Hamel, *Eur. J. Med. Chem.* **46** (2011) 2786–2796.
140. M. S. T. Makki, R. M. Abdel-Rahman, M. S. El-Shahawi, *Int. J. Chem.* **3** (2011) 181–192.
141. A. Bacchi, M. Carcelli, P. Pelagatti, C. Pelizzi, G. Pelizzi, F. Zani, *J. Inorg. Biochem.* **75** (1999) 123–133.
142. M. A. Al-Omair, A. R. Sayed, M. M. Youssef, *Molecules* **20** (2015) 2591–2610.
143. W. K. AND, L. J. SHAM, *Phys. Rev* **385** (1965) A1133–A1138.
144. Y. Zhao, D. G. Truhlar, *Theor. Chem. Acc.* **120** (2008) 215–241.
145. Y. Zhao, D. G. Truhlar, *Acc. Chem. Res.* **41** (2008) 157–167.
146. H. Elshaflu, *Univ. Belgrade* **DOCTORAL D** (2018) 1–227.
147. F. Ž. Vlahović.pdf, Density functional theory for studying electronic states of aqua- and oxo- first row transition metal complexes, UNIVERSITY OF BELGRADE, 2020.
148. J. N. Harvey, *Annu. Reports Prog. Chem. - Sect. C* **102** (2006) 203–226.
149. M. Lundberg, P. E. M. Siegbahn, *J. Chem. Phys.* **122** (2005).
150. S. Grimme, *Angew. Chemie - Int. Ed.* **45** (2006) 4460–4464.
151. S. Grimme, *J. Comput. Chem.* **25** (2004) 1463–1473.
152. P. Hohenberg, W. Kohn, *Phys. Rev.* **136** (1964).
153. V. Sahni, A. Solomatin, *Recent Developments in the Electronic Structure of Metal Surfaces*, Elsevier Masson SAS, 1998.
154. J. P. Perdew, J. A. Chevary, S. H. Vosko, K. A. Jackson, M. R. Pederson, D. J. Singh, C. Fiolhais, *Phys. Rev. B* **48** (1993) 4978.
155. J. P. Perdew, K. Burke, M. Ernzerhof, *Phys. Rev. Lett.* **77** (1996) 3865–3868.
156. A. D. Becke, *Phys. Rev. A* **38** (1988) 3098–3100.
157. A. D. Becke, *J. Chem. Phys.* **98** (1993) 1372–1377.
158. R. Wang, Y. Chen, B. Yang, S. Yu, X. Zhao, C. Zhang, C. Hao, D. Zhao, M. Cheng, *Bioorg. Chem.* **94** (2020) 103474.
159. H. F. Abd El-Halim, M. M. Omar, G. G. Mohamed, *Spectrochim. Acta - Part A Mol. Biomol. Spectrosc.* **78** (2011) 36–44.
160. E. Van Lenthe, E. J. Baerends, J. G. Snijders, *J. Chem. Phys.* **101** (1994) 9783–9792.
161. M. Bühl, C. Reimann, D. A. Pantazis, T. Bredow, F. Neese, *J. Chem. Theory Comput.* **4** (2008) 1449–1459.
162. S. D. W. and S. B. N. Jung-Seop Lee, Matthias Zeller, *Crystals* **9** (2019) 1–10.
163. N. Ramesh Babu, S. Subashchandrabose, M. Syed Ali Padusha, H. Saleem, Y. Erdoğdu, *Spectrochim. Acta - Part A Mol. Biomol. Spectrosc.* **120** (2014) 314–322.

164. K. C. Bible, S. H. Kaufmann, *Cancer Res.* **56** (1996) 4856–4861.
165. R. L. Sutherland, R. E. Hall, I. W. Taylor, *Cancer Res.* **43** (1983) 3998–4006.
166. C. A. Kunos, T. Stefan, J. W. Jacobberger, *Front. Oncol.* **3 SEP** (2013) 1–10.
167. C. Soranzo, G. Della Torre, A. Ingrosso, *Tumori* **72** (1986) 459–467.
168. E. Pavez Lorie, N. Stricker, B. Plitta-Michalak, I. P. Chen, B. Volkmer, R. Greinert, A. Jauch, P. Boukamp, A. Rapp, *Sci. Rep.* **10** (2020) 1–20.
169. S. L. Tran, A. Puhar, M. Ngo-Camus, N. Ramarao, *PLoS One* **6** (2011) 2–6.
170. F. Miles, J. Lynch, R. Sikes, *J. Biol. Methods* **2** (2015) e29.
171. H. Zhao, J. Oczos, P. Janowski, D. Trembecka, J. Dobrucki, Z. Darzynkiewicz, D. Wlodkowic, *Cytom. Part A* **77** (2010) 399–405.
172. H. Y. Chen, Y. M. Yang, B. M. Stevens, M. Noble, *EMBO Mol. Med.* **5** (2013) 723–736.
173. I. Lakshmanan, S. Batra, *Bio-Protocol* **3** (2013).
174. L. Galluzzi, I. Vitale, S. A. Aaronson, J. M. Abrams, D. Adam, P. Agostinis, E. S. Alnemri, L. Altucci, I. Amelio, D. W. Andrews, M. Annicchiarico-Petruzzelli, A. V. Antonov, E. Arama, E. H. Baehrecke, N. A. Barlev, N. G. Bazan, F. Bernassola, M. J. M. Bertrand, K. Bianchi, M. V. Blagosklonny, K. Blomgren, C. Borner, P. Boya, C. Brenner, M. Campanella, E. Candi, D. Carmona-Gutierrez, F. Cecconi, F. K. M. Chan, N. S. Chandel, E. H. Cheng, J. E. Chipuk, J. A. Cidlowski, A. Ciechanover, G. M. Cohen, M. Conrad, J. R. Cubillos-Ruiz, P. E. Czabotar, V. D'Angiolella, T. M. Dawson, V. L. Dawson, V. De Laurenzi, R. De Maria, K. M. Debatin, R. J. Deberardinis, M. Deshmukh, N. Di Daniele, F. Di Virgilio, V. M. Dixit, S. J. Dixon, C. S. Duckett, B. D. Dynlacht, W. S. El-Deiry, J. W. Elrod, G. M. Fimia, S. Fulda, A. J. García-Sáez, A. D. Garg, C. Garrido, E. Gavathiotis, P. Golstein, E. Gottlieb, D. R. Green, L. A. Greene, H. Gronemeyer, A. Gross, G. Hajnoczky, J. M. Hardwick, I. S. Harris, M. O. Hengartner, C. Hetz, H. Ichijo, M. Jäättelä, B. Joseph, P. J. Jost, P. P. Juin, W. J. Kaiser, M. Karin, T. Kaufmann, O. Kepp, A. Kimchi, R. N. Kitsis, D. J. Klionsky, R. A. Knight, S. Kumar, S. W. Lee, J. J. Lemasters, B. Levine, A. Linkermann, S. A. Lipton, R. A. Lockshin, C. López-Otín, S. W. Lowe, T. Luedde, E. Lugli, M. MacFarlane, F. Madeo, M. Malewicz, W. Malorni, G. Manic, J. C. Marine, S. J. Martin, J. C. Martinou, J. P. Medema, P. Mehlen, P. Meier, S. Melino, E. A. Miao, J. D. Molkentin, U. M. Moll, C. Muñoz-Pinedo, S. Nagata, G. Nuñez, A. Oberst, M. Oren, M. Overholtzer, M. Pagano, T. Panaretakis, M. Pasparakis, J. M. Penninger, D. M. Pereira, S. Pervaiz, M. E. Peter, M. Piacentini, P. Pinton, J. H. M. Prehn, H. Puthalakath, G. A. Rabinovich, M. Rehm, R. Rizzuto, C. M. P. Rodrigues, D. C. Rubinsztein, T. Rudel, K. M. Ryan, E. Sayan, L. Scorrano, F. Shao, Y. Shi, J. Silke, H. U. Simon, A. Sistigu, B. R. Stockwell, A. Strasser, G. Szabadkai, S. W. G. Tait, D. Tang, N. Tavernarakis, A. Thorburn, Y. Tsujimoto, B. Turk, T. Vanden Berghe, P. Vandenabeele, M. G. Vander Heiden, A. Villunger, H. W. Virgin, K. H. Vousden, D. Vucic, E. F. Wagner, H. Walczak, D. Wallach, Y. Wang, J. A. Wells, W. Wood, J. Yuan, Z. Zakeri, B. Zhivotovsky, L. Zitvogel, G. Melino, G. Kroemer, *Cell Death Differ.* **25** (2018) 486–541.
175. F. P. Wilson, J. S. Berns, *Adv. Chronic Kidney Dis.* **21** (2014) 18–26.
176. T. Otto, P. Sicinski, *Nat. Rev. Cancer* **17** (2017) 93–115.
177. K. J. Barnum, M. J. O'Connell, *Methods Mol. Biol.* **1170** (2014) 29–40.
178. J. J. Bower, L. D. Vance, M. Psioda, S. L. Smith-Roe, D. A. Simpson, J. G. Ibrahim, K. A. Hoadley, C. M. Perou, W. K. Kaufmann, *Npj Breast Cancer* **3** (2017) 1–9.
179. D. R. McIlwain, T. Berger, T. W. Mak, *Cold Spring Harb. Perspect. Biol.* **5** (2013) 1–28.
180. P. Li, L. Zhou, T. Zhao, X. Liu, P. Zhang, Y. Liu, X. Zheng, Q. Li, *Oncotarget* **8** (2017) 23996–24008.

181. X. Xu, Y. Lai, Z. C. Hua, *Biosci. Rep.* **39** (2019) 1–17.
182. S. P. Jackson, J. Bartek, *Nature* **461** (2009) 1071–1078.
183. U. S. Srinivas, B. W. Q. Tan, B. A. Vellayappan, A. D. Jeyasekharan, *Redox Biol.* **25** (2019) 101084.
184. D. B. Zorov, M. Juhaszova, S. J. Sollott, *Physiol. Rev.* **94** (2014) 909–950.
185. D. Munro, J. R. Treberg, *J. Exp. Biol.* **220** (2017) 1170–1180.
186. C. Lennicke, J. Rahn, R. Lichtenfels, L. A. Wessjohann, B. Seliger, *Cell Commun. Signal.* **13** (2015) 1–19.
187. L. J. Marnett, *Carcinogenesis* **21** (2000) 361–370.
188. A. V. Snezhkina, A. V. Kudryavtseva, O. L. Kardymon, M. V. Savvateeva, N. V. Melnikova, G. S. Krasnov, A. A. Dmitriev, *Oxid. Med. Cell. Longev.* **2019** (2020) 1–17.
189. H. Piotrowska, M. Kucinska, M. Murias, *Mol. Cell. Biochem.* **383** (2013) 95–102.
190. and R. A. W. Arthur W. Lambert, Diwakar R. Pattabiraman, *Hydrocarb. Eng.* **9** (2004) 46.
191. J. Pijuan, C. Barceló, D. F. Moreno, O. Maiques, P. Sisó, R. M. Marti, A. Macià, A. Panosa, *Front. Cell Dev. Biol.* **7** (2019) 1–16.
192. G. Nasiri, N. Azarpira, A. Alizadeh, S. Goshtasbi, L. Tayebi, *Stem Cell Res. Ther.* **11** (2020) 1–11.
193. C. Y. Ng, C. B. Chen, M. Y. Wu, J. Wu, C. H. Yang, R. C. Y. Hui, Y. C. Chang, C. W. Lu, *J. Immunol. Res.* **2018** (2018) 1–9.
194. A. van Summeren, J. Renes, F. G. Bouwman, J. P. Noben, J. H. M. van Delftf, J. C. S. Kleinjans, E. C. M. Mariman, *Toxicol. Sci.* **120** (2011) 110–122.
195. A. R. Božić, N-Heteroaromatični Hidrazoni I Dihidrazoni Dihidrazida Ugljene I Tiougljene Kiseline: Karakterizacija, Kvantnomehanička Studija I Biološka Aktivnost, University of Belgrade, 2017.
196. Z. Shi, Z. Zhao, M. Liu, X. Wang, *Comptes Rendus Chim.* **16** (2013) 977–984.
197. D. Maity, A. K. Manna, D. Karthigeyan, T. K. Kundu, S. K. Pati, T. Govindaraju, *Chem. - A Eur. J.* **17** (2011) 11152–11161.
198. A. Bacchi, A. Bonini, M. Carcelli, F. Ferraro, E. Leporati, C. Pelizzi, G. Pelizzi, *J. Chem. Soc. - Dalt. Trans.* (1996) 2699–2704.
199. K. S. T. Dias, C. T. de Paula, T. dos Santos, I. N. O. Souza, M. S. Boni, M. J. R. Guimarães, F. M. R. da Silva, N. G. Castro, G. A. Neves, C. C. Veloso, M. M. Coelho, I. S. F. de Melo, F. C. V. Giusti, A. Giusti-Paiva, M. L. da Silva, L. E. Dardenne, I. A. Guedes, L. Pruccoli, F. Morroni, A. Tarozzi, C. Viegas, *Eur. J. Med. Chem.* **130** (2017) 440–457.
200. M. H. Assaleh, S. K. Bjelogrlic, N. Prlainovic, I. Cvijetic, A. Bozic, I. Arandjelovic, D. Vukovic, A. Marinkovic, *Arab. J. Chem.* **15** (2022) 103532.
201. M. S. Blois, *Nature* **181** (1958) 1199–1200.
202. Z. W. Jiang, X. C. Weng, Y. Huang, J. P. Hou, X. Y. Liao, *Grasas y Aceites* **65** (2014) 1–7.
203. O. Erel, *Clin. Biochem.* **37** (2004) 277–285.
204. P. Prieto, M. Pineda, M. Aguilar, *Anal. Biochem.* **269** (1999) 337–341.
205. S. D. Çekiç, K. S. Başkan, E. Tütem, R. Apak, *Talanta* **79** (2009) 344–351.
206. P. Wayne, *Approv. Stand. M7-A7, CLSI, USA* (2006) 91.
207. P. E. A. D. S. and J. C. Palomin, *J Antimicrob Chemother* **66** (2011) 1417–1430.
208. M. Seifert, D. Catanzaro, A. Catanzaro, T. C. Rodwell, *PLoS One* **10** (2015) 1–13.
209. N. Trotsko, J. Golus, P. Kazimierczak, A. Paneth, A. Przekora, G. Ginalska, M. Wujec, *Bioorg. Chem.* **97** (2020) 103676.
210. S. N. Danchuk, F. McIntosh, F. B. Jamieson, K. May, M. A. Behr, *Clin. Microbiol. Infect.* **26** (2020) 384.e5-384.e8.

211. N. Galić, A. Dijanošić, D. Kontrec, S. Miljanić, *Spectrochim. Acta - Part A Mol. Biomol. Spectrosc.* **95** (2012) 347–353.
212. T. A. Halgren, *J. Comput. Chem.* **20** (1999) 720–729.
213. R. W. Harrison, *J. Comput. Chem.* **14** (1993) 1112–1122.
214. A. Pedretti, L. Villa, G. Vistoli, *J. Comput. Aided. Mol. Des.* **18** (2004) 167–173.
215. T. Yanai, D. P. Tew, N. C. Handy, *Chem. Phys. Lett.* **393** (2004) 51–57.
216. K. Wolinski, J. F. Hinton, P. Pulay, *J. Am. Chem. Soc.* **112** (1990) 8251–8260.
217. J. Da Chai, M. Head-Gordon, *Phys. Chem. Chem. Phys.* **10** (2008) 6615–6620.
218. M. J. Frisch, G. W. Trucks, H. B. Schlegel, G. E. Scuseria, M. A. Robb, J. R. Cheeseman, G. Scalmani, V. Barone, B. Mennucci, G. A. Petersson, H. Nakatsuji, M. Caricato, X. Li, H. P. Hratchian, A. F. Izmaylov, J. Bloino, G. Zheng, J. L. Sonnenberg, M. Hada, M. Ehara, K. Toyota, R. Fukuda, J. Hasegawa, M. Ishida, T. Nakajima, Y. Honda, O. Kitao, H. Nakai, T. Vreven, J. A. Montgomery, J. E. Peralta, F. Ogliaro, M. Bearpark, J. J. Heyd, E. Brothers, K. N. Kudin, V. N. Staroverov, R. Kobayashi, J. Normand, K. Raghavachari, A. Rendell, J. C. Burant, S. S. Iyengar, J. Tomasi, M. Cossi, N. Rega, J. M. Millam, M. Klene, J. E. Knox, J. B. Cross, V. Bakken, C. Adamo, J. Jaramillo, R. Gomperts, R. E. Stratmann, O. Yazyev, A. J. Austin, R. Cammi, C. Pomelli, J. W. Ochterski, R. L. Martin, K. Morokuma, V. G. Zakrzewski, G. A. Voth, P. Salvador, J. J. Dannenberg, S. Dapprich, A. D. Daniels, Farkas, J. B. Foresman, J. V Ortiz, J. Cioslowski, D. J. Fox, *Gaussian 09, Revis. B.01, Gaussian, Inc., Wallingford CT* (2009).
219. M. Pastor, G. Cruciani, I. McLay, S. Pickett, S. Clementi, *J. Med. Chem.* **43** (2000) 3233–3243.
220. M. Pastor, *Alignment-independent Descriptors from Molecular Interaction Fields*, in *Mol. Interact. Fields Appl. Drug Discov. ADME Predict.*, Wiley-VCH Verlag GmbH & Co. KGaA, 2006, pp. 117–143.
221. J. J. P. Stewart, *J. Mol. Model.* **19** (2013) 1–32.
222. J. J. P. Stewart, (2016).
223. J. J. P. Stewart, *J. Comput. Aided. Mol. Des.* **4** (1990) 1–103.
224. P. J. Goodford, *J. Med. Chem.* **28** (1985) 849–857.
225. F. Fontaine, M. Pastor, F. Sanz, *J. Med. Chem.* **47** (2004) 2805–2815.
226. Á. Durán, G. C. Martínez, M. Pastor, *J. Chem. Inf. Model.* **48** (2008) 1813–1823.
227. M. Baroni, G. Costantino, G. Cruciani, D. Riganelli, R. Valigi, S. Clementi, *Quant. Struct. Relationships* **12** (1993) 9–20.
228. B. K. Momidi, V. Tekuri, D. R. Trivedi, *Spectrochim. Acta - Part A Mol. Biomol. Spectrosc.* **180** (2017) 175–182.
229. P. Kovaříková, K. Vávrová, K. Tomalová, M. Schöngut, K. Hrušková, P. Hašková, J. Klimeš, *J. Pharm. Biomed. Anal.* **48** (2008) 295–302.
230. F. Milletti, A. Vulpetti, *J. Chem. Inf. Model.* **50** (2010) 1062–1074.
231. W. M. F. Fabian, L. Antonov, D. Nedeltcheva, F. S. Kamounah, P. J. Taylor, *J. Phys. Chem. A* **108** (2004) 7603–7612.
232. Z. Kuodis, A. Rutavičius, A. Matijoška, O. Eicher-Lorka, *Cent. Eur. J. Chem.* **5** (2007) 996–1006.
233. L. Lin, W. Fan, S. Chen, J. Ma, W. Hu, Y. Lin, H. Zhang, R. Huang, *New J. Chem.* **36** (2012) 2562–2567.
234. S. Uchiyama, M. Ando, S. Aoyagi, *J. Chromatogr. A* **996** (2003) 95–102.
235. N. Galić, Z. Cimerman, V. Tomišić, *Spectrochim. Acta - Part A Mol. Biomol. Spectrosc.* **71** (2008) 1274–1280.
236. G. M. Abu El-Reash, O. A. El-Gammal, A. H. Radwan, *Spectrochim. Acta - Part A Mol. Biomol. Spectrosc.* **121** (2014) 259–267.
237. A. Cembran, F. Bernardi, M. Garavelli, L. Gagliardi, G. Orlandi, *J. Am. Chem. Soc.* **126**

(2004) 3234–3243.
238. R. Cimiraglia, H. J. Hofmann, *Chem. Phys. Lett.* **217** (1994) 430–435.
239. M. A. Gordillo, M. Soto-Monsalve, C. C. Carmona-Vargas, G. Gutiérrez, R. F. D'vries, J. M. Lehn, M. N. Chaur, *Chem. - A Eur. J.* **23** (2017) 14872–14882.
240. Z. J. Li, L. Cai, R. F. Mei, J. W. Dong, S. Q. Li, X. Q. Yang, H. Zhou, T. P. Yin, Z. T. Ding, *Tetrahedron Lett.* **56** (2015) 7197–7200.
241. T. Matsuhira, H. Yamamoto, T. A. Okamura, N. Ueyama, *Org. Biomol. Chem.* **6** (2008) 1926–1933.
242. I. K. Cheah, B. Halliwell, *Biochim. Biophys. Acta - Mol. Basis Dis.* **1822** (2012) 784–793.
243. M. T. Zimmerman, C. A. Bayse, R. R. Ramoutar, J. L. Brumaghim, *J. Inorg. Biochem.* **145** (2015) 30–40.
244. V. Calcatierra, Ó. López, J. G. Fernández-Bolaños, G. B. Plata, J. M. Padrón, *Eur. J. Med. Chem.* **94** (2015) 63–72.
245. L. Hernández-García, J. Sandoval-Lira, S. Rosete-Luna, G. Niño-Medina, M. Sanchez, *Struct. Chem.* **29** (2018) 1265–1272.
246. N. C. Institute, *Https://Www.Cancer.Gov/Research/Areas/Treatment* (2021) 2021.
247. H. Sung, J. Ferlay, R. L. Siegel, M. Laversanne, I. Soerjomataram, A. Jemal, F. Bray, *CA. Cancer J. Clin.* **71** (2021) 209–249.
248. H. Murad, M. Hawat, A. Ekhtiar, A. AlJapawe, A. Abbas, H. Darwish, O. Sbenati, A. Ghannam, *Cancer Cell Int.* **16** (2016) 1–11.
249. J. H. Zhang, M. Xu, *Cell Res.* **10** (2000) 205–211.
250. C. H. Jung, E. M. Kim, J. Y. Song, J. K. Park, H. D. Um, *Exp. Mol. Med.* **51** (2019) 1–10.
251. R. B. Rodríguez, D. Iguchi, R. Erra-Balsells, M. Laura Salum, P. Froimowicz, *Polymers (Basel).* **12** (2020) 1–11.
252. R. C. Montes, A. L. A. L. Perez, C. I. S. Medeiros, M. O. De Araújo, E. D. O. Lima, M. T. Scotti, D. P. De Sousa, *Molecules* **21** (2016).
253. L. B. Rice, *Infect. Control Hosp. Epidemiol.* **31** (2010) S7–S10.
254. J. Garnacho-Montero, R. Amaya-Villar, *Curr. Opin. Infect. Dis.* **23** (2010) 332–339.
255. A. Ulu-Kilic, S. Ahmed, E. Alp, M. Doğanay, *OA Crit. Care* **1** (2013).
256. L. Malone, D. H. Kwon, *Int. J. Antimicrob. Agents* **41** (2013) 70–74.
257. A. Al-Mulla, *Der Pharma Chem.* **9** (2017) 141–147.
258. G. F. Viana, S. M. dos Santos Saalfeld, L. B. Garcia, C. L. Cardoso, M. Pelisson, M. C. B. Tognim, *Lett. Appl. Microbiol.* **53** (2011) 374–378.
259. Y. Zhang, C. Zhao, Q. Wang, X. Wang, H. Chen, H. Li, F. Zhang, H. Wang, *J. Antimicrob. Chemother.* **75** (2020) 2609–2615.
260. D. N. A. Chee, M. A. Affan, F. B. Ahmad, M. R. Asaruddin, N. Sam, M. A. Salam, A. Ismail, S. H. Tan, *J. Coord. Chem.* **64** (2011) 4191–4200.
261. Z. H. Chohan, H. Pervez, K. M. Khan, C. T. Supuran, *J. Enzyme Inhib. Med. Chem.* **20** (2005) 81–89.
262. F. S. Castelo-Branco, E. C. de Lima, J. L. de O. Domingos, A. C. Pinto, M. C. S. Lourenço, K. M. Gomes, M. M. Costa-Lima, C. F. Araujo-Lima, C. A. F. Aiub, I. Felzenszwalb, T. E. M. M. Costa, C. Penido, M. G. Henriques, N. Boechat, *Eur. J. Med. Chem.* **146** (2018) 529–540.
263. S. Hofmann-Thiel, H. Hoffmann, D. Hillemann, L. Rigouts, A. Van Deun, K. Kranzer, *Int. J. Tuberc. Lung Dis.* **21** (2017) 721–726.
264. K. W. Jo, Y. Yeo, H. Sung, M. N. Kim, T. S. Shim, *Respir. Med.* **122** (2017) 12–17.
265. J. Y. Kang, J. Hur, S. Kim, S. Jeon, J. Lee, Y. J. Kim, S. C. Kim, Y. J. Park, Y. K. Kim, H. S. Moon, *J. Thorac. Dis.* **11** (2019) 400–409.

266. P. Wang, K. Pradhan, X. bo Zhong, X. Ma, *Acta Pharm. Sin. B* **6** (2016) 384–392.
267. H. Singh, P. Thangaraj, A. Chakrabarti, *J. Clin. Diagnostic Res.* **7** (2013) 2602–2605.
268. M. A. Smith, V. B. Weaver, D. M. Young, L. N. Ornston, *Appl. Environ. Microbiol.* **69** (2003) 524–532.
269. C. Ratledge, L. G. Dover, *Annu. Rev. Microbiol.* **54** (2000) 881–941.
270. F. Runci, V. Gentile, E. Frangipani, G. Rampioni, L. Leoni, M. Lucidi, D. Visaggio, G. Harris, W. Chen, J. Stahl, B. Averhoff, P. Visca, *Infect. Immun.* **87** (2019) 1–16.
271. M. S. Dragset, G. Poce, S. Alfonso, T. Padilla-Benavides, T. R. Ioerger, T. Kaneko, J. C. Sacchettini, M. Biava, T. Parish, J. M. Argüello, M. Steigedal, E. J. Rubin, *Antimicrob. Agents Chemother.* **59** (2015) 2256–2264.
272. A. D. Tiwari, A. K. Mishra, S. B. Mishra, B. B. Mamba, B. Maji, S. Bhattacharya, *Spectrochim. Acta - Part A Mol. Biomol. Spectrosc.* **79** (2011) 1050–1056.
273. Mohamed H Assaleh, Sanja Jeremić, Ilija Cvijetić, Aleksandar Marinković, Nevena Prlainović, *J. Mol. Struct.* **1262** (2022) 1–11.

## 6. Appendix

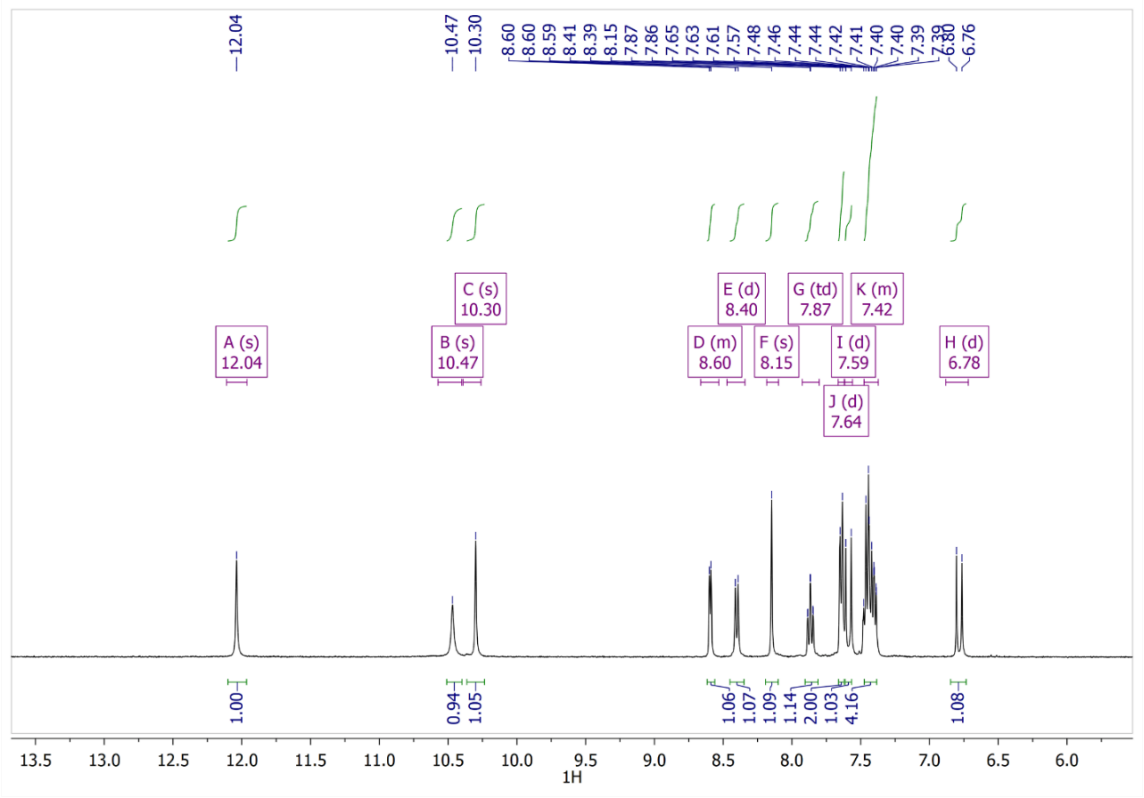


Figure 48. $^{1}$H NMR spectrum of **CimTCH$_{2fp}$**

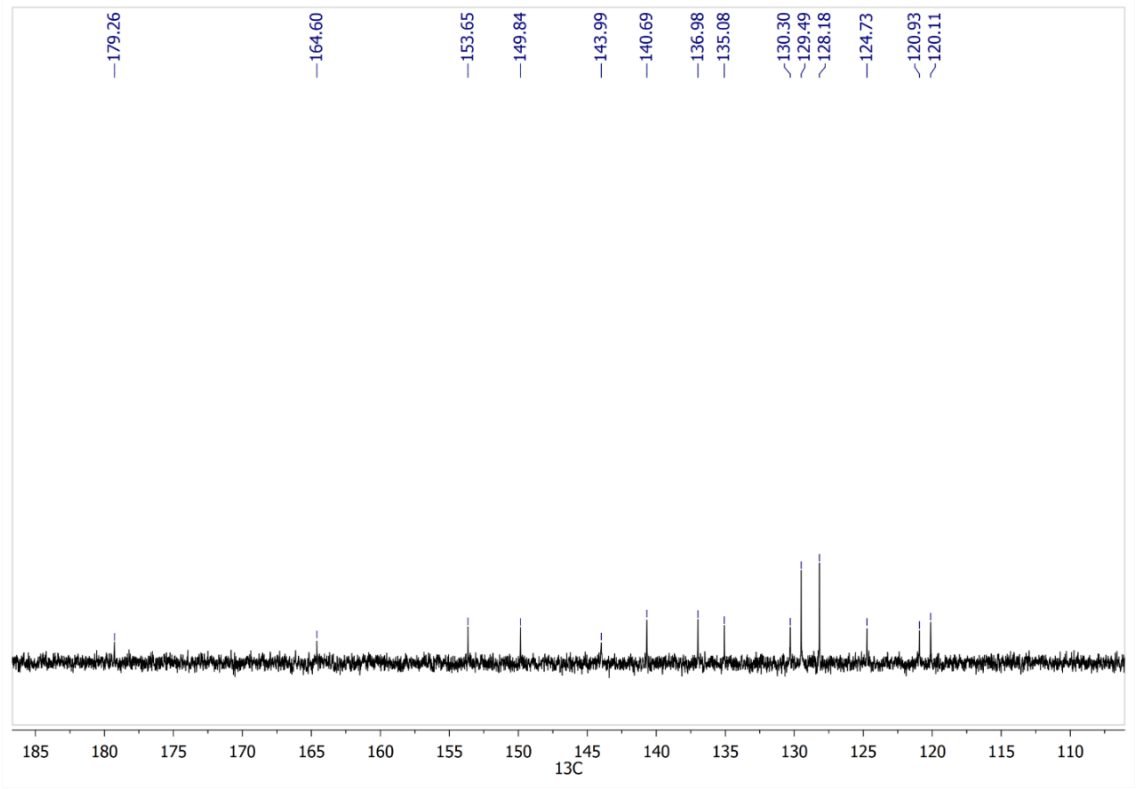


Figure 49. $^{13}$C NMR spectrum of **CimTCH$_{2fp}$**

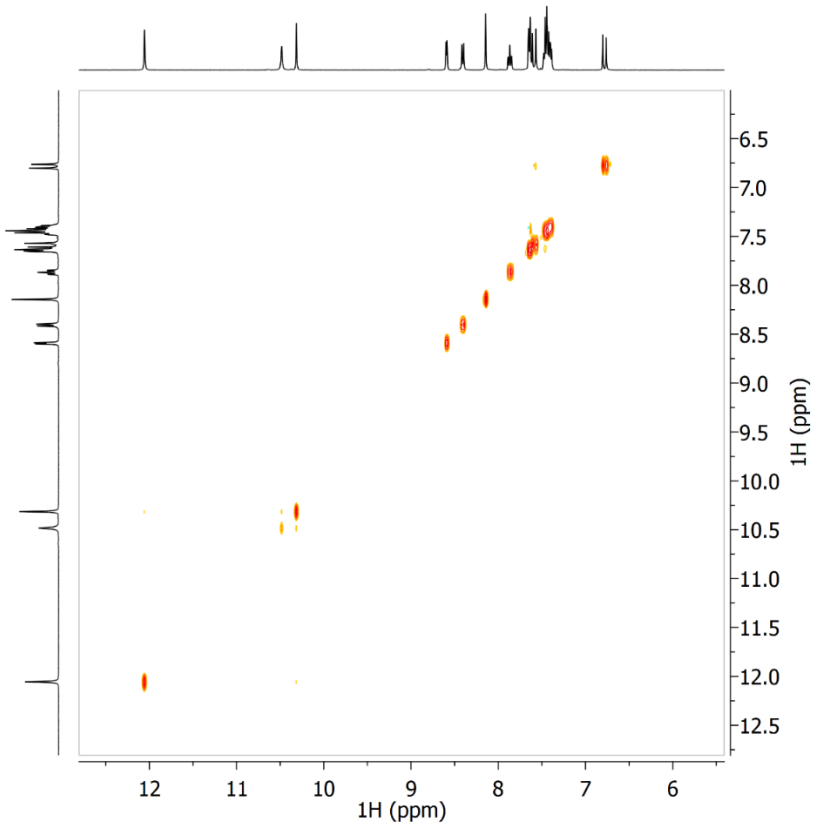


Figure 50. NOESY NMR spectrum of **CimTCH$_{2fp}$**

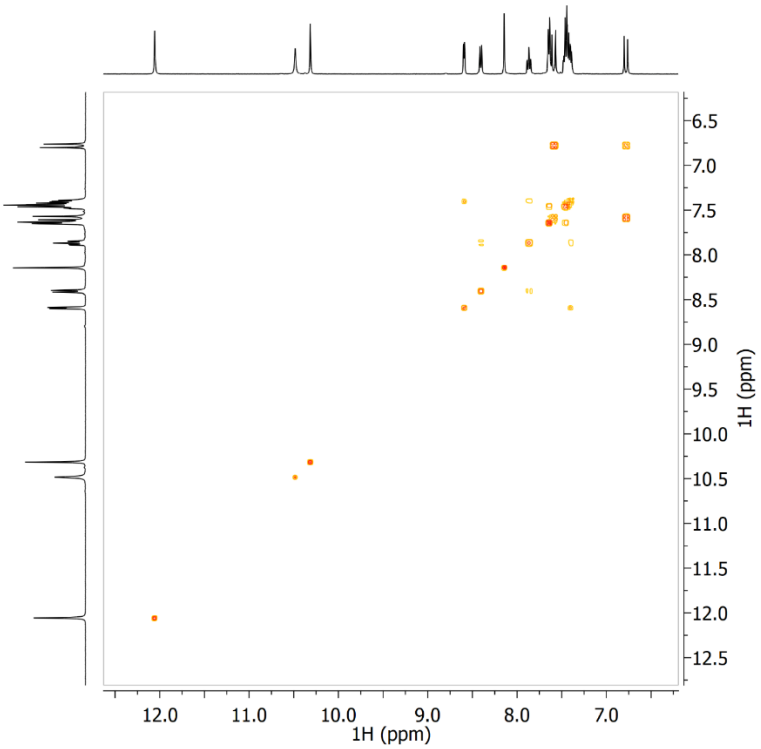


Figure 51. COSY NMR spectrum of **CimTCH$_{2fp}$**

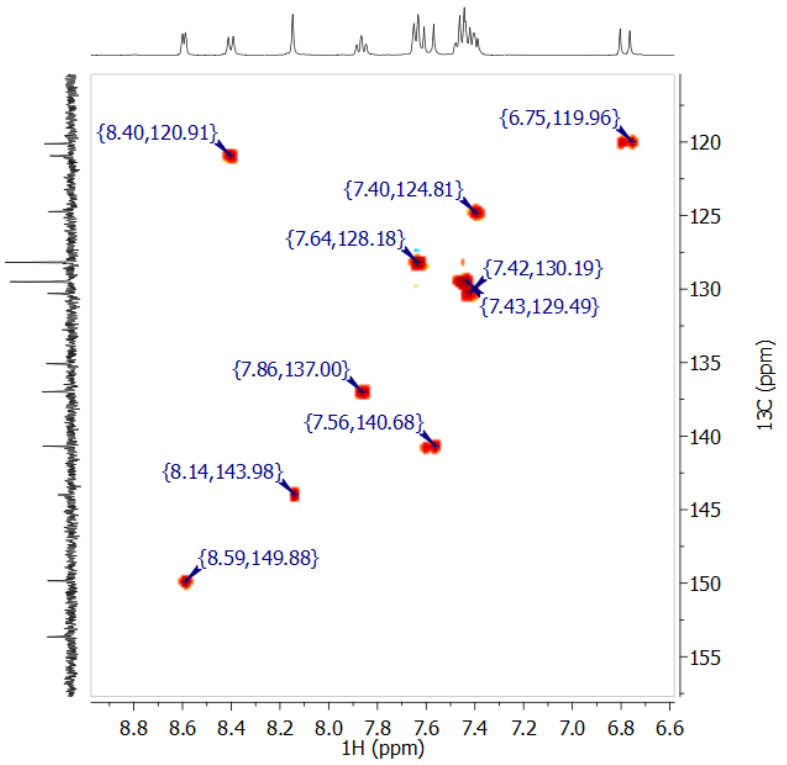


Figure 52**.** HSQC NMR spectrum of **CimTCH$_{2fp}$**

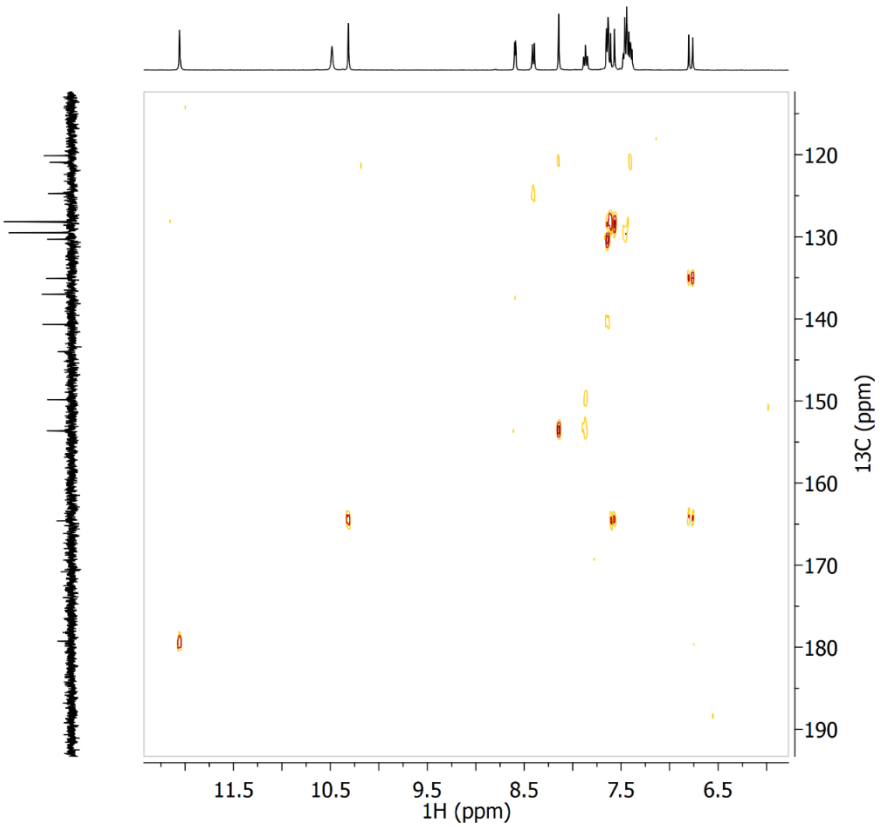


Figure 53. HMBC NMR spectrum of **CimTCH$_{2fp}$**

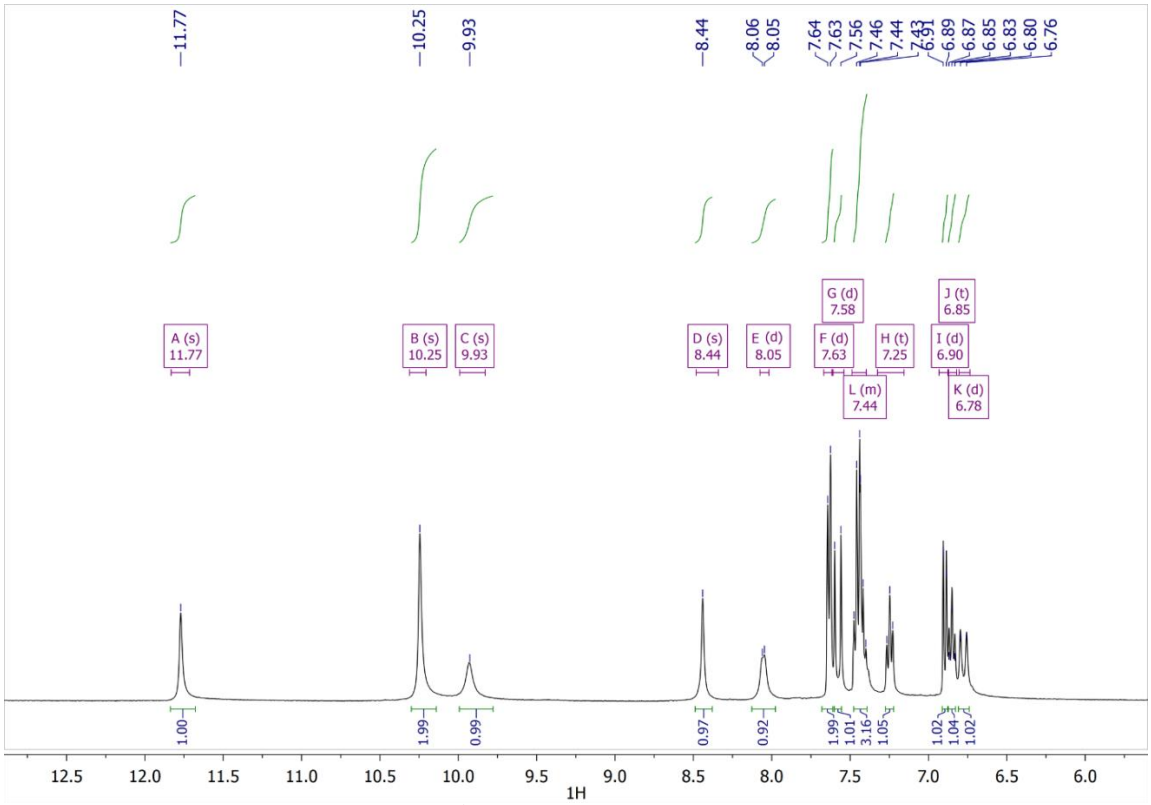


Figure 54. $^{1}$H NMR spectrum of **CimTCH$_{sal}$**

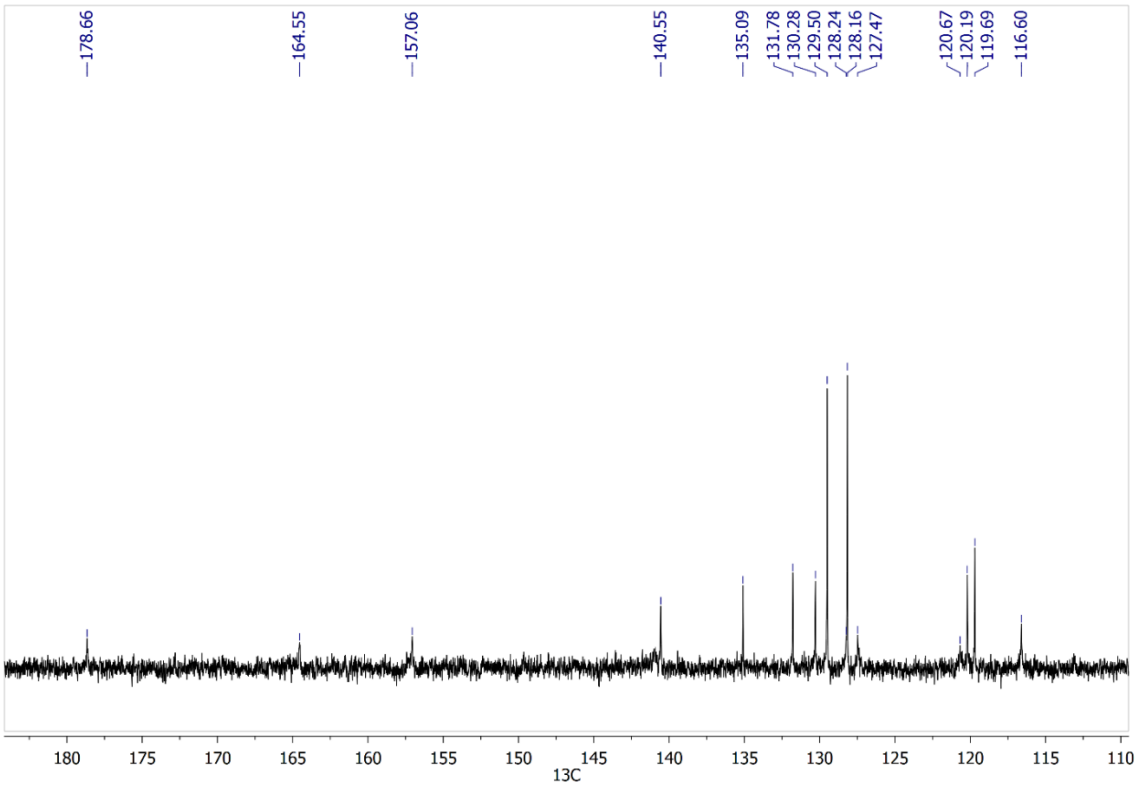


Figure 55. $^{13}$C NMR spectra of **CimTCH$_{sal}$**

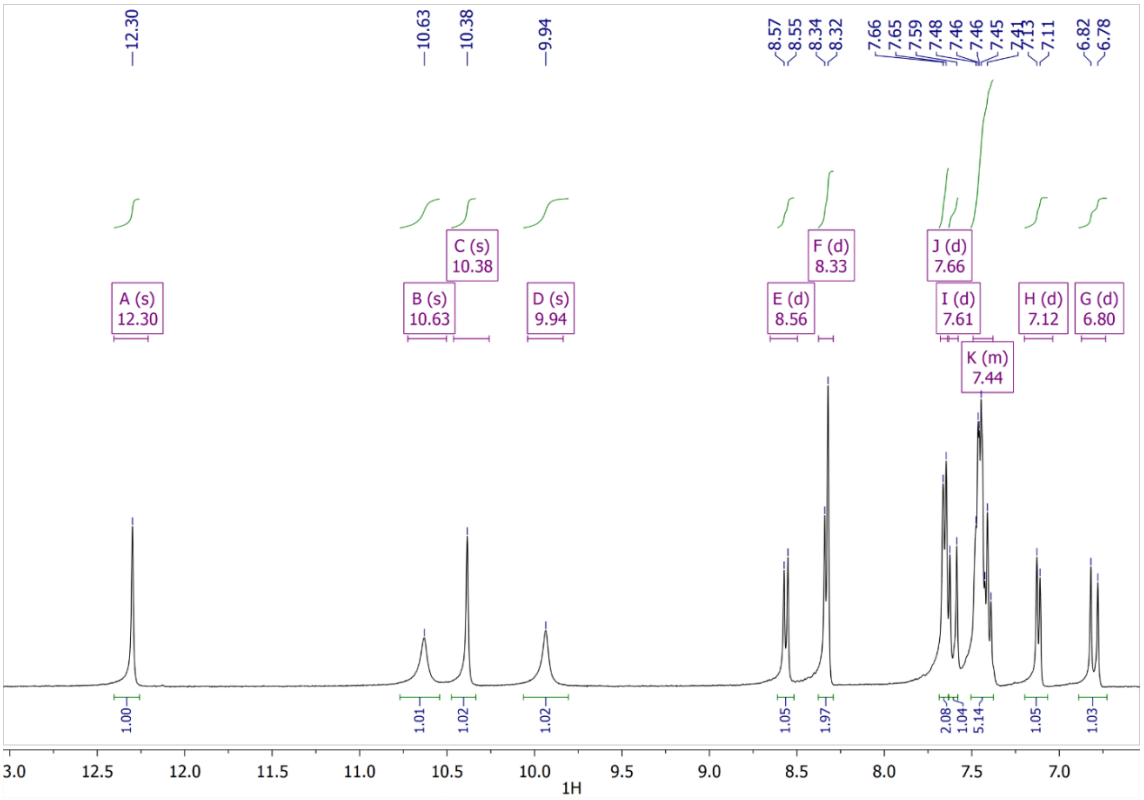


Figure 56. $^{1}$H NMR spectra of **CimTCH$_{8OH2qu}$**

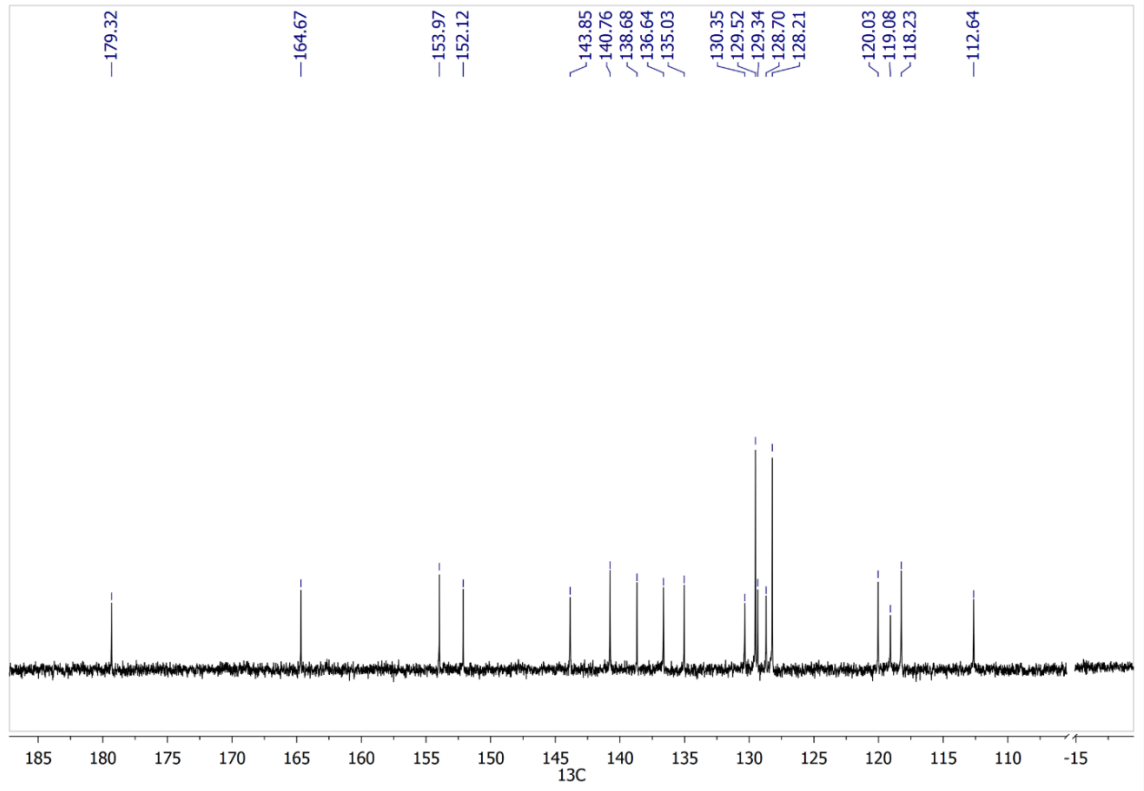


Figure 57. $^{13}$C NMR spectra of **CimTCH$_{8OH2qu}$**

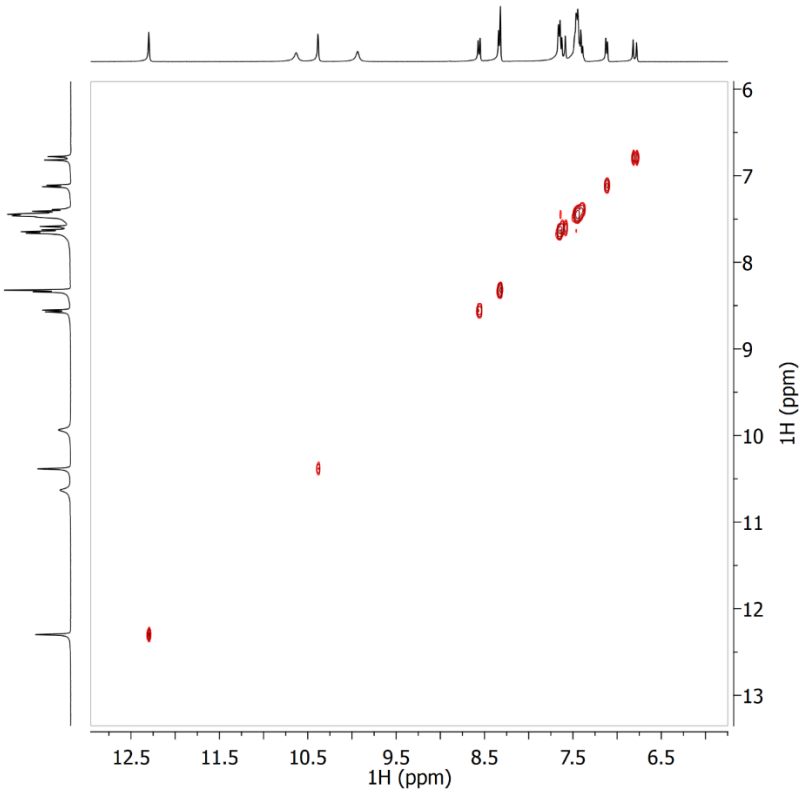


Figure 58. COSY spectra of **CimTCH$_{8OH2qu}$**

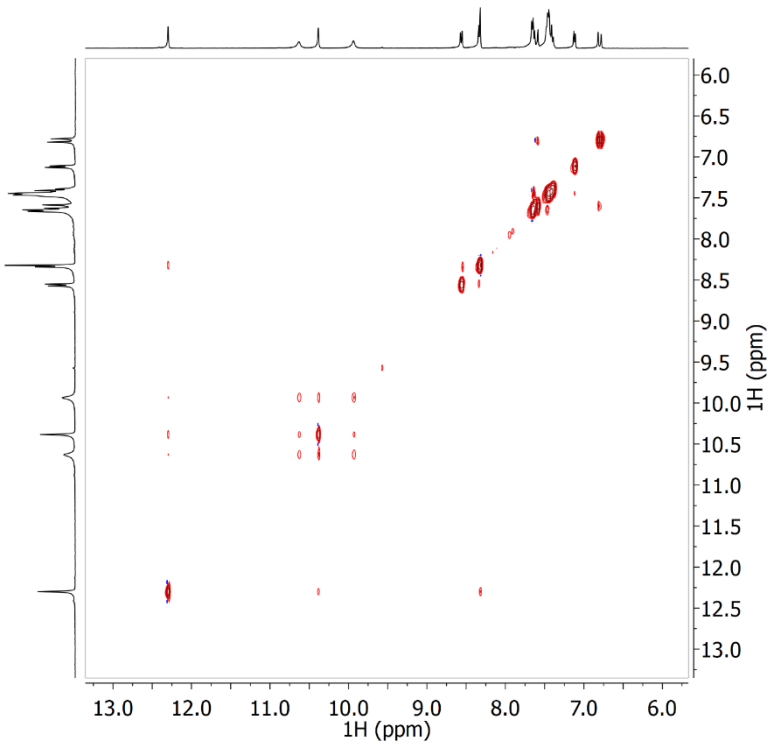


Figure 59. NOESY spectra of **CimTCH$_{8OH2qu}$**

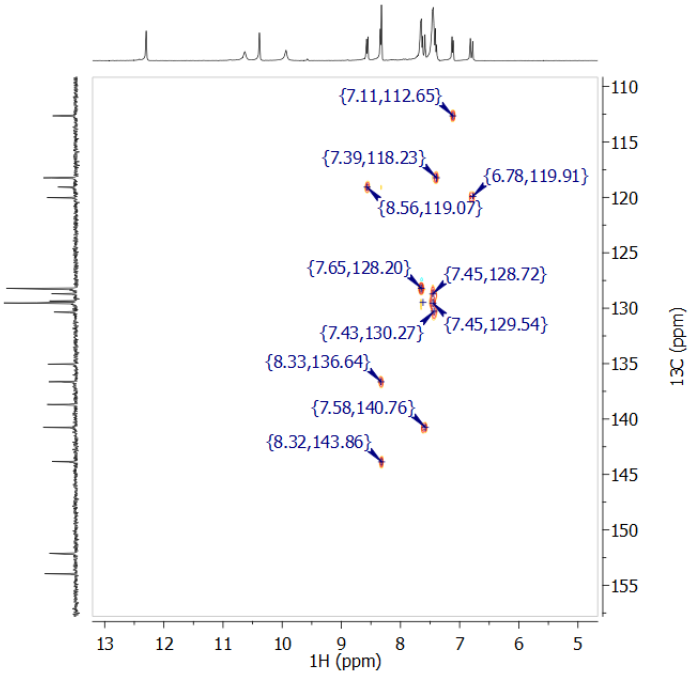


Figure 60. HSQC NMR spectra of **CimTCH$_{8OH2qu}$**

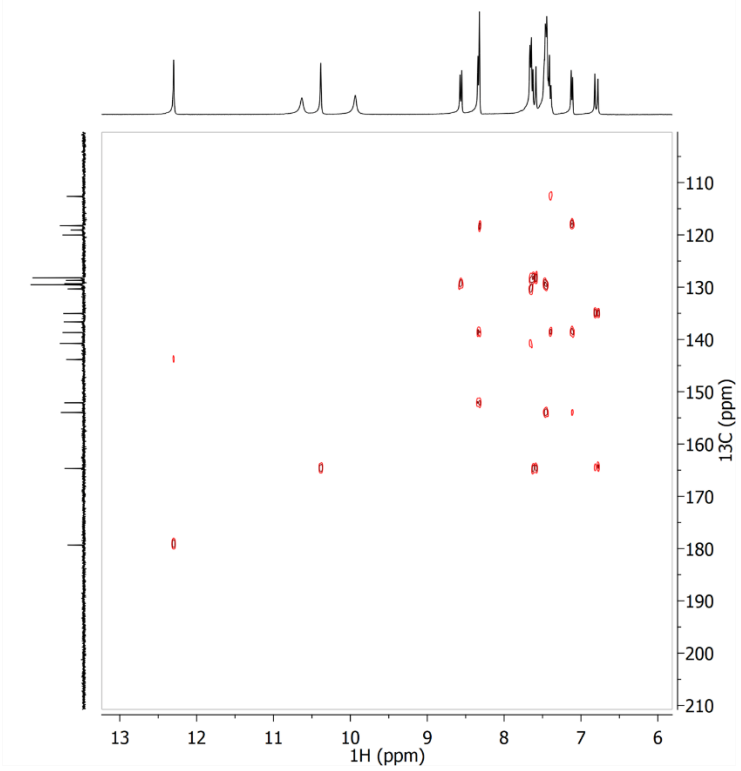


Figure 61. HMBC NMR spectra of **CimTCH$_{8OH2qu}$**

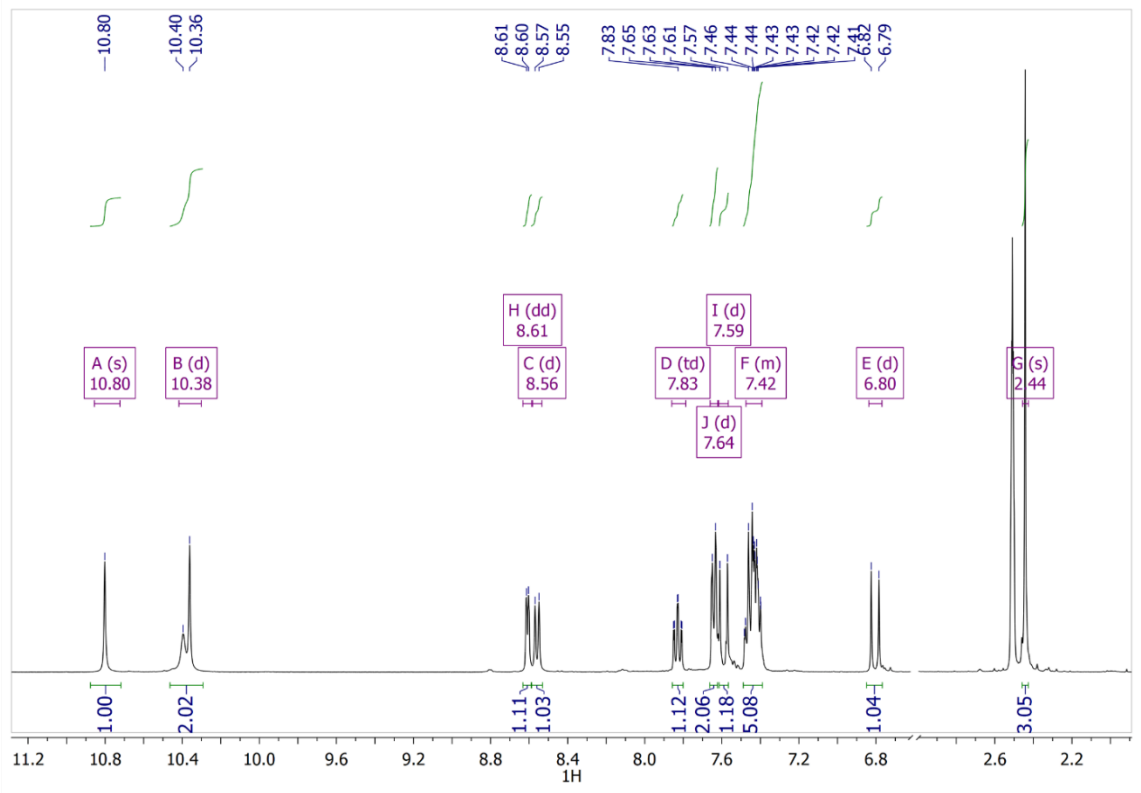


Figure 62. $^{1}$H NMR spectra of **CimTCH$_{2ap}$**

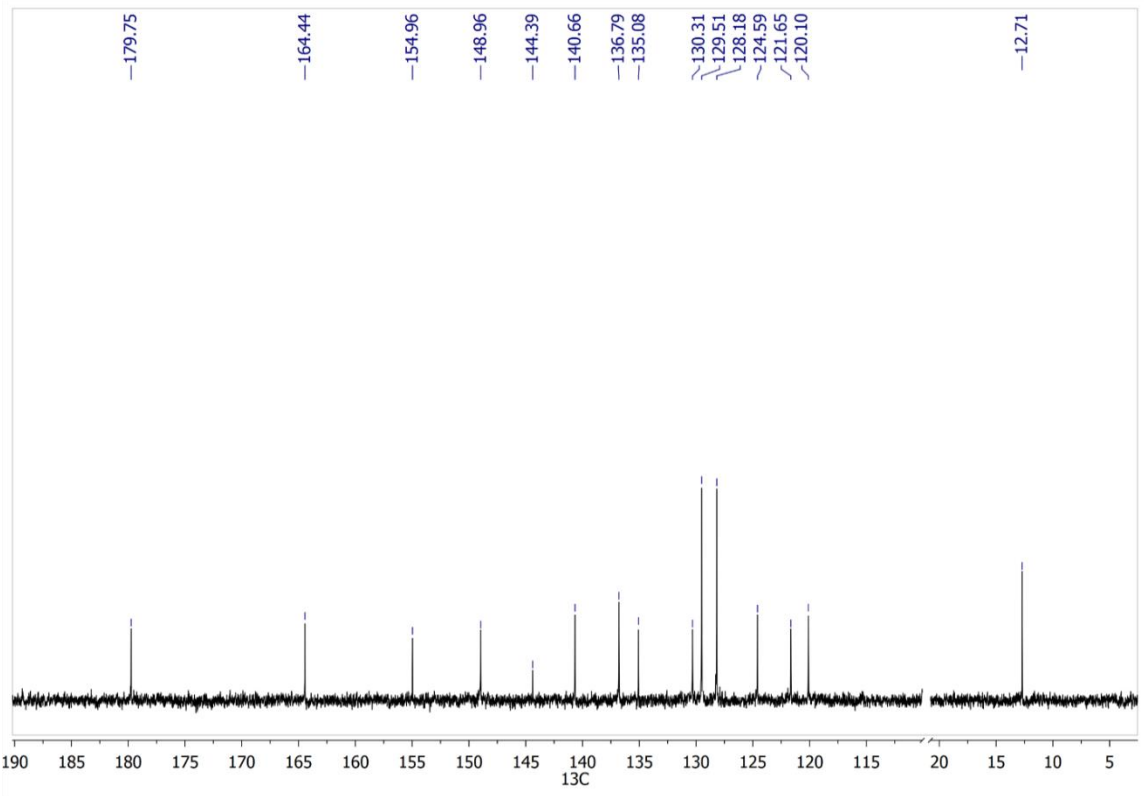


Figure 63. $^{13}$C NMR spectra of **CimTCH$_{2ap}$**

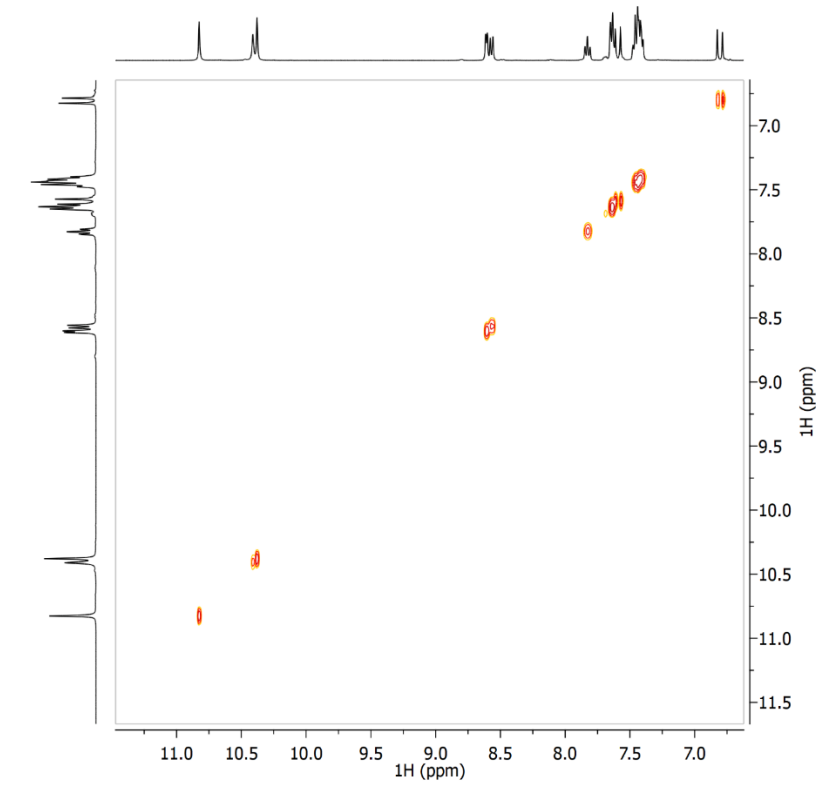


Figure 64. COSY NMR spectra of **CimTCH$_{2ap}$**

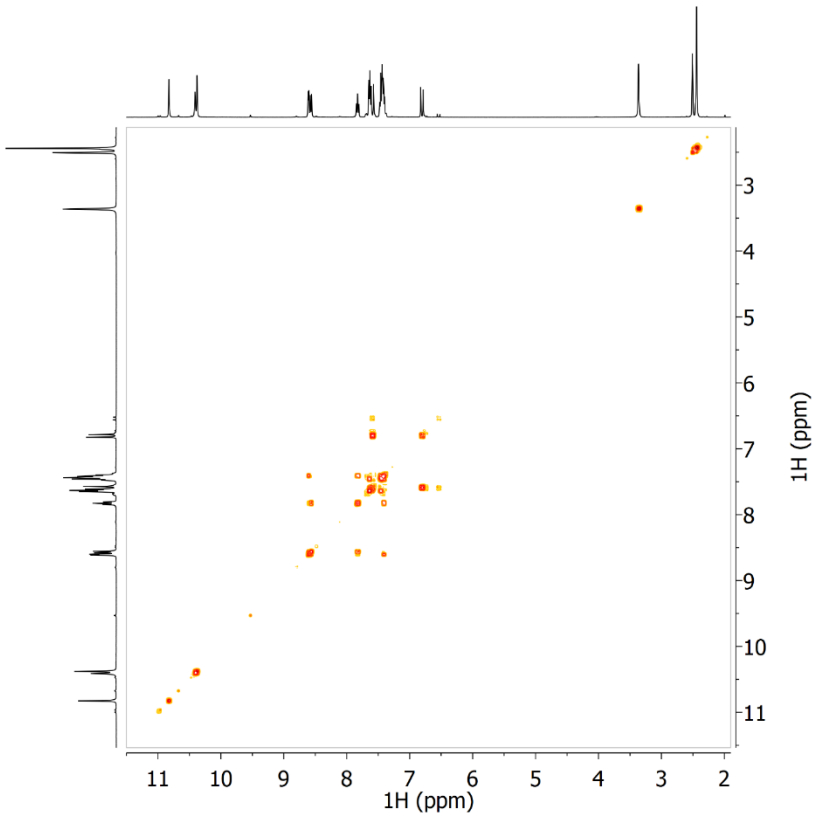


Figure 65. NOESY NMR spectra of **CimTCH$_{2ap}$**

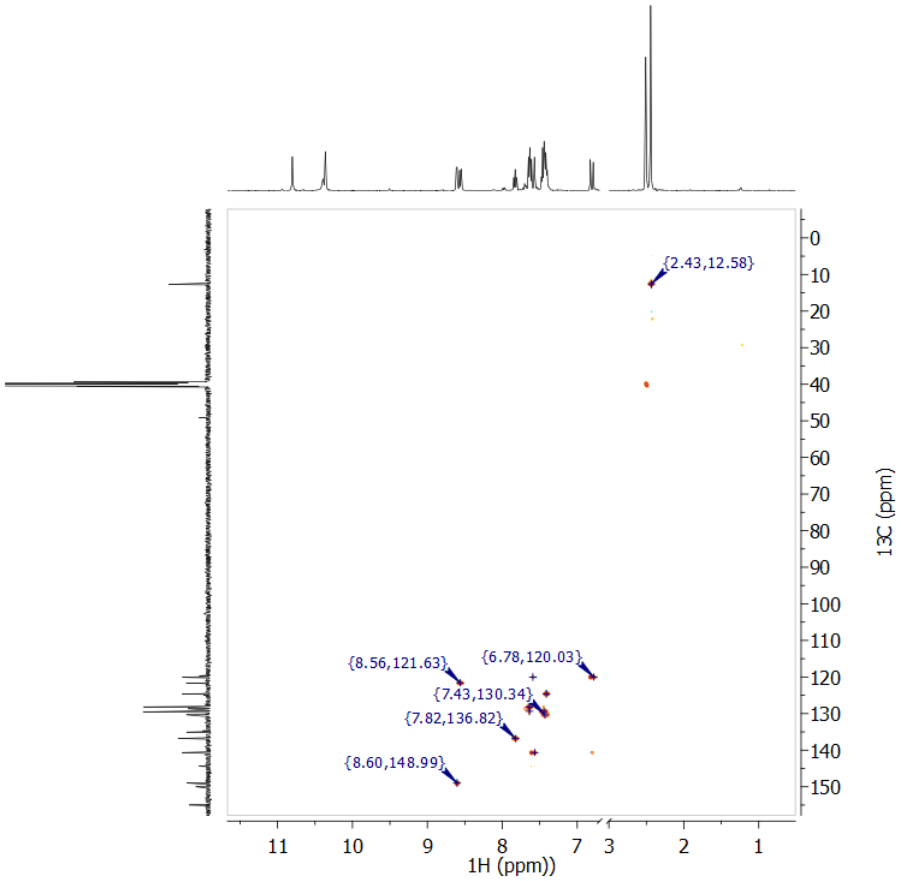


Figure 66. HSQC NMR spectra of **CimTCH$_{2ap}$**

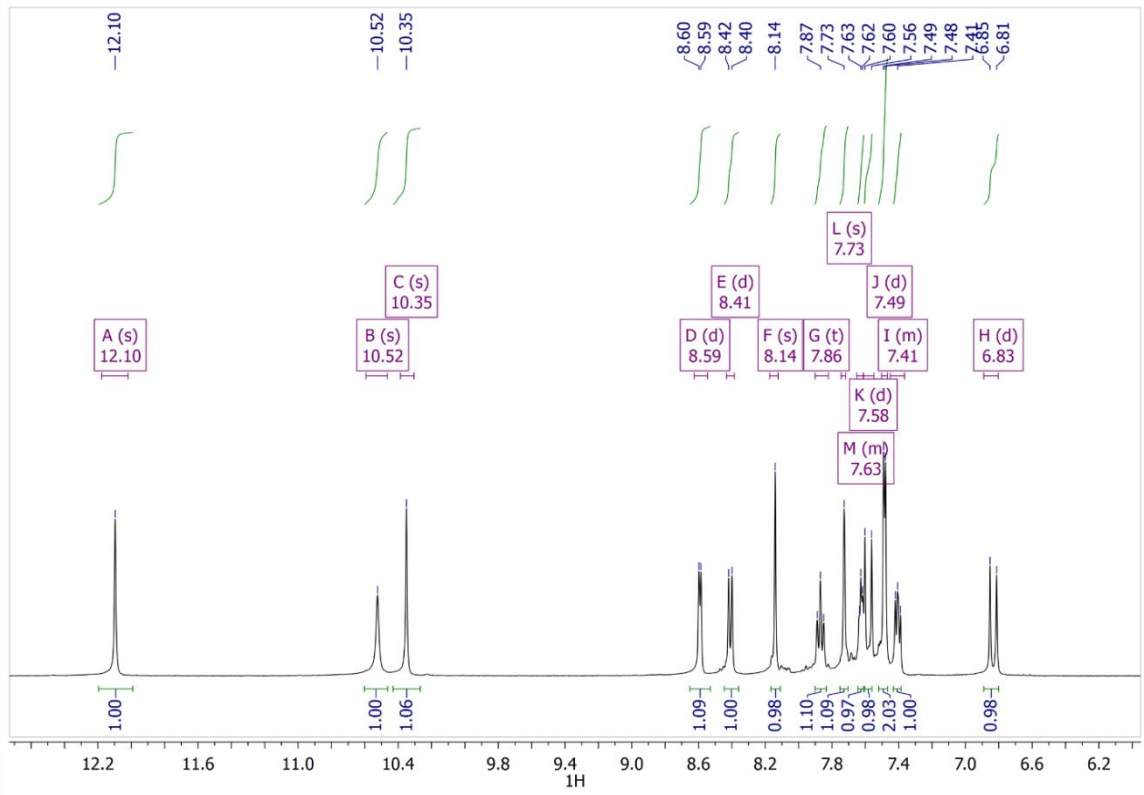


Figure 67. $^{1}$H NMR spectra of **3-ClCimTCH$_{2fp}$**

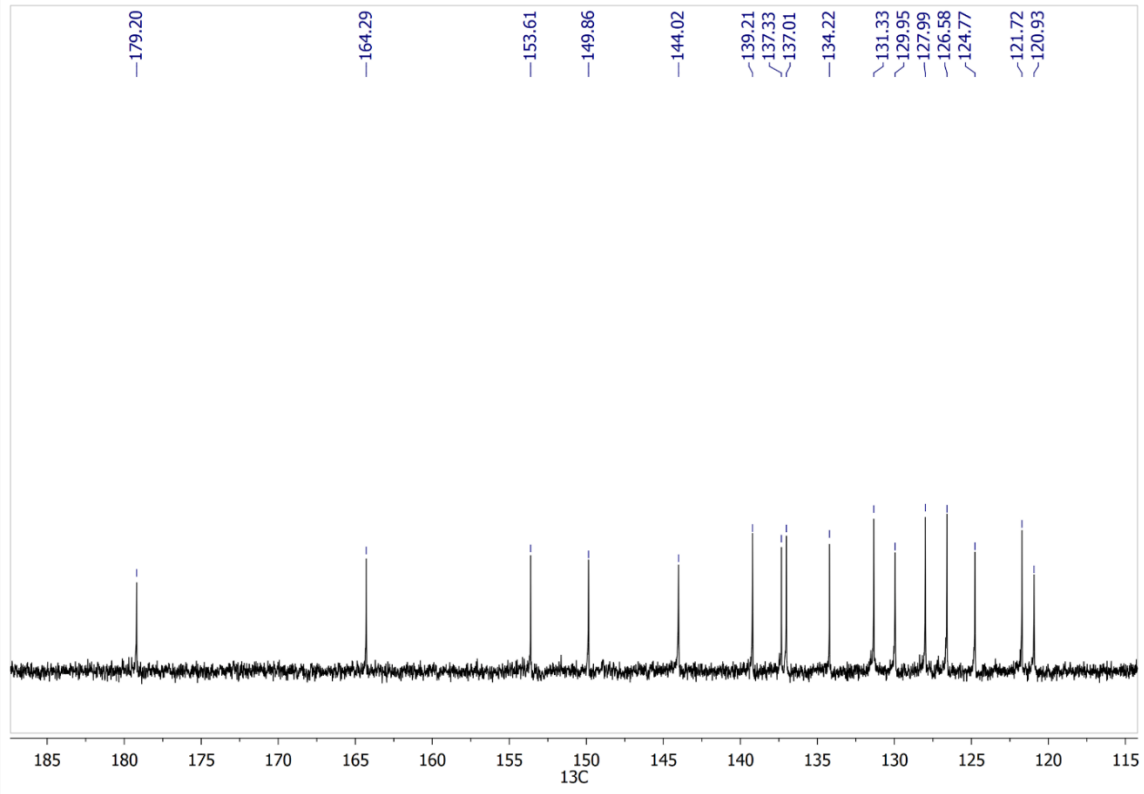


Figure 68. $^{13}$C NMR spectra of **3-ClCimTCH$_{2fp}$**

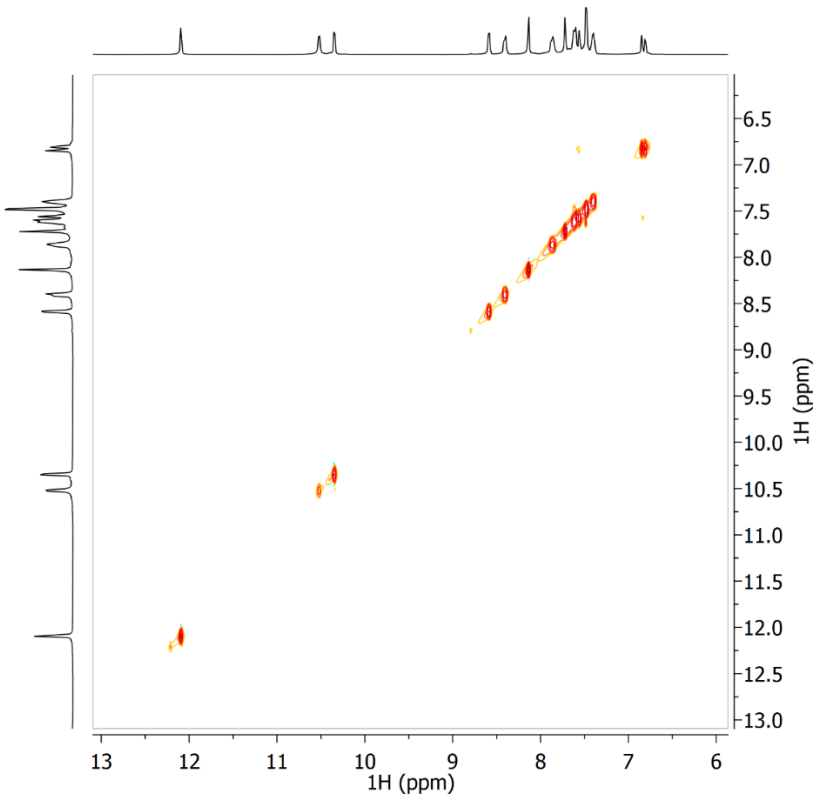


Figure 69. COSY NMR spectra of **3-ClCimTCH$_{2fp}$**

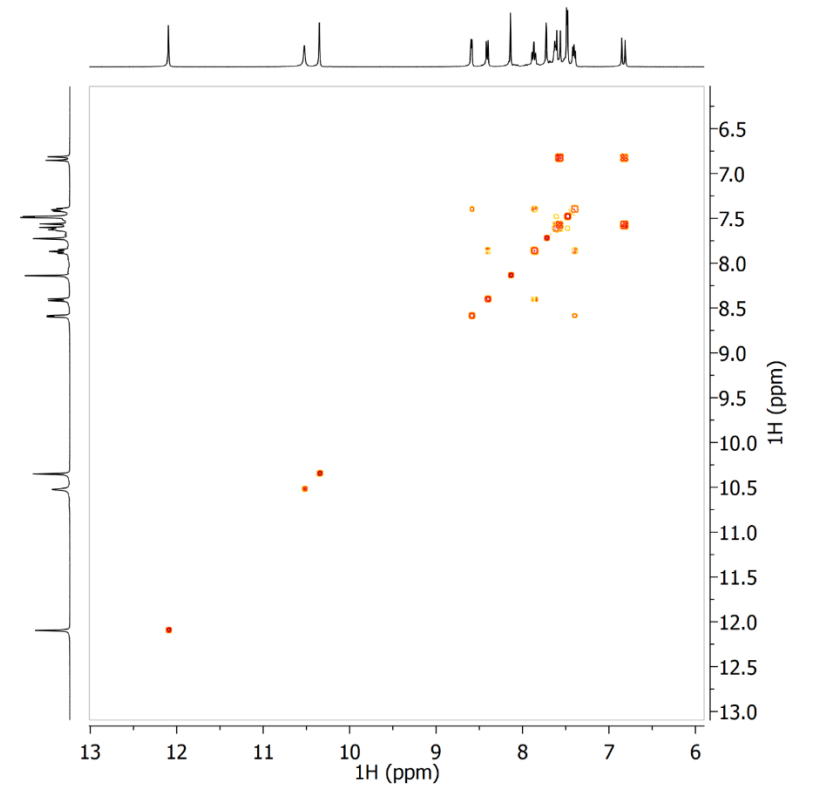


Figure 70. NOESY NMR spectra of **3-ClCimTCH$_{2fp}$**

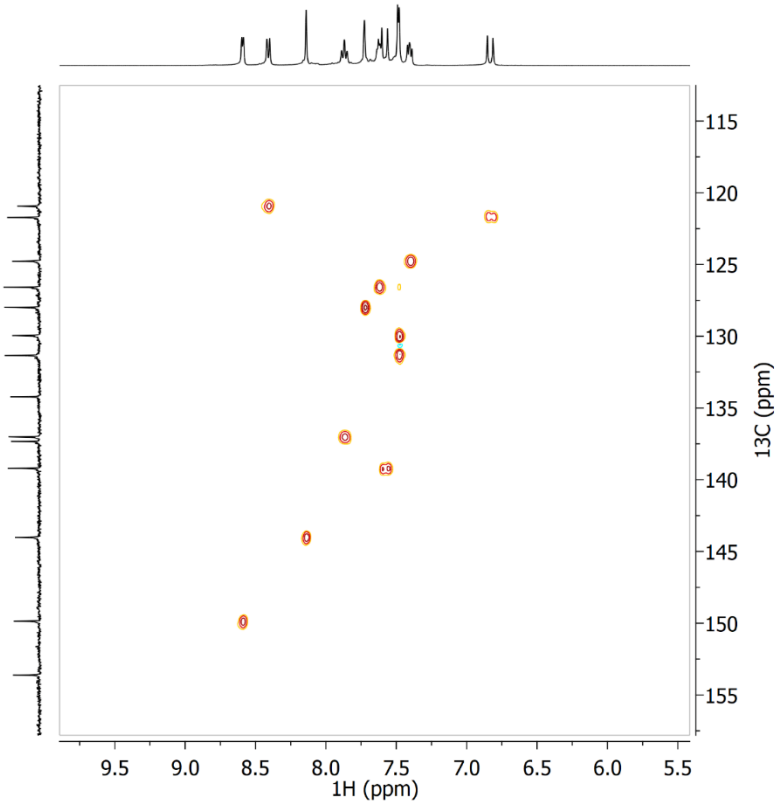


Figure 71. HSQC NMR spectra of **3-ClCimTCH$_{2fp}$**

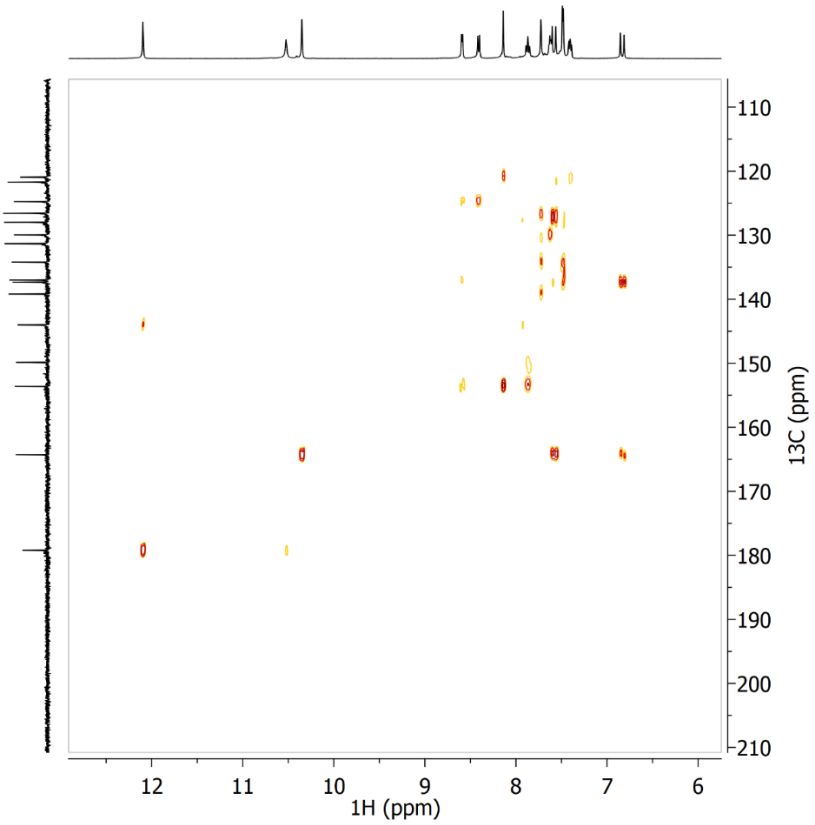


Figure 72. HMBC NMR spectra of **3-ClCimTCH$_{2fp}$**

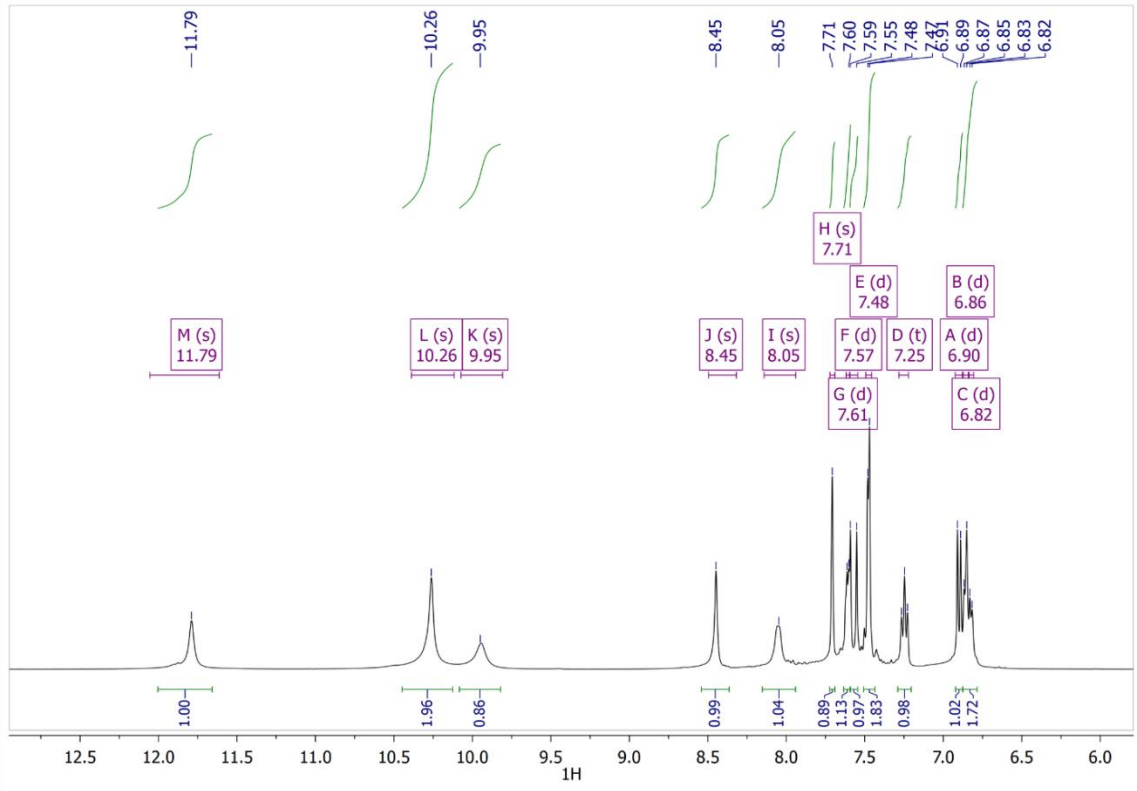


Figure 73. $^{1}$H NMR spectra of **3-ClCimTCH$_{sal}$**

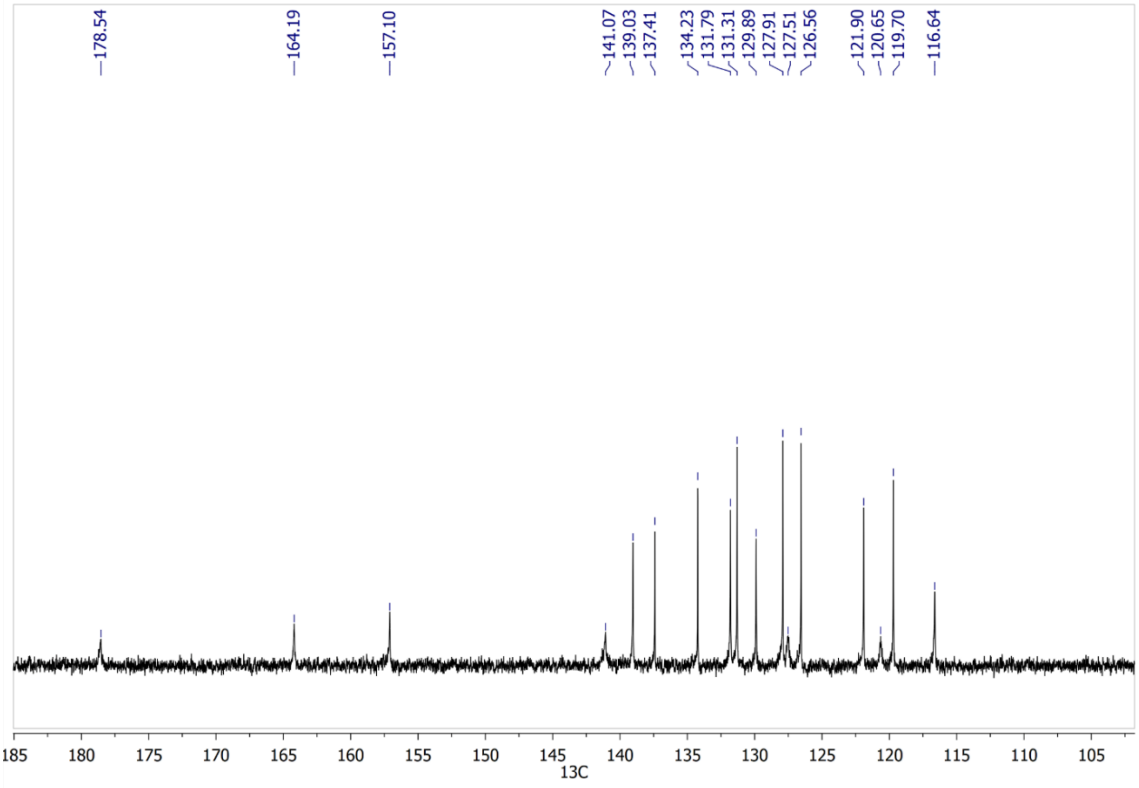


Figure 74. $^{13}$C NMR spectra of **3-ClCimTCH$_{2fp}$**

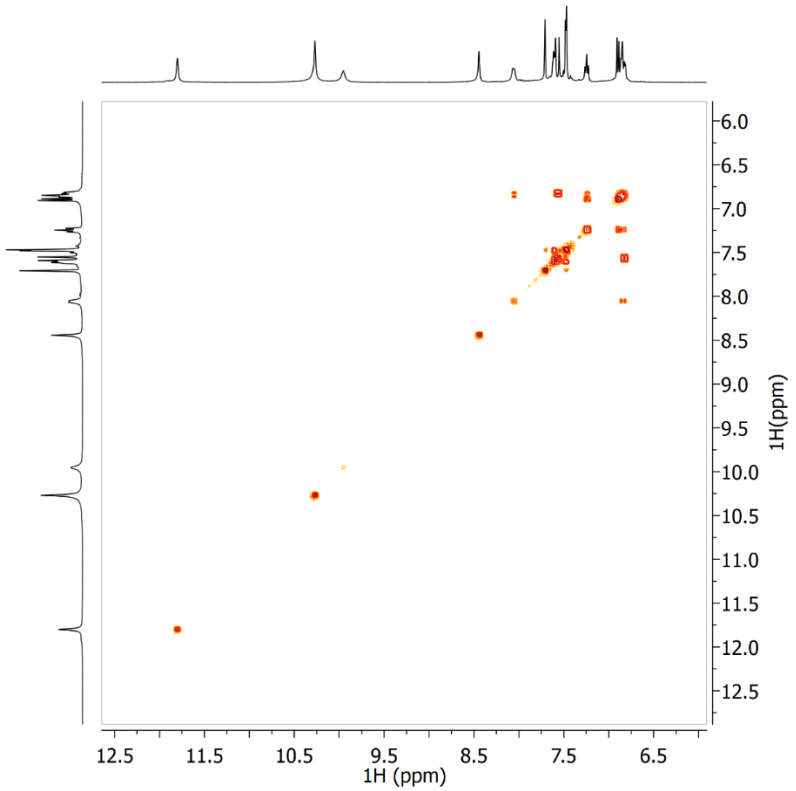


Figure 75. COSY NMR spectra of **3-ClCimTCH$_{2fp}$**

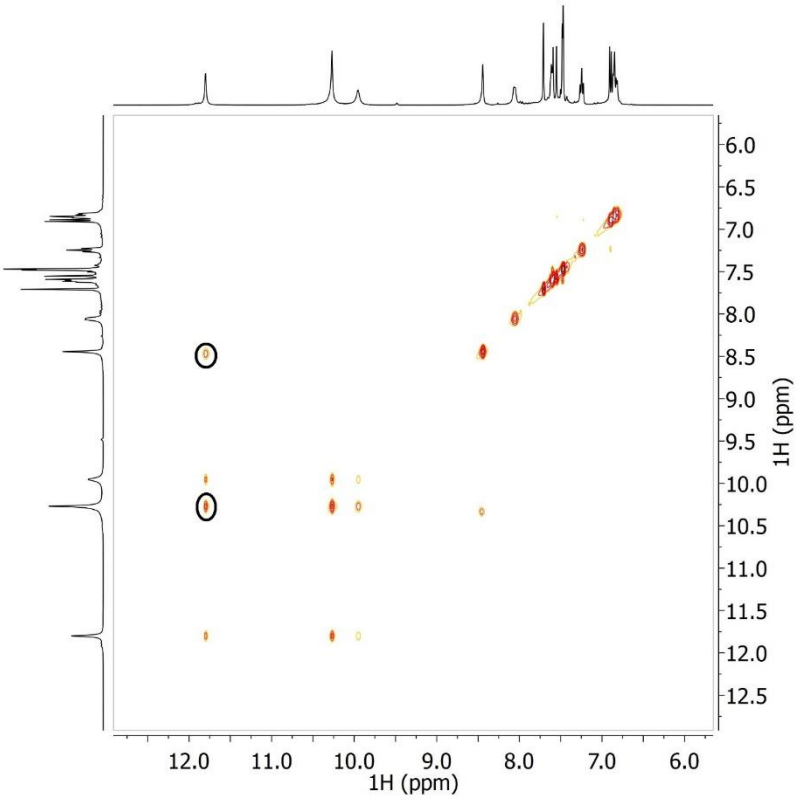


Figure 76. NOESY NMR spectra of **3-ClCimTCH$_{2fp}$**

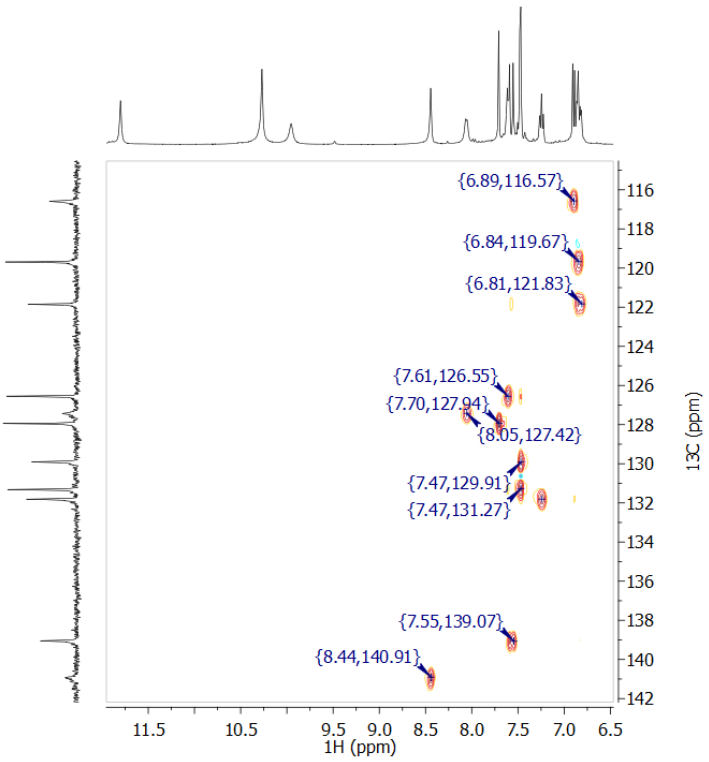


Figure 77. HSQC NMR spectra of **3-ClCimTCH$_{2fp}$**

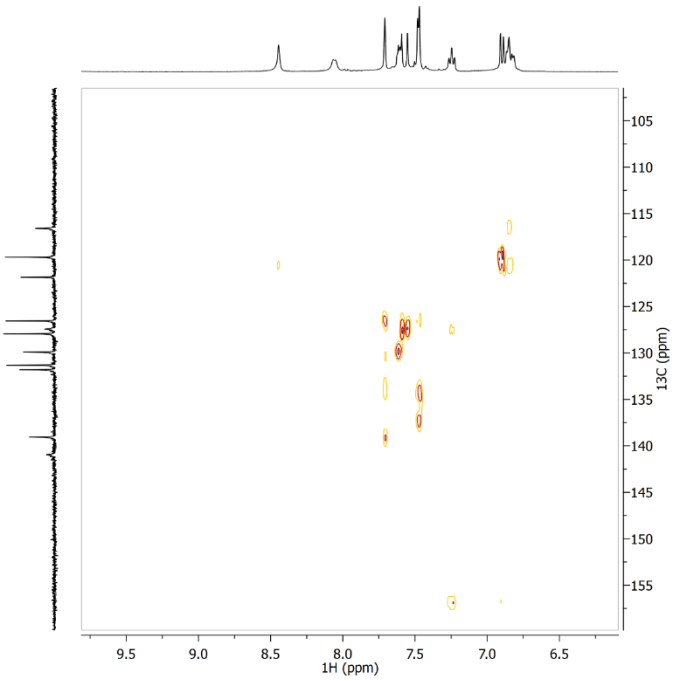


Figure 78. HMBC NMR spectra of **3-ClCimTCH$_{2fp}$**

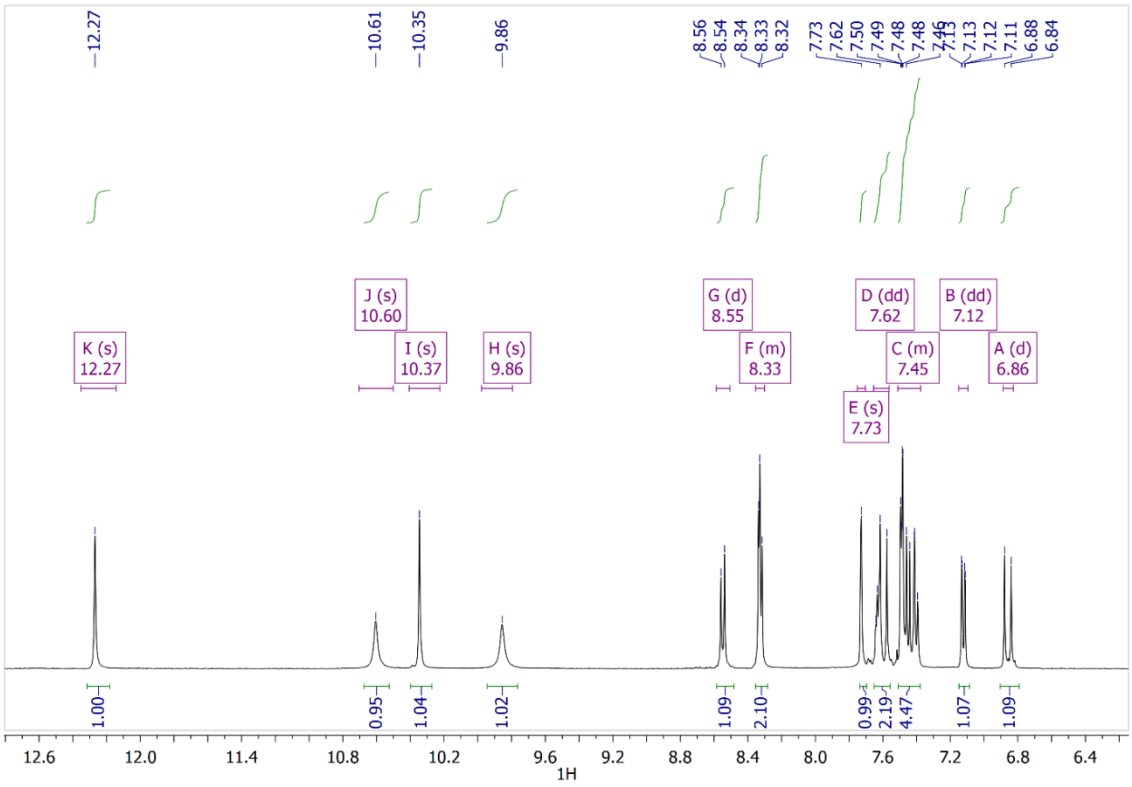


Figure 79. $^{1}$H NMR spectra of **3-ClCimTCH$_{8OH2qu}$**

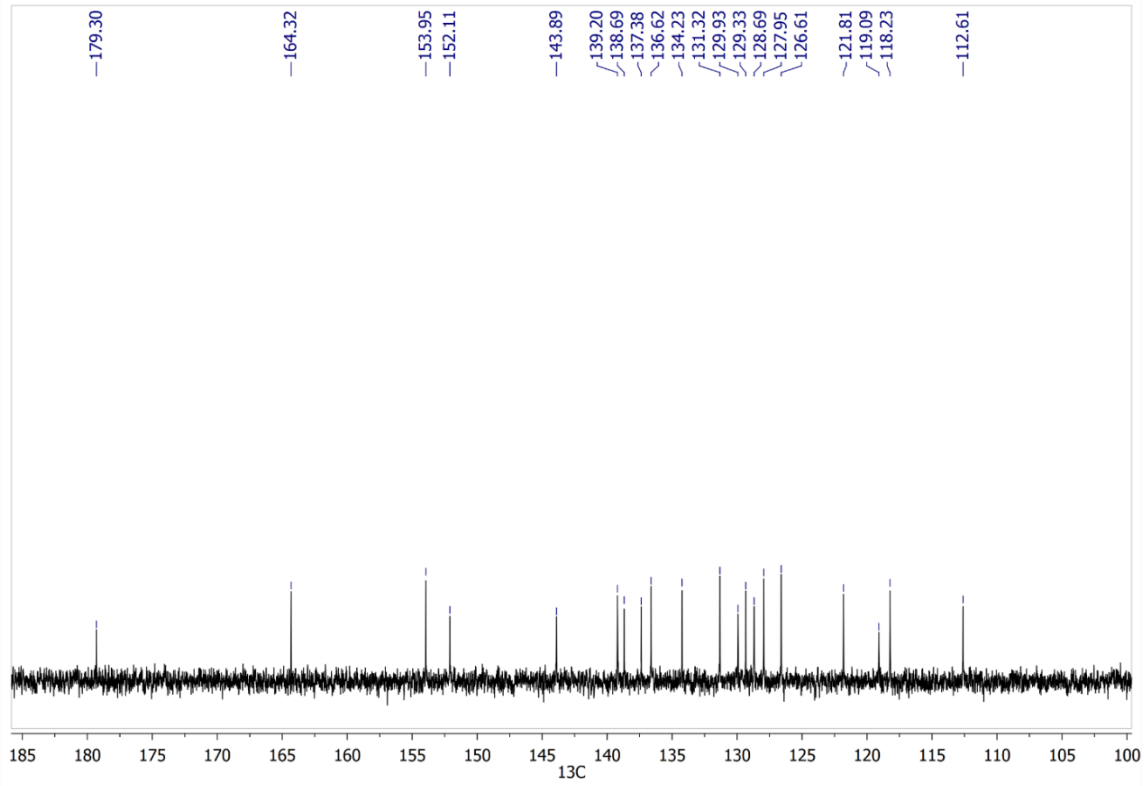


Figure 80. $^{13}$C NMR spectra of **3-ClCimTCH$_{8OH2qu}$**

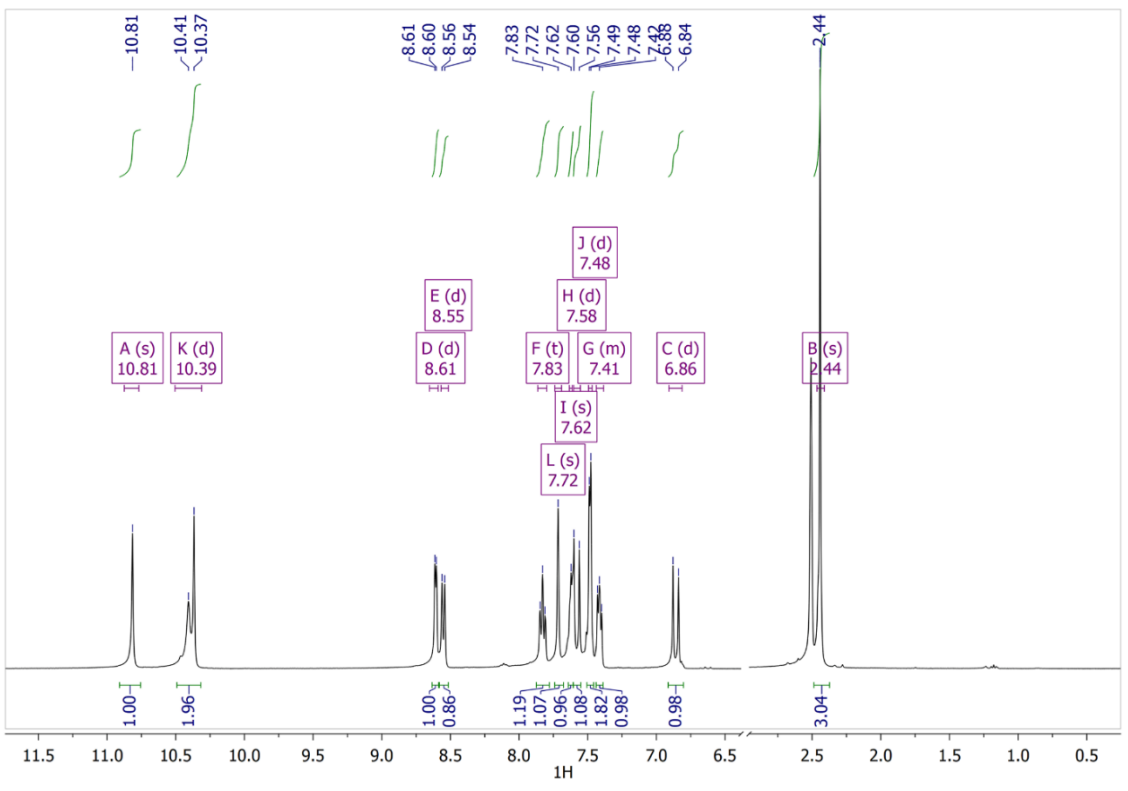


Figure 81. $^{1}$H NMR spectra of **3-ClCimTCH$_{2ap}$**

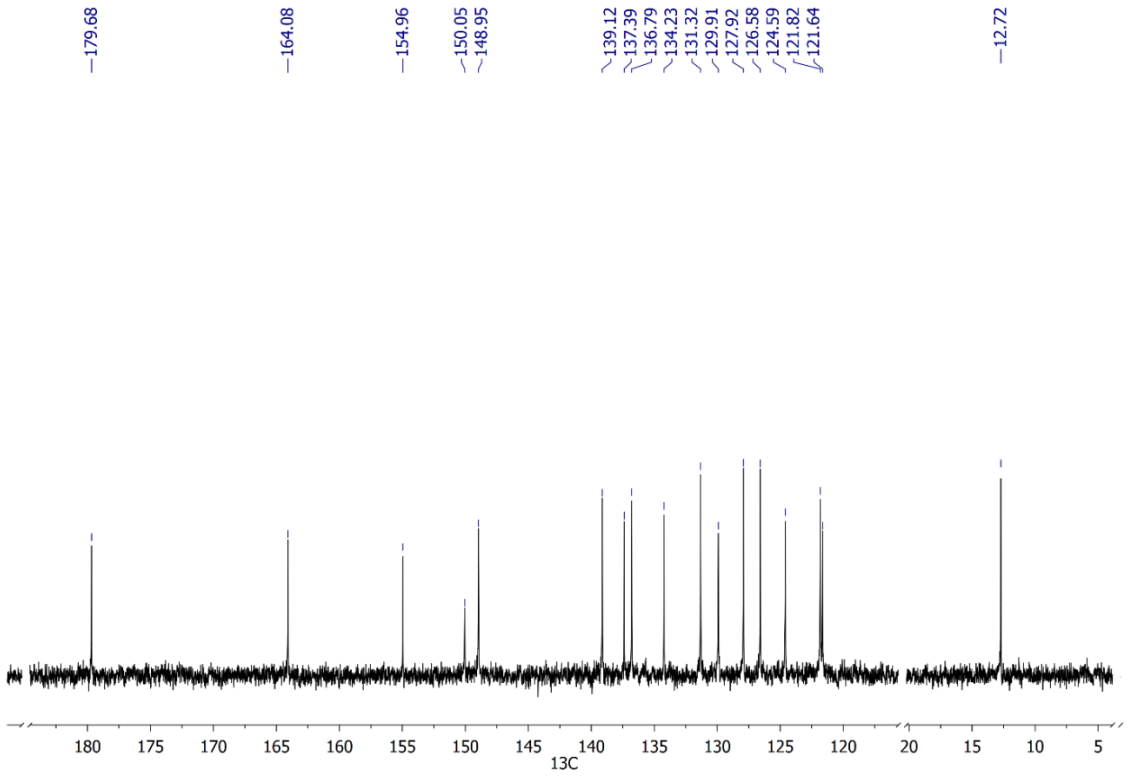


Figure 82. $^{13}$C NMR spectra of **3-ClCimTCH$_{2ap}$**

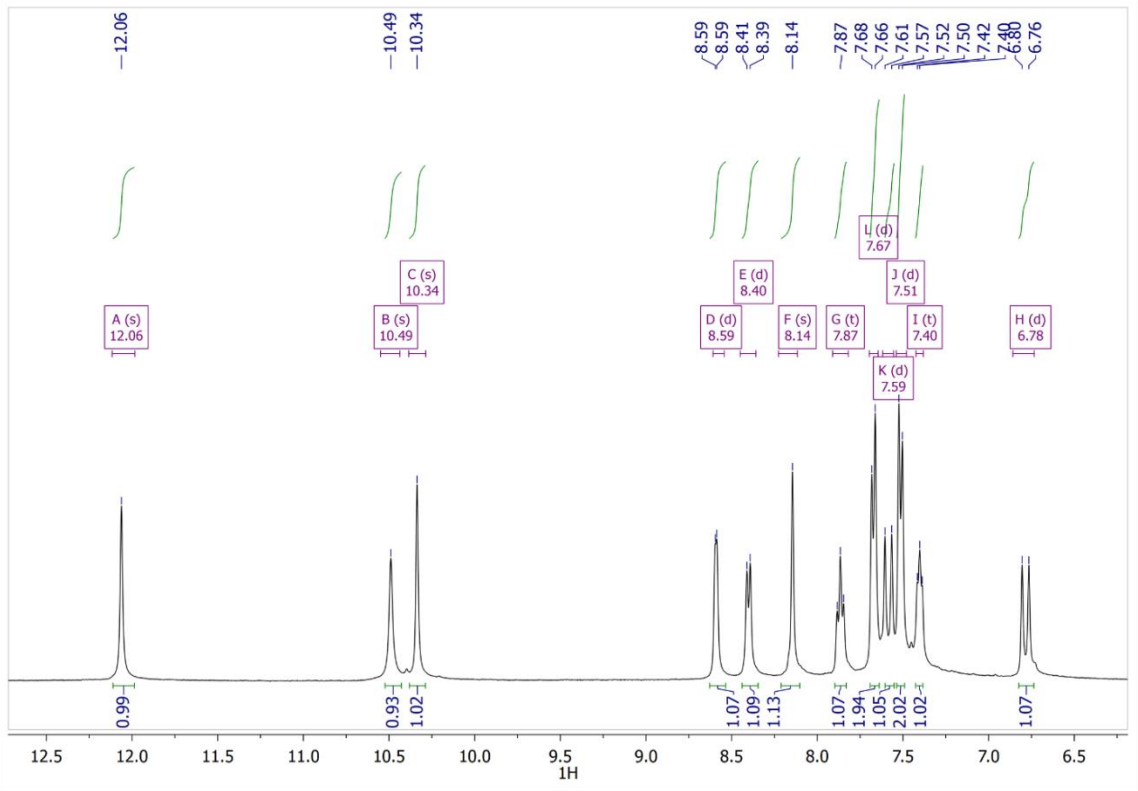


Figure 83. $^{1}$H NMR spectra of **4-ClCimTCH$_{2fp}$**

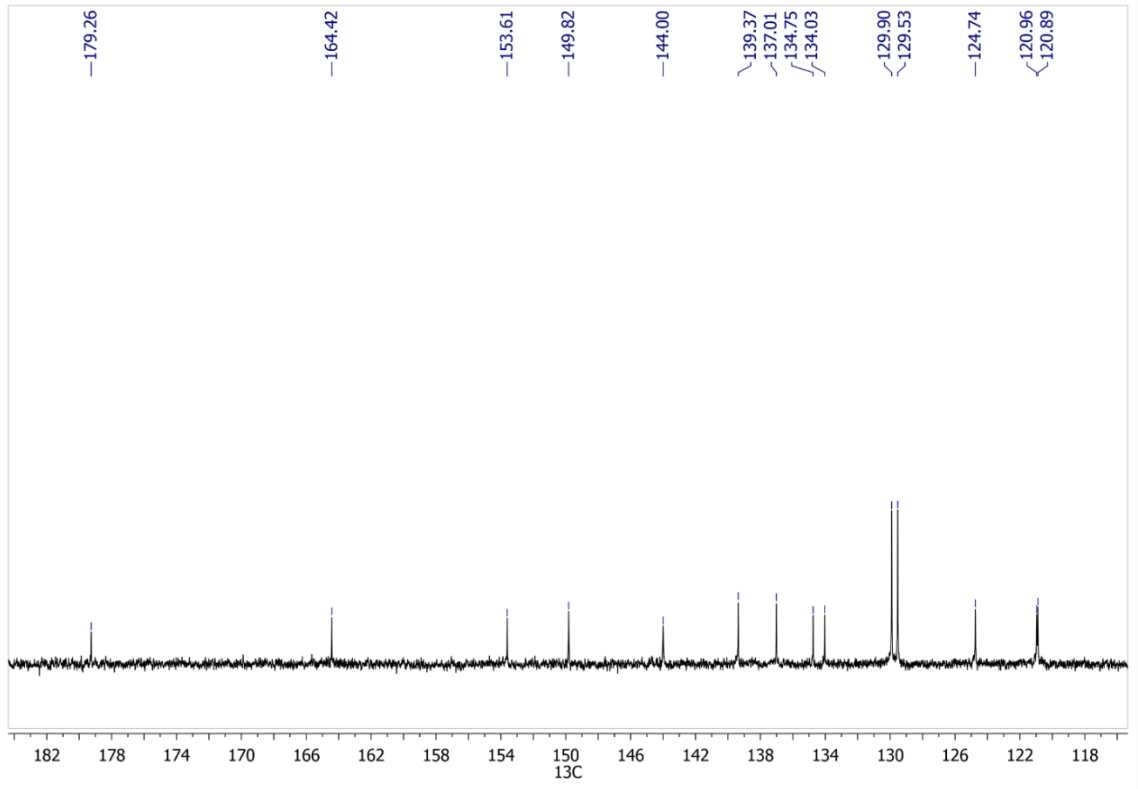


Figure 84. $^{13}$C NMR spectra of **4-ClCimTCH$_{2fp}$**

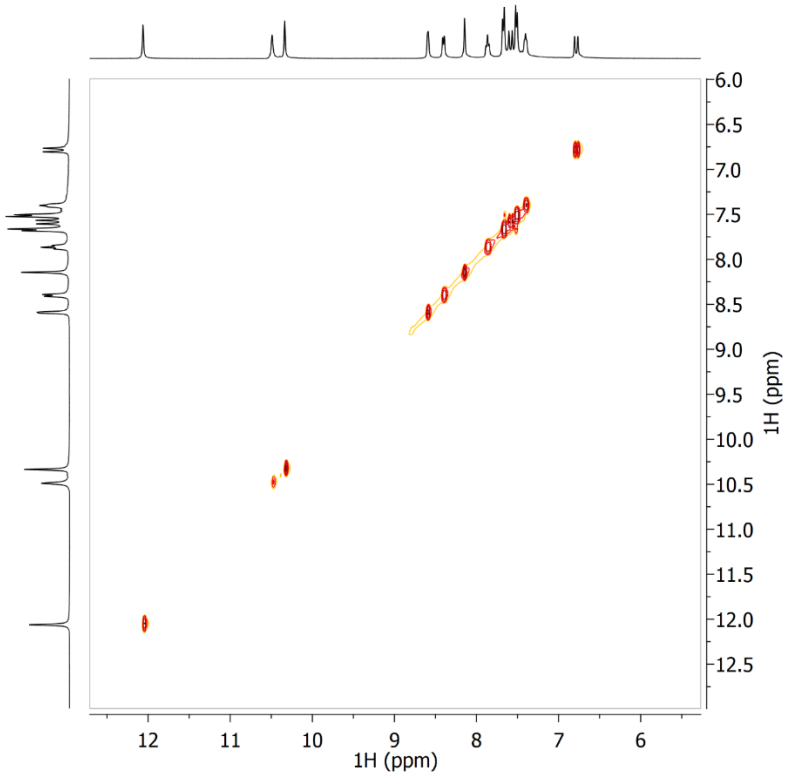


Figure 85. COSY NMR spectra of **4-ClCimTCH$_{2fp}$**

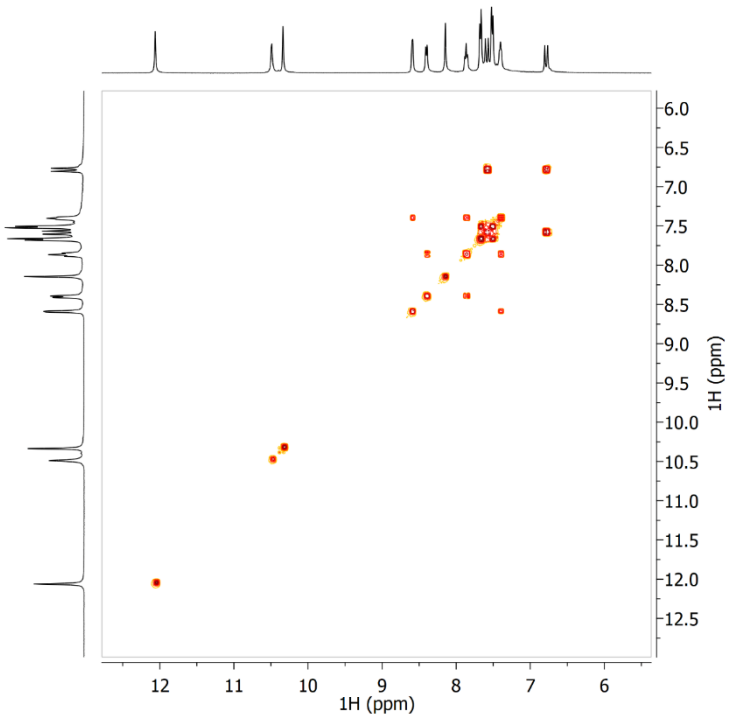


Figure 86. NOESY NMR spectra of **4-ClCimTCH$_{2fp}$**

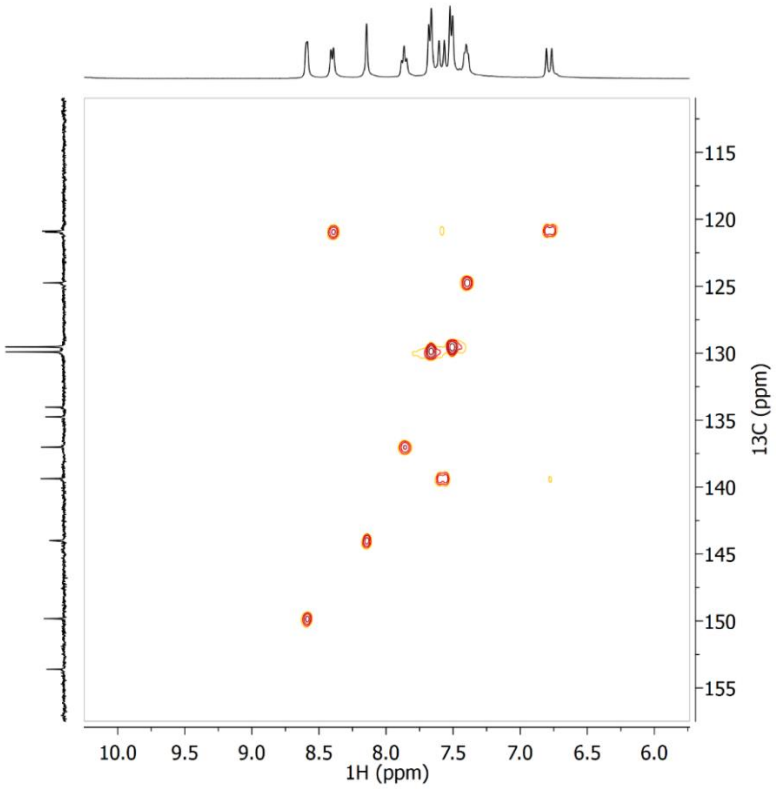


Figure 87. HSQC NMR spectra of **4-ClCimTCH$_{2fp}$**

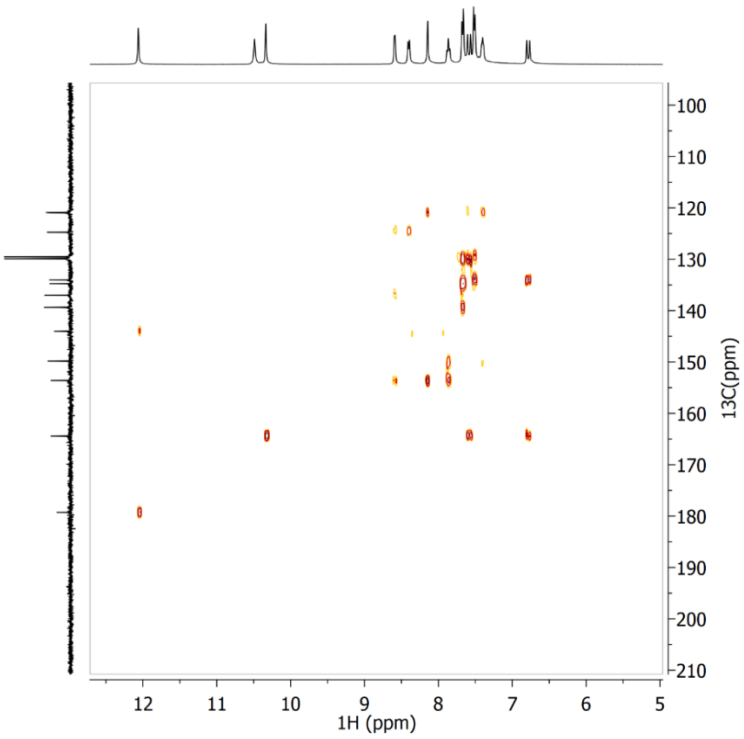


Figure 88. HBMC NMR spectra of **4-ClCimTCH$_{2fp}$**

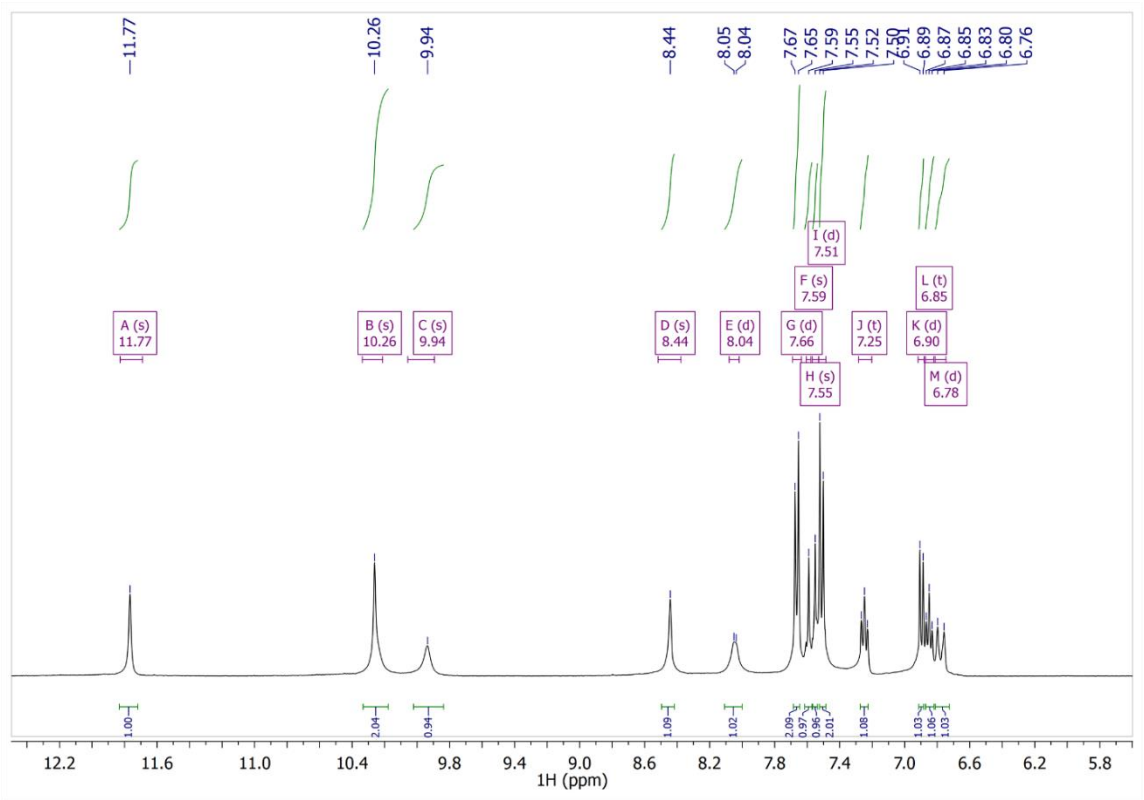


Figure 89. $^{1}$H NMR spectra of **4-ClCimTCH$_{sal}$**

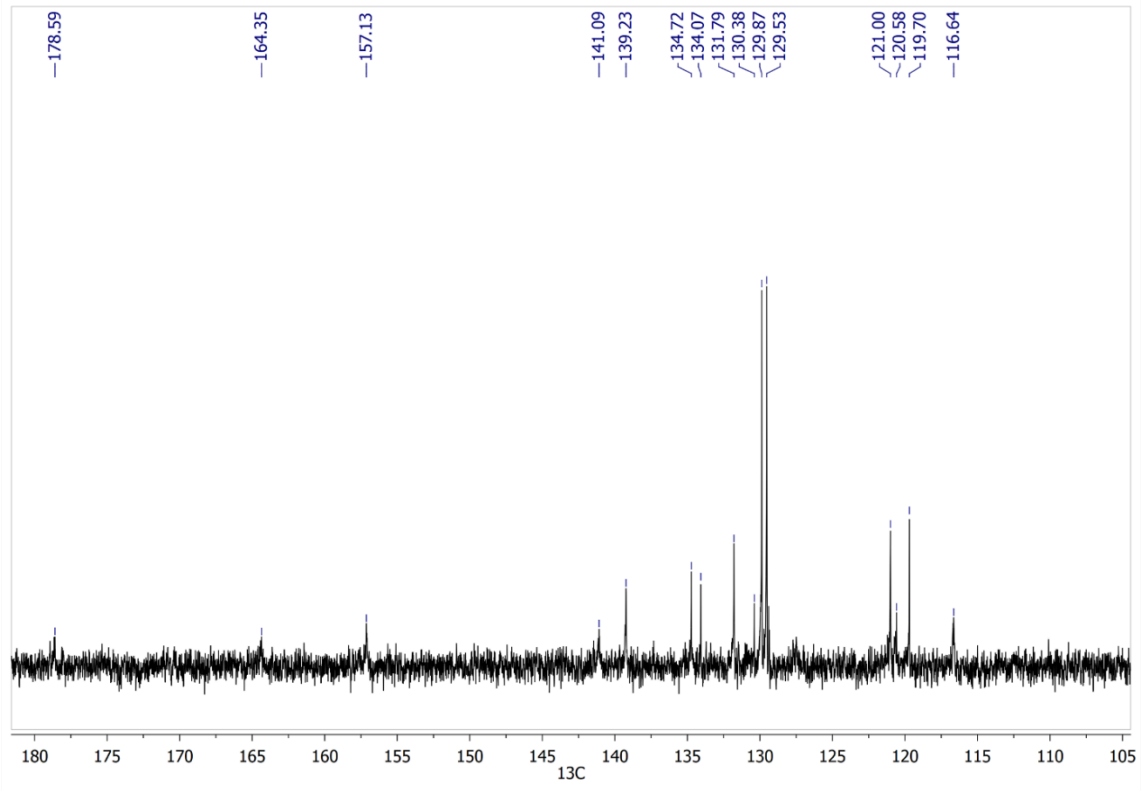


Figure 90. $^{13}$C NMR spectra of **4-ClCimTCH$_{sal}$**

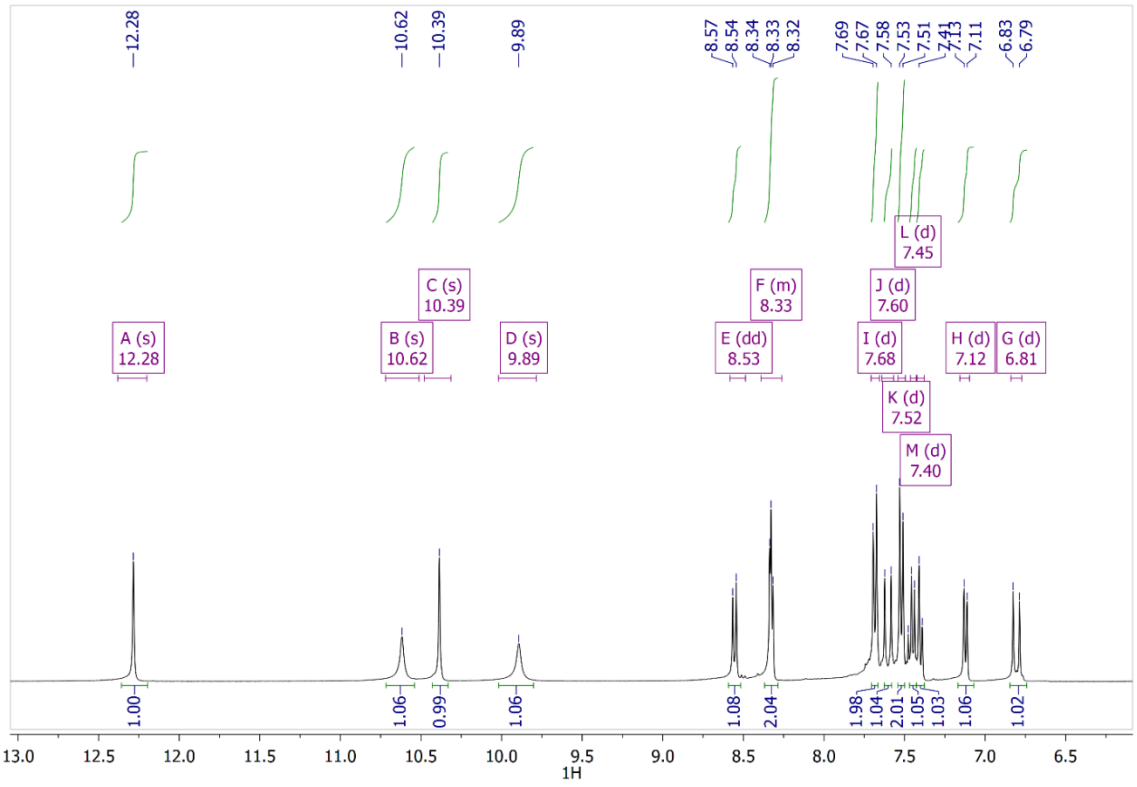


Figure 91. $^{1}$H NMR spectra of **4-ClCimTCH$_{8OH2qu}$**

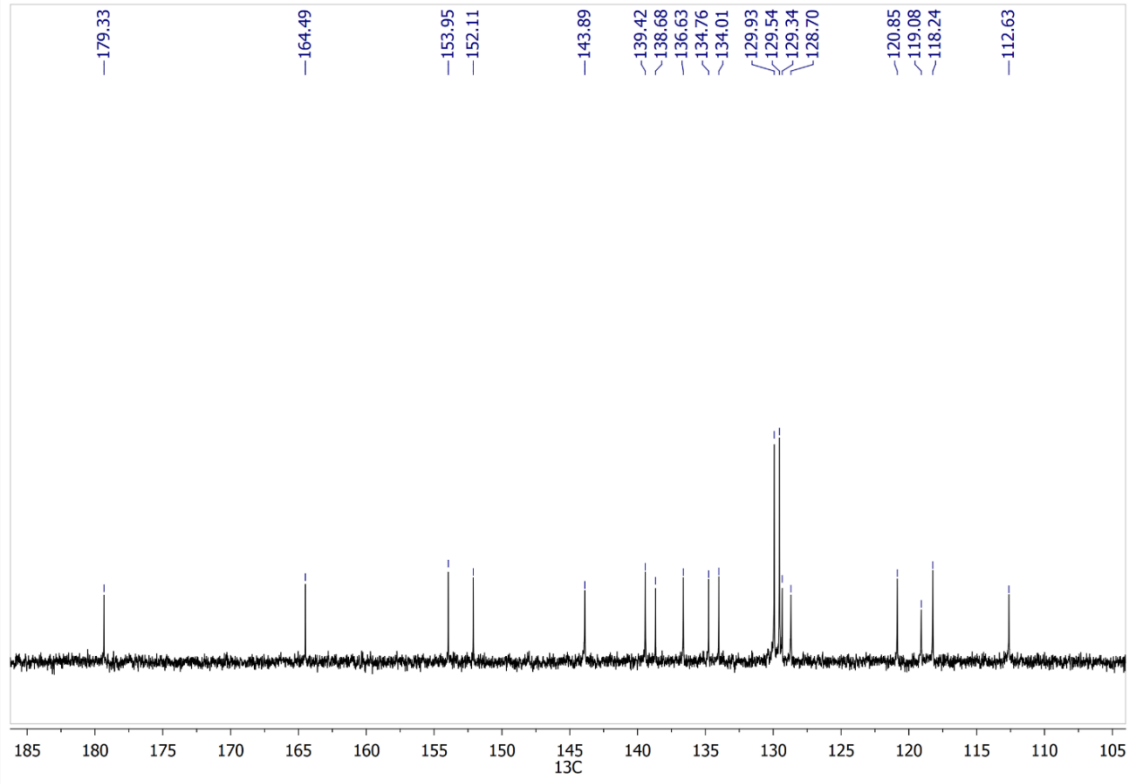


Figure 92. $^{13}$C NMR spectra of **4-ClCimTCH$_{8OH2qu}$**

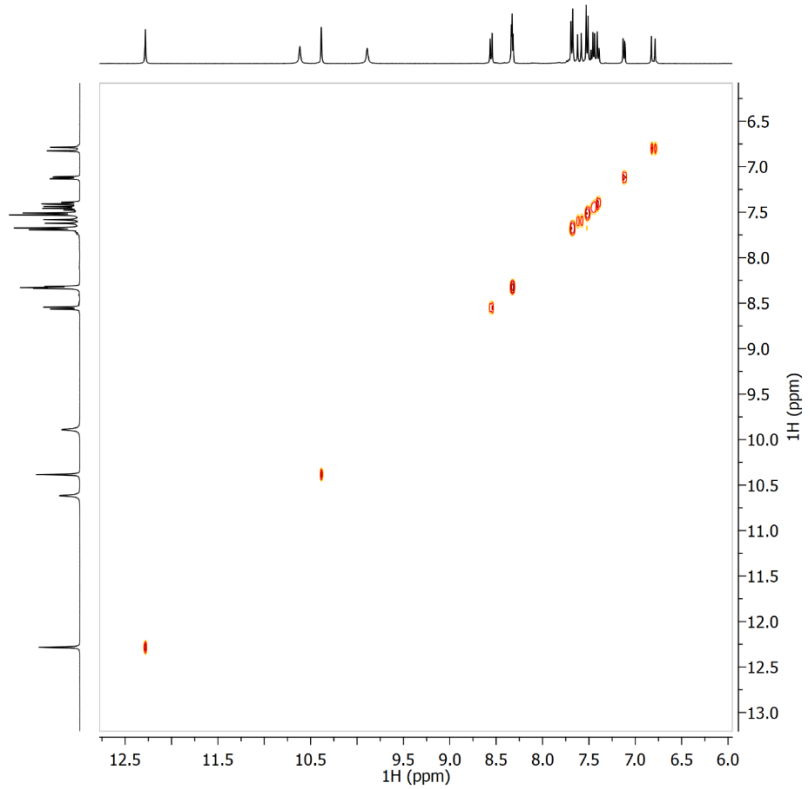


Figure 93. COSY NMR spectra of 4-ClCimTCH$_{8OH2qu}$

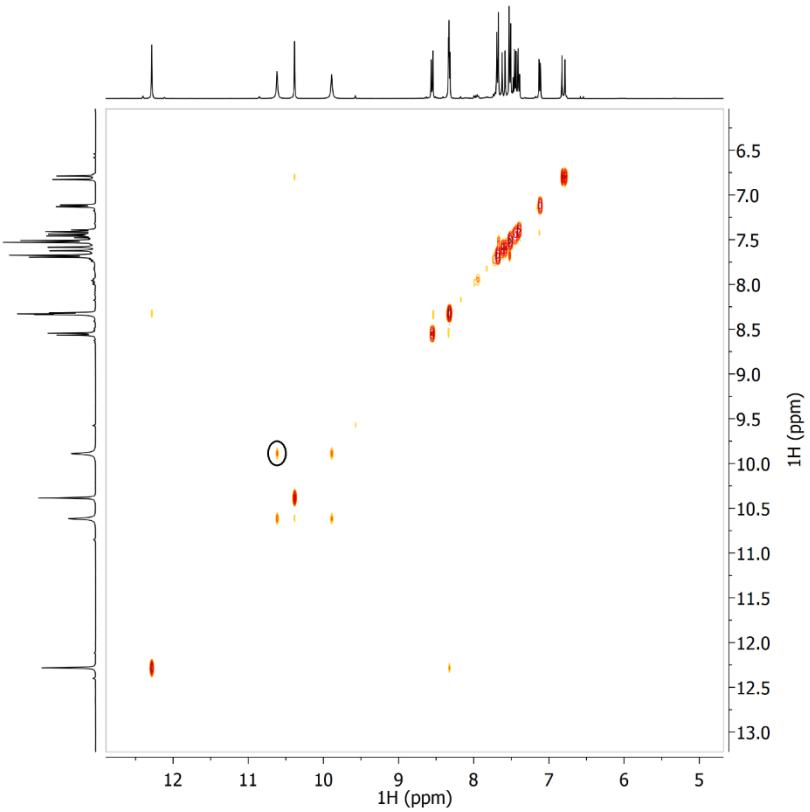


Figure 94. NOESY NMR spectra of **4-ClCimTCH$_{8OH2qu}$**

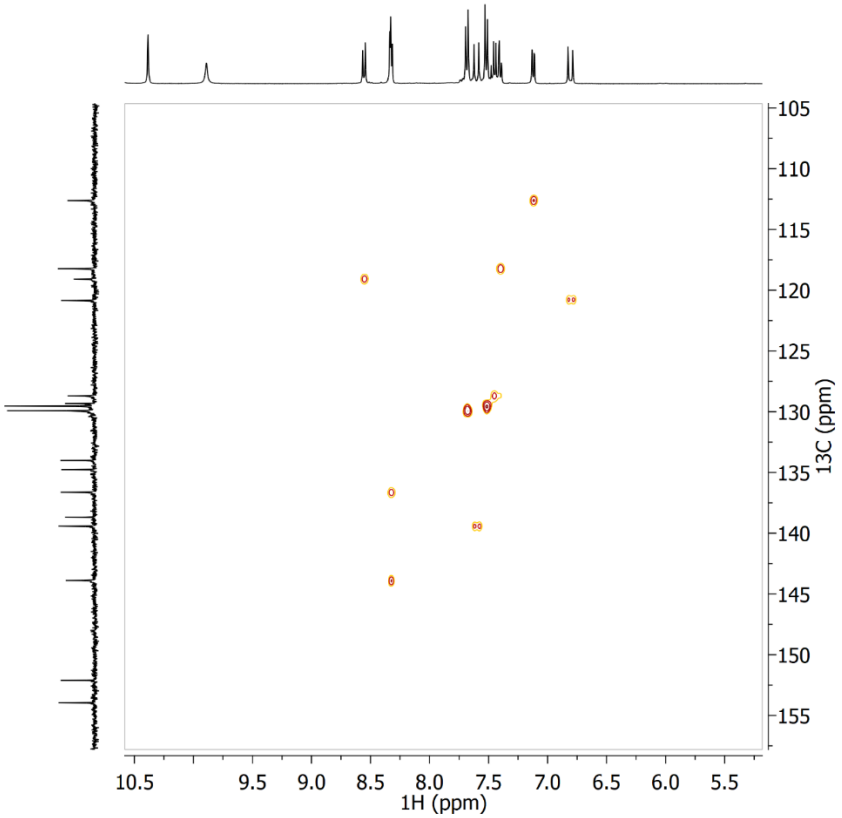


Figure 95. HSQC NMR spectra of **4-ClCimTCH$_{8OH2qu}$**

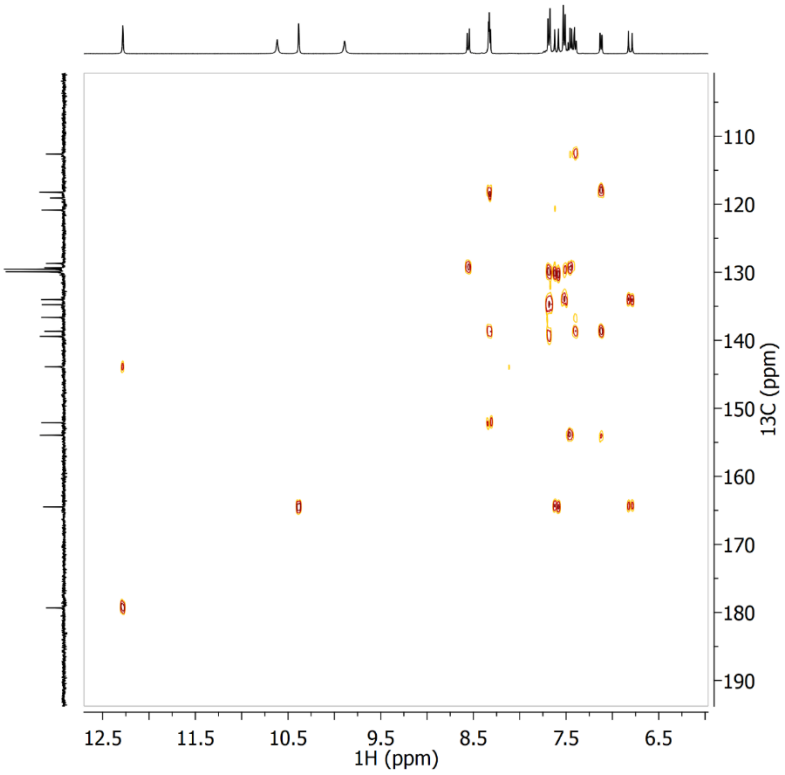


Figure 96. HMBC NMR spectra of **4-ClCimTCH$_{8OH2qu}$**

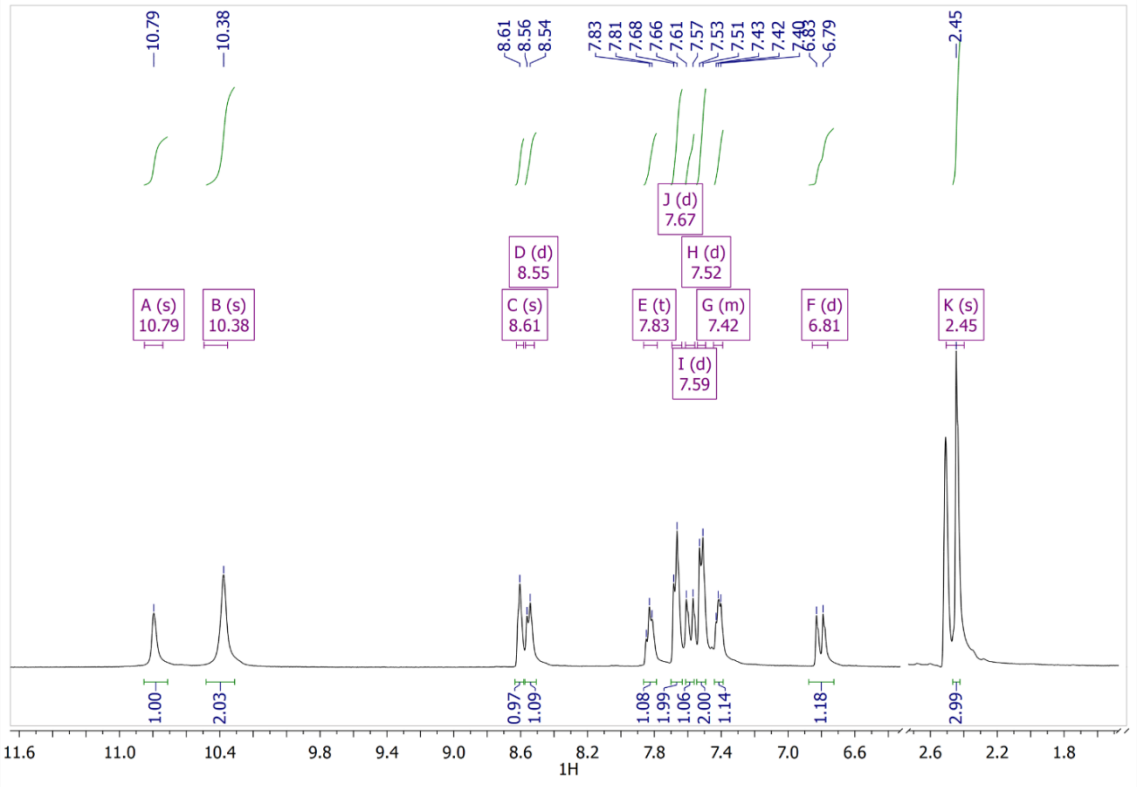


Figure 97. $^{1}$H NMR spectra of **4-ClCimTCH$_{2ap}$**

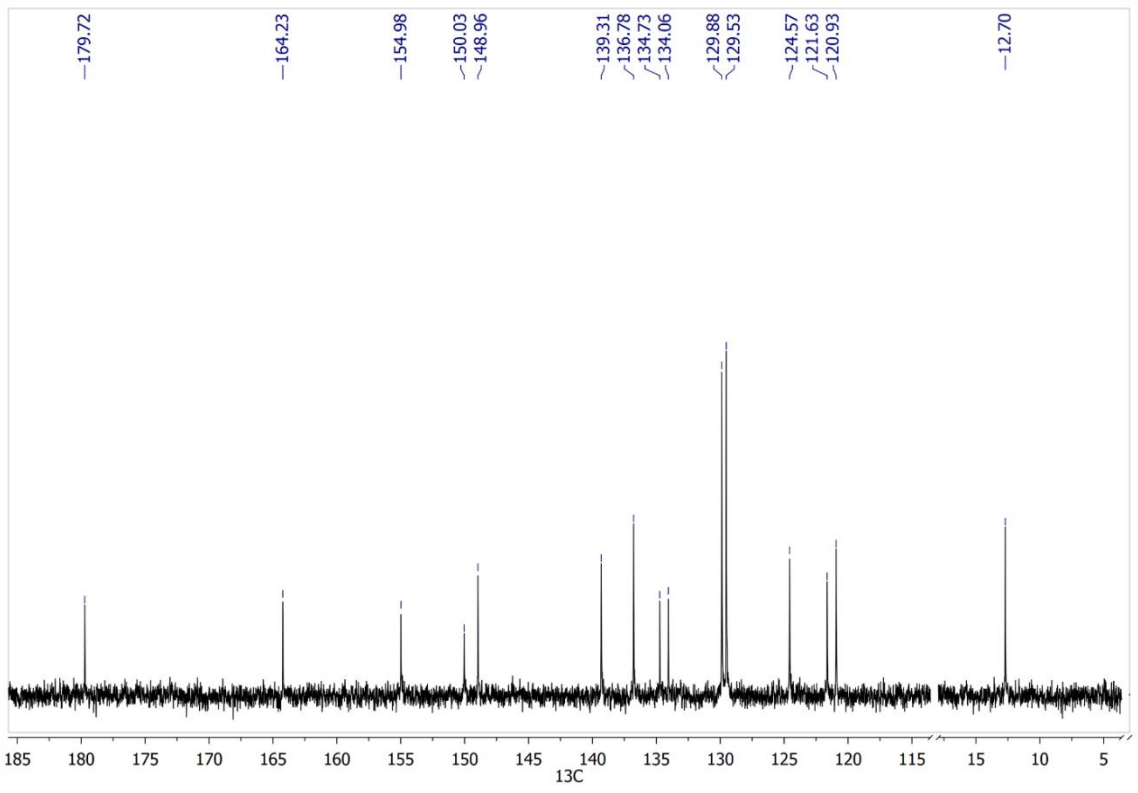


Figure 98. $^{13}$C NMR spectra of **4-ClCimTCH$_{2ap}$**

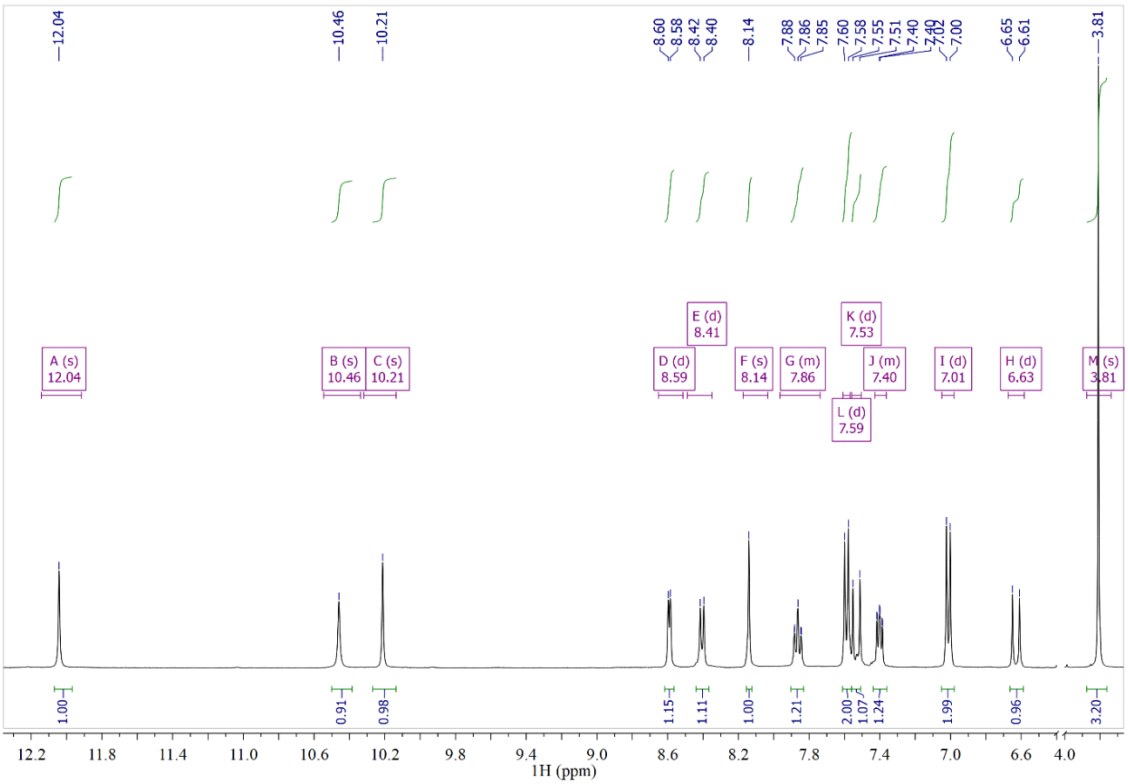


Figure 99. $^{1}$H NMR spectra of **4-MeOCimTCH$_{2fp}$**

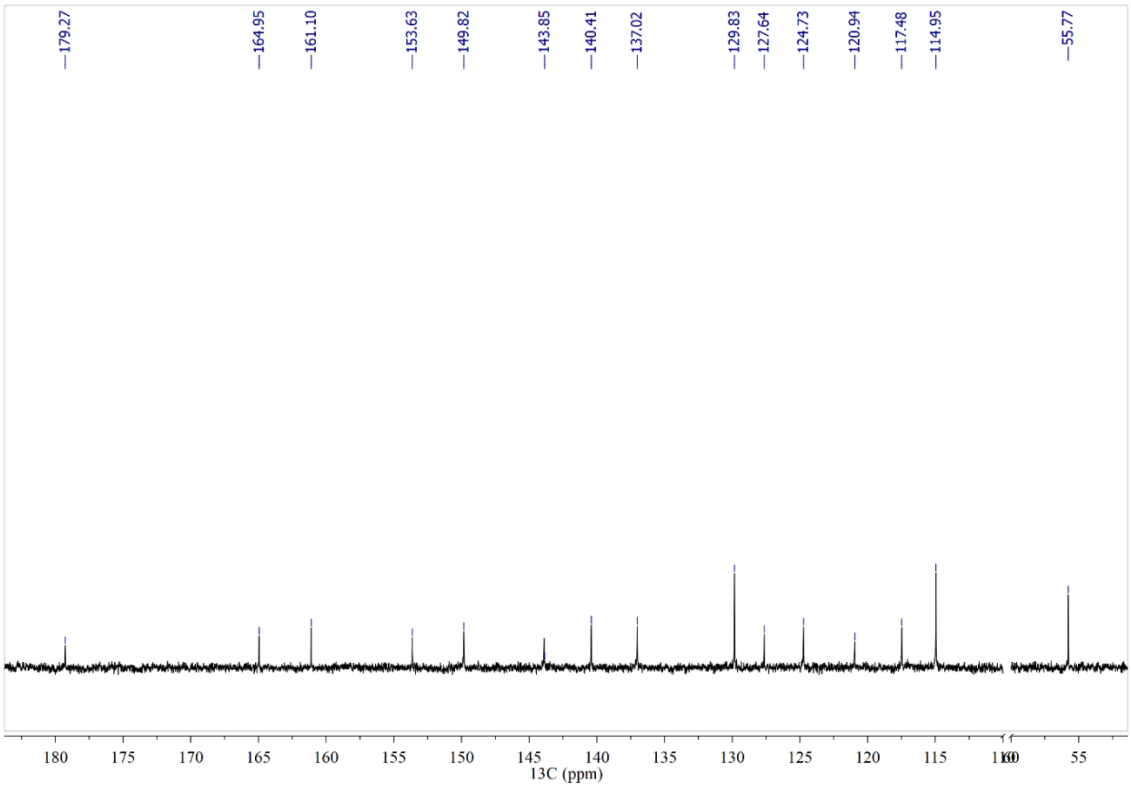


Figure 100. $^{13}$C NMR spectra of **4-MeOCimTCH$_{2fp}$**

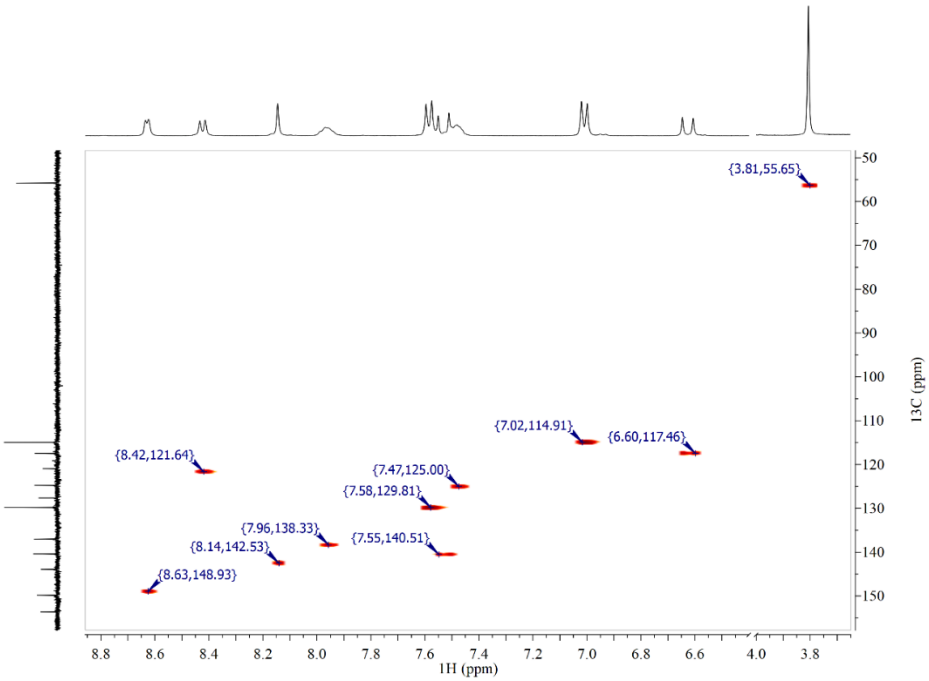


Figure 101. HSQC NMR spectra of **4-MeOCimTCH$_{2fp}$**

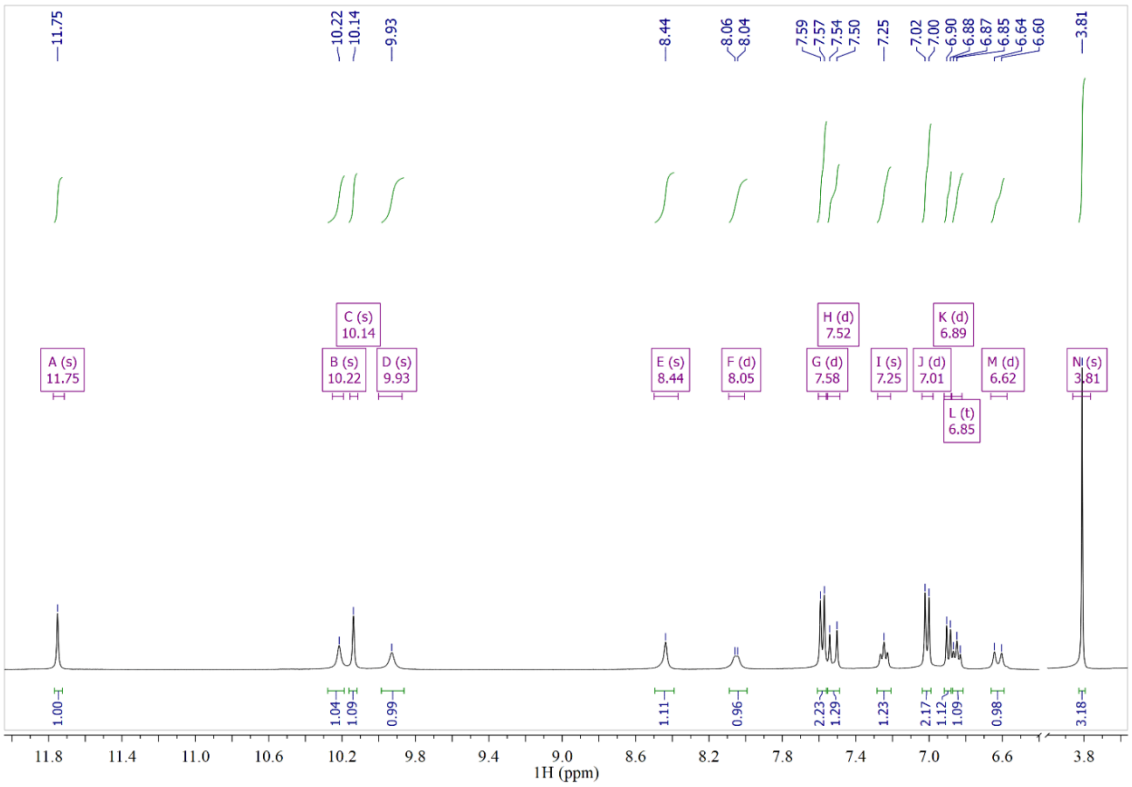


Figure 102. $^{1}$H NMR spectra of **4-MeOCimTCH$_{sal}$**

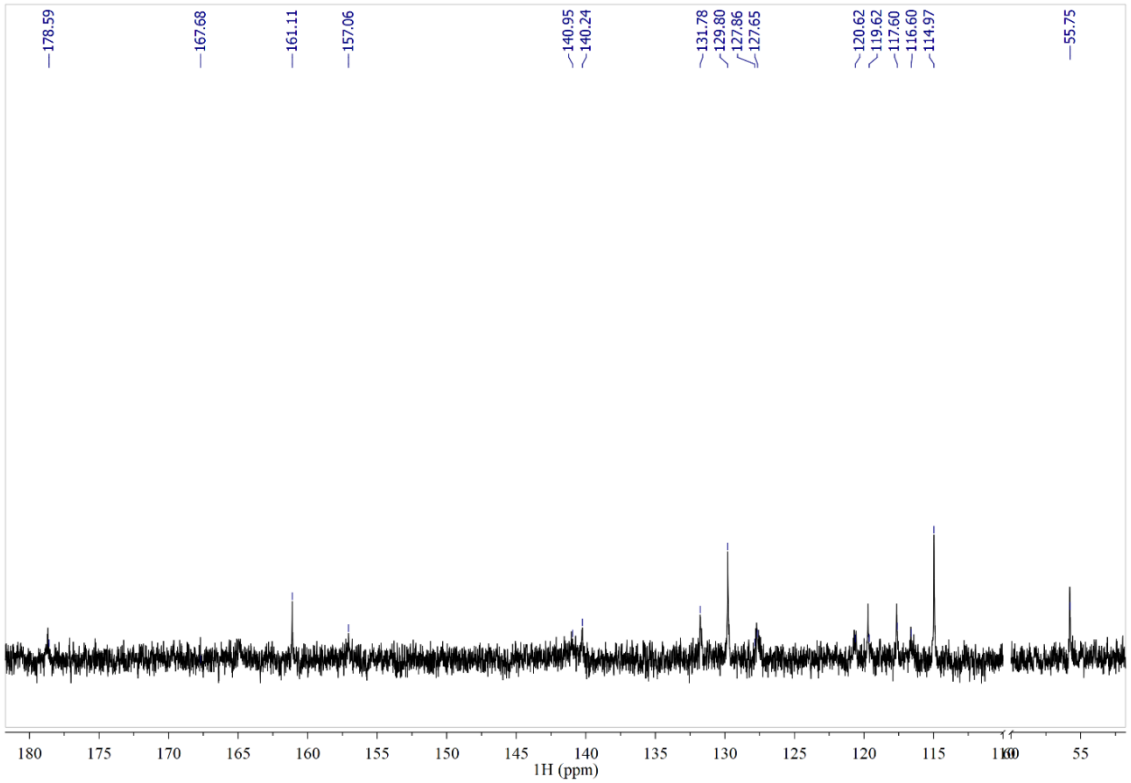


Figure 103. $^{13}$C NMR spectra of **4-MeOCimTCH$_{sal}$**

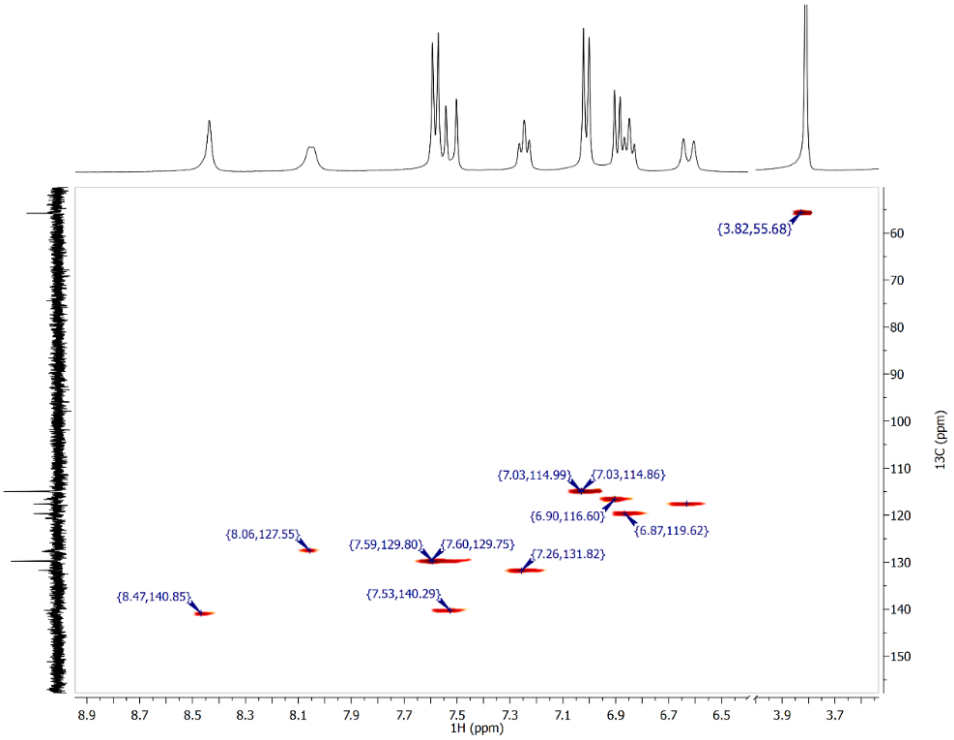


Figure 104. HSQC NMR spectra of **4-MeOCimTCH$_{sal}$**

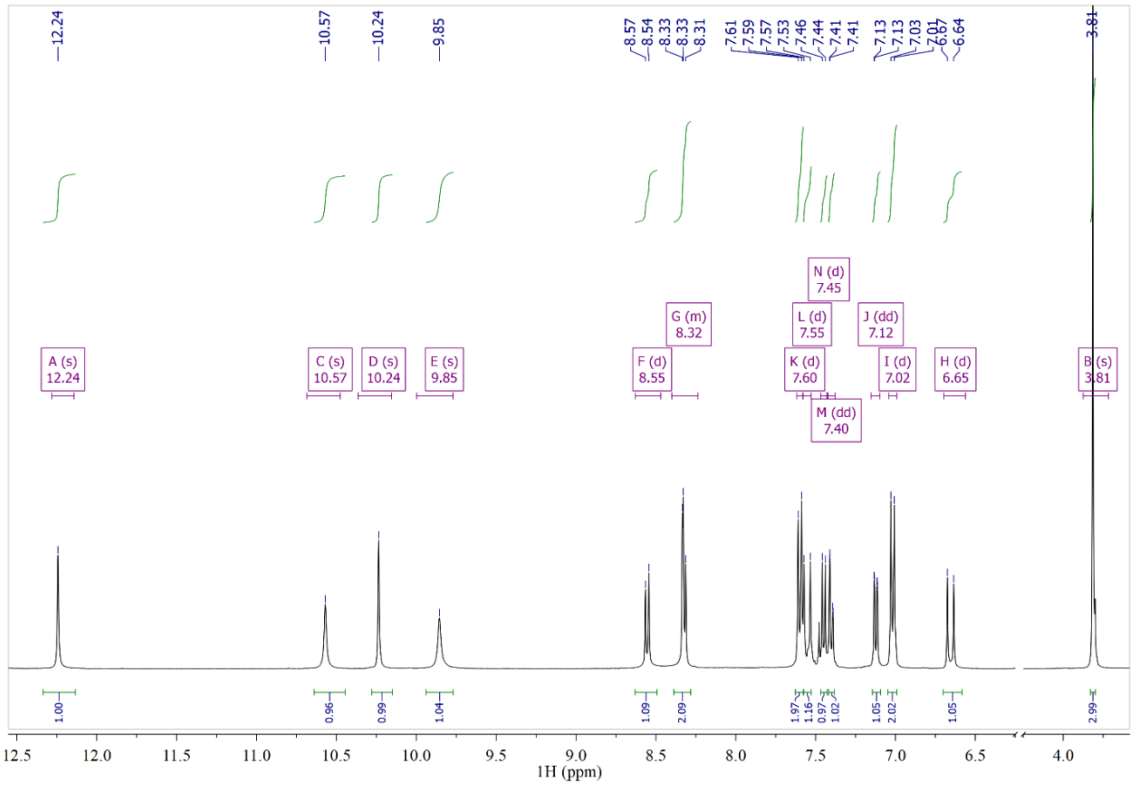


Figure 105. $^{1}$H NMR spectra of **4-MeOCimTCH$_{8OH2qu}$**

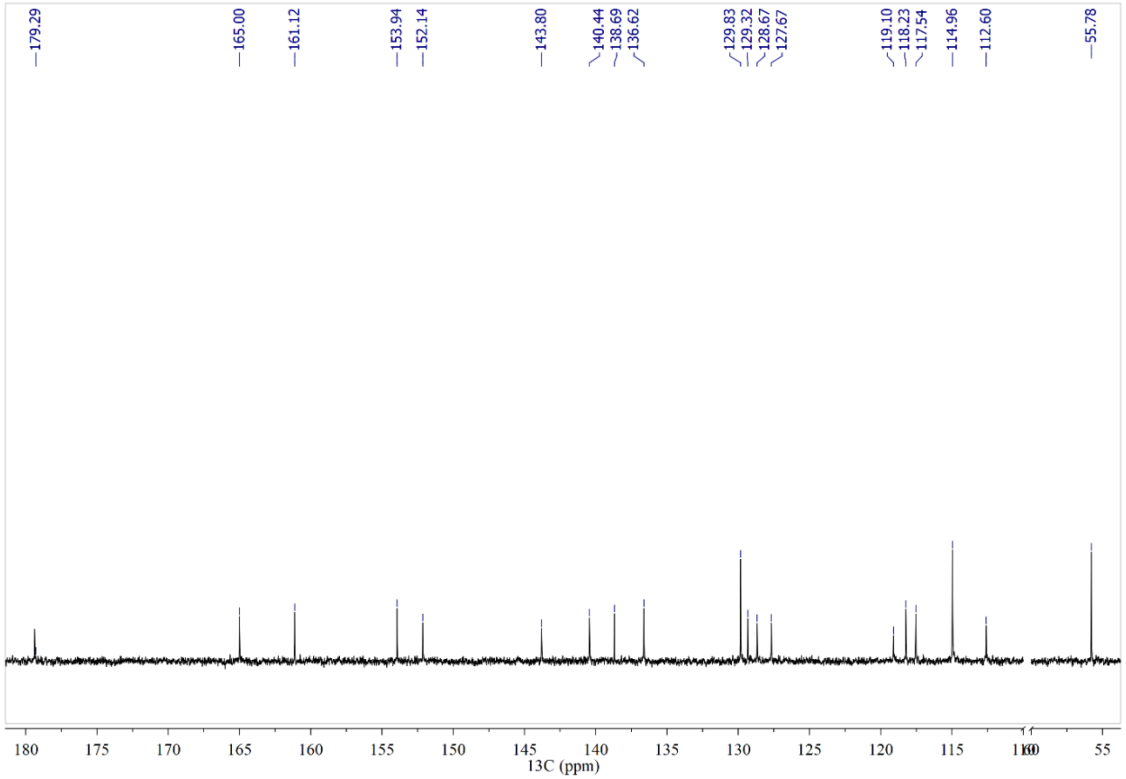


Figure 106. $^{13}$C NMR spectra of **4-MeOCimTCH$_{8OH2qu}$**

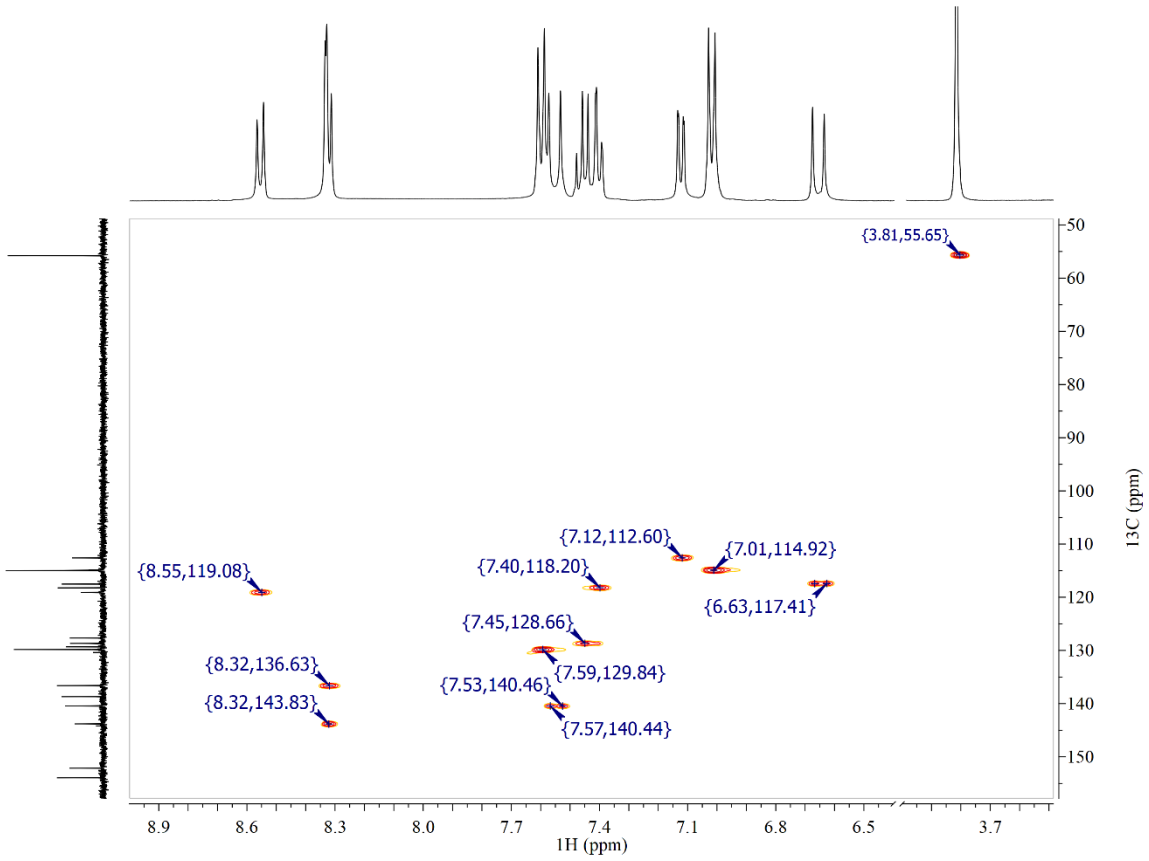


Figure 107. HSQC NMR spectra of **4-MeOCimTCH$_{8OH2qu}$**

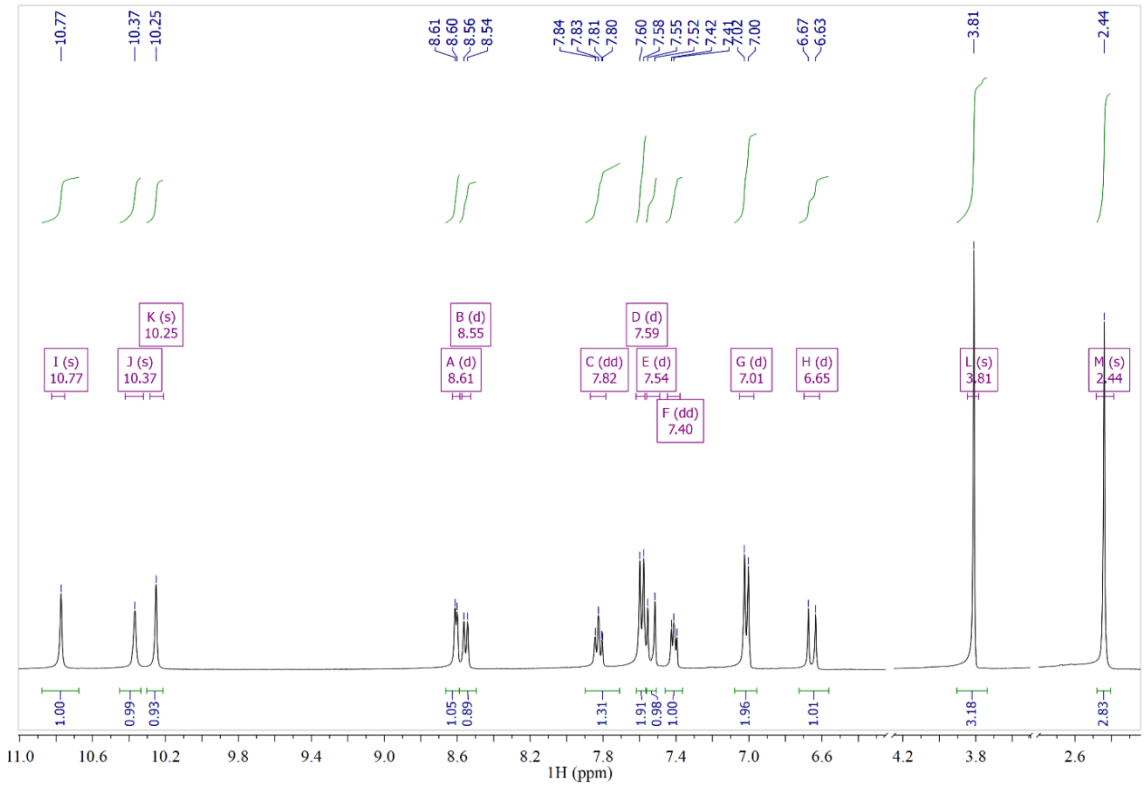


Figure 108. $^{1}$H NMR spectra of **4-MeOCimTCH$_{2ap}$**

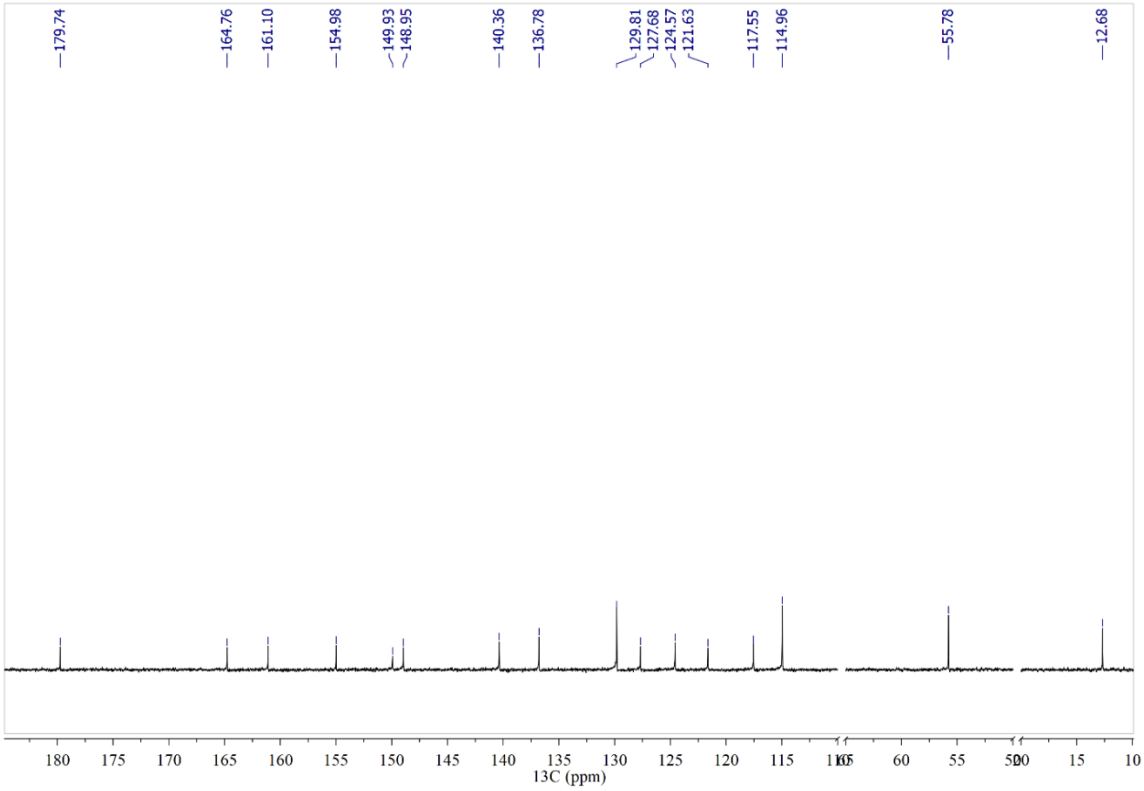


Figure 109. $^{13}$C NMR spectra of **4-MeOCimTCH$_{2ap}$**

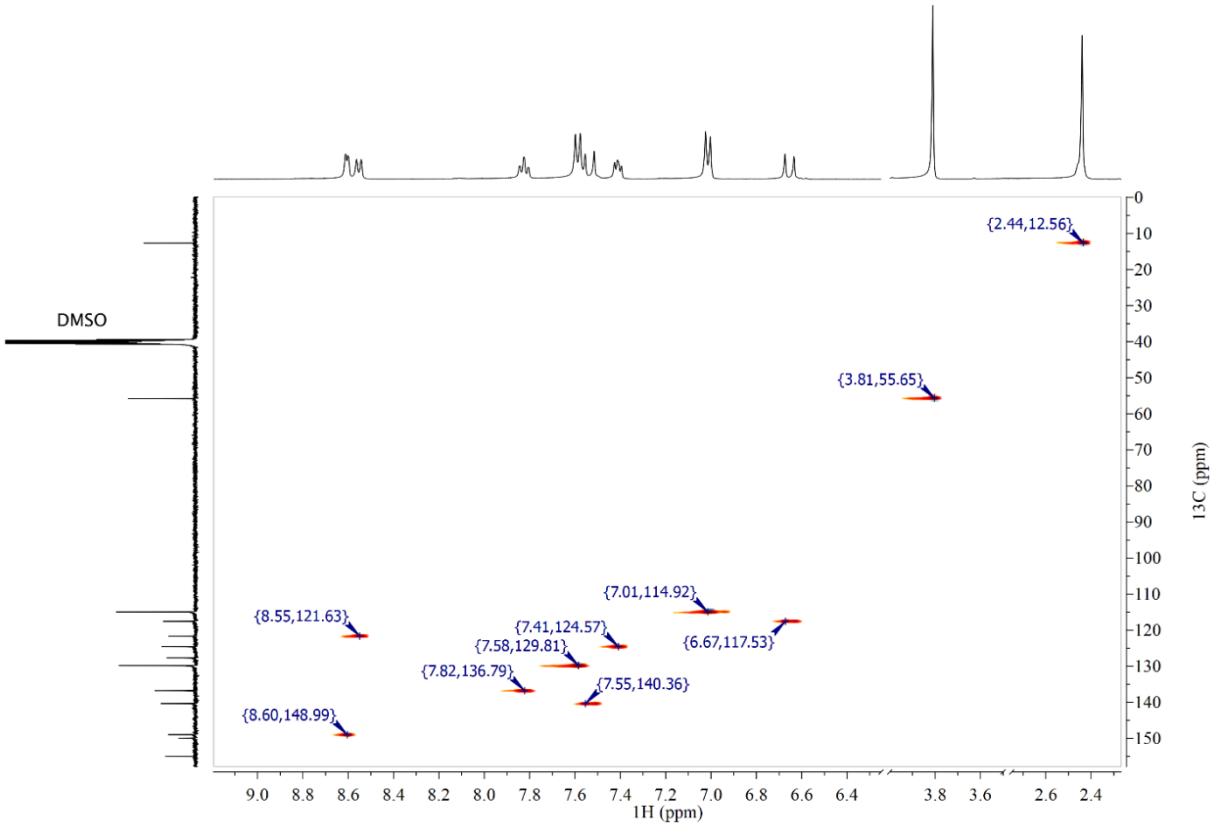


Figure 110. HSQC NMR spectra of **4-MeOCimTCH$_{2ap}$**

## 7. Биографија

Мохамед Х. Асалех (Mohamed H. Assaleh) је рођен 1982. године у Алзавији (Alzawiyah), Либија (Libya). Школске 2003/2004. завршио је основне студије и дипломирао на одсеку за Хемију Универзитета Алгабал Алгарби (Algabal Algarbi), Факултет за науку, Алзавија, Либија са просечном оценом 57,33%. Кандидат је 2009. године похађао курс за међународну дозволу за коришћење рачунара International Computer Driving License (Excel, Word, PowerPoint, Access, and Internet) и курс за обуку у Лабораторији за хемијске анализе Универзитета Триполи, Либија. Мохамед Х. Асалех је 2012. године завршио курс за обуку о Примени токсикологије, Laboratory of the Government (LGC) Forensics, Oxford (Оксфорд), Велика Британија и курс за Менаџмент квалитетом (примењени курс) Универзитета у Хадерсфилду (Huddersfield), Велика Британија. Кандидат је истовремено 2012. године завршио мастер студије на смеру форензичка токсикологија под насловом: Испитивање уличних дрога (Roadside drug testing) на Универзитету у Хадерсфилду, Велика Британија . Програм је похађао на Енглеском језику уз просечну оцену од 72%. Након тога, 2015. године Мохамед Х. Асалех је уписао докторске студије на Технолошко-металуршком факултету Универзитета у Београду, студијски програм Хемија, и положио све испите, а школске 2016/2017 положио завршни испит.

Од 2016. до 2019. године, у оквиру истраживачке групе на катедри за Органску хемију , као сарадник је учествовао на међународној сарадњи истраживача COST Action CM1407 „*Challenging organic synthesis inspired by nature: from natural product chemistry to drug discovery*“.

Научно-истраживачки рад Мохамеда Х. Асалеха обухвата синтезу, физичко-хемијску карактеризацију, теоријска проучавања и испитивање биолошке активности имино деривата дихидразида тиоугљене и амида циметних киселина уз успостављање повезаности између структуре и биолошке активности ових класа једињења.

Мохамед Х. Асалех је објавио три рада у часописима међународног значаја (М22), једно саопштење са међународног скупа штампаног у целини (М33)) и два саопштења са међународних скупова штампаних у изводу (М34).

## 8. List of publications

Радови објављени у часописима међународног значаја – М20

Рад у истакнутом међународном часопису (М22)

1. **Assaleh M. H**., Jeremić S., Cvijetić I., Marinković A., Prlainović N., *In vitro* activity of novel cinnamic acids hydrazides against clinically important pathogens – *Journal of Molecular Structure, In Press*, vol. 1262, pp. 133016 (1-11), 2022 (IF(2020)=3,196) (ISSN: 0022-2860), https://doi.org/10.1016/j.molstruc.2022.133016

2. **Assaleh M. H**., Bjelogrlic S. K., Prlainovic N., Cvijetic I., Bozic A., Arandjelovic I., Vukovic D., Marinkovic A.: Antimycobacterial and anticancer activity of newly designed cinnamic acid hydrazides with favorable toxicity profile: Antimycobacterial and anticancer activity of newly designed cinnamic acid - *Arabian Journal of Chemistry*, vol. 15, no. 1, pp. 103532 (1-18), 2021 (IF(2020)=5,165) (ISSN: 1878-5352) https://doi.org/10.1016/j.arabjc.2021.103532.

3. **Assaleh M. H**., Božić A.R., Bjelogrlić S., Milošević M., Simić M., Marinković A. D., Cvijetić I. N.: Water-induced isomerism of salicylaldehyde and 2-acetylpyridine mono- and bis-(thiocarbohydrazones) improves the antioxidant activity: spectroscopic and DFT study - *Structural Chemistry*, vol. 30, no. 6, pp. 2447–2457, 2019 (IF(2019)=2,081) (ISSN: 1040-0400), https://doi.org/10.1007/s11224-019-01371-4.

Саопштење са међународног скупа штампан у целини (М33)

1. **Assaleh M. H**., Božić A., Prlainović N., Milošević M., Stojiljković I., Cvijetić I., Marinković A.: *Synthesis, characterization, and antioxidant activity of novel 4-chlorocinnamamide monothiocarbohydrazones*, - 13th International Symposium Novel Technologies and Economic Development, Leskovac, Republic of Serbia, 2019, pp. 41-50, ISBN: 978-86-89429-36-7.

## 9. ИЗЈАВА О АУТОРСТВУ

Име и презиме аутора Mohamed Assaleh
Број индекса 4036/2015

**Изјављујем**

да је докторска дисертација под насловом
**Имино деривати дихидразида тиоугљене и амида циметних киселина: корелације структуре и активности**

**Imino derivatives of carbonothioic dihydrazides and cinnamic acids amides: structure-activity relationship studies**

- резултат сопственог истраживачког рада;
- да дисертација у целини ни у деловима није била предложена за стицање друге дипломе према студијским програмима других високошколских установа;
- да су резултати коректно наведени и
- да нисам кршио/ла ауторска права и користио/ла интелектуалну својину других лица.

**Потпис аутора**

У Београду, 02.03..2022

_____

## 10. ИЗЈАВА О ИСТОВЕТНОСТИ ШТАМПАНЕ И ЕЛЕКТРОНСКЕ ВЕРЗИЈЕ ДОКТОРСКОГ РАДА

Име и презиме аутора Mohamed Assaleh
Број индекса 4036/2015
Студијски програм Хемија
Наслов рада
**Имино деривати дихидразида тиоугљене и амида циметних киселина: корелације структуре и активности**

**Imino derivatives of carbonothioic dihydrazides and cinnamic acids amides: structure-activity relationship studies**

Ментори: Александар Маринковић и Снежана Бјелогрлић

Изјављујем да је штампана верзија мог докторског рада истоветна електронској верзији коју сам предао/ла ради похрањена у **Дигиталном репозиторијуму Универзитета у Београду.**
Дозвољавам да се објаве моји лични подаци везани за добијање академског назива доктора наука, као што су име и презиме, година и место рођења и датум одбране рада. Ови лични подаци могу се објавити на мрежним страницама дигиталне библиотеке, у електронском каталогу и у публикацијама Универзитета у Београду.

**Потпис аутора**

У Београду, 02.03.2022

_____

## 11. ИЗЈАВА О КОРИШЋЕЊУ

Овлашћујем Универзитетску библиотеку „Светозар Марковић“ да у Дигитални репозиторијум Универзитета у Београду унесе моју докторску дисертацију под насловом:

**Имино деривати дихидразида тиоугљене и амида циметних киселина: корелације структуре и активности**

**Imino derivatives of carbonothioic dihydrazides and cinnamic acids amides: structure-activity relationship studies**

која је моје ауторско дело.
Дисертацију са свим прилозима предао/ла сам у електронском формату погодном за трајно архивирање.
Моју докторску дисертацију похрањену у Дигиталном репозиторијуму Универзитета у Београду и доступну у отвореном приступу могу да користе сви који поштују одредбе садржане у одабраном типу лиценце Креативне заједнице (Creative Commons) за коју сам се одлучио/ла.

1. Ауторство (CC BY)
2. Ауторство – некомерцијално (CC BY-NC)
3. Ауторство – некомерцијално – без прерада (CC BY-NC-ND)
4. Ауторство – некомерцијално – делити под истим условима (CC BY-NC-SA)
5. Ауторство – без прерада (CC BY-ND)
6. Ауторство – делити под истим условима (CC BY-SA)

(Молимо да заокружите само једну од шест понуђених лиценци.
Кратак опис лиценци је саставни део ове изјаве).

**Потпис аутора**

У Београду, 02.03.2022

_____

**ПРОВЕРА ОРИГИНАЛНОСТИ ДОКТОРСКЕ ДИСЕРТАЦИЈЕ**

На основу Правилника о поступку провере оригиналности докторских дисертација које се бране на Универзитету у Београду, коришћењем програма iThenticate извршена је провера оригиналности докторске дисертације кандидата Мохамеда Х. Асалеха (Mohamed H. Assaleh) под називом **„ИМИНО ДЕРИВАТИ ДИХИДРАЗИДА ТИОУГЉЕНЕ И АМИДА ЦИМЕТНИХ КИСЕЛИНА: КОРЕЛАЦИЈЕ СТРУКТУРЕ И АКТИВНОСТИ (IMINO DERIVATIVES OF CARBONOTHIOIC DIHYDRAZIDES AND CINNAMIC ACIDS AMIDES: STRUCTURE-ACTIVITY RELATIONSHIP STUDIES)“**. Извештај који садржи резултате провере оригиналности ментор је добио дана 13.03.2022. Утврђени проценат подударности је 23%. Овај проценат је последица општих места, односно употребе стручних термина и података који се тичу обрађене теме, назива коришћених метода и њихових скраћеница, личних имена, инструмената, цитиране литературе и изјава кандидата. Део подударности се односи на претходно публиковане резултате докторандових истраживања, који су проистекли из његове дисертације.

На основу свега изнетог, а у складу са чланом 8. став 2. Правилника о поступку провере оригиналности докторских дисертација које се бране на Универзитету у Београду, изјављујемо да извештај указује на оригиналност докторске дисертације, те се прописани поступак припреме за њену одбрану може наставити.

**Ментори**

---

др Александар Маринковић, ванредни професор Универзитета у Београду, Технолошко-металуршки факултет

---

др сц. мед. Снежана Бјелогрлић, виши научни сарадник Института за онкологију и радиологију Србије